Development of Soluble Manganese Sorptive Contactors for Enhancing Potable Water Treatment Practices

Lauren Zuravnsky

Thesis submitted to the faculty of the Virginia Polytechnic Institute and State University in partial fulfillment of the requirements for the degree of

Master of Science
In
Environmental Engineering

Dr. William R. Knocke, Co-Chair
Dr. John C. Little, Co-Chair
Dr. Peter J. Vikesland

September 11, 2006
Blacksburg, VA

Keywords: manganese, oxide-coated media, adsorption, water treatment

Development of Soluble Manganese Sorptive Contactors for Enhancing Potable Water Treatment Practices

Lauren Zuravnsky

ABSTRACT

Without proper removal at a water treatment facility, the soluble manganese (Mn) concentration can reach and exceed the Secondary Maximum Contaminant Level (SMCL) of 0.05 mg/L in the water distribution system. At this level, soluble Mn can be oxidized to solid Mn-oxide particulates, leading to water discoloration events and resulting in numerous consumer complaints. Manganese-laden water can severely stain fixtures and laundry as well as increase turbidity and foul tastes. A major discoloration event can cause a decrease in consumer confidence in the quality of water provided to their taps. Currently, there is no other treatment alternative available that can remove soluble Mn with the high efficiency of the "natural greensand effect."

Therefore, researchers are developing ways to effectively create the natural greensand effect in a post-filtration sorptive contactor for application at water treatment facilities. The process of adsorption and oxidation of Mn onto oxide-coated media grains in the contactor will be used for the removal of soluble Mn. However, small media grains, such as sand or anthracite, could produce prohibitive head loss in a sorptive contactor. The focus of this research project was to show that Mn could be effectively removed via adsorption onto larger media (2.0-6.4mm) at hydraulic loading rates of 16-24 gpm/ft^2, thus producing less head loss and furthering the development of soluble Mn sorptive contactors to be implemented in water treatment facilities.

Research was conducted by executing laboratory- and pilot-scale experiments using columns packed with oxide-coated media. Three types of media were used: large grain "torpedo sand," pyrolucite granules, and small gravel. Before being packed into the columns, the torpedo sand and gravel media was coated with an oxide coating using a technique previously developed by Merkle (1995). Manganese uptake capacity was determined for each media type prior to use and after a number of contactor column experiments were completed. Water samples were collected during the experiments and analyzed for soluble Mn concentration. The Mn removal profile was determined by taking water samples at a certain time and at various depths in the media bed.

Experiments were conducted to determine the removal profile of the media types under different operating conditions. Hydraulic loading rate, influent Mn concentration, influent free chlorine concentration, and pH were the operational parameters varied. The effect of these parameters of the Mn removal profile was evaluated.

Although each media type was able to remove some percentage of soluble manganese from the applied water, pyrolucite media was the most effective media, often providing approximately 80-90% removal of initial manganese concentration. The removal performance of the large-sized media beds was affected by operational parameters as expected from knowledge of prior research. The contactor media beds also provided adequate soluble manganese removal under conditions available at the water treatment facility as determined from the pilot-scale experiments conducted at the Blacksburg-Christiansburg-VPI Water Authority.

Another important and complementing facet of this research was the development of a proven model that would predict soluble Mn removal performance of various oxide-coated media types and the development of recommendations that could be used for implementing and operating such post-filtration sorptive contactors. A model was developed from first principles for the prediction of soluble Mn removal and fitted to the experimental data. The predictive model showed that removal performance depended on the specific surface area of the contactor media, HLR, and the mass transfer coefficient.

Recommendations for the operation of a sorptive contactor containing large oxide-coated media include an applied hydraulic loading rate of 16-24 gpm/ft^2 with an initial free chlorine concentration of 1.0-2.0 mg/L and a slightly alkaline pH of 7.0-8.0. Greater hydraulic loading rates are recommended to provide capital cost savings due to the decreased contactor footprint required. Alkaline pH is recommended for improved Mn removal. Facilities with a slightly acidic pH due to enhanced coagulation practices should consider adjusting the pH of the finished water for corrosion control prior to the Mn removal contactor for improved Mn adsorption performance.

ACKNOWLEDGEMENTS

I would like to thank my co-advisors Dr. W. Knocke and Dr. J. Little, not only for their patient and helpful guidance of my research but also for the knowledge and professional development I gained while working with them. Thank you to Dr. P. Vikesland for providing insight as a member of my committee.

Funding for this research was provided by the following sources: American Water Works Association Research Foundation (AWWARF), the Charles E. Via, Jr. Department of Civil and Environmental Engineering Endowment, and the Edna Bailey Sussman Foundation. Thank you for providing the resources to make this research possible.

Thank you to Ying Xu for her collaboration in the development of the model by sharing her astute knowledge of MatLab and numerical analysis.

Thank you to Jeff Parks and Jody Smiley for teaching me how to use the ICP-MS and the AA-MS. Without your assistance and constant troubleshooting, I may not have had any data.

Thank you to Julie Petruska for providing support and insight during the development of my lab experiments. Your expertise is invaluable.

A special thank you to my parents and family for their constant love and unwavering support.

CONTENTS

TABLES

FIGURES

CHAPTER 1
INTRODUCTION

In the past decade water treatment processes have changed due to the fact that the US Environmental Protection Agency (EPA) has introduced the Enhanced Coagulation Rule, the Disinfection/Disinfectant By-Product (D/DBP) Rule and other regulations aimed at reducing the health risks associated with the chlorination of drinking water. As a result of these regulations, some water treatment utilities have recently stopped applying free chlorine to their filtration beds. However, in many utilities it has been the presence of the free chlorine in contact with the oxide-coated surface of the filtration media that has created a "natural greensand effect" that efficiently removed soluble manganese (Mn) from the drinking water. Without proper removal, Mn concentration can reach and exceed the Secondary Maximum Contaminant Level (SMCL) of 0.05 mg/L in the finished water. At this level, water utilities can begin to experience water discoloration events throughout the distribution system, resulting in numerous consumer complaints. Complaints regarding water discoloration have been observed by municipal water treatment utilities even when the finished water Mn level exceeds 0.02 mg/L on a consistent basis (Sly *et al.* 1990). Manganese-laden water can severely stain fixtures and laundry as well as increase turbidity and foul tastes. A major discoloration event can cause a decrease in consumer confidence in the quality of water provided to their taps. Currently, there is no other treatment alternative available that can remove soluble Mn with the high efficiency of the "natural greensand effect."

Previous research has determined that oxide-coated media could be used to remove soluble Mn from water at treatment facilities by adsorption and oxidation of the soluble Mn onto the media (Knocke *et al.* 1988; Knocke *et al.* 1990; Knocke *et al.* 1991). Different media configurations have been evaluated for improved head loss and Mn removal (Coffey *et al.* 1993). Two operational modes have been proposed for this type of oxide-coated media use: intermittent regeneration without the presence of an oxidant and continuous regeneration in the presence of an oxidant. The continuous regeneration mode requires an oxidant which provides rapid and effective oxidation at the media surface without oxidizing the soluble Mn in solution. Free chlorine was determined to be the most effective oxidant for this situation (Knocke *et al.* 1987). Modeling of the adsorption and oxidation processes is helpful for practical application of the Mn removal system to treatment situations. Previous models have been developed (with certain limitations) that attempt to predict soluble Mn removal profiles across oxide-coated media beds (Coffey *et al.* 1993; Merkle *et al.* 1997b).

The research reported on in this thesis focused on the further development of the "natural greensand effect" with application as a post-filtration contactor. Contactors composed of oxide-coated media could be applied to water treatment as a tertiary treatment process after filtration. The location of the contactor downstream of the filters would ensure that additional Mn found in the source water, present after primary treatment, and released during the treatment process could be removed. Contactor location would also provide minimal concern of clogging due to solid particles and require less frequent backwashing. Since oxidant addition is still required for disinfection and distribution system residual, research suggests that placing a free chlorine addition point just prior to the oxide-coated media contactor will provide sufficient oxidant for continuous contactor regeneration as well as disinfection. If influent concentrations of Mn were

in excess of 0.3 mg/L, the water treatment facility may also require a primary method of Mn removal at the head of the plant.

Previously, the Mn removal process was investigated using small sand-sized media and hydraulic loading rates of 2-5 gpm/ft^2. Research reported on in this thesis was conducted with large-sized media and higher flow rates of 16-24 gpm/ft^2. Three types of oxide-coated media were used in this research: large grain "torpedo sand," pyrolucite granules, and small gravel. The focus on large-sized media and increased hydraulic loading rates was important for further developing a practical contactor to be implemented at water treatment facilities. Large media was required for increased loading rates without large head loss concerns. Increased loading rates were preferred for design of a contactor with a small footprint requiring less disruption and capital investment for a utility. Therefore, evaluating the performance of large media with decreased surface area was important. Specific research objectives include the following:

1. Conduct laboratory-scale and pilot-scale treatment experiments to demonstrate the post-filtration contactor concept for soluble Mn removal,

2. Evaluate the impacts of important operational variables such as initial Mn concentration, free chlorine concentration, hydraulic loading rate and pH on overall process performance,

3. Develop from first principles a proven model that would predict soluble Mn removal performance of various oxide-coated media types in a post-filtration contactor model; and,

4. Develop recommendations that could be used by water process designers and water utility personnel for implementing and operating such post-filtration contactors within their treatment operations.

CHAPTER 2
LITERATURE REVIEW

This chapter presents brief summaries of previous research conducted in areas relevant to the removal of soluble manganese by adsorption onto manganese oxide. A literature review of previous research is important for development of successful experimental methods and progressive research objectives to further enhance knowledge of the subject. This chapter includes sections on manganese chemistry, sources of manganese in drinking water, related water quality issues and regulations, health effects, common removal techniques, sorption of soluble manganese onto filter media, and modeling of manganese removal via sorption and oxidation.

MANGANESE CHEMISTRY – SOLID AND AQUEOUS SPECIES

Manganese is a widely abundant and naturally occurring element. Most commonly found in solid form as pyrolucite (essentially manganese dioxide, MnO_2), manganese is mined and used in steel alloy and dry battery production. Manganese is also ubiquitous in animal and plant tissue, functioning as an important trace nutrient. Oceanic research has even resulted in the discovery of the abundance of manganese nodules on the ocean floor (Rona 2003).

As a transition metal, manganese has numerous oxidation states between 0 and +7. The most commonly encountered states are Mn(II), Mn(III), Mn(IV), and Mn(VII). The reduced Mn (II) is generally found as the soluble Mn^{2+} cation. The highly oxidized Mn(VII) is widely known as permanganate and found in the form of the soluble MnO_4^- anion. The insoluble oxides of manganese are formed from Mn(III) and Mn(IV) and are often found as $MnOOH_{(s)}$ and $MnO_{2(s)}$, respectively. Mixed oxides also exist in the form of MnO_x, where x varies from 1.1 to 1.8 (Morgan and Stumm 1964).

SOURCES OF MANGANESE IN DRINKING WATER

Manganese is naturally found in both surface water and groundwater throughout the United States. Aerated or oxidized sources of water generally have low concentrations (< 0.05 mg/L) due to the oxidation of manganese to the insoluble form of $MnO_x(s)$. The reducing conditions found in groundwater sources and the hypolimnion of deep reservoirs produce greater soluble manganese concentrations (up to approximately 1.0 mg/L). Under reducing conditions, manganese is commonly found as Mn(II). Biological activity can also introduce reduced manganese into a water source.

The presence of manganese in source water is the most common source of manganese in the drinking water system. However, contamination of coagulants can also introduce manganese into the system. Coagulant sludge generally contains higher concentrations of manganese than found in source water. Recycle from a sludge thickener or a hydraulic upset in a tradition settling basin may release spikes of manganese into the plant flow (American Water Works Association 1999).

WATER QUALITY ISSUES AND REGULATIONS

If manganese is not removed during the treatment process, it will enter the distribution system and continue to interact with oxidants in the water, piping materials, and biofilms. Residual free chlorine has been shown to chemically oxidize the remaining soluble manganese via the same process used to treat manganese in the plant as discussed later in this chapter. Manganese oxidizing bacteria are present in biofilms along the pipe walls. Pipe material has been shown to affect the buildup of both manganese oxidizing biofilms and associated manganese oxide scale (Murdoch and Smith 1999; Cerrato *et al.* 2006).

Pipe capacity reductions due to the production and deposition of particulate manganese oxides can cause problems in the distribution system. Significant aesthetic water quality issues at the tap, including brown to black water, bitter tastes, discolored laundry and stained fixtures, are also caused by particulate manganese oxides. Concentrations of greater than 0.05 mg/L are generally considered to trigger problematic oxide formation. However, consumer complaints regarding these aesthetic issues have been found to plague municipal treatment plants when finished water manganese levels exceed 0.02 mg/L on a consistent basis (Sly *et al.* 1990).

As directed by the amended Safe Drinking Water Act (SDWA), the U.S. Environmental Protection Agency (EPA) maintains a Drinking Water Contaminant Candidate List (DWCCL). Manganese was originally an item on this list and considered a candidate for National Primary Drinking Water Regulation (NPDWR). However, in July of 2003, the EPA announced that primary regulation was not required and a Secondary Maximum Contaminant Level (SMCL) of 0.05 mg/L for manganese was set for drinking water.

HEALTH EFFECTS OF MANGANESE

Manganese is an essential trace nutrient for human growth and development. As with most metals, large doses of manganese can produce toxic effects. Research in the area of health effects of manganese has commonly focused on the inhalation of manganese dust. For manganese to be removed from the DWCCL, research on the effects of ingesting manganese through the pathway of water consumption was conducted.

Although the EPA task group was convinced that the effects of manganese consumption did not validate the creation of primary drinking water regulations, there is still research and academic discussions being conducted on the health effects of manganese in potable water. Researchers at the Wake Forest University School of Medicine have begun evaluating the concerns related to the inhalation of manganese laden water particles during showering with a critical literature review and model based estimations (Elsner and Spangler 2005; Spangler and Elsner 2006). Inhalation is considered to be a more direct pathway of exposure than consumption due to the direct connection of the olfactory pathway with the brain. The researchers estimated that humans, specifically children, can develop deposition of manganese in the olfactory system after chronic exposure to shower aerosols containing manganese (0.1-0.5 mg/L). Although stating the limitations of their estimations, the researchers believe that this pathway deserves further evaluation relating to neurological health concerns.

Table 2.1
Reactions of Mn(II) with alternative oxidants (Adapted from (Knocke *et al.* 1990))

Reaction	Equation Number
$Mn^{2+} + HOCl + H_2O \leftrightarrows MnO_{2(s)} + Cl^- + 3H^+$	2.1
$3Mn^{2+} + 2MnO_4^- + 2H_2O \leftrightarrows 5MnO_{2(s)} + 4H^+$	2.2
$Mn^{2+} + 2ClO_2 + 2H_2O \leftrightarrows MnO_{2(s)} + 2ClO_2^- + 4H^+$	2.3
$Mn^{2+} + O_{3(aq)} + H_2O \leftrightarrows MnO_{2(s)} + O_{2(aq)} + 2H^+$	2.4

COMMON REMOVAL TECHNIQUES

There are a number of common technologies used to remove manganese from water: aeration, chemical oxidation, sequestration, and sorption. Sorption using oxide coated media is discussed in more detail in the following section.

The removal of soluble manganese can be accomplished through the physical process of aeration. Researchers have investigated source reduction of manganese levels by using bubble aerators to mix deep water reservoirs and reduce the effect of thermal stratification (Burns 1998). Water from either an underground or surface source can be aerated using various techniques during treatment. However, the rate of reaction between manganese and oxygen is slow and a retention tank with several hours of detention time is recommended to allow conversion (Wong 1984). Alkaline pH (> 9.0) is generally required for soluble manganese to be oxidized in this way within the duration of water treatment (Morgan and Stumm 1964). Filtration is then used for the removal of the solid manganese oxide particles. Aeration is not often used for large plants or high levels of manganese. The slow reaction time and capital cost of constructing large retention basins do not promote widespread usage.

Manganese removal has been accomplished by the addition of chemical oxidants, including free chlorine, chlorine dioxide, potassium permanganate and ozone. Table 2.1 shows the reactions between four different chemical oxidants and soluble manganese.

The use of free chlorine as an oxidant for water treatment has a long history. A study conducted by Knocke *et al*. (1987) has shown that alkaline conditions (pH > 8) are required for adequate manganese removal by chlorine addition. Low temperatures (< 5°C) were also shown to inhibit the process. Since traditional coagulation-flocculation treatment benefits from acidic pH conditions, the sole use of chlorine as an oxidant for manganese removal is not recommended. Chlorine is the oxidant preferred to enhance removal via oxide coated media as discussed later in this chapter.

Chlorine dioxide (ClO_2) is an effective disinfectant and commonly used in water treatment. For manganese oxidation, the theoretical stoichiometric amount of chlorine dioxide needed is 2.45 mg/mg Mn^{2+}. Laboratory testing showed that twice the theoretical amount could be required for effective soluble manganese removal (Knocke *et al.* 1987). The concentration of organic material in the water greatly affects the dosage of chlorine dioxide required. At low organic concentrations (< 2.5 mg/L), measured as total organic carbon (TOC), a chlorine dioxide dose between 1.0–1.5 mg/L was effective across a large range of pH values. However, higher

organic demands (8-10 mg/L TOC) resulted in required doses of over 3 mg/L of ClO_2 for similar removal. Due to concerns of chlorite and chlorate presence in drinking water, most regulatory agencies do not permit dosage of chlorine dioxide outside the range of 0.5-2.0 mg/L. Therefore, chlorine dioxide is an effective oxidant for manganese removal but should be used in conjunction with another oxidant when high concentrations of organic material and or high initial soluble manganese levels are present.

Potassium permanganate ($KMnO_4$) has been conventionally used for manganese oxidation. Also affected by organic concentrations, the permanganate dosage increases to much higher than the theoretical stoichiometric amount as the TOC levels increase above 3 mg/L. The increased permanganate dose also satisfies the organic oxidation demand as well as the manganese oxidation demand. The chemical cost per unit of potassium permanganate is higher than the cost per unit required for oxidation by free chlorine (Knocke *et al.* 1987).

Ozone (O_3) is a strong and rapid-acting oxidant. Ozone has become a more widely accepted disinfectant in water treatment since its use will not produce disinfection by-products, except when bromide is present in the water. Ozone is also used to oxidize manganese for removal. A study was conducted by Reckhow *et al*. (1991) to determine the stoichiometry and kinetic rates of the oxidation reaction between ozone and manganese under both low and moderate organic concentration conditions. The study found that the reaction rate increased with increasing pH; further, at a pH of 8.0 the required dose was practically equal to the theoretical stoichiometry. However, with the addition of organics, between 2-5 times the stoichiometric dose was required to oxidize the manganese. To reduce the dose of ozone required, bicarbonate was added to minimize the formation of unproductive radicals. Ozone use is therefore more often recommended for oxidizing manganese in water with low organic content.

Most of the removal methods mentioned above chemically or physically oxidize manganese to its solid form. These oxide particles then require physical removal. Often utilities use the traditional treatment consisting of coagulation, flocculation, clarification, and filtration to remove the oxides along with other water impurities. Oxidized manganese often forms particles in the colloidal range which are not efficiently removed when applied directly to filtration media (Knocke *et al.* 1988). Research on membrane filtration as a viable method for removing oxidized manganese particulate has also been conducted (Suzuki *et al.* 1998; Rahman *et al.* 2000).

Sequestration of manganese is another limited-use method of controlling manganese oxidation issues. The addition of polyphosphates or a combination of sodium silicate and chlorine has been shown to sequester the inorganic with varying degrees of success. However, there has been limited research in developing this treatment method (Trace Inorganic Substances Committee 1987).

SORPTION OF MANGANESE ONTO FILTER MEDIA

Another removal method and the focus of this research is the adsorption of soluble manganese onto manganese oxide. The oxide can be present as a coating on the surface of the filtration media (coated sand or gravel) or as the media (pyrolucite). The soluble manganese adsorbs to available oxide sites and, in the presence of an oxidant, these adsorbed ions are oxidized to create more available sites. The following section reviews the relevant research related to this process.

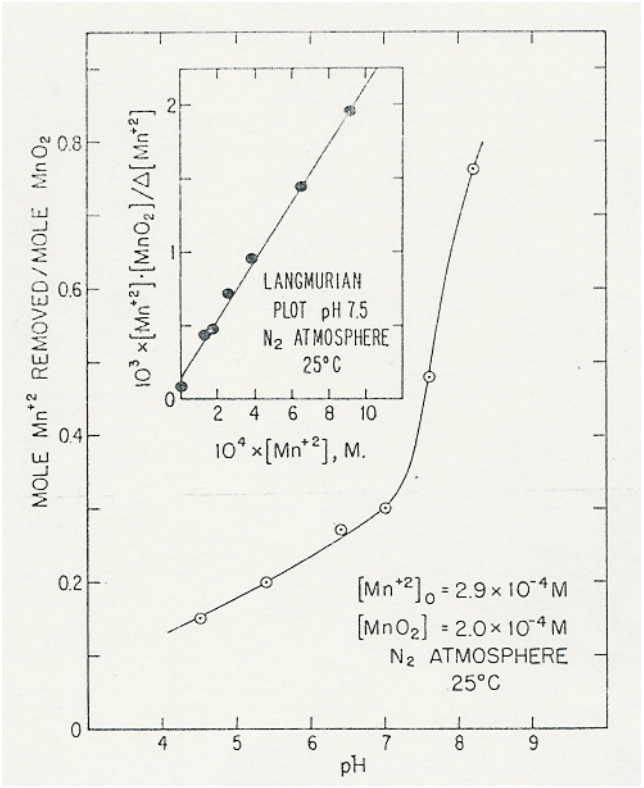

Figure 2.1 Plot showing pH dependent sorption of manganese(II) on manganese dioxide (Reprinted from Morgan and Stumm 1964, with permission from Elsevier)

Morgan and Stumm (1964) conducted a study to evaluate the surface chemical properties of hydrous manganese dioxide. Colloidal manganese dioxide suspensions were manipulated and evaluated for certain properties. The zero point of charge was found to be at pH 2.8 ± 0.3. The colloid surface charge becomes increasingly negative as the pH of the solution increases. Manganese dioxide was shown to have an affinity for soluble manganese (Mn^{2+}) adsorption. Figure 2.1 shows the capacity for soluble manganese sorption onto the colloids also increased as the solution pH increase. At a pH of approximately 9.0, the capacity approaches 2 moles of Mn^{2+} per mole of MnO_2.

The process of manganese removal through sorption and oxidation on manganese greensand has been utilized for decades, primarily in treating groundwater with elevated soluble manganese levels. Knowledge of this process developed into the use of oxide-coated media in a filter bed with an oxidant residual (e.g. HOCl) across the bed. There are a number of parameters that affect the manganese removal performance of oxide coated media (OCM). Researchers have noted the significance of the type of oxidant applied, the pH of water applied to the bed, and the capacity of the media as related to the available surface sites on the oxide coating.

Knocke *et al.* (1988) evaluated the use of four different oxidants to promote manganese removal across the OCM filter bed. Oxidants were applied to the water before the filter bed. Strong oxidants such as permanganate, chlorine dioxide, and ozone oxidized the soluble manganese almost immediately. In these cases, colloidal solid manganese was reaching the filter

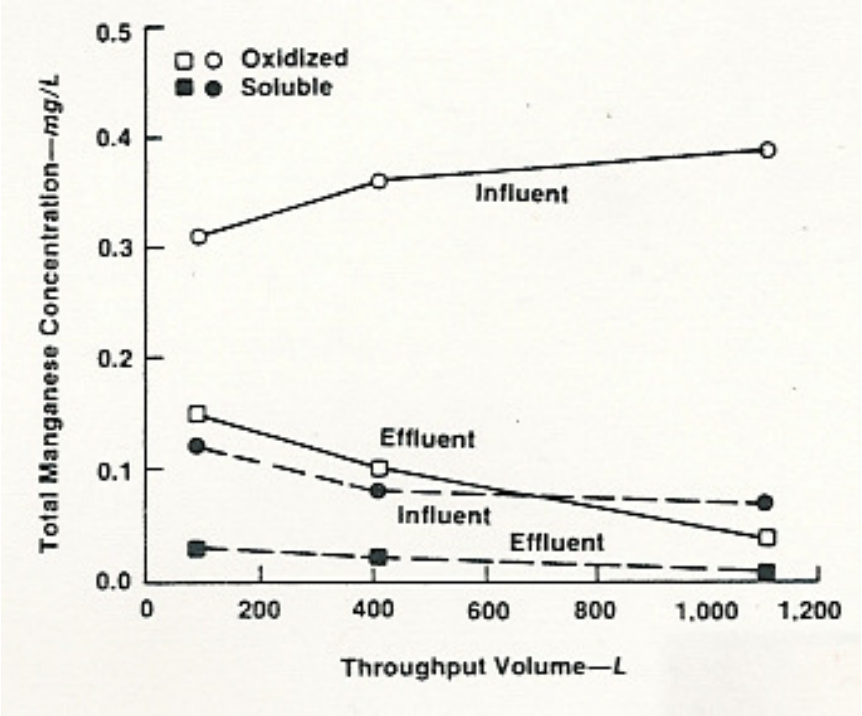

Figure 2.2 Plot of manganese removal characteristics across a coal bed with pre-filter $KMnO_4$ addition ($KMnO_4$ = 0.5 mg/L, pH = 7.3) (Reprinted from Knocke *et al.* 1988, with permission from AWWA)

and the removal mechanism was filtration instead of sorption. Figure 2.2 shows the characteristics of the manganese reaching a filter bed when permanganate is applied before the filter. Due to the highly negative charge of the colloidal manganese dioxide, these particles were found to be not easily removed through filtration (Wong 1984). In the oxidant study by Knocke *et al*. (1988), the failure of the filter bed was defined as a colloidal breakthrough of $MnO_x(s)$ when using the strong oxidants.

The addition of free chlorine prior to the OCM filter bed did not oxidize the manganese in the bulk solution. Instead, the majority of the manganese reaching the filter bed was in the soluble form. The removal mechanism was determined to be direct sorption of soluble manganese onto the media surface. The chlorine residual provided the necessary oxidant to regenerate the active sites on the media. The capacity of the media in combination with the regenerative properties of the free chlorine provided the necessary manganese removal at both low and high loading rate conditions. The results indicated that the presence of free chlorine at a concentration of >1-2 mg/L was sufficient for rapid soluble manganese removal (Knocke *et al.* 1988). Figure 2.3 shows that continuous removal of manganese can occur with the application of free chlorine, while without free chlorine, the capacity of the media is eventually exhausted.

Knocke *et al*. (1991) used shallow bed depths (5-6 in) and high influent manganese concentrations (1.0 mg/L) to promote rapid exhaustion of the available sorption sites to evaluate the effects of the absence of chlorine on manganese removal. There was no evidence of auto-oxidation found and no active sites were being regenerated without the presence of an oxidant.

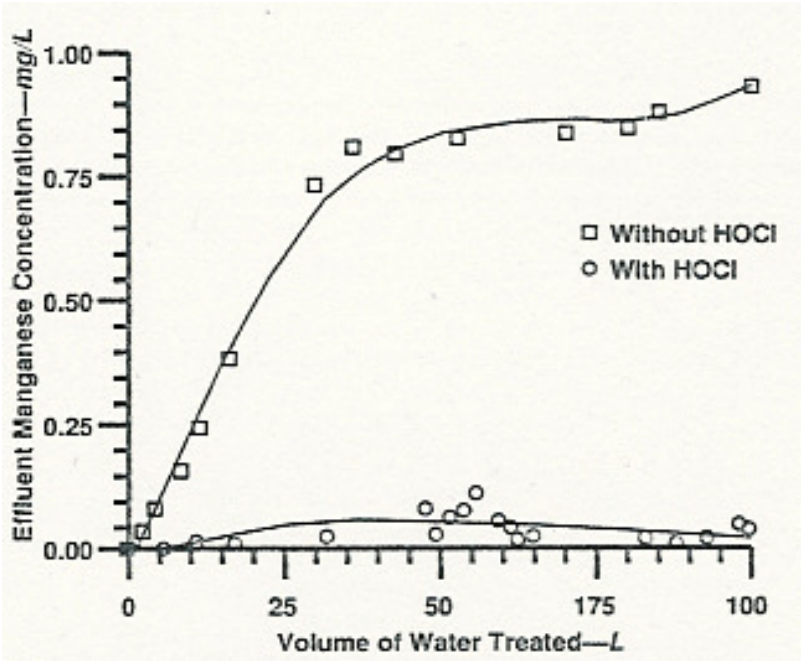

Figure 2.3 Plot showing the Mn(II) with and without the presence of HOCl (2 mg/L) at pH = 7.8 (Reprinted from Knocke *et al.* 1991, with permission from AWWA)

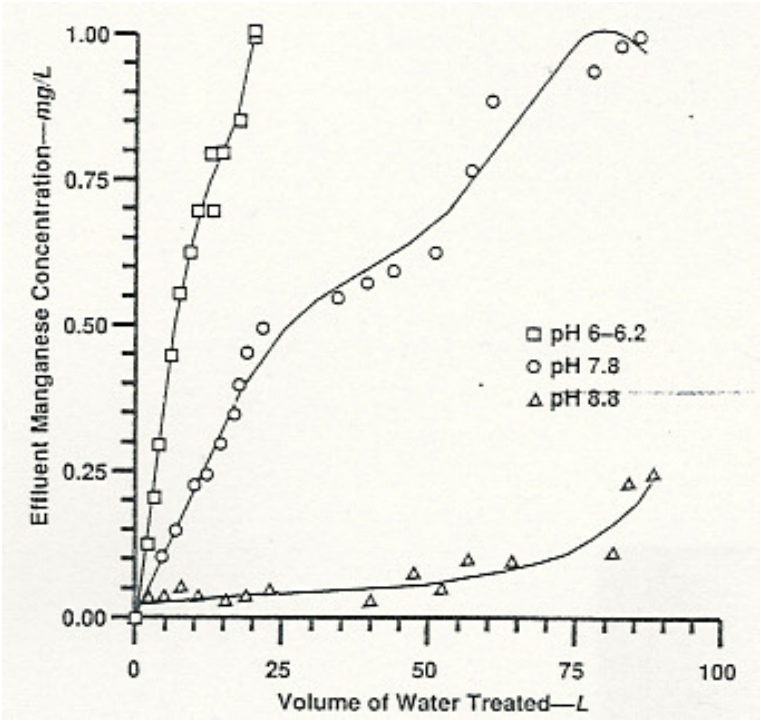

Figure 2.4 Plot showing the effect of pH on Mn(II) adsorption without free chlorine (Reprinted from Knocke *et al.* 1991, with permission from AWWA)

A number of studies have found significant effects related to the pH of the applied water on oxide-coated filter media performance (Knocke *et al.* 1988; Knocke *et al.* 1990). These effects were observed under conditions with and without applied chlorine. In the absence of free chlorine, the effect of pH on the media capacity was observed. Figure 2.4 shows the detrimental effects of acidic pH on the media manganese adsorption capacity and the benefits of alkaline conditions for effective removal. These results correlate well with the findings of Morgan and Stumm (1964) as discussed earlier in this section.

Earlier research was able to show the relationship between removal efficiency and the amount of extractable manganese oxide present on the media as seen in Figure 2.5. As the extractable amount increased, the capacity of the media to remove more manganese seemed to increase. However, in more recent research, the correlation between extractable coating and manganese adsorption capacity has been evaluated more directly. A 4-hour capacity test was developed to determine the manganese absorptive capacity of the media. This test was used by Bouchard (2005) to evaluate media capacity as related to bed depth in an active surface water treatment plant. The capacity results were also compared to the amount of extracted manganese oxide. The plot of absorptive capacity versus extractable manganese (shown in Figure 2.6) indicates that capacity increases with increasing MnO_x coating until approximately 12 mg coating per mg of media. Beyond this point there does not seem to be an increase in capacity with an increase in extractable coating, suggesting that layering of MnO_x coatings covers previously available adsorption sites, making them thusly inaccessible

This agrees with the kinetic studies conducted by Morgan and Stumm (1964). The kinetic rates of manganese adsorption were different between colloidal and flocculated manganese dioxide particles. The colloidal suspensions reacted more rapidly than the flocculated suspensions. It was suggested that the reaction between soluble manganese and manganese dioxide is a surface related phenomena and the colloidal sites were more available, allowing for a faster reaction (Morgan and Stumm 1964). Together, these findings point to a sorption reaction that is surface related.

Since the cycle of adsorption and oxidation adds layers of manganese oxide to the filter media grains, research was conducted to determine the effect of oxide coatings on the physical properties of the media. There were no significant changes in the physical size or density of the media (Knocke *et al.* 1990). Therefore, no significant changes in the hydraulic properties in the media bed should be expected.

Recently, the change in physical properties was also evaluated in combination with the effects of backwashing and the long-term fate of manganese on the filter media (Hargette and Knocke 2001). The regular operation of filters involves frequent backwashing to maintain the effective removal of solid particles across the media bed. The authors conducted filter experiments at two pH values (6.0 & 7.3), where the backwash of these filters was the primary focus. It was found that during backwash an initial spike of particulate manganese was detected in the backwash effluent; however, this spike tailed off quickly as the backwash proceeded. The backwash rate slightly affected the amount of manganese removed from the filter but profile shape over the backwash period was unaffected. The pH of the influent water caused a change in the magnitude of the backwash spike. At pH 6.0, the vast majority (>98%) was soluble and removed by sorption. At pH 7.3, 93-96% was soluble, with the remaining 4-7% being particulate. The small amount of particulate manganese was found to be removed by the filter media via physical separation. Therefore, the backwash spike from the filters subject to an

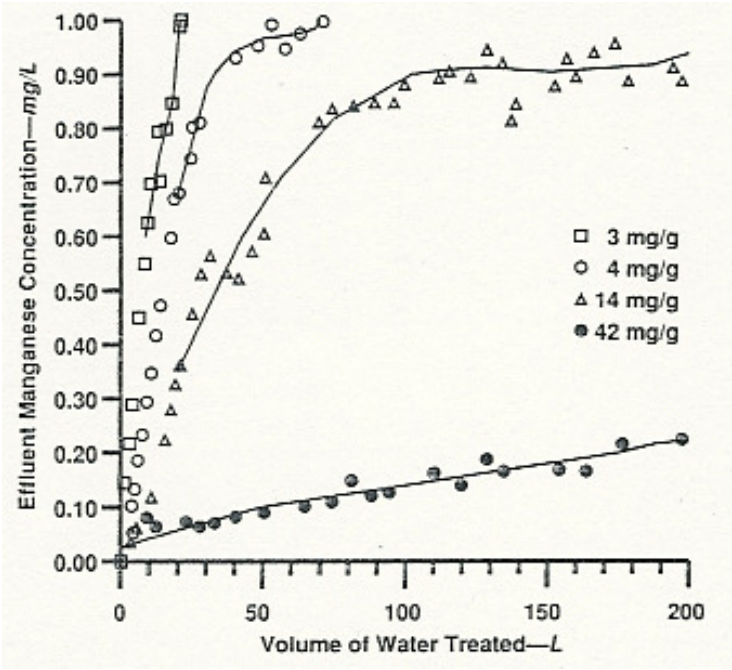

Figure 2.5 Effect of surface oxide concentration on Mn(II) uptake (influent water at pH=6.0-6.2, Mn^{2+}=1.0 mg/L, no oxidant) (Reprinted from Knocke *et al.* 1991, with permission from AWWA)

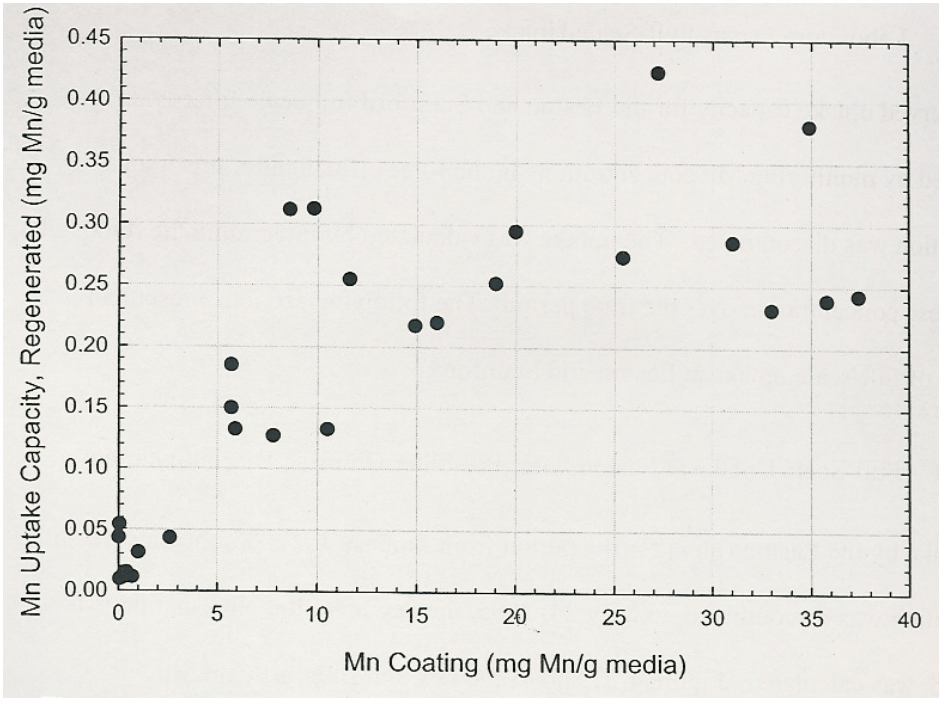

Figure 2.6 Plot of manganese uptake capacity versus extractable coating filter media (Reprinted from Bouchard 2005, with permission from R. Bouchard)

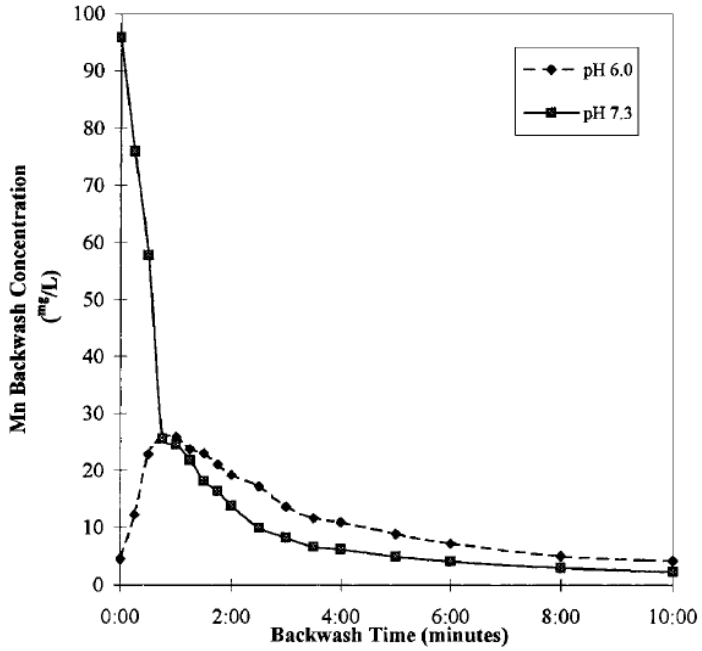

Figure 2.7 Effect of influent pH on manganese release during backwash at 30 gpm/ft2 (Reprinted from Hargette and Knocke 2001, with permission from ASCE)

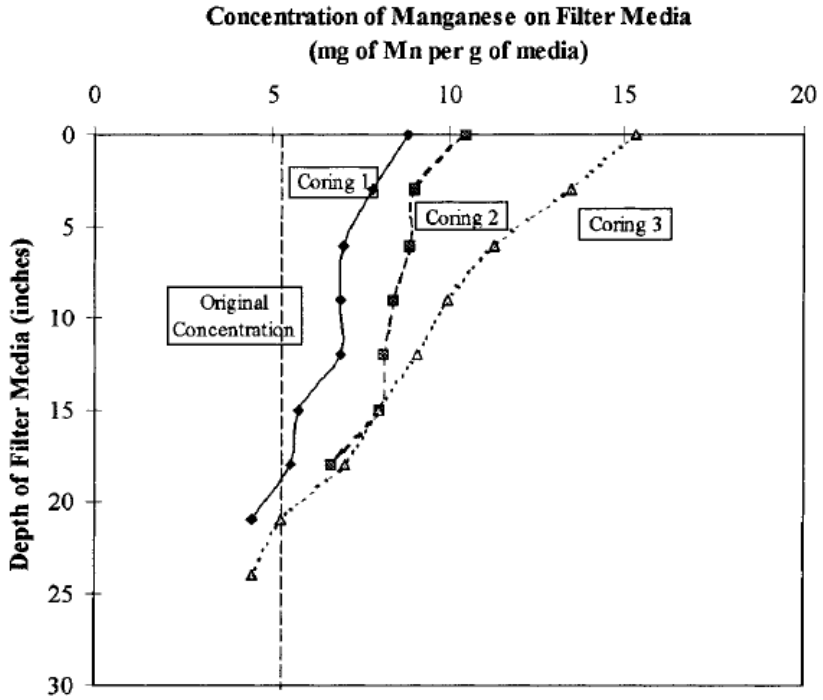

Figure 2.8 Progression of extractable manganese coating on filter media (three filtration and backwash cycles between corings) (Reprinted from Hargette and Knocke 2001, with permission from ASCE)

influent pH of 7.3 showed a much greater spike is initial manganese in the backwash effluent as seen in Figure 2.7.

The amount of manganese remaining on the filter media after backwashing was sufficient to continued adsorptive removal of manganese. Even with the application of air scour, 50-90% of the manganese applied to the filter remained on the media, depending on the pH of the influent solution. The coating continued to accumulate after subsequent backwashing and no considerable changes to the physical properties of the media were determined over the duration of the study.

The accumulation of manganese oxide coating is often concentrated in the upper portions of the filter bed. This phenomena has been observed in both operating utilities (Bouchard 2005) and pilot-scale experiments (Hargette and Knocke 2001). Data in Figure 2.8 show the progression of oxide coating growth as continuous filter operation occurs.

MODELING OF SORPTION AND OXIDATION REMOVAL OF MANGANESE

Modeling the removal of soluble manganese through the coupled process of sorption and oxidation is beneficial for the prediction of oxide-coated media performance and the design of media beds for manganese control. There are two different modes of operating OCM beds that required slightly different models. The first mode is referred to as intermittent regeneration. In this mode of operation, oxidant is not continuously applied to the OCM bed and removal occurs until the capacity of the bed is fully exhausted. At this point, the bed is regenerated with a strong oxidant over a short period of time. The second mode of operation is referred to as continuous regeneration. As it suggests, the oxidant is continuously applied to the OCM bed, allowing the media to be regenerated during operation and maintain its capacity.

Coffey *et al*. (1993) used a mass balance approach to further develop the model provided by Nakanishi (1967). The following chemical equations were the basis for this model.

$$Mn^{2+} + MnO(OH)_{2(s)} \leftrightarrow MnO_2MnO_{(s)} + 2H^+ \quad (2.5)$$

$$MnO_2MnO_{(s)} + HOCl \rightarrow 2MnO_{2(s)} + H^+ + Cl^- \quad (2.6)$$

The use of these equations assumed that the number of potential sites was unchanging but these sites were continuously regenerated. The model for the continuously regenerated mode took into account the concentration of manganese in the influent and effluent as well as the effects of hydraulic loading rate, media depth, chlorine concentration, pH, and sorption capacity. The manganese adsorption capacity in this case was determined by extractable manganese concentration on the media surface.

The model developed for intermittent regeneration considered the maximum amount of soluble manganese that can be absorbed. The solution used a linear adsorption isotherm and a first-order adsorption rate. The effect of pH on sorption capacity was included indirectly in the rate constants. Coffey *et al*. (1993) have shown that both models agree with the experimental data collected in that study. However, the continuous regeneration model was only valid for steady state operation; further intermittent regeneration model was considered to be empirical in nature.

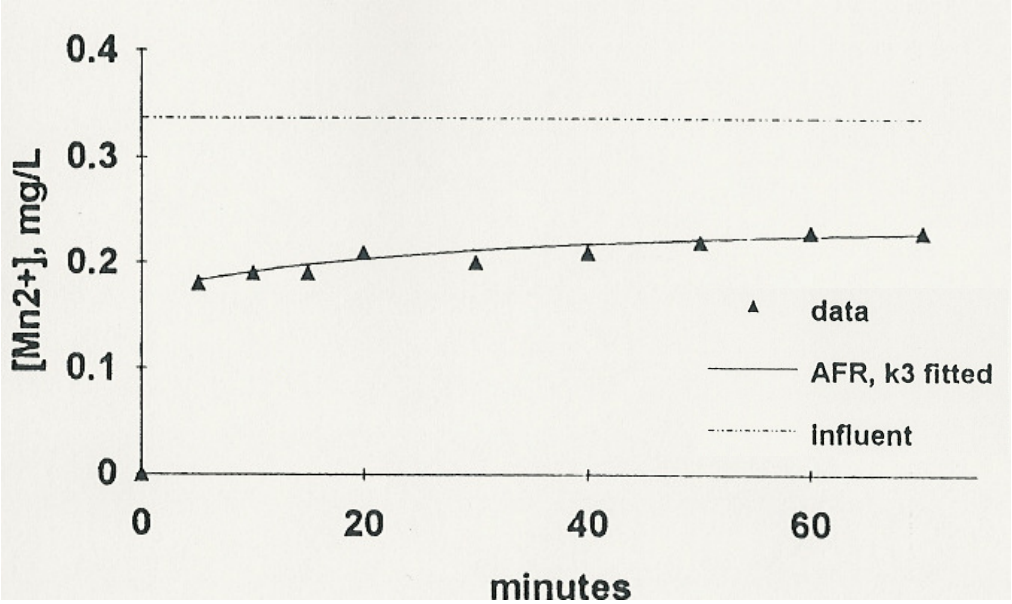

Figure 2.9 Continuous regeneration model calibration at pH=7.5, HLR=5.0 gpm/ft^2, HOCl=1.0 mg/L (Reprinted from Merkle *et al.* 1997b, with permission from ASCE)

Merkle *et al*. (1997b) combined the equations (2.5-2.6) used by Coffey *et al*. (1993) to create an overall reaction for manganese adsorption and surface oxidation. The reaction was then simplified because the specific knowledge of sorption site chemistry has not been well developed. The simplified reaction is stated as Equation 2.7.

$$Mn^{2+} + SITE + HOCl \rightarrow MnO_{x(s)} + SITE \qquad (2.7)$$

This reaction states that the soluble manganese first adsorbs to a site, and then is oxidized to replace and regenerate the previous oxide site. Models were developed for both modes of operation (intermittent and continuous regeneration). The Freundlich isotherm was selected for the models due to the agreement with the data at manganese concentrations consistently seen in water treatment (< 2 mg/L). For intermittent regeneration, a linear driving force (LDF) approximation was used to predict the sorption process. However, LDF did not agree with desorption data and consistently over-predicted the effluent soluble manganese concentration.

The continuous regeneration model was developed as an adaptation of the intermittent model to include the surface oxidation reaction. The oxidation was assumed to be limited to the surface because the oxidant ($HOCl/OCl^-$) is not considered to diffuse past the surface to interior sites. The continuous regeneration model as developed by Merkle *et al.* (1997b) predicted effluent soluble Mn concentration as a function of time in minutes as shown in Figure 2.9.

The calibration parameter used in both models was referred to as the kinetically available fraction of sorption capacity (AFR). The value determined for AFR refers to the sites available through surface diffusion. The continuous regeneration model included another fitted parameter, k_f, the mass transport coefficient of Mn from the bulk fluid to the particle surface.

The model predictions were valid under conditions generally found in water treatment. The model did not agree with the data when subjected to high flows at low manganese adsorption capacity. The previous work conducted by Merkle *et al*. (1997a) focused on the physical structure of oxide coated media supports the assumptions made during the modeling process.

CHAPTER 3
EXPERIMENTAL METHODS & MATERIALS

The purpose of this chapter is to describe the experimental setup and analytical methods used to complete the research objectives previously stated. Descriptions of contactor column design including media characteristics determination constitutes the majority of the experimental methods and materials discussed in this section. These methods and materials were selected and adapted based on a review of the literature and previously conducted research in the area of soluble manganese (Mn) removal using oxide coated media.

CONTACTOR COLUMN DESIGN

Contactor columns were the main focus of the laboratory experiments. The full experimental setup was designed to direct water from the tap through holding drums and a constant head tank, subsequently feeding water to the columns at a constant flow and specified water quality parameters as seen in Figure 3.1. Clear vinyl tubing was attached to the tap water source, guiding water flow into the first plastic 55-gallon drum. A second plastic 55-gallon drum was connected to the first drum via a short length of PVC pipe to provide a constant water source for the pump and allow the chlorine solution to fully mix with the tap water. Water levels were stabilized so that the hydraulic detention time in each drum was approximately 20-30 minutes depending on desired flow rate. Water was then pumped into a constant head tank by a Dayton ½ horsepower pump (plastic, non-submersible, purchased from Grainger, Lake Forest, IL). The constant head tank was constructed from a 40 L Nalgene carboy and supported above the column support rack. Two overflow lines were connected from 15" above the bottom of the head tank to the second drum using clear vinyl tubing (¾" OD x ⅝" ID) and 1" PVC pipe. Column feed water flowed, through clear vinyl tubing (½" OD x ⅜" ID) via gravity, from an outlet at the bottom of the head tank to an inlet in the column wall above the top of the media bed. There was a T-joint approximately halfway between the head tank and the column to allow for two columns to be online at once if necessary. Generally, only one column was online at a time. Water exited the column after flowing through the media bed and was conveyed to a floor drain.

Free chlorine concentration in each experiment was controlled by the addition of a dilute bleach (NaOCl) solution. The concentration of this solution was batch prepared and varied as necessary while the pumping rate was held constant (70-75 mL/min). A Master-Flex peristaltic pump was used to add the solution to the first drum at a location directly adjacent to the tap water influent point. Clear vinyl tubing of various sizes was used to convey the free chlorine solution to the drum.

Tap water was used as the main water source in the laboratory experiments. The local water treatment facility practiced chloramination for disinfection purposes. Free and total chlorine concentrations at the tap were measured during each experiment; free chlorine concentrations were <0.2 mg/L and total chlorine concentrations were 1.8-2.2 mg/L. The concentration of free chlorine in the stock solution was prepared as to provide enough free chlorine beyond the chloramine concentration present at the tap. Other tap water characteristics included a pH of 7.4-8.1 and an alkalinity of approximately 34 mg/L as $CaCO_3$.

Influent soluble Mn concentration was controlled by the addition of a $MnCl_2$ solution. The concentration of this solution was varied as necessary while the pumping rate was

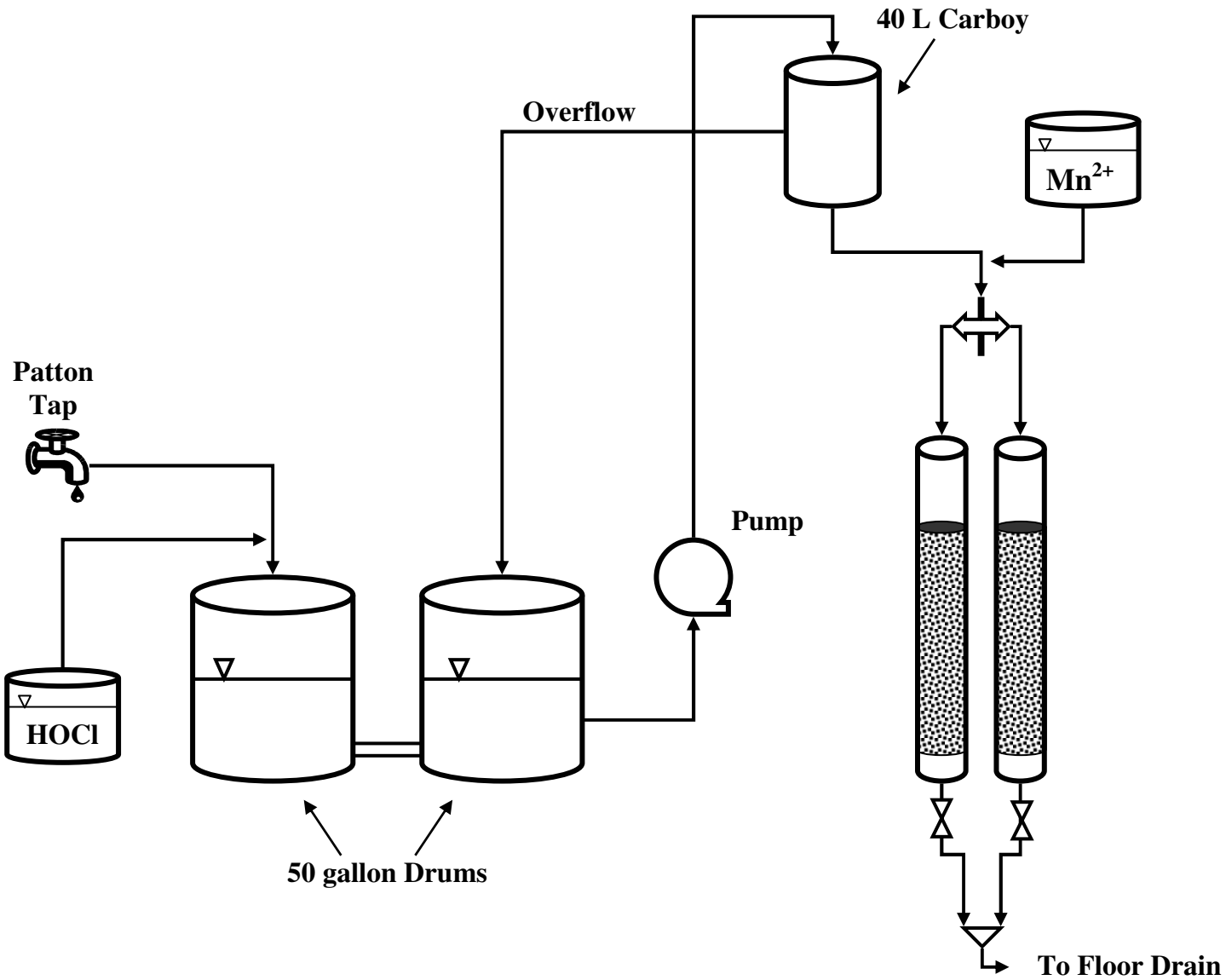

Figure 3.1 Flow diagram of lab-scale contactor column experimental setup

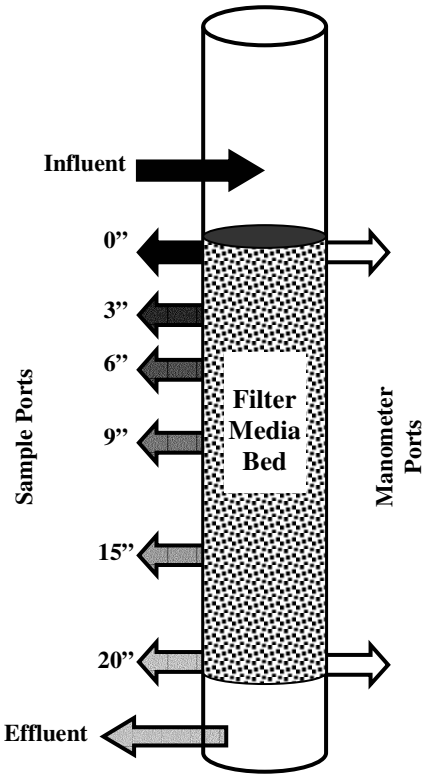

Figure 3.2 Diagram of column port detail

held constant (10-12 mL/min). The soluble Mn solution, consisting of a known mass of $MnCl_2$ in deionized water, was batch prepared in a Pyrex glass vessel. A Master-Flex peristaltic pump was used to add the solution at a joint in the tubing leading from the head tank to the columns. Clear vinyl tubing ($^3/_8$” OD x $^1/_4$” ID) was used to convey the soluble Mn solution. The pH of the column feed water was controlled by sulfuric acid (1.0 N) addition to the $MnCl_2$ solution.

The blended mix of the previously described solutions and tap water flowed through media beds contained in the experimental contactor columns. These columns were constructed from six-foot-long, 3” ID clear PVC pipes. PVC caps were attached to the bottom of the pipes and the tops were left open to the atmosphere. The media bed within the column was constructed by placing approximately two inches of each of the three support gravel sizes obtained from the Blacksburg-Christiansburg-VPI Water Authority (1”- $^5/_8$”, $^3/_8$”- $^5/_8$”, and #10 sieve – $^3/_{16}$”) into the bottom of the pipe.

Twenty inches of the active oxide-coated media were placed over the support gravel. For the purpose of this discussion, this depth of oxide-coated media will be referred to as the media bed. Bulk media was added or removed from the column through the top of the PVC pipe.

All holes drilled into the pipe walls were $^9/_{16}$” in diameter and are represented as arrows in Figure 3.2. Influent water was applied to the column at a point 3” above the top of the media bed, while effluent water flowed from the column at a point 4” below the media bed within the support gravel. Influent and effluent lines were clear vinyl tubing ($^1/_2$” OD x $^3/_8$” ID).

A manometer was constructed from two lengths of glass tubing (3/8" ID) attached to the column through short sections of clear vinyl tubing and 3/8" plastic elbow joints. One glass tube was connected to the column 0" from the top of the media bed, while the other glass tube was connected at 20" from the top of the media bed. The head loss across the media bed was measured as the difference in inches between the water levels in the two glass tubes.

Measurements of soluble Mn concentrations at different depths in the media bed were required to determine the soluble Mn removal profile. Sample points for water collection were drilled at 0", 3", 9", 15", and 20" measured from the top of the media bed. The sample points were fitted with a rubber stopper (size 0), through which a narrow, 3" long glass tube was positioned to reached to the approximate centerline of the column. On the exterior of the column, a flexible tube (5/16" OD x 3/16" ID) was connected to the glass tube and clamped. Water samples for soluble Mn determination were collected by loosening the clamp to allow water flow through the tubing while sample water was captured in 25 mL plastic sample jars with lids. Solid media samples were collected from the column by removing the rubber stopper and gently extracting media grains from the bed. Influent and effluent free chlorine samples were collected from the top (0") sample point and the column effluent tubing, respectively.

Hydraulic flow through the system originated at the tap and ended at the column effluent tubing which led to a floor drain. Water flow from the tap and column effluent was measured and balanced to ensure a narrow range of detention time in the system. The hydraulic loading rate of the media bed was ultimately controlled by a clamp on the column effluent tubing. Flow rate was determined by measuring the time required to collect a known volume of effluent water. The clamp was tightened or loosened to generate the desired flow rate.

CONTACTOR MEDIA SELECTION

Previous research has been conducted on filter sand grain media. Larger sized media was selected for this study to determine the effectiveness of the process under conditions that included decreased media surface area (9-18 cm^2/cm^3 as compared to 34 cm^2/cm^3) and increased hydraulic loading rate (16-20 gpm/ft^2 as compared to 2-5 gpm/ft^2). Sorptive contactors with large media grains provide a more practical design for use in water treatment plants as a tertiary treatment step after filtration since such contactors could be implemented without a large disruption in the plant hydraulic grade line. Three types of contactor media were evaluated in this research study: commercially available pyrolucite, gravel, and torpedo sand. Table 3.1 shows the properties of each media. Pyrolucite was particles of manganese oxide which required activation with an oxidant. Pyrolucite media was LayneOx™ brand material obtained from the Layne Christensen Co. (Mission Woods, KS); received at 8x20 mesh size and then sieved to

Table 3.1
Summary of contactor media properties

	Gravel	Sand	Pyrolucite
Specific gravity	2.42	2.67	4.15
Porosity (ε)	0.35-0.39	0.43-0.44	0.51-0.53
Particle size (mm)	3.2-6.4	2.0-2.5	2.0-2.4

Table 3.2
Summary of operational parameters of experimental influent water

Operational parameter	Numerical value	Description
Hydraulic loading rate	16 gpm/ft^2	Lower flow rate condition
	20 gpm/ft^2	Upper flow rate condition
Mn^{2+} concentration	0.05 – 0.10 mg/L	Desired range of applied Mn concentration
	0.25 mg/L	High Mn concentration ("stress" condition)
Free chlorine concentration	1.0 – 2.0 mg/L	Desired range of applied concentration
	0.2 – 4.0 mg/L	Range of concentrations evaluated
pH	6.5	Lower Boundary
	7.5	Upper Boundary

obtain the 8x10 mesh size used in the columns. Gravel and torpedo sand had to be coated to develop the required oxide coating. Gravel media with a size range of ⅛ - ¼ inches was obtained from the Roberts Filter Group (Darby, PA). Torpedo sand media with a size range of 2.0 – 2.5 mm was obtained from R.W. Sidley, Inc. (Painesville, OH). The procedure for depositing a manganese oxide coating on the gravel and torpedo sand is presented later in this chapter.

EXPERIMENTAL MATRIX

Column influent water characteristics were defined to ensure that water experimentally applied to the media bed could be reasonably compared to post-filtration water in typical surface water treatment utilities. Four operational parameters were measured and controlled in each experimental situation: hydraulic loading rate, soluble Mn concentration, free chlorine concentration (as Cl_2), and pH. Table 3.2 is a summary of the operational parameters and the associated experimental values.

Large-size media was evaluated in this research not only to determine soluble Mn removal effectiveness but also because it is expected that greater hydraulic flow rates can be applied to a large grain media bed with less head loss than in a typical filtration media bed (e.g. sand or anthracite). The ability to apply greater flow rates with smaller head loss would improve the marketability of this absorptive contactor to water treatment utilities because small footprints would be preferred with minimal hydraulic disruption to the plant. The hydraulic loading rates used experimentally in this research were 16 and 20 gpm/ft^2, which are larger than the typical filtration flow of 1.0-5.0 gpm/ft^2.

Soluble Mn concentration was commonly varied between 0.05-0.10 mg/L in the influent water. This concentration range was considered a typical range of soluble Mn concentrations found in water treatment utilities with manganese concerns in the United States. A high concentration "stress" of 0.25 mg/L Mn was applied to the pyrolucite to consider situations in which system or seasonal changes may periodically increase the loading on the contactor.

The desired optimal range of free chlorine concentrations was 1.0-2.0 mg/L, which was chosen after reviewing previous research. Narrow ranges of concentrations during experimental

Table 3.3
Volumetric additions to initial batch coating solution

At Time (minutes)	Oxidant Solution (mL)	Bicarbonate Solution (mL)
0	50	250
20	50	150
40	100	100
50	50	~
60	250	~

hydraulic loading of the column were preferred for modeling purposes. If insignificant amounts of free chlorine were present, the number of available adsorptions sites would have decreased and the soluble Mn removal profile would have shifted during the time of operation. The large range of measured concentrations listed in Table 3.2 does not reflect the conditions experienced in every experiment but shows the variance in concentrations measured during different experiments.

Two pH values commonly found in water treatment situations were considered for the effect of pH on soluble Mn removal. Slightly alkaline pH values positively affect the adsorption of soluble Mn onto oxides and pH values of close to 7.5 are often found in finished water. Slightly acidic pH values negatively affect soluble Mn adsorption but are preferred for better coagulation effectiveness (Morgan and Stumm 1964; Knocke *et al.* 1988). Therefore, a pH value of 6.5 was evaluated as a lower process boundary.

DEVELOPMENT OF OXIDE-COATING ON GRAVEL & TORPEDO SAND

A two-step method developed by Merkle *et al*. (1997) for fixing a $MnO_x(s)$ coating on filter media was used to prepare gravel and torpedo sand for use in the column experiments. The first step used a batch procedure to initialize the coating. For each batch coating, 500g of the media was rinsed with tap water and placed in a continuously mixed (60-100 rpm) Pyrex vessel with 9 L of tap water, 13.25 g $MnCl_2 \bullet 4H_20$, and approximately 36 mg $SnCl_2 \bullet 2H_20$. Two separate solutions were prepared and added to the Pyrex vessel in the pattern shown in Table 3.3. The oxidant solution was prepared by adding 10 mL of 6% bleach (NaOCl) to 500 mL of tap water. The bicarbonate solution was prepared by adding 3.36 g $NaHCO_3$ to 500 mL of tap water. After both solutions were completely added to the vessel at 60 minutes, the resulting solution was allowed to mix for an additional 60 minutes. Then the reactor was drained and the media rinsed with tap water and allowed to air dry. This first step produced an extractable coating of approximately 0.2 mg/g media on both the gravel and sand.

Two different methods were used for the second step of the coating process. A short bed depth (6") with flow recycle was used for the gravel, while a large bed depth (20") without recycle was used for the sand. Initially, a six-inch bed was chosen to provide a more uniformly coated supply of media to be used in the column experiments. Manganese deposition was expected to be greater in the upper portion of the media bed; thus, the use of short beds was considered to reduce the effect of a deposition gradient across the bed. However, the repetition required to produce a full twenty-inch bed depth of media was cumbersome and the recycle

Table 3.4
Properties of solution used to determine 4-hr soluble Mn adsorption capacity

Parameter	Property
Water	5L of Lab Deionized
pH	Adjusted by NaOH & H_2SO_4 addition
Alkalinity	25 mg/L as $CaCO_3$
Calcium	10 mg/L
Mn^{2+}	0.5 mg/L

process increased the extractable coating to only 0.3 mg/g media. A twenty-inch bed without recycle using a similar setup to the contactor experiment was later used due to ease of operation.

The short bed (6") second step used a recycle process to build up the coating on the media. Six inches of media from the batch step was placed in a short column of PVC pipe (3" ID). The media was supported in the middle of the column with a wire mesh. Holes were drilled near the top and bottom of the column to provide influent and effluent flow. Initially, a solution of tap water with 400 mg/L free chlorine flowed through the media until the influent and effluent chlorine concentrations were equal. The media was rinsed, removed from the column, and allowed to air dry.

The dry media was returned to the short column with 2.5 L of a tap water solution containing 10^{-3} M HCO_3^- and 1.9 mg/L Mn. An oxidant solution was created by adding 230 mL 6% bleach to 1 L deionized water. Initial, 50 mL of the oxidant solution was added above the media. A Master-Flex peristaltic pump was used to continuously draw the solution through the media in an up-flow mode at a constant rate of 250 mL/min for two hours. Additional oxidant solution was added every 15 minutes during the first hour. The pH was adjusted to 7.0 between additions of the oxidant solution. At the end of the two hours, the solution was drained from the column and replaced with tap water plus the remaining 250 mL of oxidant solution. This rinse solution was recirculated for 15 minutes. The media was removed from the column and allowed to air dry.

The alternative large bed second step used the full contactor column experimental setup. A full bed depth (20") of media was supported by a short gravel bed. Water was applied to the bed with 1.0 mg/L Mn^{2+} and >2.0 mg/L of free chlorine. This water was allowed to flow through the column (16 gpm/ft^2) for 7 hours per application. Water with only free chlorine was applied to the column for a short time (30 min) between applications to regenerate any available sites. Media was removed from the column and mixed before being placed into an experimental contactor column to provide a more homogenous extractable coating amount throughout the experimental bed depth.

SOLUBLE MANGANESE ADSORPTION CAPACITY DETERMINATION

Short-term soluble Mn adsorption capacity of the media was determined by a four-hour recycle method developed by Bouchard (2005). A bed depth of 2.5 cm of media with a known weight was supported by glass wool in a 1.5 cm diameter glass tube as shown in Figure 3.3. A dilute bleach solution (2 mL of 6% bleach in 5 L tap water) was pumped by a Master-Flex

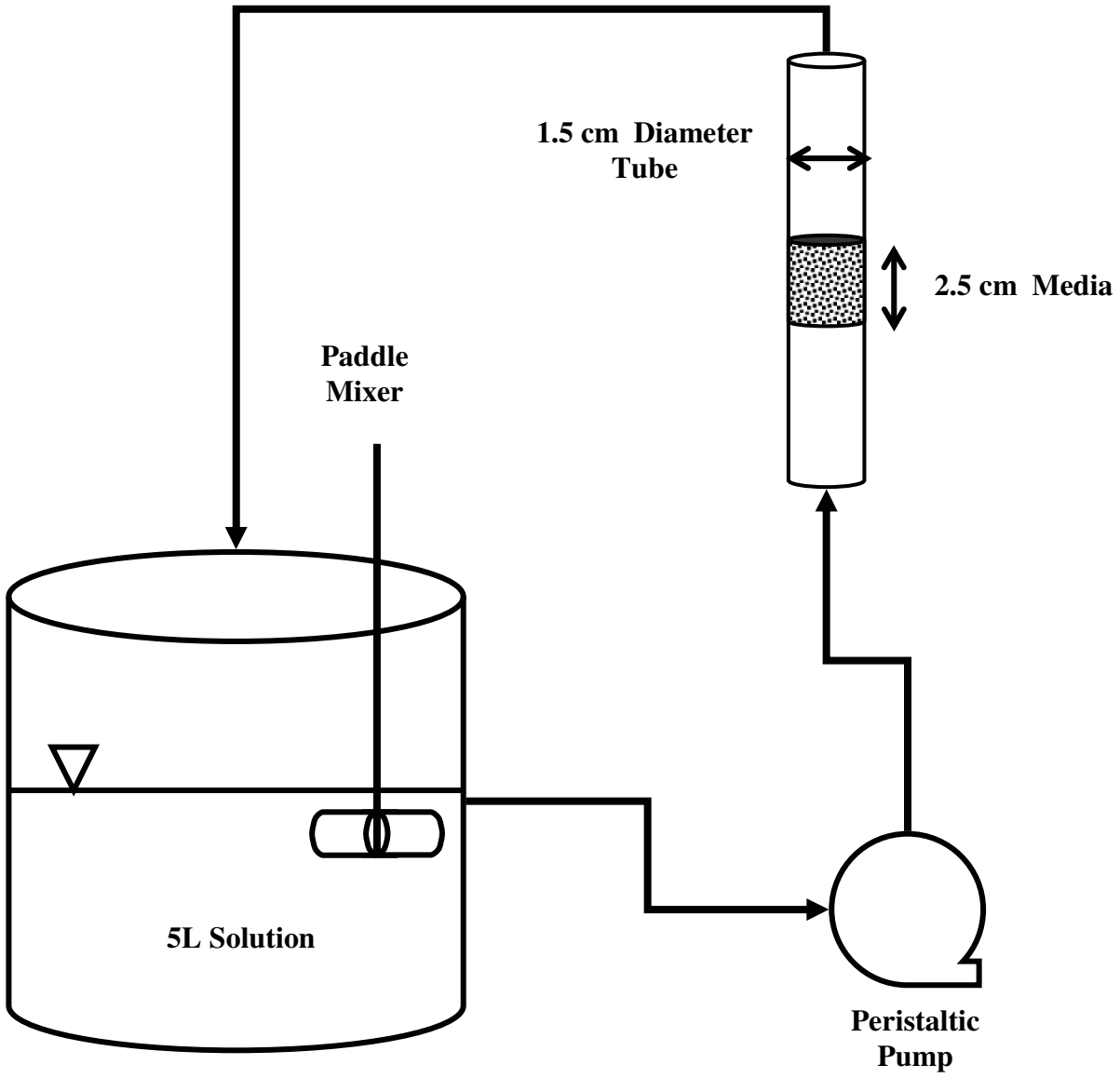

Figure 3.3 Flow diagram of 4-hr recycle to determine short-term soluble Mn adsorption capacity

peristaltic pump from a continuously mixed (100 rpm) reservoir through tubing at a rate of between 10-11 gpm/ft^2. The solution circulated through the media for four hours, after which the media was rinsed, removed, and allowed to air dry. This regeneration step was to ensure that all available sorption sites were oxidized before the short-term capacity was measured, providing a more accurate measurement.

The media was returned to the glass tube once dry. A prepared solution containing the properties listed in Table 3.4 was placed in the continuously mixed reservoir and pumped through the media at a rate of between 10-11 gpm/ft^2. An initial and final sample of the solution reservoir were collected and filtered for soluble Mn concentration analysis using the ICP. Only the initial and final measurements were used in the capacity calculation. Additional samples were taken at 60, 120, 180, and 240 minutes to be filtered and analyzed by the HACH method for soluble Mn analysis. Since sorption capacity is related to bulk Mn concentration, the additional samples were taken to monitor the soluble Mn concentration in the reservoir. If more than 10% of the initial concentration was adsorbed during the four-hour period, soluble Mn was added as necessary to keep the concentration within the desired range.

Short-term soluble Mn adsorption capacity was calculated from the difference of initial and final soluble Mn concentrations using Equation 3.1.

$$\text{Capacity} = [(C_i - C_f) * V_{solution}] / M_{media} \quad (3.1)$$

where:
C_i = initial concentration of Mn^{2+} in the reservoir (mg/L)
C_f = final concentration of Mn^{2+} in the reservoir (mg/L)
$V_{solution}$ = volume of solution in reservoir (L)
M_{media} = mass of media in glass tube (g)

PILOT-SCALE EXPERIMENTAL SETUP

Pilot-scale experiments were conducted at the Blacksburg-Christiansburg-VPI Water Authority water treatment facility. The experimental setup at the utility was similar to the laboratory experimental setup as described earlier in this chapter. The feed water delivery system including the same size pumps, tubing, and tanks was re-assembled on-site. Post filtration water from Filter #6 was the water source for the pilot-scale experiments. Source water was piped into a single plastic 55-gallon drum along with a solution of dilute bleach. The water was pumped up to a head tank and flowed via gravity through tubing to the contactor columns. The soluble Mn solution was pumped into the tubing between the head tank and the contact column. Only one contactor column was online in the system at a time. Water flow exited the base of the column and flowed to a nearby floor drain.

The purpose of the pilot-scale experiments was to determine the effectiveness of the contactor columns for removing soluble Mn under conditions typically found at a water treatment facility. The solution pH was not altered to provide such conditions. The free chlorine concentration of the water was increased by approximately 1.5 mg/L to simulate the continuous regeneration mode of operation proposed for the soluble Mn removal contactor units. Initial Mn concentrations were varied from 0.02-0.09 mg/L and hydraulic loading rates were varied from

16-24 gpm/ft^2 to observe the soluble Mn removal performance of the contactor columns under different loading situations.

METHOD FOR EXTRACTION OF MANGANESE OXIDE COATING

A method published by Knocke *et al*. (1990) was used to determine the extractable amount of manganese oxide coating on the media. Media samples were air dried and placed into a 250 mL Erlenmeyer flask with 100 mL of 0.5% Nitric Acid and approximately 300 mg of hydroxylamine sulfate (HAS). The flask was periodically agitated and the solution was allowed to react for two hours. After two hours, the solution was agitated and a sample of the solution was removed and filtered. The soluble Mn concentration was analyzed using the atomic absorption spectrophotometer or the ICP. The extractable manganese (mg/g media) was calculated using Equation 3.2.

$$EMC = [C * V] / W \tag{3.2}$$

where: EMC = extractable manganese (mg/g media)
C = measured soluble Mn concentration (mg/L)
V = volume of nitric acid (L)
W = mass of media placed in the flask (g)

ANALYTICAL METHODS

Samples collected for soluble Mn concentration determination were filtered through 0.45 μm filters and acidified with the addition of concentrated nitric acid for sample preservation.

The Hach Low Range Method (0.006 – 0.700 mg/L) for soluble Mn analysis (Method 8149, 1-(2-Pyridylazo)-2-Naphthol PAN Method) was used to obtain immediate results. Reagents were obtained from the Hach Company and a Hach DR/2400 was used for analysis. The machine was zeroed with a blank cell, which was prepared with 10 mL of deionized water and reagents. The samples were prepared by placing 10 mL of filtered sample in a sample cell. An ascorbic acid pillow was added to each cell. Fifteen drops of alkaline-cyanide solution were added, followed by 21 drops of PAN indicator. The cell was inverted multiple times after the addition of each reagent. The sample cell was allowed to rest for two minutes before analysis.

An inductively coupled plasma mass spectrometer (ICP-MS) was also used for soluble Mn analysis. The calibration curve was created using five standard solutions (1, 10, 50,100, 1000 ppb). A quality assurance check of a blank (zero manganese) and a 50 ppb standard solution was evaluated after every nine unknown samples.

Free chlorine was measured using the Hach Method 8021 (DPD Method) with a detection range of 0.02 – 2.00 mg/L Cl_2. Reagents were obtained from the Hach Company and a Hach DR/2400 was used for the analysis. The machine was zeroed with a blank cell, which was prepared by placing 10 mL of sample to the sample cell. Samples were prepared by placing 10 mL and a DPD Free Chlorine Powder Pillow in a sample cell. The cell was inverted to mix the reagent and allowed to rest for 30 seconds before analysis.

Temperature was measured with a Fisher Scientific Ever-Safe™ Thermometer with a range of -20°C – 110°C. The solution pH was measured with a portable Fisher Scientific Accumet Model AP62 meter with an Accumet Liquid Electrode. The meter was calibrated with pH 7 buffer solution.

All plastic sample containers and glassware were cleaned before use in the following manner. Items used for soluble Mn analysis (sample containers and filter syringes) were double rinsed with tap water and placed in a 10% nitric acid bath for at least 14 hours. After the acid bath, containers and syringes were double rinsed with tap water and allowed to dry. All other glassware was rinsed before and after each use and acid washed when necessary.

Data collected from the ICP-MS output were stored in Microsoft Excel. Data collected in the laboratory were stored in a carbon copy notebook as well as in Microsoft Excel. Microsoft Excel was also used for data organization and comparison. SigmaPlot 8.0 was used for plotting graphical representations of data. Model code was developed and executed in MatLab 7.1. All files were backed up periodically.

CHAPTER 4
EXPERIMENTAL RESULTS

The purpose of this chapter is to describe the characteristic experimental results collected during contactor column experiments, pilot-scale experiments, and uptake capacity experiments. This chapter is arranged in five sections. The first through third sections describe the results of the laboratory-scale contactor column experiments for pyrolucite, gravel, and torpedo sand media, respectively. Each of these sections includes representative plots showing data from individual experiments as well as comparison plots showing the effect of influent free chlorine (HOCl) concentration, pH, initial manganese (Mn) concentration, and hydraulic loading rate on soluble Mn removal performance. The fourth section describes the results of the pilot-scale contactor column experiments that were conducted at the Blacksburg-Christiansburg-VPI Water Authority treatment facility. Post-filtration water at the local water treatment utility was applied to each media. The soluble Mn adsorption profiles in this section reflect a range of initial soluble Mn concentrations and a range of applied hydraulic loading rates that could be expected at the local utility. The fifth section describes the results of the soluble manganese absorption capacity determination experiments. Uptake capacities were determined both before and after the media was used in the contactor columns. Due to the volume of data collected, representative plots were included in this chapter and supplementary plots were included in the Appendix. All soluble Mn concentration measurements analyzed by the ICP-MS were determined to be above the instrument's detection limit of 0.02 ppb.

COLUMN EXPERIMENTS INVOLVING THE USE OF PYROLUCITE MEDIA

The matrix of water influent parameters applied in the laboratory-scale contactor column experiments containing pyrolucite can be found in Table 3.2. Soluble Mn concentration profiles were collected at six depths in the media bed as described in Chapter 3. The frequency of profile collection was in either thirty-minute or one-hour time steps over each four-hour experiment. Various combinations of operational parameters were applied in separate experiments to the contactor column to provide data for comparisons of parameter effects.

Prior to data collection, the pyrolucite was exposed to the applied water for an hour without Mn addition to achieve regeneration by free chlorine oxidation. During an additional fifteen minutes after regeneration, the soluble Mn feed was activated and the pyrolucite contactor was acclimated to the operational conditions. Fifteen minutes was determined to provide enough time for acclimation due to the flow rate and position of the soluble Mn feed. After this acclimation period, the first soluble Mn profile was collected and labeled as time zero (0 mins). Each subsequent profile was identified with the amount of time in minutes that elapsed past time zero when samples for that profile were collected.

Figures 4.1 and 4.2 present data from individual experiments. Each plot shows soluble Mn concentration versus depth of pyrolucite media as a function of time. The soluble Mn adsorption profiles in these figures are considered stable as there is no significant movement of the Mn concentration profile with time. In later data analysis, these stable profiles were routinely averaged and displayed as a single profile for ease of comparison. Often suitable individual profiles were used for comparison.

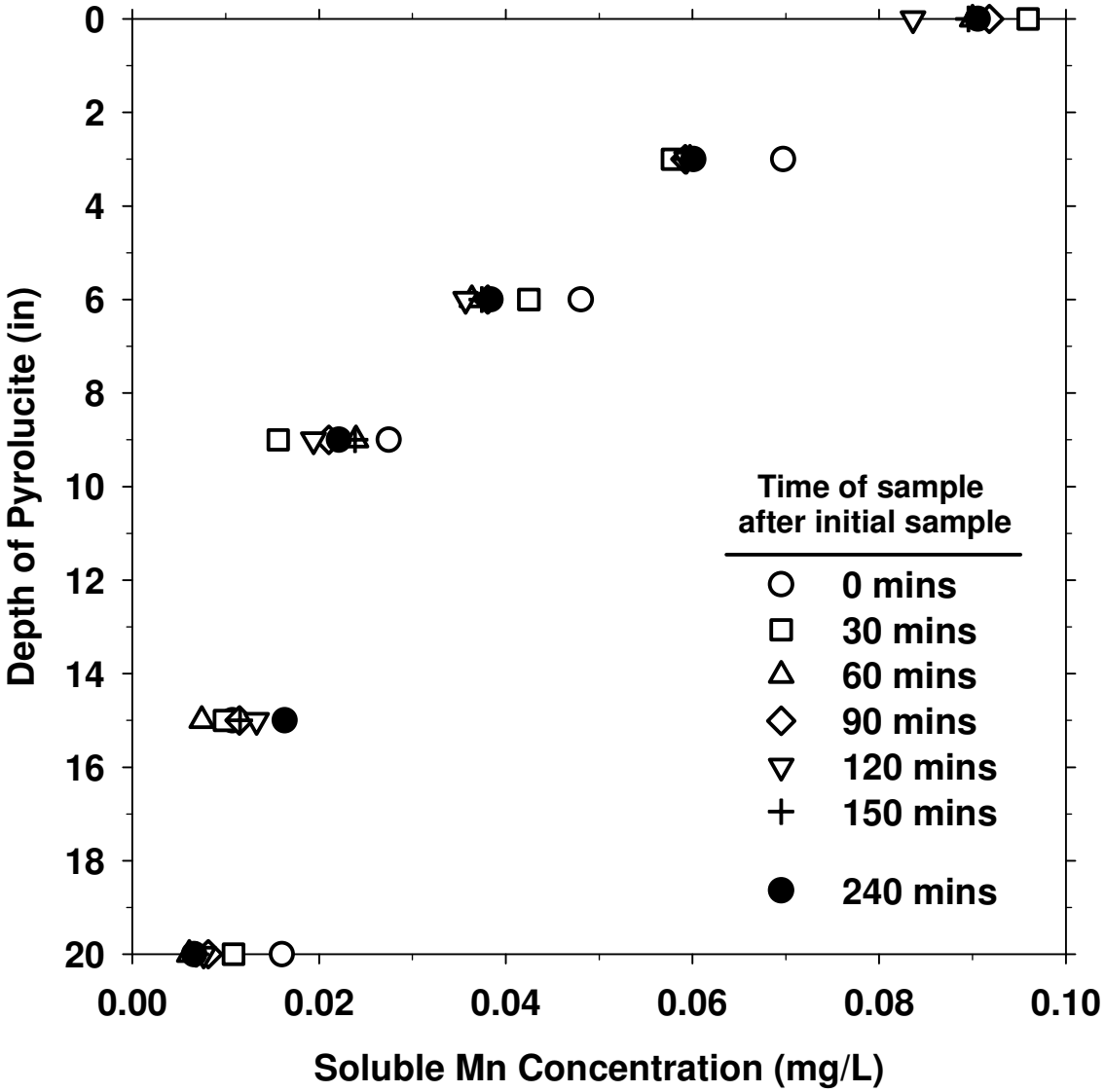

Figure 4.1 Soluble Mn removal profiles over depth of pyrolucite as a function of time (Influent water: HLR=16 gpm/ft^2, HOCl=1.3-1.9 mg/L, pH=7.6)

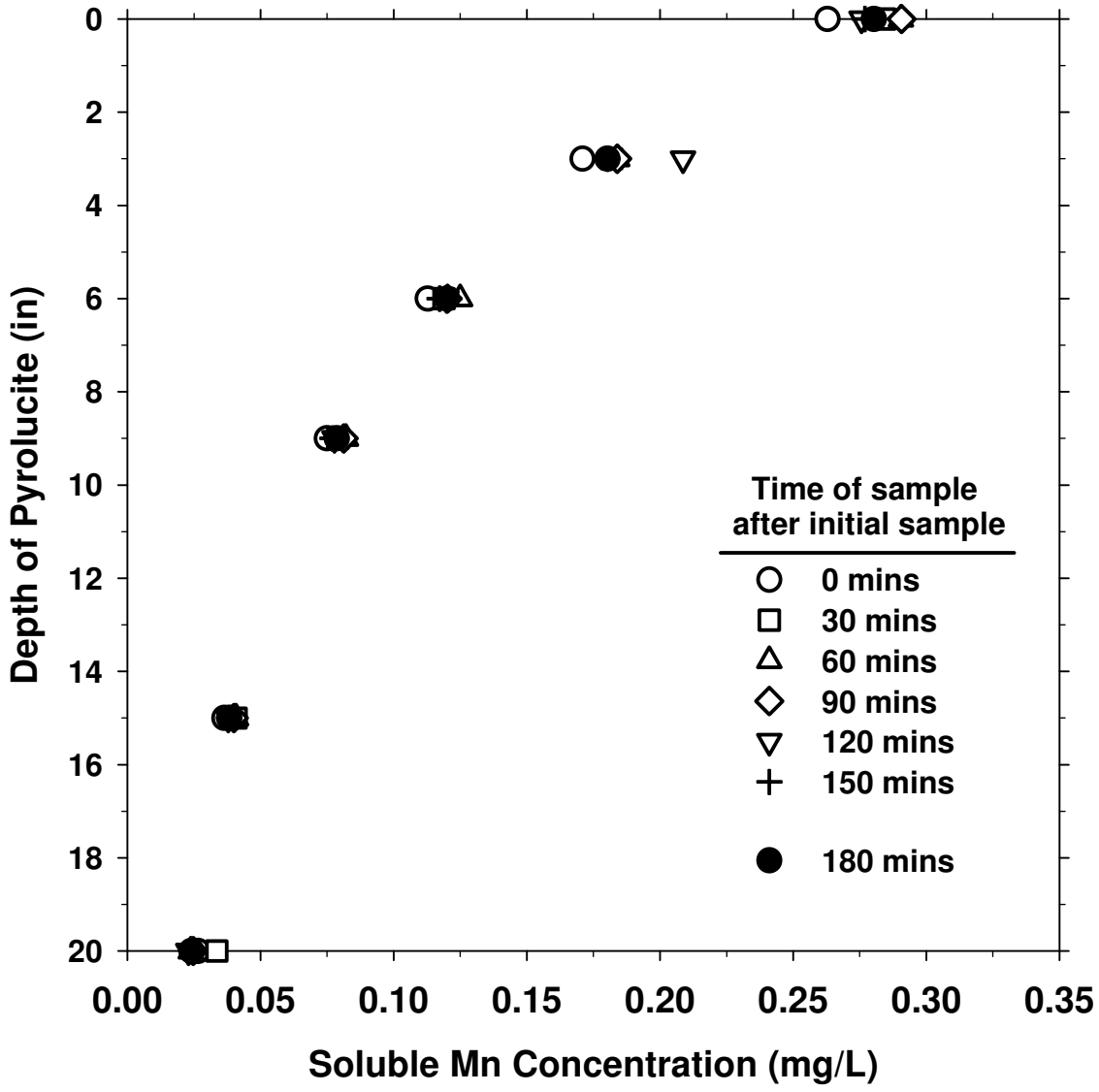

Figure 4.2 Soluble Mn removal profiles over depth of pyrolucite as a function of time with minimal oxidant addition (Influent water: HLR=16 gpm/ft^2, HOCl=0.6-0.9 mg/L, pH=7.9)

The contactor column containing pyrolucite provided effective Mn removal. The removal profiles observed in the pyrolucite contactor columns typically showed a rapid initial absorption as the water moved through the media. Under most conditions, the influent soluble Mn concentration decreased by approximately 50% in the upper third of the media depth. The remaining two thirds of the media depth contributed additional manganese adsorption, although at a lower amount per unit depth. Data plotted in Figures 4.1 and 4.2 show a total of 90% of the influent soluble Mn concentration adsorbed across the column depth. The applied water condition for data plotted in Figure 4.1 was a hydraulic loading rate (HLR) of 16 gpm/ft^2, a pH of 7.6, an initial soluble Mn concentration of 0.1 mg/L, and a free chlorine concentration of 1.3-1.9 mg/L. The applied water condition for data plotted in Figure 4.2 was similar to Figure 4.1 with a HLR of 16 gpm/ft^2 and a pH of 7.9. However, this experiment was meant to stress the contactor with a minimal free chlorine concentration of 0.6-0.9 mg/L and an increased initial Mn concentration of 0.3 mg/L. The pyrolucite contactor was still able to successfully adsorb 90% of the initial Mn concentration under these influent conditions.

Adequate oxidant concentration is required to oxidize the adsorbed soluble Mn on the surface of the media. Although the rate of oxidation is considered rapid, the concentration of available oxidant can have an effect on the shape of the adsorption profile. Profiles from laboratory-scale experiments were compared to determine the effect of free chlorine concentration on soluble Mn adsorption in the pyrolucite contactor at both 16 gpm/ft^2 and 20 gpm/ft^2 as well as for different pH conditions.

Figures 4.3 and 4.4 display soluble Mn adsorption profiles over a similar range of free chlorine concentrations. Figure 4.3 compares profiles collected at 16 gpm/ft^2 and pH 7.5-7.7. Data presented in this figure indicate that the free chlorine concentration does not create a discernable difference in soluble Mn adsorption profile over the range of free chlorine concentrations investigated. Figure 4.4 compares profiles at the same hydraulic loading rate but at a more acidic pH. Data plotted in Figure 4.4 show an improved soluble Mn adsorption profile at a higher free chlorine concentration of 1.8 mg/L.

Bulk solution pH has been shown to have an effect on the adsorption capacity of media which directly affects the shape of the adsorption profile (Morgan and Stumm 1964). Profiles from laboratory-scale experiments were compared to determine the effect of pH on soluble Mn removal in the pyrolucite contactor at both 16 gpm/ft^2 and 20 gpm/ft^2. Representative data presented in Figure 4.5 compare profiles under the conditions of 20 gpm/ft^2 and free chlorine concentration of 1.3 mg/L. The more alkaline pH (pH 7.1 instead of pH 6.6) provided an improved soluble Mn removal profile with the pyrolucite media.

The concentration of Mn in solution affects the adsorption capacity of media which directly affects the shape of the adsorption profile. Profiles from laboratory-scale experiments were compared to determine the effect of initial soluble Mn concentration on the soluble Mn removal performance of the pyrolucite contactor at both 16 gpm/ft^2 and 20 gpm/ft^2.

Data plotted in Figures 4.6 and 4.7 show a minimal improvement of soluble Mn removal with an increase of initial soluble Mn concentration. The influent water was applied at a HLR of 16 gpm/ft^2 with a pH of 7.5-7.6. Data plotted in Figure 4.6 were collected with a free chlorine concentration of 1.3 mg/L, whereas data plotted in Figure 4.7 were collected with an increased free chlorine concentration of 1.9-2.1 mg/L.

Increased loading rates (>15 gpm/ft^2) will allow for the design of small contactor footprints and, hence, reduced unit costs for soluble Mn control. Profiles from laboratory-scale

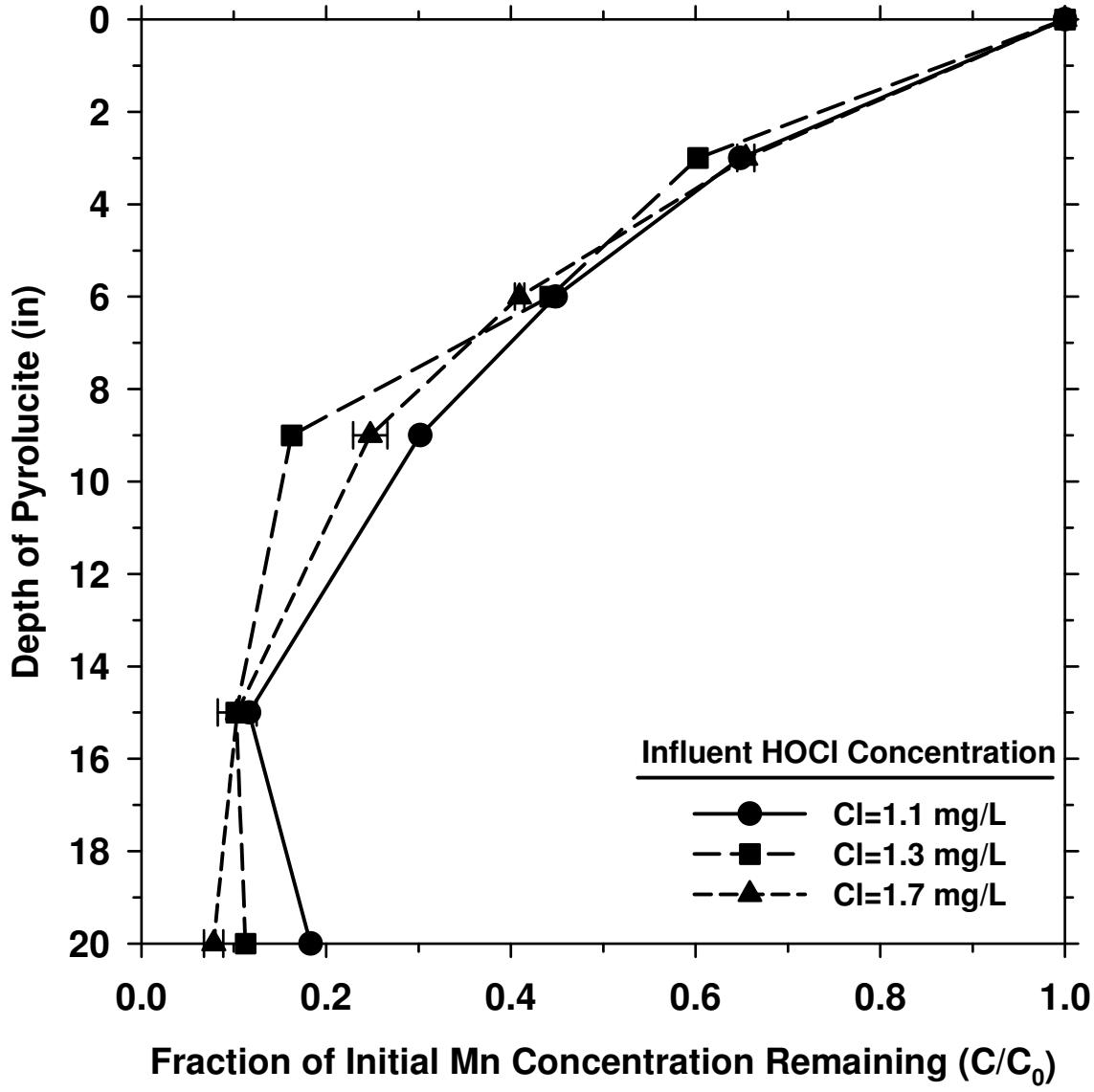

Figure 4.3 Effect of free chlorine concentration on soluble Mn removal profile over depth of pyrolucite (Influent water: HLR=16 gpm/ft^2, pH=7.5-7.7, Mn^{2+}=0.09-0.11mg/L)

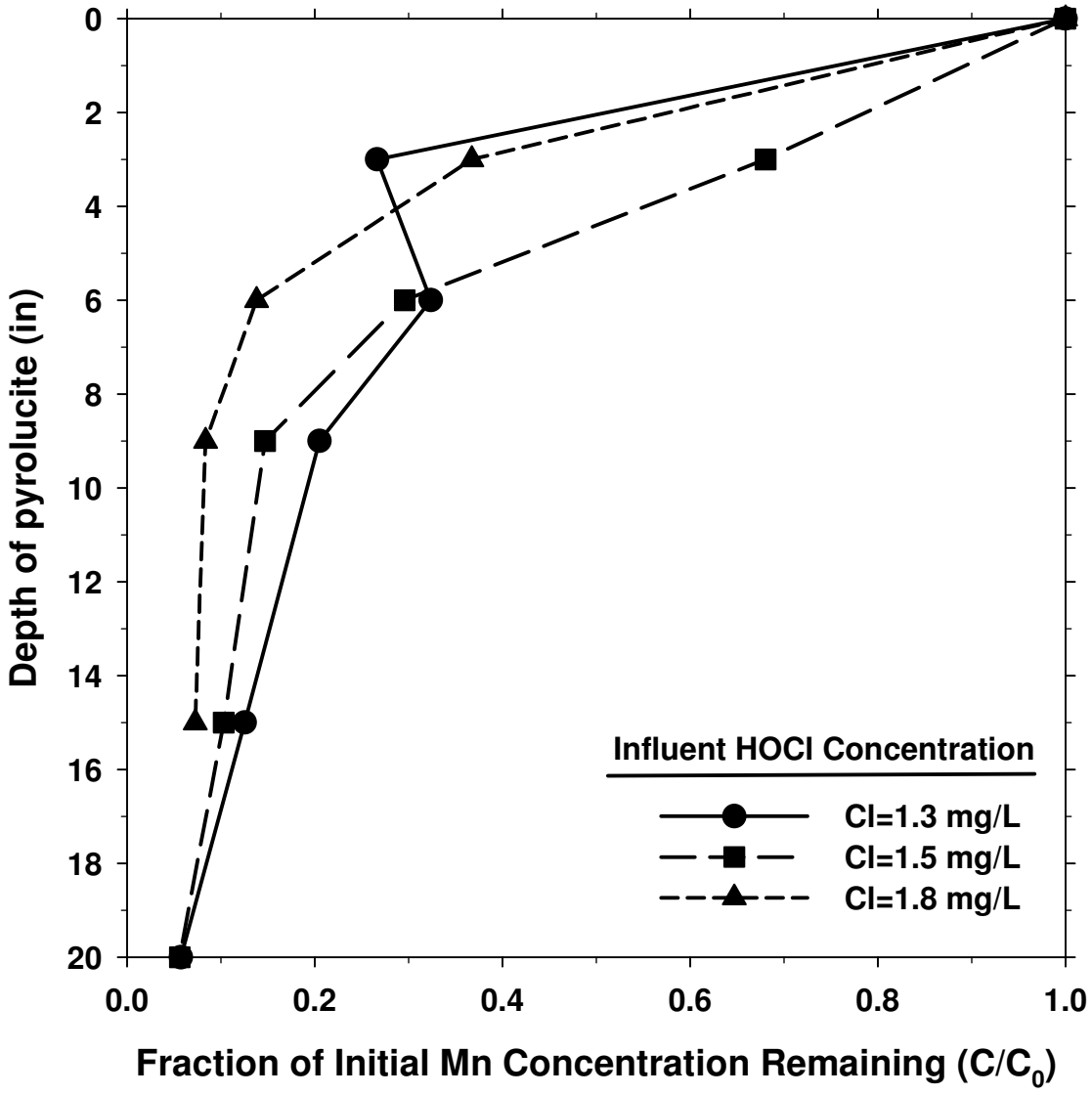

Figure 4.4 Effect of free chlorine concentration on soluble Mn removal profile over depth of pyrolucite (Influent water: HLR=16 gpm/ft^2, pH=6.5-6.6, Mn^{2+}=0.05-0.06mg/L)

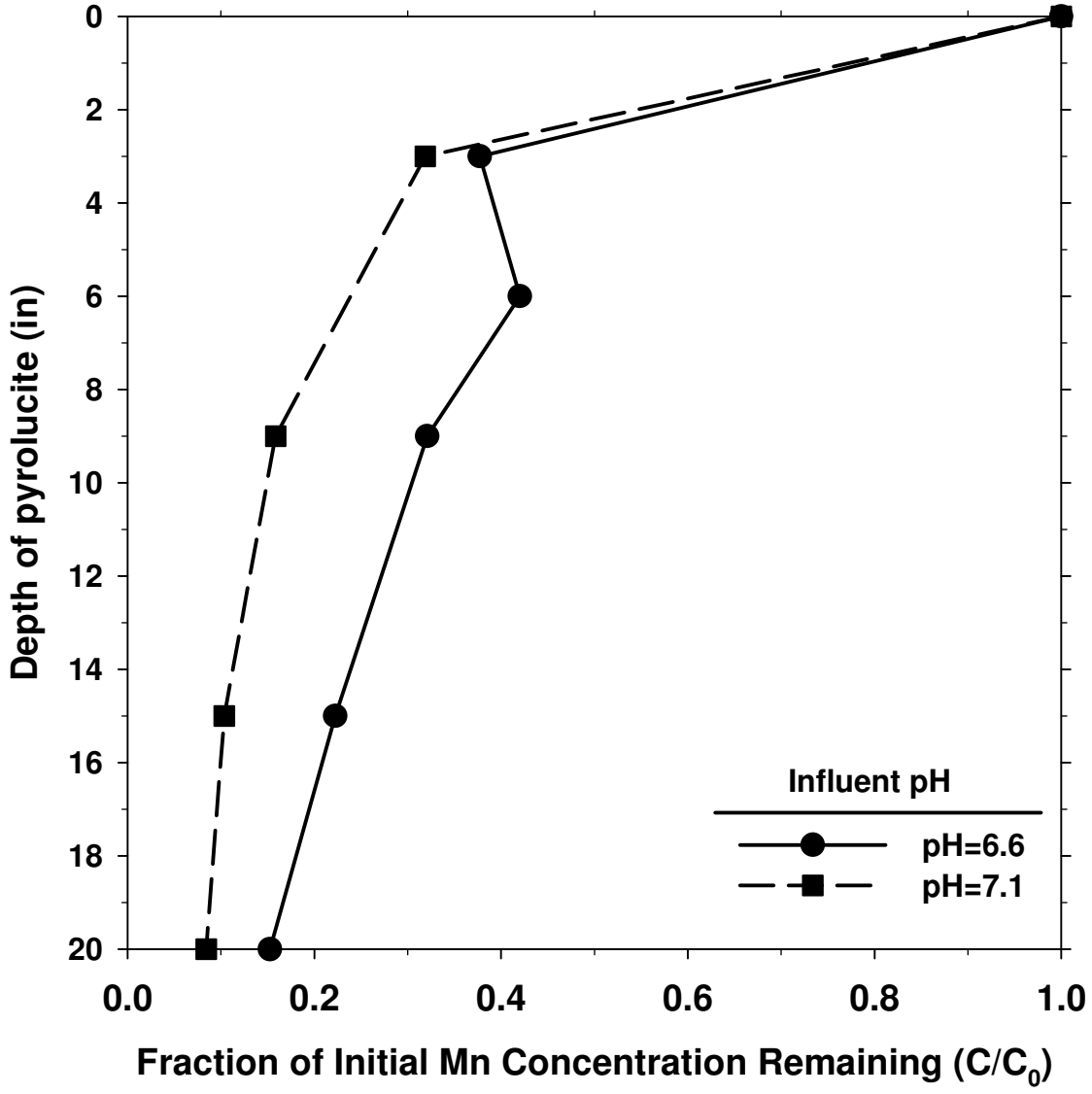

Figure 4.5 Effect of pH on soluble Mn removal profile over depth of pyrolucite (Influent water: HLR=20 gpm/ft^2, HOCl=1.3 mg/L, Mn^{2+}=0.09 mg/L)

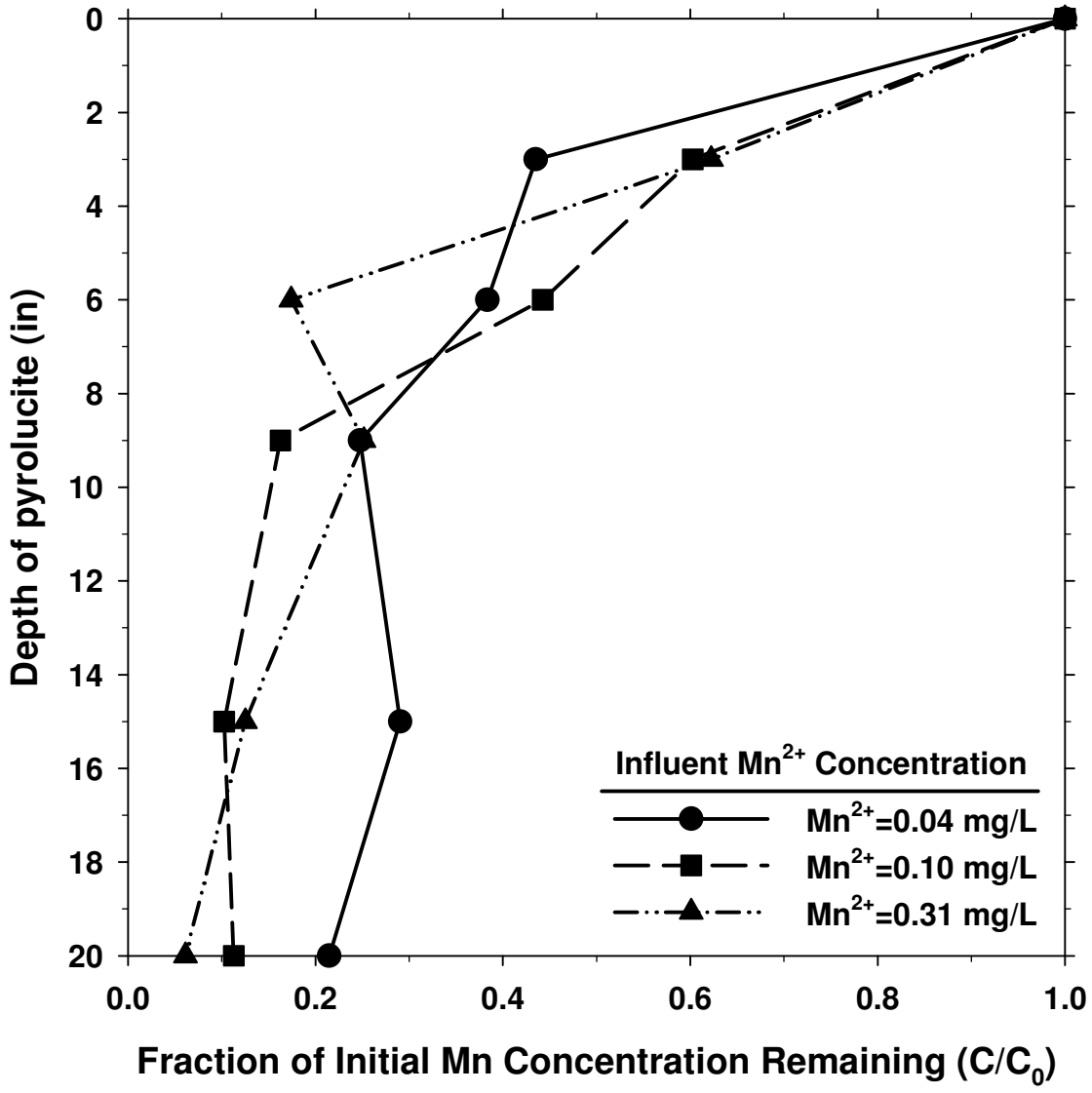

Figure 4.6 Effect of influent soluble Mn concentration on soluble Mn profile over depth of pyrolucite (Influent water: HLR=16 gpm/ft^2, HOCl=1.3 mg/L, pH=7.5)

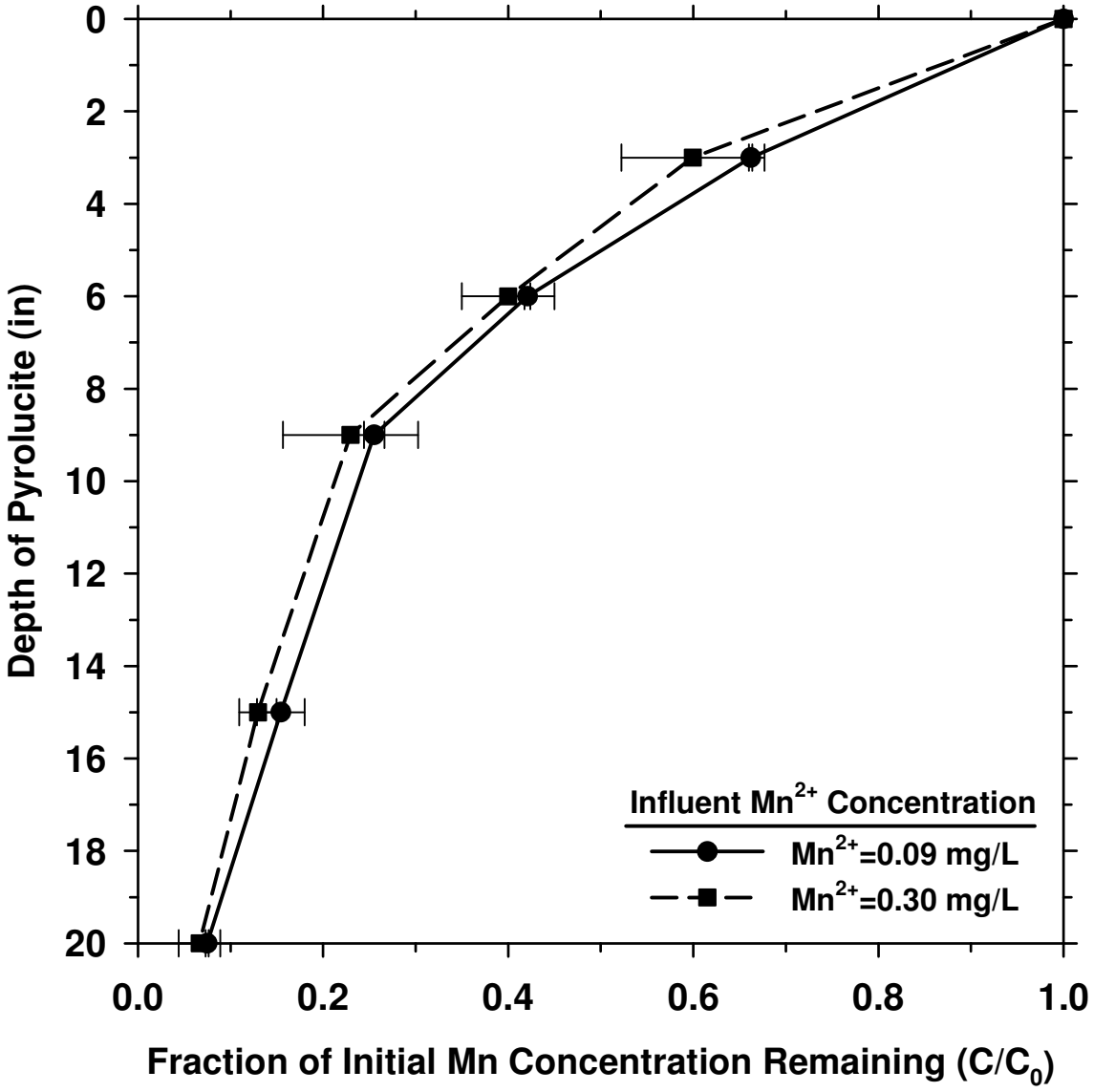

Figure 4.7 Effect of influent soluble Mn concentration on soluble Mn removal profile over depth of pyrolucite (Influent water: HLR=16 gpm/ft^2, HOCl=1.9-2.1 mg/L, pH=7.5-7.6)

experiments were compared to determine the effect of hydraulic loading rate on soluble Mn removal by the pyrolucite media.

Data plotted in Figure 4.8 compare two hydraulic loading rates under slightly acidic pH conditions. The hydraulic loading rate of 16 gpm/ft^2 provides a better adsorption profile with a total soluble Mn removal percentage increase from 82% to 90% of the initial soluble Mn concentration removed.

Overall, contactor columns containing pyrolucite media provided good soluble Mn removal with 80-90% of the initial soluble Mn concentration being adsorbed across the contactor bed. Applied water conditions with a slightly alkaline pH (7.0-8.0) and a free chlorine concentration of 1.0-2.0 mg/L should provide satisfactory conditions for continued and adequate absorption of soluble Mn in a contactor containing pyrolucite.

COLUMN EXPERIMENTS INVOLVING THE USE OF GRAVEL MEDIA

Laboratory-scale contactor column experiments containing gravel coated with MnO_x were conducted using the same methods as described previously in the opening paragraphs of the pyrolucite section of this chapter. Water was applied to the contactor column under various conditions. After a period of acclimation, soluble Mn profiles were collected over a known period of time. These profiles were then compared to show parameter effects on soluble Mn removal over a depth of gravel.

Data plotted in Figure 4.9 present the soluble Mn removal profile collected during a single laboratory-scale experiment with a contactor column containing gravel. Soluble Mn concentration decreased over the depth of gravel with a total removal of 70% of the initial soluble Mn concentration. The influent water conditions were conducive to a sustained soluble Mn removal profile at a hydraulic loading rate of 16 gpm/ft^2, free chlorine concentration of 1.0-1.4 mg/L, and a slightly alkaline pH of 7.5. The soluble Mn adsorption profile was considered stable as there was no distinguishable movement of the soluble Mn concentration profile with time. In later data analysis, some profiles were averaged and displayed as a single profile for ease of comparison. Often suitable individual profiles were used for comparison.

Data plotted in Figure 4.10 show an unstable soluble Mn profile under conditions meant to stress the removal performance of the contactor column containing gravel. Water was applied at a HLR of 16 gpm/ft^2 with an acidic pH of 6.6 and insufficient oxidant (free chlorine concentration of 0.2-0.4 mg/L) for continued removal. Data plotted in Figure 4.10 show an increasingly poor removal from a total soluble Mn removal of approximately 55% to, after three hours of operation, a removal percentage of 25% of the initial soluble Mn concentration. Profile instability was most likely due to a lack of oxidant to provide regeneration of available absorption sites.

The application of free chlorine to the water flowing through the media provides the necessary oxidant for available adsorption site regeneration during contactor operation. Data from laboratory-scale experiments were compared to determine the effect of free chlorine concentration on soluble Mn removal performance in the gravel contactor at both 16 gpm/ft^2 and 20 gpm/ft^2. Data plotted in Figure 4.11 show profiles at a slightly alkaline pH of 7.4 and a hydraulic loading rate of 20 gpm/ft^2. These plots show an increase of free chlorine concentration from 0.7 mg/L to 3.1 mg/L improved the soluble Mn adsorption profile from 45% to 60% total removal of the initial soluble Mn concentration.

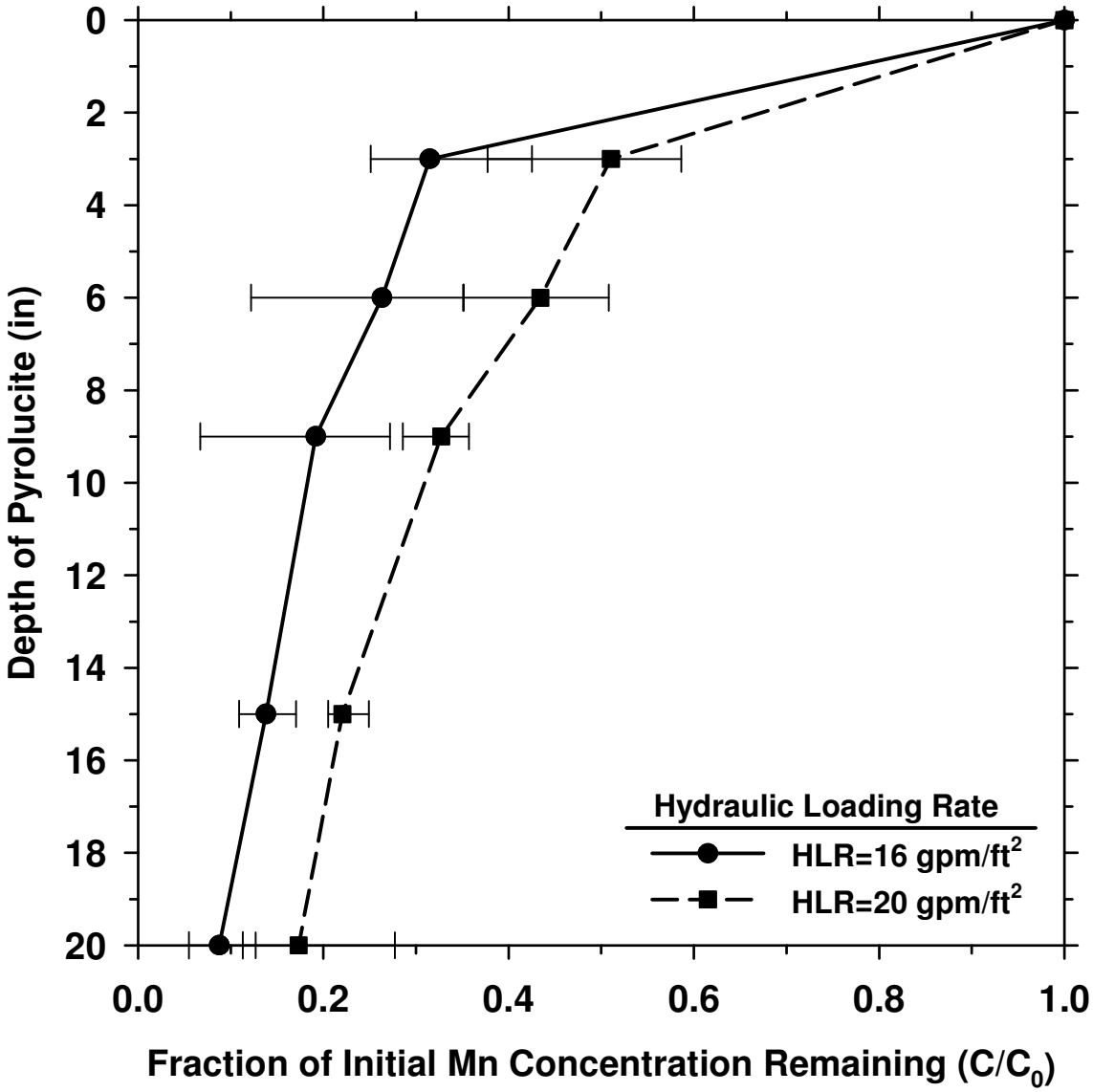

Figure 4.8 Effect of HLR on soluble Mn removal profile over depth of pyrolucite (Influent water: HOCl=1.2-1.4 mg/L, pH=6.5-6.7, Mn^{2+}=0.07-0.09 mg/L)

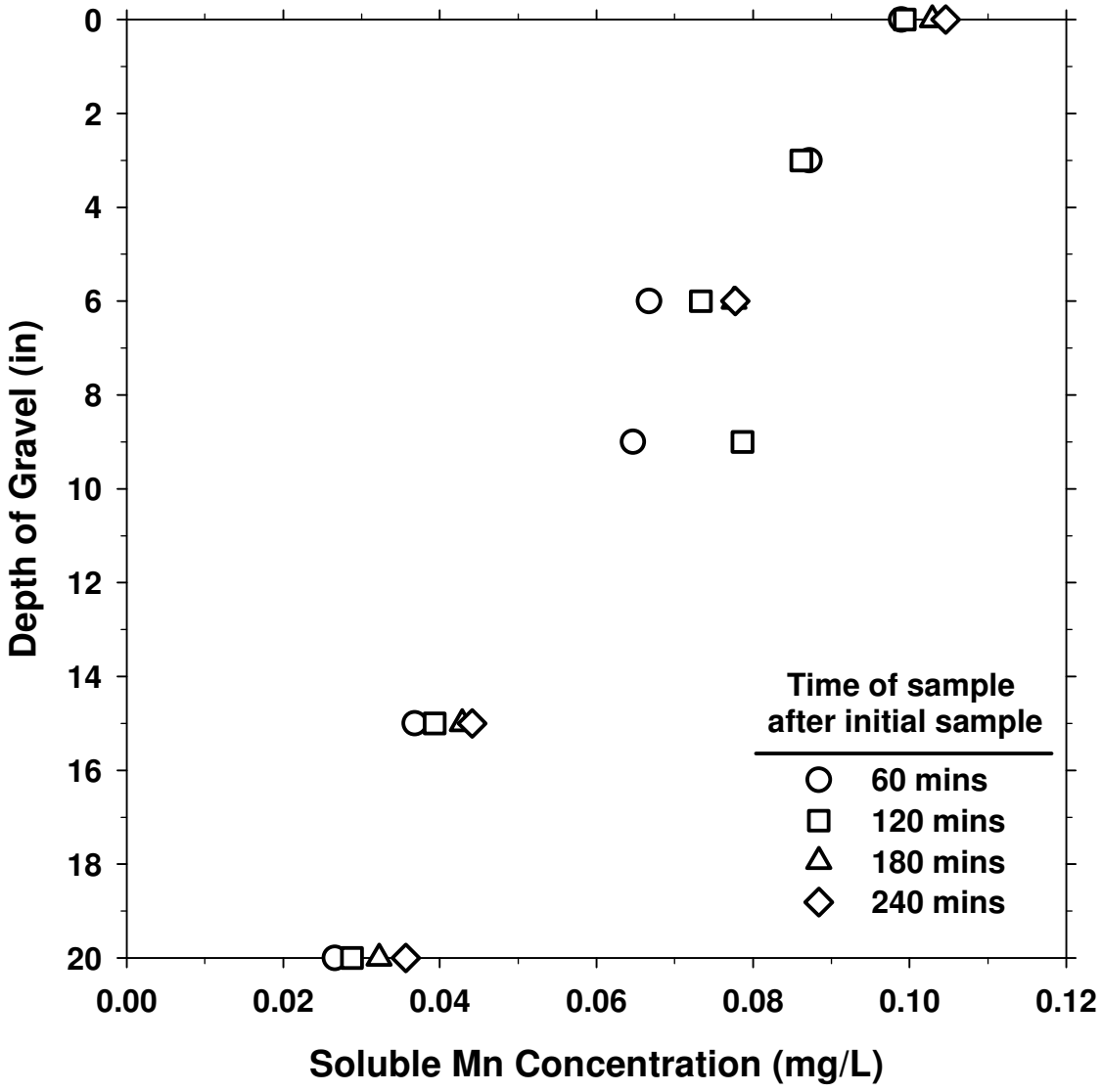

Figure 4.9 Soluble Mn removal profiles over depth of gravel as a function of time (Influent water: HLR=16 gpm/ft^2, HOCl=1.0-1.4 mg/L, pH=7.5)

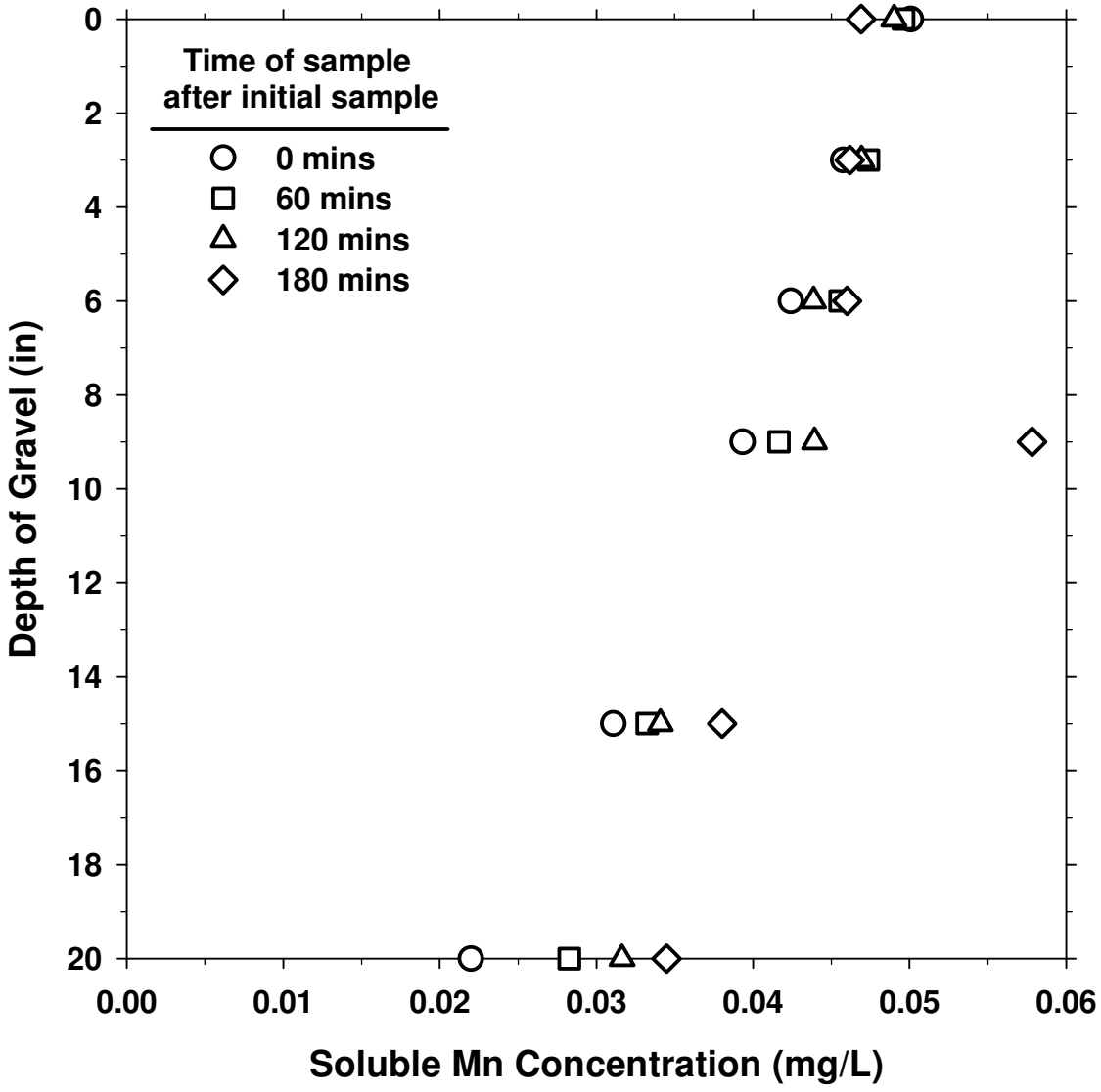

Figure 4.10 Soluble Mn removal profiles over depth of gravel as a function of time (Influent water: HLR=20 gpm/ft^2, HOCl=0.2-0.4 mg/L, pH=6.6)

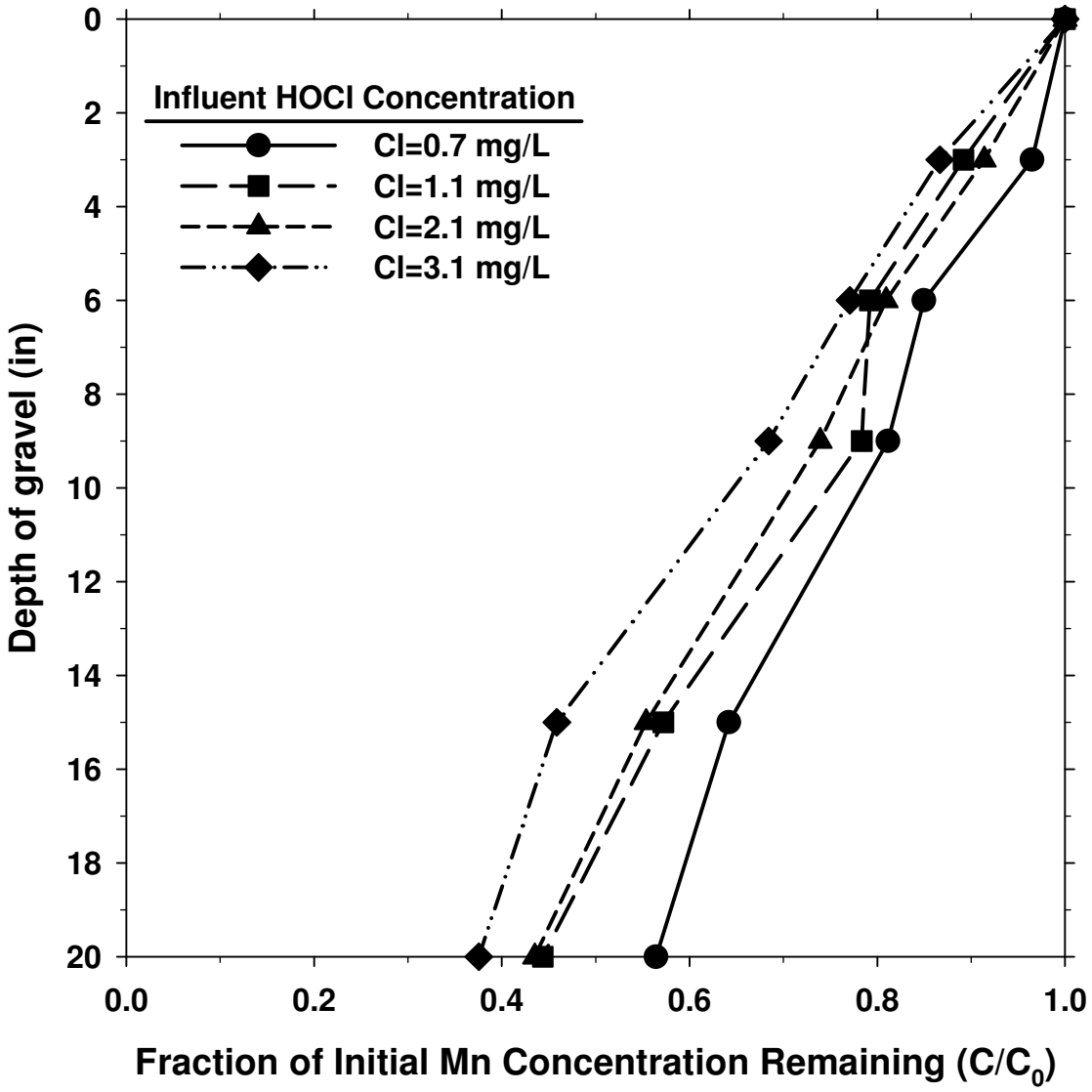

Figure 4.11 Effect of free chlorine concentration on soluble Mn removal profile over depth of gravel (Influent water: HLR=20 gpm/ft^2, pH=7.4, Mn^{2+}=0.09-0.10mg/L)

Bulk solution pH affects the adsorption capacity of media which directly affects the shape of the adsorption profile (Morgan and Stumm 1964). Profiles from laboratory-scale experiments were compared to determine the effect of pH on soluble Mn removal in the gravel contactor at both 16 gpm/ft^2 and 20 gpm/ft^2. Data plotted in Figure 4.12 show that a more alkaline pH of 7.7 (when compared to a slightly acidic pH of 6.6) provided an improved soluble Mn adsorption profile from 35% to 65% total removal of the initial soluble Mn concentration.

The concentration of manganese in solution can affect the adsorption capacity of media which directly affects the shape of the adsorption profile. Profiles from laboratory-scale experiments were compared to determine the effect of influent soluble Mn concentration on soluble Mn removal in the contactor column containing gravel.

Data plotted in Figure 4.13 present an indistinguishable difference in soluble Mn adsorption profiles at different initial soluble Mn concentrations. The soluble Mn profile with a total removal of 60% of the initial soluble Mn concentration of 0.05 mg/L remained stable after doubling the initial soluble Mn concentration to 0.10 mg/L.

Profiles from laboratory-scale experiments were compared to determine the effect of hydraulic loading rate on soluble Mn removal in the gravel contactor. Data plotted in Figure 4.14 compare two hydraulic loading rates under slightly alkaline pH conditions (pH of 7.4-7.6). Soluble Mn removal improved by 25% of initial soluble Mn concentration under a HLR of 16 gpm/ft^2 as compared to a HLR of 20 gpm/ft^2.

Overall, contactor columns containing gravel media provided acceptable soluble Mn adsorption under conditions of free chlorine concentrations of >1.5 mg/L, slightly alkaline pH (7.0-8.0), and HLR of 16 gpm/ft^2. Fluctuations in operating parameters such as influent soluble Mn or free chlorine concentrations can be adequately handled as long as the pH is slightly alkaline. Acidic pH conditions do not provide sufficient soluble Mn removal conditions. Generally, the shape of soluble Mn absorption profiles in the contactor column containing gravel was linear and showed a semi-constant soluble Mn absorption rate over contactor depth.

COLUMN EXPERIMENTS INVOLVING THE USE OF TORPEDO SAND MEDIA

Laboratory-scale contactor column experiments containing torpedo sand coated with MnO_x were conducted using the same methods as described previously in the opening paragraphs of the pyrolucite section of this chapter. Water was applied to the contactor column under various conditions. After a period of acclimation, soluble Mn profiles were collected over a known period of time. These profiles were then compared to show parameter effects on soluble Mn removal over depth of torpedo sand. Representative plots of data from single laboratory-scale experiments are included in the Appendix.

Applied free chlorine concentrations provide the necessary oxidant for available adsorption site regeneration during contactor operation. Data from laboratory-scale experiments were compared to determine the effect of free chlorine concentration on soluble Mn removal performance in the torpedo sand contactor at both 16 gpm/ft^2 and 20 gpm/ft^2. Data plotted in Figure 4.15 show profiles at a slightly acidic pH of 6.6 and a hydraulic loading rate of 16 gpm/ft^2. These plots show an increase of free chlorine concentration from 1.5 mg/L to 1.9 mg/L improved the soluble Mn adsorption profile from a total removal of 50% to 70% of the initial soluble Mn concentration.

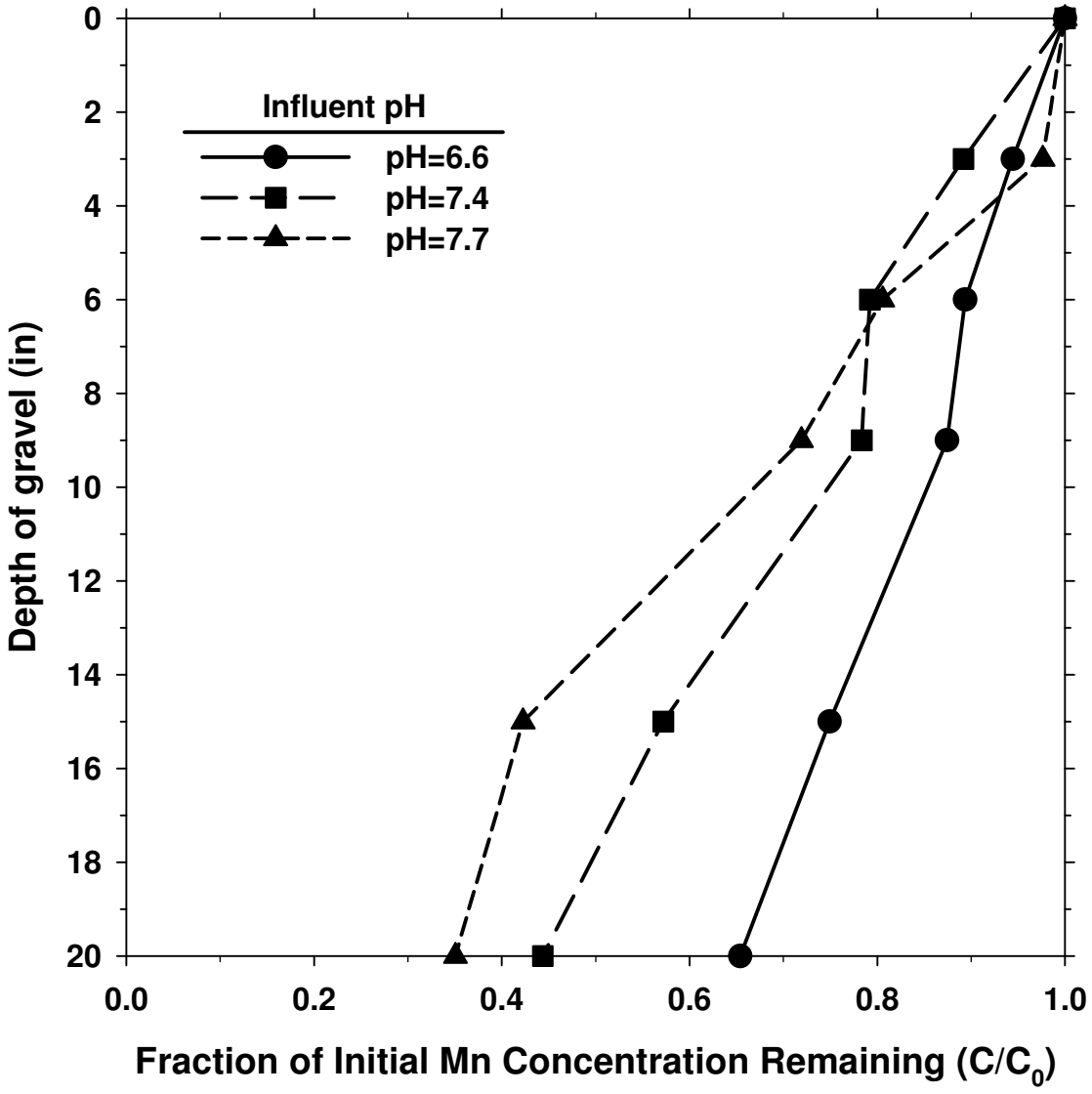

Figure 4.12 Effect of pH on soluble Mn removal profile over depth of gravel (Influent water: HLR=20 gpm/ft^2, HOCl=1.1 mg/L, Mn^{2+}=0.06-0.09 mg/L)

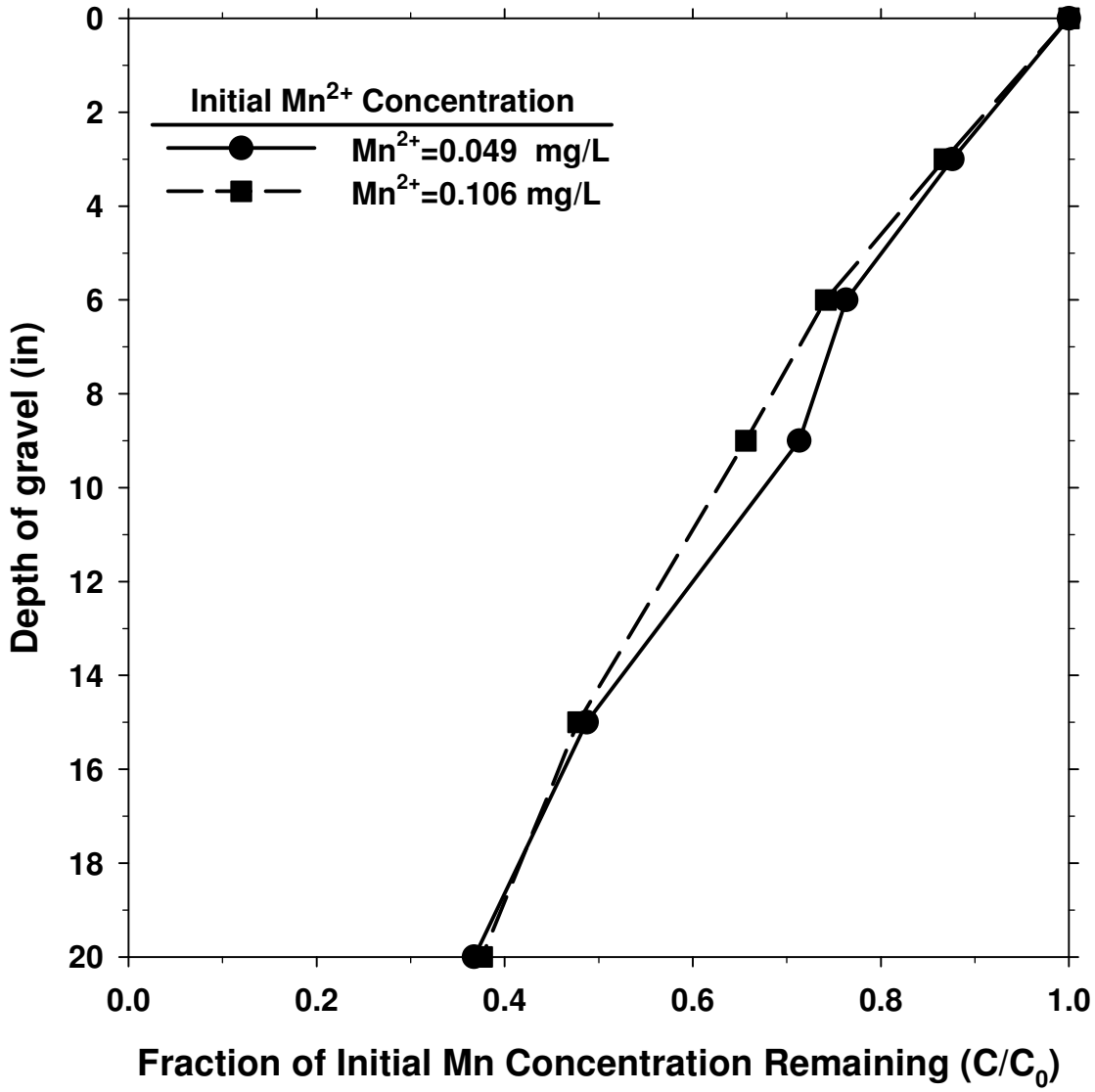

Figure 4.13 Effect of influent soluble Mn concentration on soluble Mn removal profile over depth of gravel (Influent water: HLR=16 gpm/ft^2, HOCl=2.3-2.4 mg/L, pH=7.7-7.8)

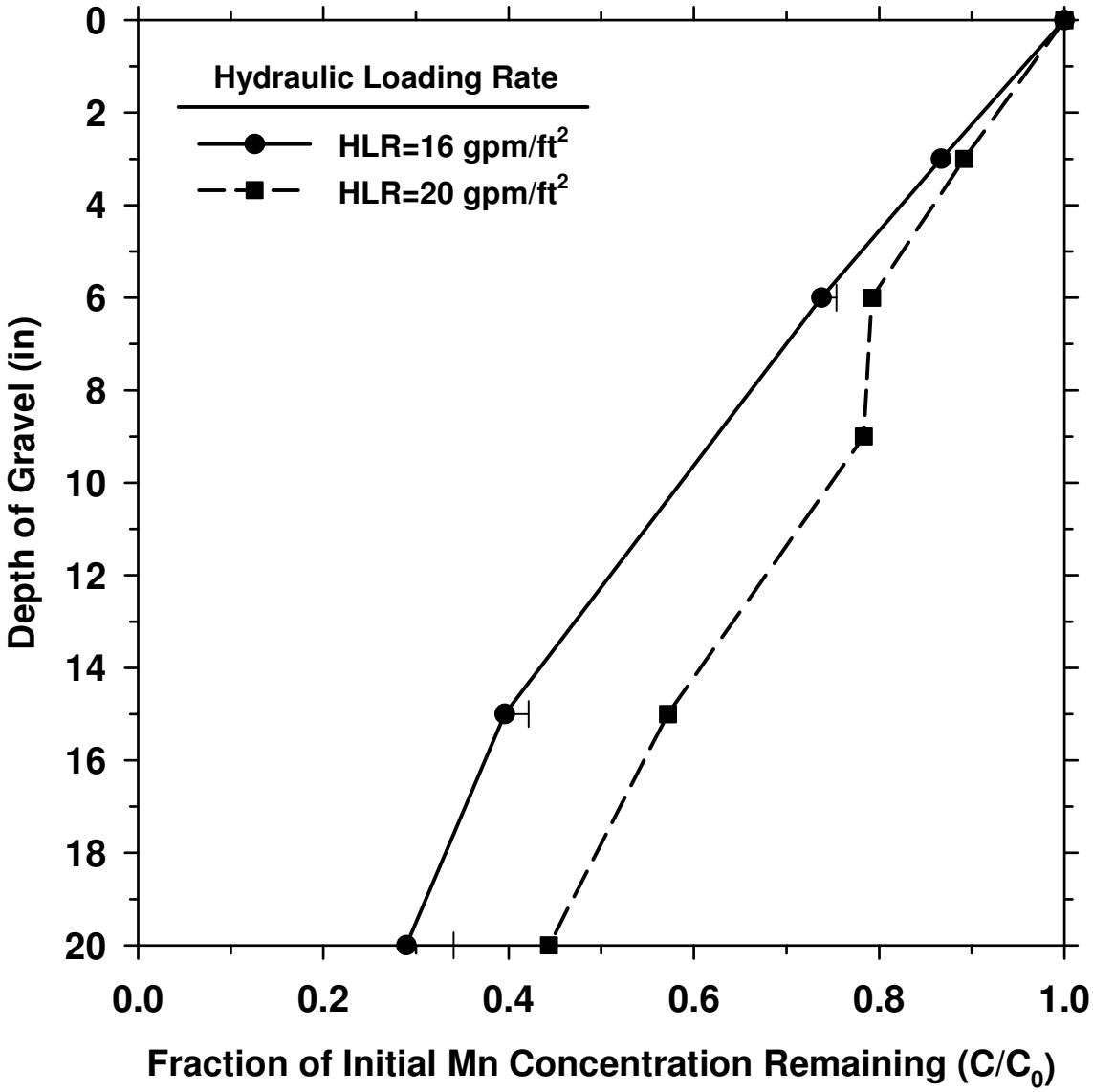

Figure 4.14 Effect of HLR on soluble Mn removal profile over depth of gravel (Influent water: HOCl=1.1-1.2 mg/L, pH=7.4-7.6, Mn^{2+}=0.09 mg/L)

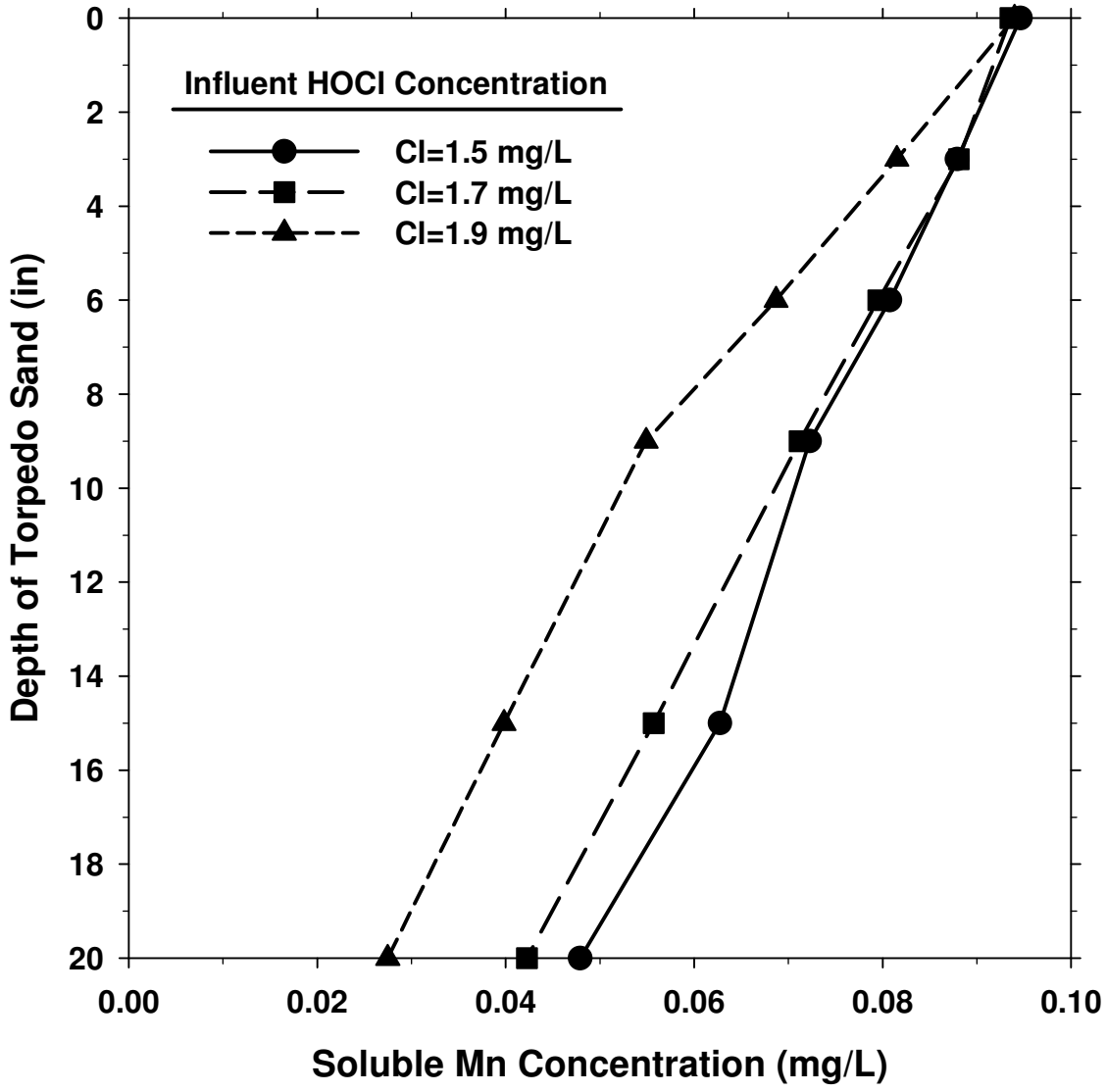

Figure 4.15 Effect of free chlorine concentration on soluble Mn removal profile over depth of torpedo sand (Influent water: HLR=16 gpm/ft^2, pH=6.6, Mn^{2+}=0.09 mg/L)

The concentration of manganese in solution can affect the adsorption capacity of media which directly affects the shape of the adsorption profile. Profiles from laboratory-scale experiments were compared to determine the effect of influent soluble Mn concentration on soluble Mn removal in the contactor column containing torpedo sand. Data plotted in Figure 4.16 were collected under conditions of a HLR of 20 gpm/ft^2, a free chlorine concentration of 2.1-2.4 mg/L, and a slightly acidic pH of 6.5-6.6. A slight improvement in soluble Mn removal was observed with an increase of initial soluble Mn concentration.

Contactor columns containing torpedo sand showed an adequate soluble Mn removal under conditions of an acidic pH of 6.5-6.8 and a free chlorine concentration of 1.5-3.1 mg/L. The shape of soluble Mn absorption profiles in the torpedo sand contactor was similar to the soluble Mn adsorption profiles in the gravel contactor. The soluble Mn removal profiles were linear and showed a semi-constant soluble Mn absorption rate over the torpedo sand contactor depth.

PILOT-SCALE EXPERIMENTS

The previous three sections of this chapter discuss the ability of each media to removal soluble Mn under varying conditions applied in the laboratory. The purpose of the pilot-scale experiments was to determine the effectiveness of the large-sized media under water quality conditions found at the Blacksburg-Christiansburg-VPI Water Authority (BCVPIWA), a local water treatment utility. The contactor columns simulated the application of soluble Mn removal post-filtration contactors on site at the utility, by being placed in the treatment sequence after Filter #6 at the BCVPIWA.

Post filtration water was supplemented with soluble Mn to simulate the range of soluble Mn concentrations that a contactor might experience in a full-scale treatment situation. The proposed contactor configuration would include a free chlorine residual across the media bed for continued regeneration and soluble Mn removal. Therefore, the minimal free chlorine residual after the filters at the utility was increased to a desired free chlorine concentration of 1.0-2.0 mg/L before reaching the contactor columns. The filtered water pH at the utility was not altered so that soluble Mn removal profiles were observed under actual utility conditions of pH 7.1-7.5.

Prior to data collection, the media in the contactor columns was exposed to the applied water for an hour without soluble Mn addition to achieve regeneration by free chlorine oxidation. During an additional thirty minutes after regeneration, the soluble Mn feed was activated and the media in the contactor was acclimated to the operational parameters. Adsorption profiles were collected after the columns were acclimated. Three profiles were taken at ten-minute intervals to demonstrate the stability of the adsorption profile. Data collection occurred in two separate phases.

During phase one, each media type was exposed to an initial soluble Mn concentration ranging from 0.02-0.09 mg/L at a HLR of 16 gpm/ft^2 and pH of 7.2-7.5. Pyrolucite media provided effective soluble Mn removal (96% of total initial soluble Mn concentration) at all three initial soluble Mn concentrations as shown by the data plotted in Figure 4.17. Gravel media removed approximately 70% of the initial soluble Mn concentration at both 0.02 mg/L and 0.09 mg/L as shown by the data plotted in Figure 4.18. Torpedo sand removed 80-90% of the initial soluble Mn concentrations at all three initial soluble Mn concentrations as shown by the data

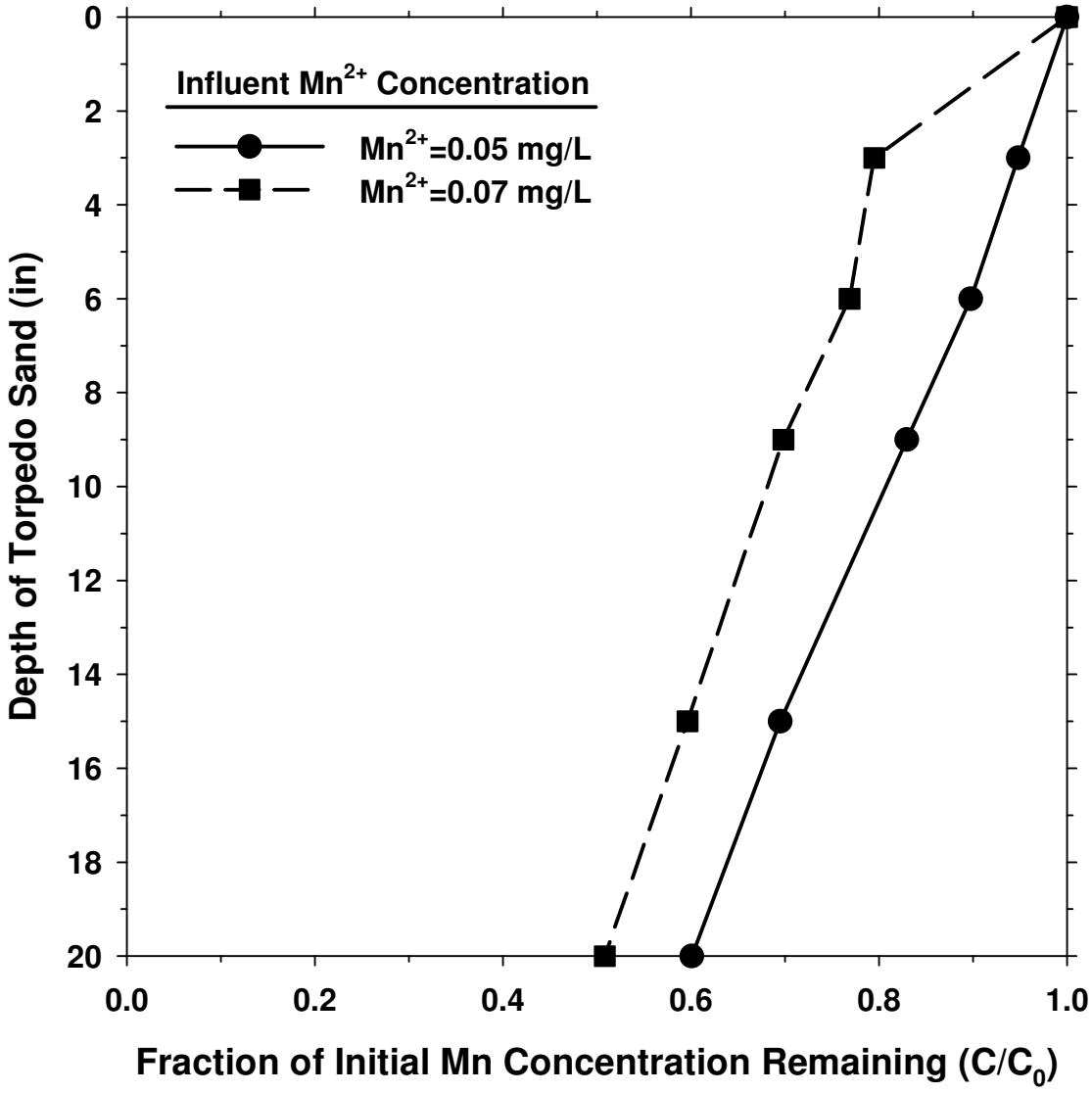

Figure 4.16 Effect of influent soluble Mn concentration on soluble Mn removal profile over depth of torpedo sand (Influent water: HLR=20 gpm/ft^2, HOCl=2.1-2.4 mg/L, pH=6.5-6.6)

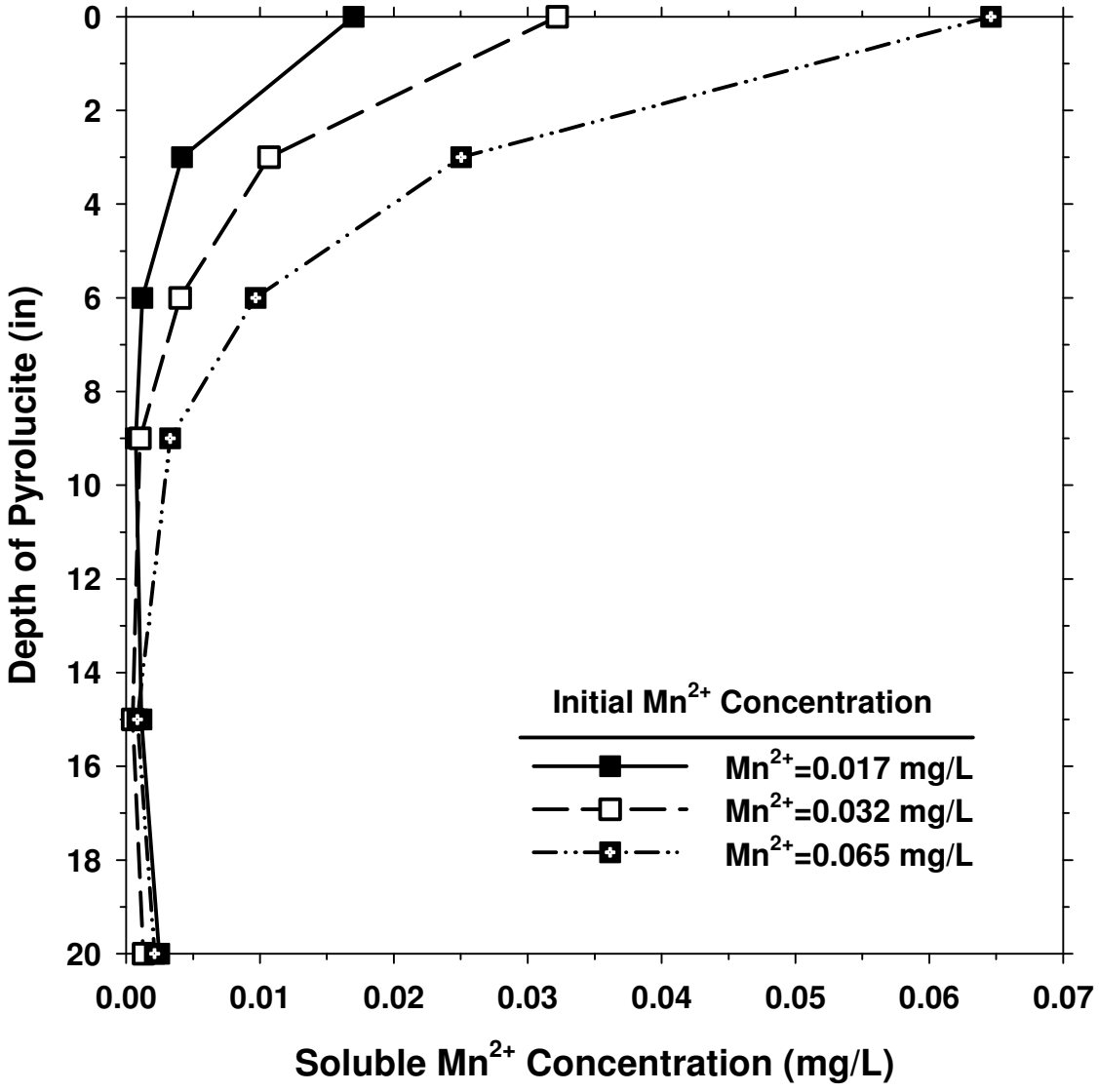

Figure 4.17 Pilot-scale soluble Mn adsorption profiles over depth of pyrolucite at increasing initial soluble Mn concentrations (Influent water: HLR=16 gpm/ft^2, HOCl=1.4-2.2 mg/L, pH=7.2-7.3)

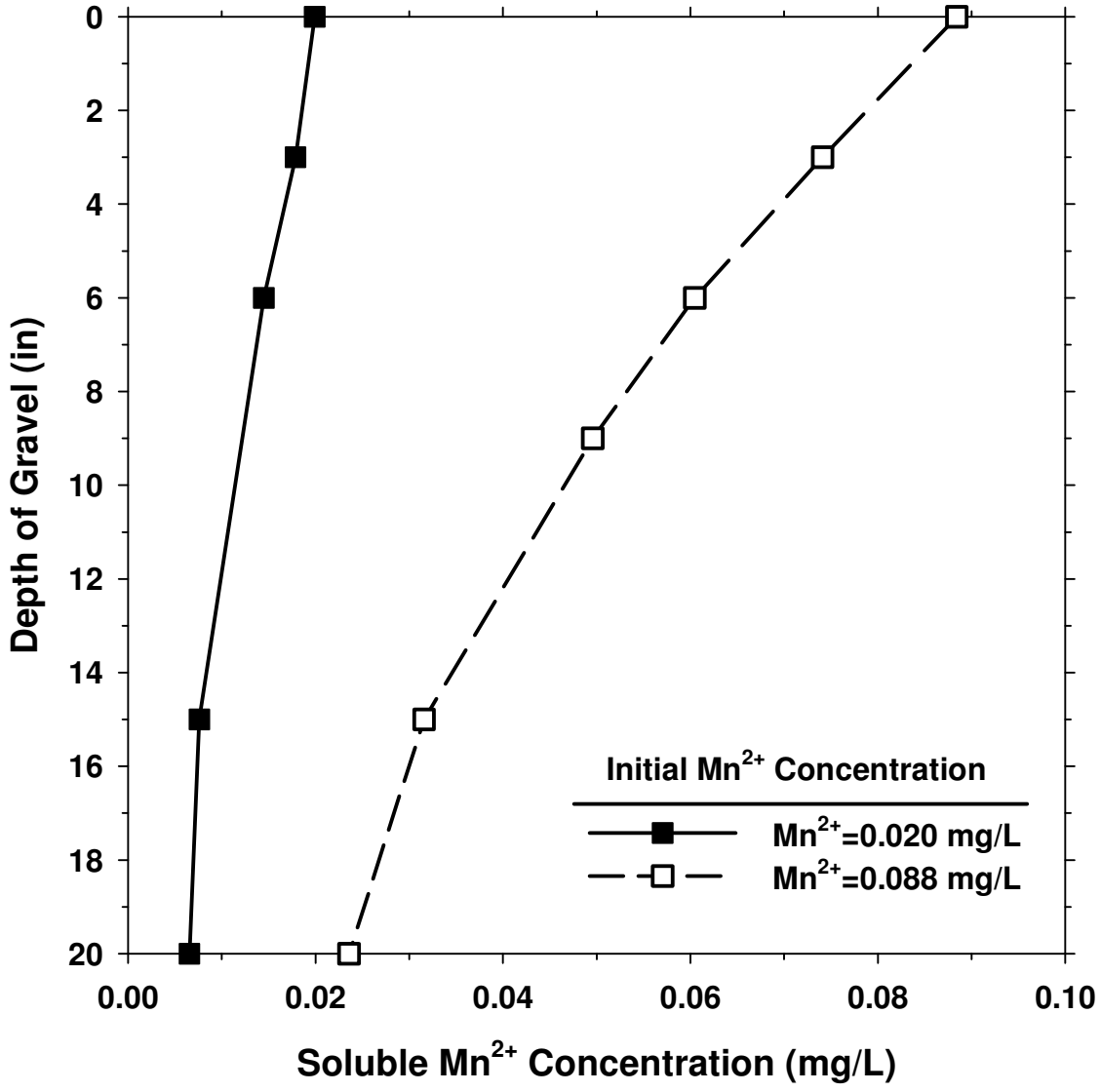

Figure 4.18 Pilot-scale soluble Mn adsorption profiles over depth of gravel at increasing initial soluble Mn concentrations (Influent water: HLR=16 gpm/ft^2, Free Cl=0.9-1.6 mg/L, pH=7.3-7.4)

plotted in Figure 4.19. Comparisons should not be made between these three plots since the chlorine concentration varied between these experiments.

During phase two, each media type was exposed to an increased hydraulic loading rate of 22-24 gpm/ft^2 and an initial soluble Mn concentration of 0.03-0.04 mg/L. Hydraulic loading rate effects on soluble Mn removal profiles were compared at similar initial soluble Mn concentrations for each media. Data plotted in Figure 4.20 present no distinguishable change in profile with increased hydraulic loading rate from 16 to 22 gpm/ft^2 for pyrolucite. Data plotted in Figure 4.21 present similar results for gravel with no distinguishable change in profile with increased hydraulic loading rate from 16 to 24 gpm/ft^2. Data plotted in Figure 4.22 present a slightly less effective soluble Mn removal profile with increased hydraulic loading rate from 16 to 24 gpm/ft^2 for torpedo sand.

Overall, each of the large-sized media effectively removed the initial soluble Mn concentrations under water quality conditions found at the BCVPIWA facility. Each contactor column also provided effective soluble Mn removal at the increased hydraulic loading rate of 22-24 gpm/ft^2. Pyrolucite provided the largest total soluble Mn removal at 96-99% of the initial soluble Mn concentration adsorbed.

UPTAKE CAPACITY EXPERIMENTS

The purpose of the Mn uptake capacity experiments was to determine the amount of soluble Mn able to be adsorbed per weight of contactor media. Soluble Mn uptake capacity experiments were conducted on new, unused media and on media that has been used across several laboratory and pilot-scale experiments. New and used Mn uptake capacity data are compared in this chapter to determine if long-term contactor use affected the Mn uptake capacity of the media. Soluble Mn uptake capacities are compared across media types in Chapter 6 to determine how differences in capacity affected soluble Mn removal performance. Freundlich adsorption isotherms are calculated from the Mn uptake capacity data for use in model prediction as discussed in Chapter 5.

Data plotted in Figure 4.23 show the Mn uptake capacity per weight of media for both new and used pyrolucite over various solution Mn concentrations at pH 7.5. Uptake capacity of pyrolucite media increased with increasing solution Mn concentration and provided the largest soluble Mn uptake capacity of the three media types. There was no significant change between new and used Mn uptake capacities of the pyrolucite media; therefore, the isotherm remained the same over the range of solution concentrations investigated.

Data plotted in Figure 4.24 show the Mn uptake capacity per weight of media for new and used gravel over various solution Mn concentrations at pH 7.5; whereas, data plotted in Figure 4.25 show the Mn uptake capacity per weight of media for new and used torpedo sand under similar conditions. Both new gravel and new torpedo sand media provided similar soluble Mn uptake capacities, appearing to reach a maximum Mn uptake capacity above a solution Mn concentration of 0.05 mg/L. However, the soluble Mn uptake capacity of both the gravel and torpedo sand media increased after repeated experimental use. The soluble Mn uptake capacity of the used gravel and torpedo sand media was observed to increase as the solution Mn concentration increased. The shape of the isotherm curves suggested that these Mn uptake capacities would reach an eventual maximum at a higher solution Mn concentration than

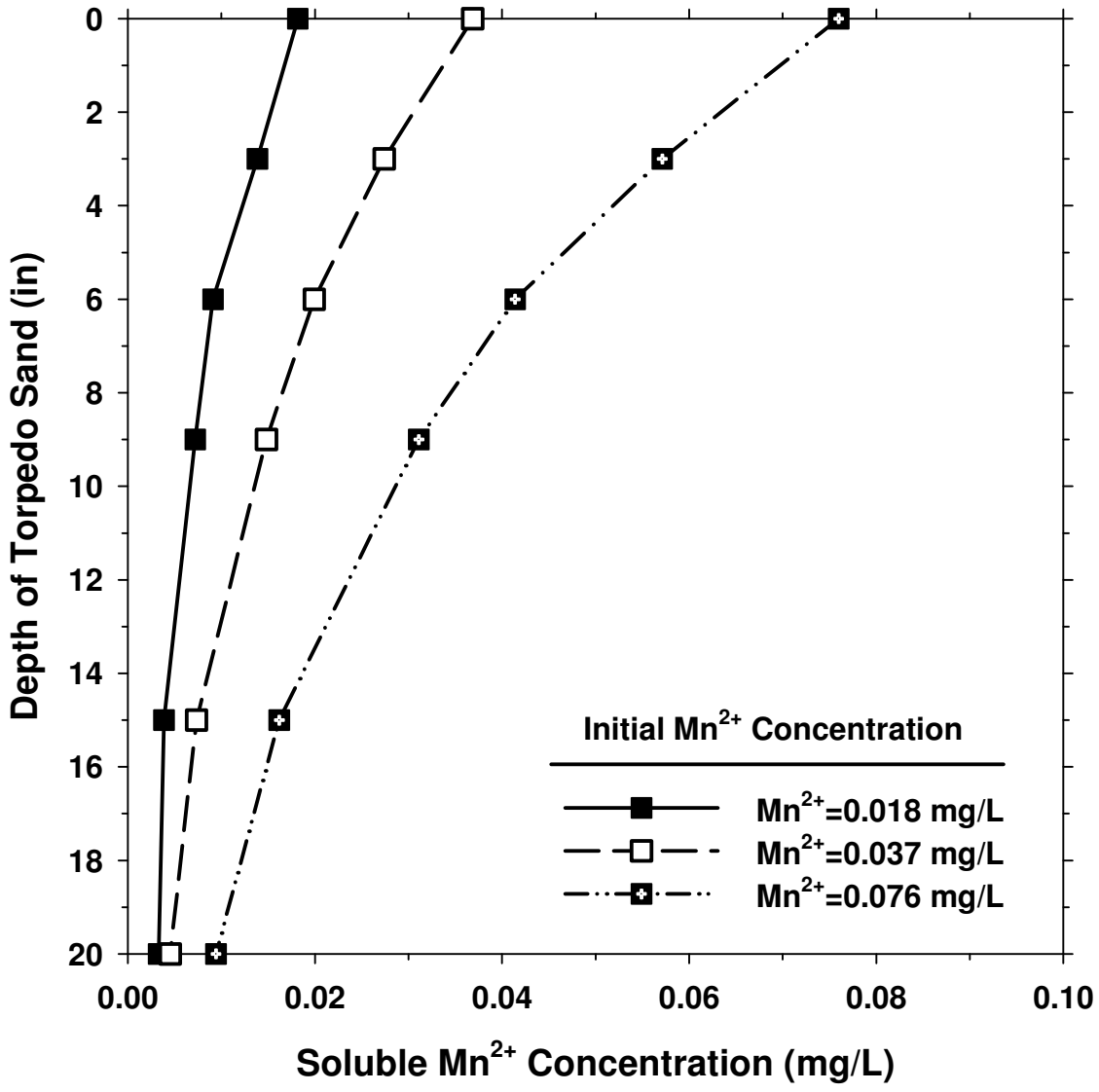

Figure 4.19 Pilot-scale soluble Mn adsorption profiles over depth of torpedo sand at increasing initial soluble Mn concentrations (Influent water: HLR=16 gpm/ft^2, Free Cl=1.1-1.8 mg/L, pH=7.2-7.5)

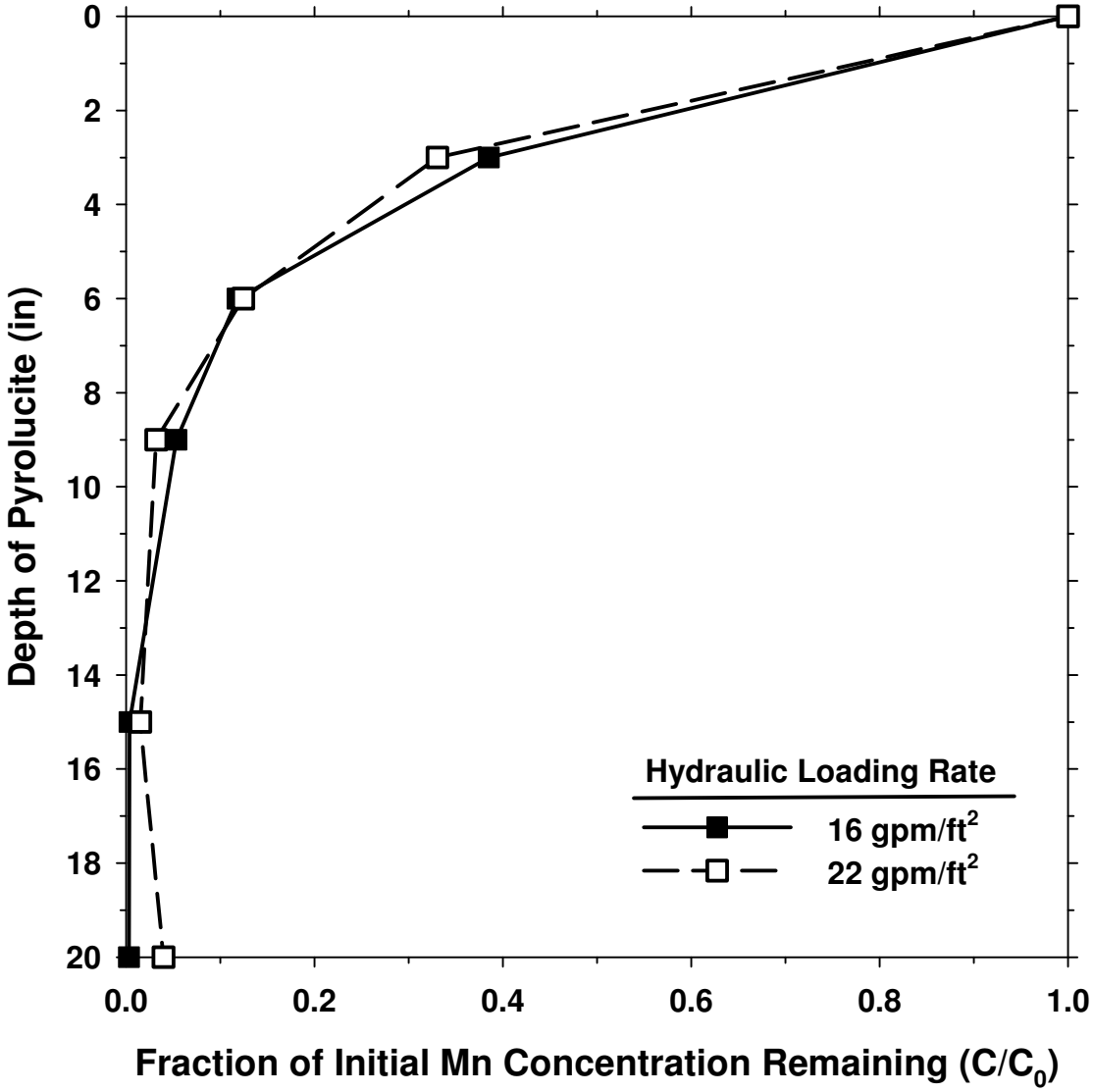

Figure 4.20 Pilot-scale soluble Mn adsorption profiles over depth of pyrolucite at increasing HLR (Influent water: Mn^{2+}=0.03 mg/L, Free Cl=1.8-1.9 mg/L, pH=7.2-7.5)

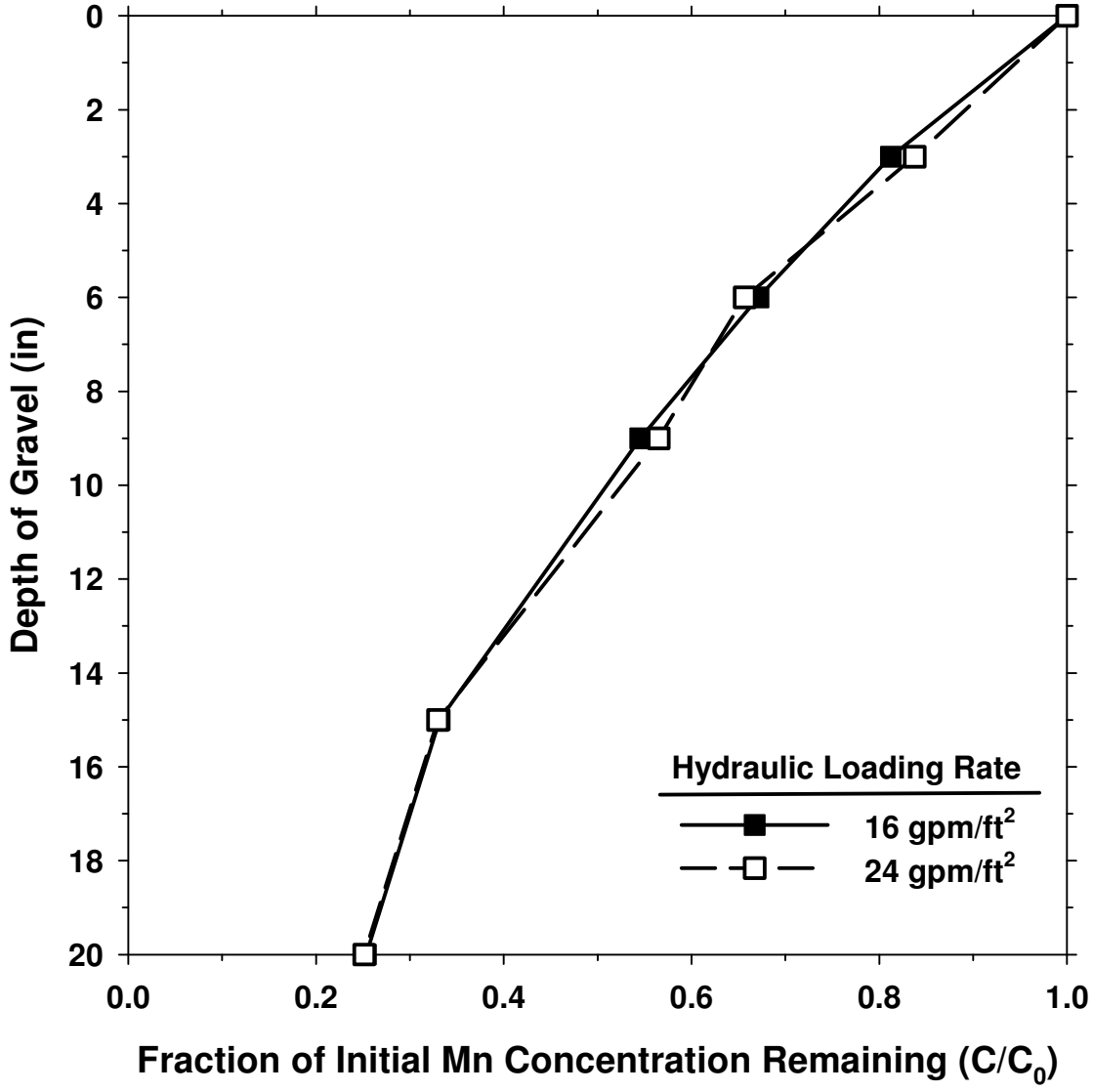

Figure 4.21 Pilot-scale soluble Mn adsorption profiles over depth of gravel at increasing HLR (Influent water: Mn^{2+}=0.04 mg/L Free Cl=1.7-2.8 mg/L, pH=7.2-7.4)

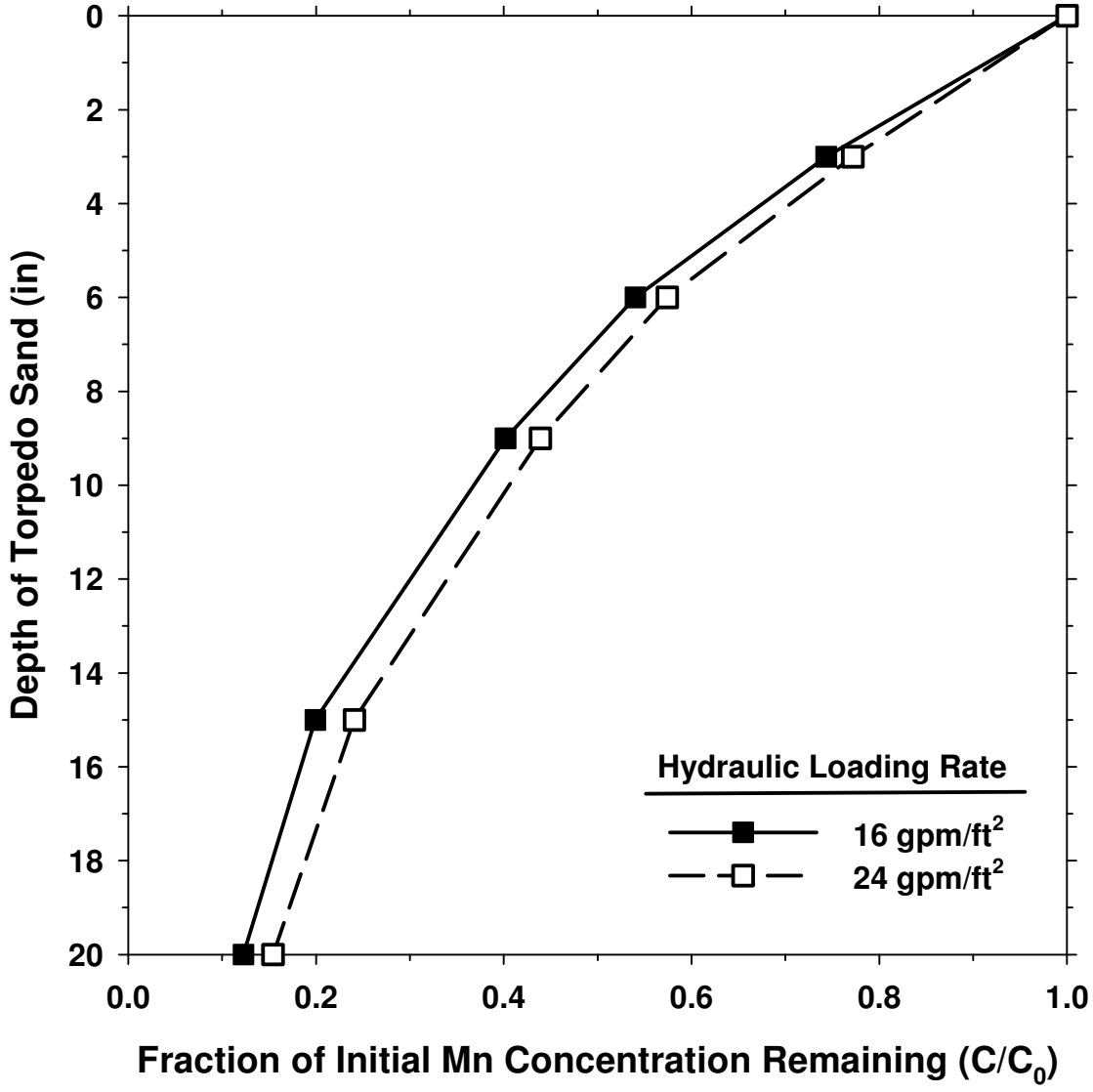

Figure 4.22 Pilot-scale soluble Mn adsorption profiles over depth of torpedo sand at increasing HLR (Influent water: Mn^{2+}=0.04 mg/L, Free Cl=1.1-1.5 mg/L, pH=7.1-7.2)

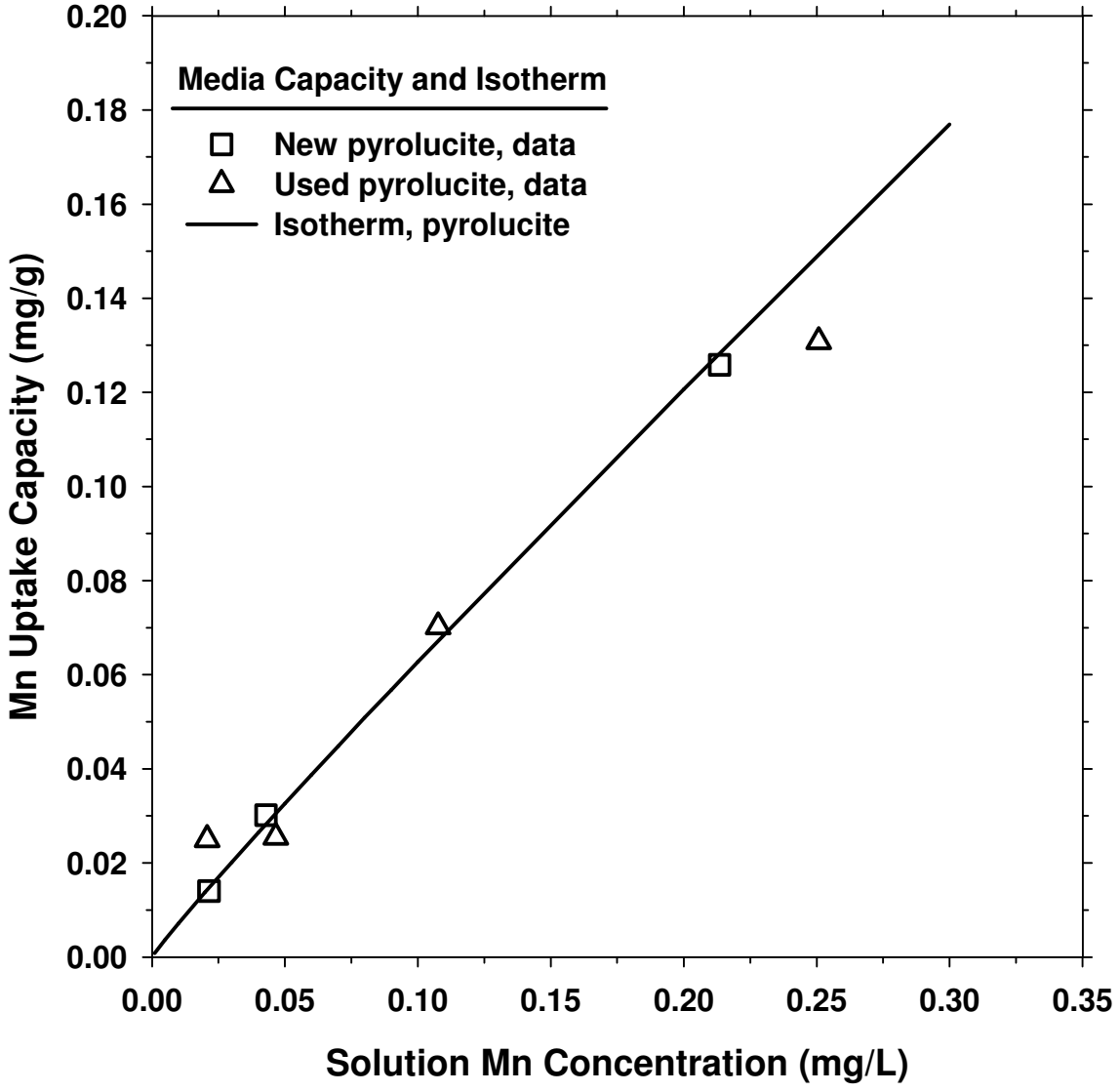

Figure 4.23 Mn adsorption capacity per weight of pyrolucite at pH=7.5 over a range of soluble Mn concentrations

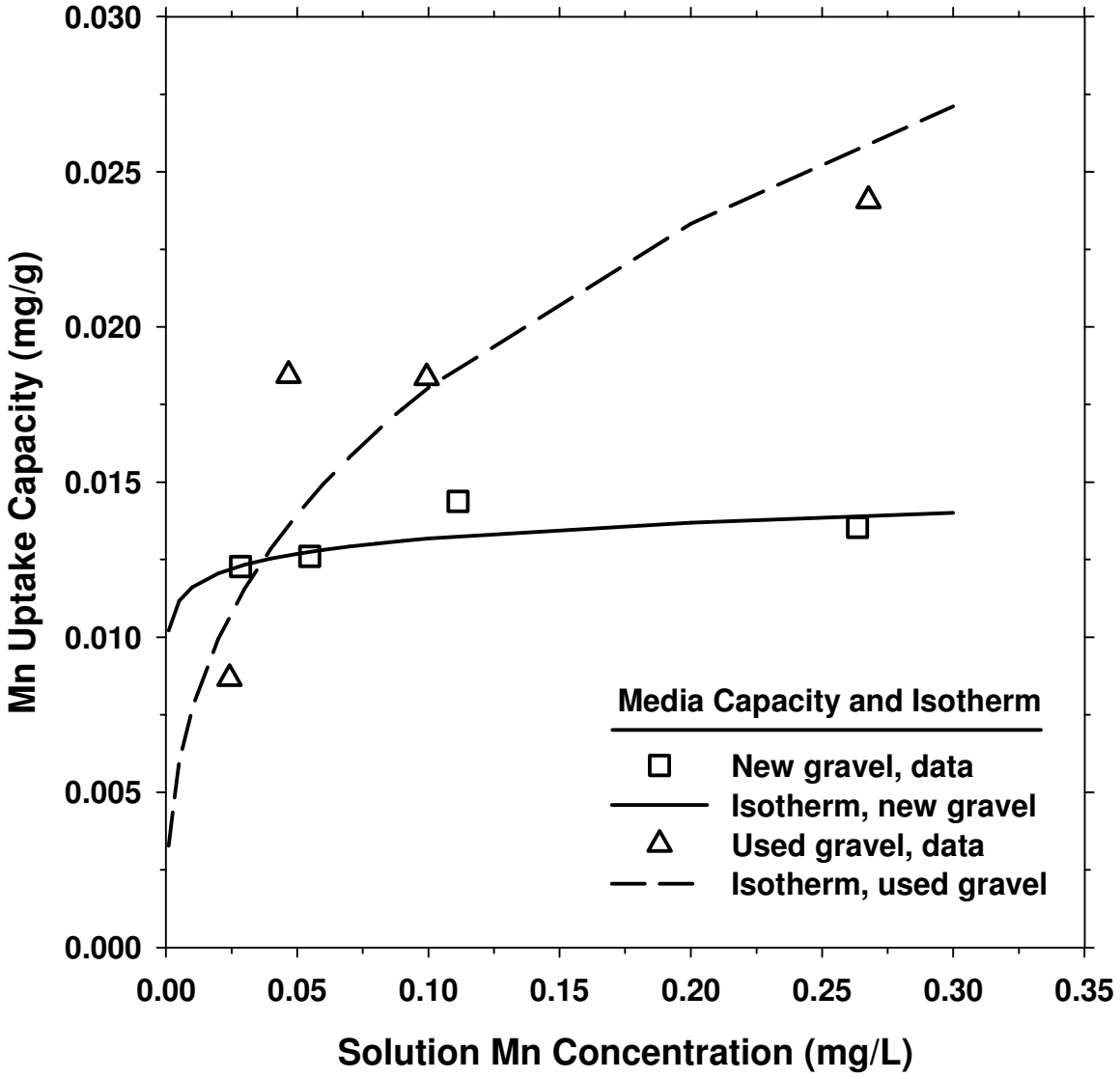

Figure 4.24 Mn adsorption capacity per weight of gravel at pH=7.5 over a range of soluble Mn concentrations

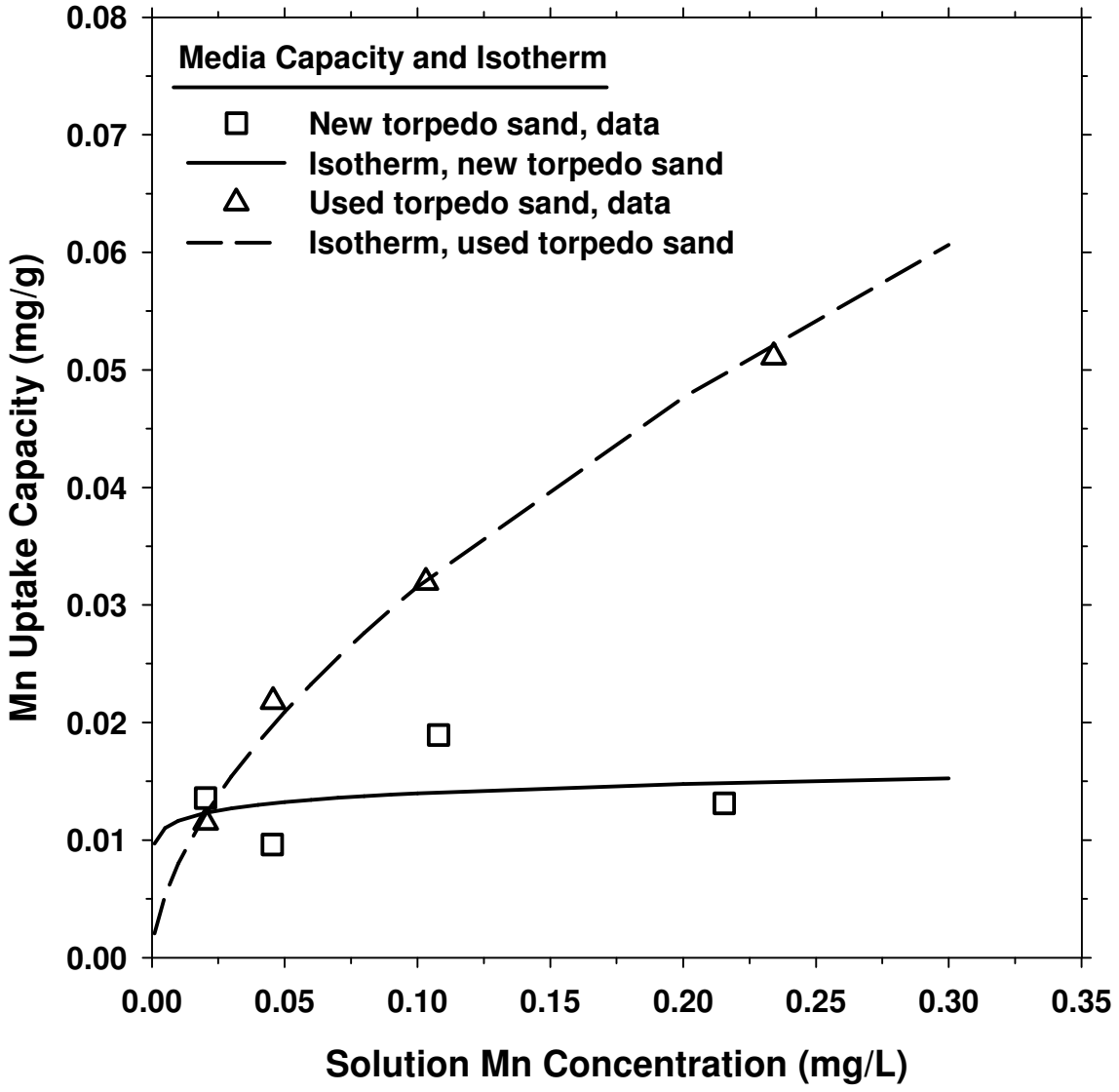

Figure 4.25 Mn adsorption capacity per weight of torpedo sand at pH=7.5 over a range of soluble Mn concentrations

Table 4.1
Summary of extractable MnOx(s) coating (mg Mn/g media) on new and used media

	Pyrolucite	Gravel	Torpedo Sand
New media	10 – 11 mg/g	0.2-0.3 mg/g	0.2-0.3 mg/g
Post-use media	25 – 26 mg/g	0.5 mg/g	0.5 mg/g

investigated. Numerical values for the Freundlich isotherm constants were required as model parameters and are provided in Table 5.1.

The relationship of new and used media uptake capacity behaved as expected. The pyrolucite media was composed of Mn-oxide material initially; therefore, deposition of additional Mn-oxide coating during use increased the extractable Mn-oxide coating but may not have provided significant added Mn uptake capacity. This is consistent with the previous finding that although extractable $MnO_x(s)$ coatings may increase above 12 mg Mn/g media, the Mn uptake capacity often does not increase (Bouchard 2005). The lack of Mn uptake capacity increase may be due to a layering of $MnO_x(s)$ coating that covers previously available adsorption sites, making them thusly inaccessible.

The gravel and torpedo sand media were initially coated using a laboratory method which had inherent limitations on Mn-oxide deposition. As the media was used, more Mn-oxide coating could have been deposited in areas that may not have been previously coated, providing an increased level of Mn uptake capacity.

The amount of extractable $MnO_x(s)$ coating on each media was measured before and after the media had been used across several laboratory and pilot-scale experiments (see Table 4.1). Since the $MnO_x(s)$ coating was deposited on the gravel and torpedo sand in the laboratory, the media was considered to be new and unused after coating procedures were completed and before the contactor column experiments began. Pyrolucite media contained a large initial amount of extractable $MnO_x(s)$ at 10-11 mg Mn per g media which increased to 25-26 mg Mn per g media. Gravel and torpedo sand contained similar amounts of extractable $MnO_x(s)$ on both new and used media. Periodic extracted samples of gravel and torpedo sand media indicated that the original extractable $MnO_x(s)$ coating may have been unstable. After an initial slight decrease, the extractable $MnO_x(s)$ coating began to deposit more permanently and increase to approximately 0.5 mg Mn per g media.

CHAPTER 5
DEVELOPMENT OF A MODEL TO PREDICT SOLUBLE MANGANESE REMOVAL VIA ADSOPRTION AND OXIDATION

The purpose of this chapter is to discuss the development and application of a model to predict soluble Mn removal via adsorption and oxidation onto MnO_x-coated media. Previous research, as discussed in Chapter 2, has been conducted with the goal of modeling the removal of soluble Mn across a bed of oxide-coated filter media. Merkle *et al.* (1997b) developed the most recent dynamic model capable of predicting soluble Mn removal profiles for small grain media (particle diameter, d_p=0.12 cm) and hydraulic loading rates (HLR) of 2.5-10 gpm/ft^2. However, the model was unstable and inaccurate under conditions of low Mn adsorption capacity and high flow rate. Therefore, the model as developed by Merkle *et al.* (1997b) could not be directly applied under the HLR conditions investigated for this report.

EQUATION DEVELOPMENT

Mass transfer and oxidation principles used to develop the previous dynamic model of Merkle *et al.* (1997b) were used as guides for the development of the current model to predict the removal of soluble Mn by large-sized media (d_p=0.22-0.48 cm) under HLR conditions of 16-24 gpm/ft^2. Although the previous model was developed for both intermittent and continuous regeneration, the current model focused solely on steady state conditions under continuous media regeneration via free chlorine addition. The development of the current model began with the application of first principles to a mass balance of soluble Mn across an incremental bed depth. The diagram in Figure 5.1 shows the representation of this incremental bed depth.

At steady state, the mass of soluble Mn entering the system was equal to the sum of the mass of soluble Mn removed by adsorption and the mass soluble Mn leaving the system (as shown in Equation 5.1). The soluble Mn flux was assumed to be driven by a linear driving force as described by Merkle *et al.* (1997b).

$$Q\,C_{1b}(z) = k_f\,(C_{1b}-C_{1s})\,A_v\,(1-\varepsilon)\,A\,\Delta z + Q\,C_{1b}(z+\Delta z) \qquad (5.1)$$

where :
- Q = volumetric water flow rate (m^3/s)
- C_{1b} = bulk aqueous-phase Mn concentration (mol/m^3)
- k_f = liquid to solid mass transfer coefficient (m/s)
- C_{1s} = aqueous-phase Mn concentration at the liquid-solid interface (mol/m^3)
- A_v = specific surface of media (m^2 media/m^3 media)
- ε = fractional pore volume (m^3 water/m^3 bed)
- A = cross sectional area of bed (m^2)

The Freundlich equilibrium isotherm was applied at the media surface to describe the relationship between the aqueous-phase soluble Mn concentration at the surface and the adsorbed Mn concentration on the surface as shown in Equation 5.2.

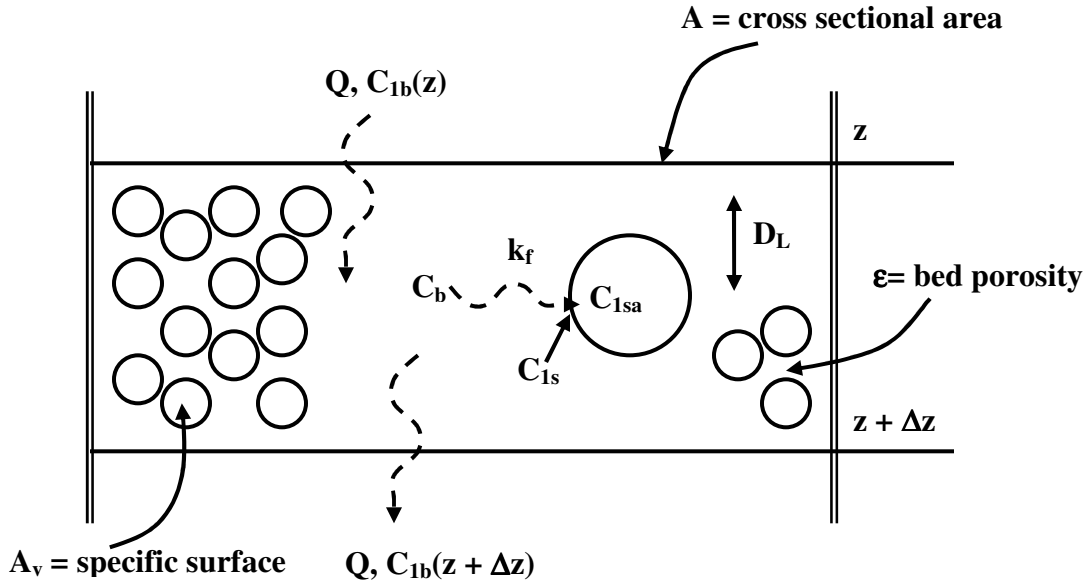

Figure 5.1 Representation of the flow of Mn across an incremental depth of media

$$C_{1s} = \left[\frac{C_{1sa}}{K}\right]^{n} \tag{5.2}$$

where : C_{1sa} = adsorbed-phase Mn concentration on the media surface (mol/kg)
K, n = Freundlich isotherm constants

Manipulation of the soluble Mn mass balance equation provided a group of three solvable steady state equations as shown in Equations 5.3-5.5. The change in soluble Mn concentration over depth is shown in Equation 5.3. The change in free chlorine concentration over depth can also be described by a mass balance approach and was manipulated into the form shown in Equations 5.4-5.5. Equations 5.3-5.5 agreed with the group of equations developed by Merkle *et al.* (1997b). However, the concept of unavailable adsorption sites developed by Merkle *et al.* (1997b) was not included in this model.

$$0 = -U\frac{\partial C_{1b}}{\partial z} + D_L\frac{\partial^2 C_{1b}}{\partial z^2} - k_f A_v\left(\frac{1-\varepsilon}{\varepsilon}\right)\left[C_{1b} - \left[\frac{C_{1sa}}{K}\right]^{n}\right] \tag{5.3}$$

$$0 = -U\frac{\partial C_{2b}}{\partial z} + D_L\frac{\partial^2 C_{2b}}{\partial z^2} - \rho_b k_r C_{1sa} C_{2b} \tag{5.4}$$

$$0 = \frac{k_f A_v}{\rho_b}(1-\varepsilon)\left[C_{1b} - \left[\frac{C_{1sa}}{K}\right]^{n}\right] - k_r \varepsilon C_{1sa} C_{2b} \tag{5.5}$$

Table 5.1
Characteristic parameters for each media type

Parameter	Pyrolucite	Gravel	Torpedo Sand
Fractional pore volume (ε)	0.52	0.37	0.44
Bulk density (kg media/m^3 bed)	1992	1525	1495
Specific surface area (m^2 media/m^3 media)	7260	2937	6895
Particle diameter (m)	0.0022	0.0048	0.0023
Freundlich isotherm constant (K), new	0.441	0.00034	0.00042
Freundlich isotherm constant (1/n), new	0.944	0.055	0.0795
Freundlich isotherm constant (K), used	0.108	0.0034	0.0245
Freundlich isotherm constant (1/n), used	0.722	0.371	0.595

where: C_{2b} = bulk aqueous-phase free chlorine concentration (mol/m^3)
ρ_b = bulk density of media (kg media/m^3 bed)
U = pore water velocity (= Q/Aε) (m/s)
D_L = axial dispersion coefficient (m^2/s)

The model equations were solved for the soluble Mn concentration and free chlorine concentration per unit depth using numerical analysis. The solution was then coded into MatLab 7.1 software. The required input parameters were modified in the file editor. The output from the model was a plot of soluble Mn concentration over media depth and a plot of free chlorine concentration over media depth.

PARAMETER ESTIMATION

Input parameters were determined for individual experiments to test the initial model output. Parameters were affected by applied water conditions and media characteristics. A summary of the media characteristics for each media type is provided in Table 5.1. Model input parameters for a specific HLR and media type are provided in Table 5.2.

Characteristic traits of each media were measured in the laboratory. Fractional pore volume, ε (m^3 water/m^3 bed) was measured as the volume of water that could be contained in a known media bed volume. The density of the media was measured as the mass of a known volume of media. This measurement was converted to bulk density of media (kg media/m^3 bed) by multiplying the media density by the fractional media volume (1–ε).

Specific surface area of the media was calculated using the known relationship of area to volume as $6/d_p$ with a fractal surface structure correction. The fractal surface correction was used because the assumption of a spherical surface structure often underestimates the specific surface area of oxide coated media (Merkle *et al.* 1997b). The corrected area per volume equation shown in Equation 5.6 was used to calculate the specific surface area (m^2 media/m^3 media).

Table 5.2
Input parameters for each media type and HLR

Parameter	HLR	Pyrolucite	Gravel	Torpedo Sand
Pore water velocity (m/s)	16	0.021	0.029	0.025
Axial dispersion coefficient (m^2/s)		$1.74x10^{-4}$	$2.42x10^{-4}$	$2.06x10^{-4}$
Pore water velocity (m/s)	20	0.026	0.037	0.031
Axial dispersion coefficient (m^2/s)		$2.18x10^{-4}$	$3.06x10^{-4}$	$2.57x10^{-4}$
Pore water velocity (m/s)	22	0.029	~	~
Axial dispersion coefficient (m^2/s)		$2.39x10^{-4}$	~	~
Pore water velocity (m/s)	24	~	0.044	0.37
Axial dispersion coefficient (m^2/s)		~	$3.66x10^{-4}$	$3.09x10^{-4}$

$$A_V = \frac{6}{d_p^{1.16}} \tag{5.6}$$

where: d_p = particle diameter (m)

Solution characteristics were measured for each experiment. Initial bulk aqueous-phase soluble Mn concentration (mol/m^3) and initial bulk aqueous-phase free chlorine concentration (mol/m^3) were measured with each soluble Mn profile collected experimentally. Pore water velocities (m/s) were calculated as the volumetric flow rate divided by the product of the cross sectional bed area and the fractional pore volume for each flow rate and media type. Axial dispersion coefficients (m^2/s) were calculated using a correlation used by Merkle *et al.* 1997b for each flow rate and media type. In this correlation the axial dispersion coefficient was equal to the pore velocity in cm/min divided by 1.2. The units were then converted for use in the model.

Freundlich isotherm constants were calculated using the soluble Mn uptake capacity experimental data for conditions under a slightly alkaline pH of 7.5. Manganese uptake capacities were measured for each media over a range of soluble Mn concentrations from 0.02-0.25 mg/L. Freundlich isotherm constants were determined for new and used media separately from a log-log plot of the appropriate uptake capacity data. Isotherm constants were verified by plotting the isotherm relationship along with the experimental data as provided in Figures 4.23-4.25. The numerical values for the Freundlich isotherm constants are provided in Table 5.1.

Two rate parameters were required for model predictions. The oxidation rate constant, k_r, was adapted from Merkle *et al.* 1997b and estimated to be $7.6x10^{-2}$ m^3bed/mol*s. This value was determined by the authors from global oxidation studies of various MnO_x-coated media. The liquid to solid mass transfer coefficient, k_f, was initially estimated to provide an input value for the model. The mass transfer coefficient was then fitted to the experimental data as discussed later in this chapter.

Initial values of k_f for each media type were calculated using a correlation proposed by Ohashi *et al.* (as shown in Equation 5.7) (Roberts *et al.* 1985). This correlation was valid over

Table 5.3
Fitted mass transfer coefficient, k_f (m/s) values for each media and flow rate

HLR	Pyrolucite	Gravel	Torpedo Sand
16, Estimated	$1.0x10^{-5}$	$1.1x10^{-5}$	$1.1x10^{-5}$
16, Lab	$1.7x10^{-5} – 2.3x10^{-5}$	$1.0x10^{-5} – 1.3x10^{-5}$	~
16, Pilot	$4.5x10^{-5} – 4.8x10^{-5}$	$1.3x10^{-5} – 1.5x10^{-5}$	$1.1x10^{-5} – 1.2x10^{-5}$
20, Lab	~	$1.0x10^{-5} – 1.5x10^{-5}$	~
22, Pilot	7.0x10-5	~	~
24, Pilot	~	2.5x10-5	1.6x10-5

the range of Reynolds numbers calculated for each media under the experimental HLR conditions from 16-24 gpm/ft^2. The initial values of k_f were calculated at a HLR of 16 gpm/ft^2 and a temperature of 20°C.

$$Sh \approx \frac{k_f d_p}{D_{L,diff}} \approx \left(2 + 1.21 R^{1/2} Sc^{1/3}\right)\left(1 + 1.5[1-\phi]\right) \qquad (5.8)$$

where:
Sh = Sherwood number
k_f = liquid to solid mass transfer coefficient (m/s)
d_p = particle diameter (m)
$D_{L,diff}$ = bulk liquid diffusivity (m^2/s) = $1x10^{-9}$ m^2/s @ 20°C
R = Reynolds number (= Ud_p/υ)
Sc = Schmidt number (= $\upsilon d_p/D_{L,diff}$)
υ = kinematic viscosity = $1.004x10^{-6}$ m^2/s @ 20°C
ϕ = fractional pore volume (m^3 water/m^3 bed)

PARAMETER FITTING: MASS TRANSFER COEFFICIENT

Model outputs generated with an initial estimate for k_f were compared to data from laboratory-scale and pilot-scale experiments. The value for k_f was then manipulated to produce a model output that well represented the experimental data. The values of k_f were still considered comparable to the initial correlation estimate due to the inherent scatter found in original data used to create comparable forms of the correlation (Wakao and Funazkri 1978; Roberts *et al.* 1985). The fitted values for k_f are included in Table 5.3. Representative plots of k_f fits are included in the Appendix.

The initial value of k_f for pyrolucite underestimated the Mn removal profile. For laboratory-scale experiments, the k_f of pyrolucite at 16 gpm/ft^2 ranged from $1.7x10^{-5}$ to $2.3x\ 10^{-5}$ m/s. However, for the pilot-scale experiments, the k_f of pyrolucite at 16 gpm/ft^2 ranged from $4.5x10^{-5}$ to $4.8x\ 10^{-5}$ m/s. This increase was unexpected and could be related to water quality parameters not evaluated in the scope of this research. For example, laboratory source water was tap water that was chloraminated and located approximately 1-2 days downstream from the treatment

Table 5.4
Initial value of parameters investigated in sensitivity analysis

Parameter	Value
Fractional pore volume (ε)	0.52
Specific surface area (m^2 media/m^3 media)	7260
Bulk density (kg media/m^3 bed)	1992
Freundlich isotherm constant (K),	0.441
Freundlich isotherm constant (1/n),	0.9442
Mass transfer coefficient, k_f (m/s)	$1.8x10^{-5}$
Oxidation rate constant, k_r (m^3bed/mol.s)	$7.6x10^{-2}$
Axial dispersion coefficient, D_L (m^2/s)	$1.7x10^{-4}$
Pore velocity (m/s)	0.021
Mn concentration (mol/m^3)	0.00091 (0.05 mg/L)
Cl concentration (mol/m^3)	0.0286 (1.5 mg/L)

facility. Additional water chemistry parameters may have affected the mass transfer in the pyrolucite contactor column. Water temperature was considered as a possible factor in the difference of k_f values. The laboratory water temperature was 18°-20°C during the majority of the pyrolucite contactor column experiments. Pilot-scale experiments were conducted at water temperatures of 27°-29°C. However, the estimate for k_f did not change significantly (<1%) with the increased temperature taken into account.

The estimated value of k_f for gravel provided a close fit to the Mn removal profile at 16 gpm/ft^2. The range of k_f values for gravel was determined to be $1.0x10^{-5}$ – $1.5x10^{-5}$ m/s. The initial value was also a close estimate at 20 gpm/ft^2, which was not expected. The estimated value of k_f for torpedo sand also provided a close fit to the Mn removal profile at 16 gpm/ft^2. The range of k_f values for torpedo sand was determined to be $1.1x10^{-5}$ – $1.2x10^{-5}$ m/s.

Single pilot-scale experiments were conducted at a HLR of 22-24 gpm/ft^2 for each media type. Values for k_f were fitted to these experimental results: $7.0x10^{-5}$ m/s for pyrolucite at 22 gpm/ft^2, $2.5x10^{-5}$ m/s for gravel at 24 gpm/ft^2, and $1.6x10^{-5}$ m/s for torpedo sand at 24 gpm/ft^2. Since only one data set was available for these HLR, further research should be conducted to verify these values.

SENSITIVITY ANALYSIS

Knowledge of parameter sensitivity was important for identifying the effect parameter estimation may have on the model output. Each input parameter was varied by approximately 0.5 and 1.5 times the original estimation used in the model. The resulting Mn removal profiles were plotted with the original profile for comparison. The initial values for each parameter are provided in Table 5.4. The media type used for the sensitivity analysis was pyrolucite. The

input parameters were chosen to reflect typical concentrations of Mn and free chlorine as expected at a water treatment facility.

The media characteristics that affected the model output were porosity (ε) (Figure 5.2) and specific surface area (Figure 5.3). Porosity was varied in a range that could be expected for contactor media; whereas, specific surface area was varied by 20%. Experimental data presented in this thesis has shown that HLR affects the Mn removal profile. Data plotted in Figure 5.4 show that the model reflects this relationship appropriately. The fitted parameter, k_f, had a large effect on the model prediction as shown in Figure 5.5. Oxidation rate, k_r, (Figure 5.6), axial dispersion coefficient, D_L, (Figure 5.7), the Freundlich constant, K, (Figure 5.8) did not show a significant effect on the model output. Since the oxidation rate value was estimated by previous research conducted by Merkle *et al.* 1997b, it was important to note that the value does not have a significant effect on the model prediction, reducing the amount of error that could be associated with the use of the estimated value. This was also true for the dispersion coefficient which was estimated from an empirical relationship used by Merkle *et al.* 1997b.

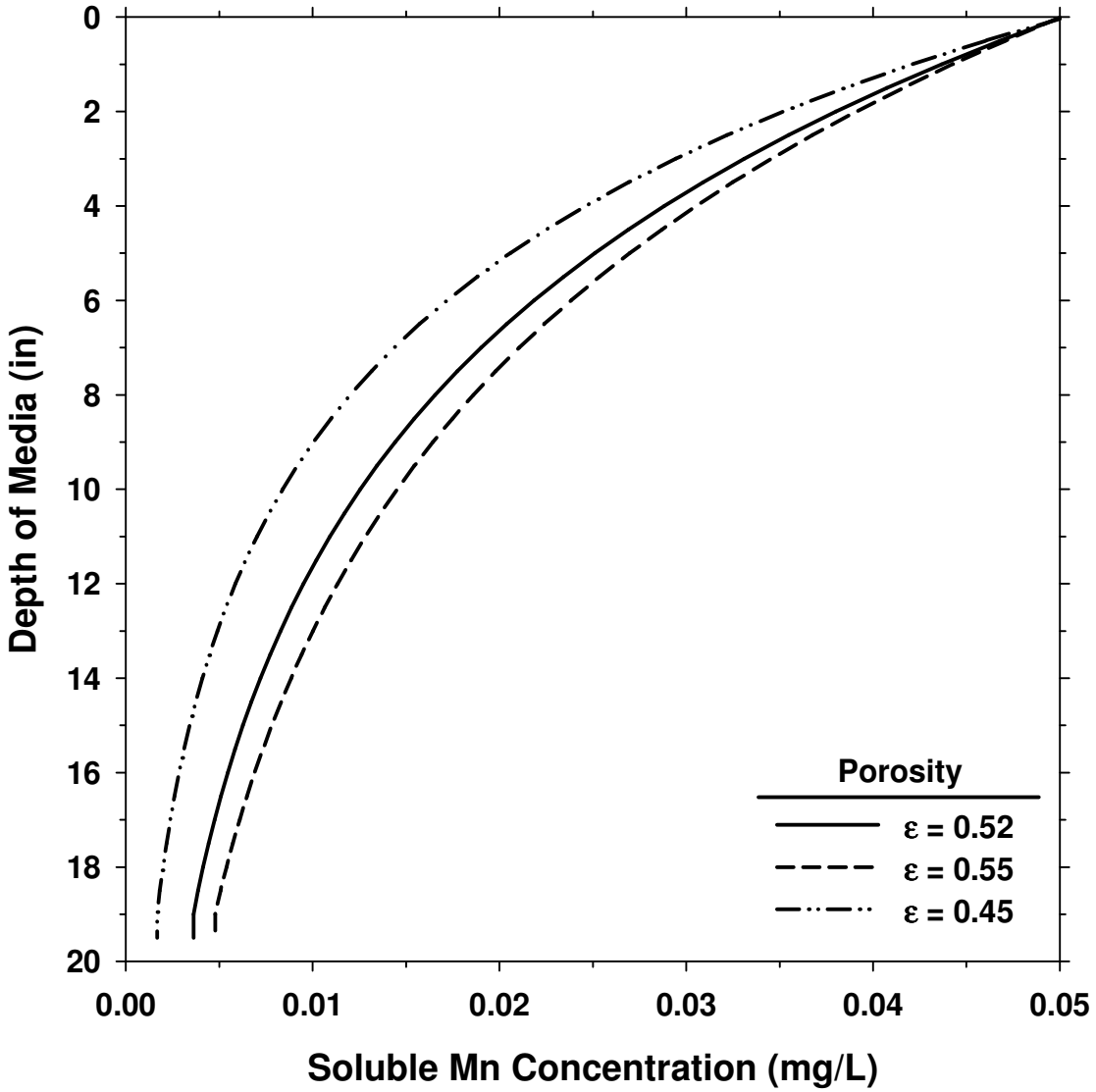

Figure 5.2 Sensitivity analysis: effect of porosity on model output

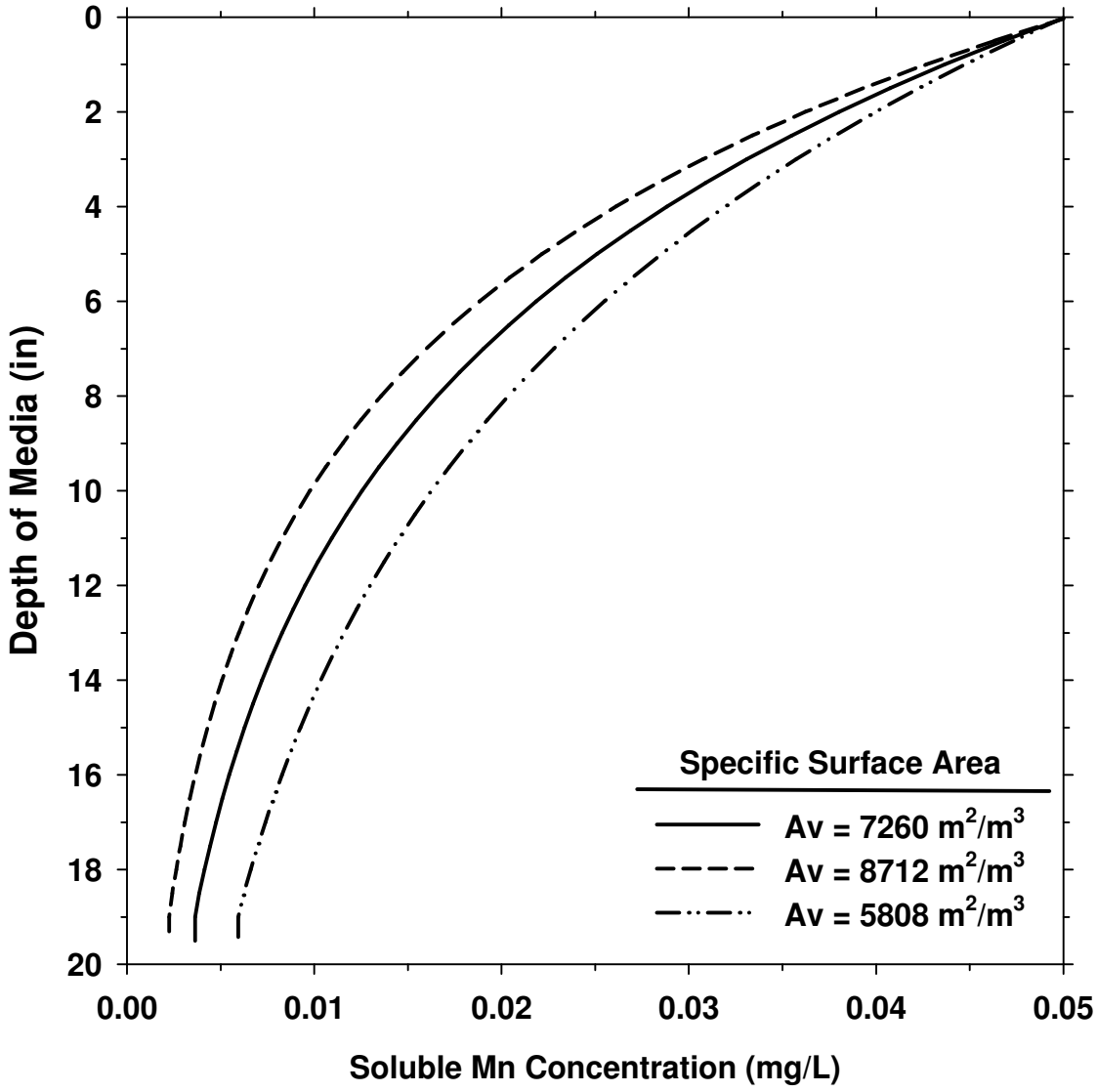

Figure 5.3 Sensitivity analysis: effect of specific surface area on model output

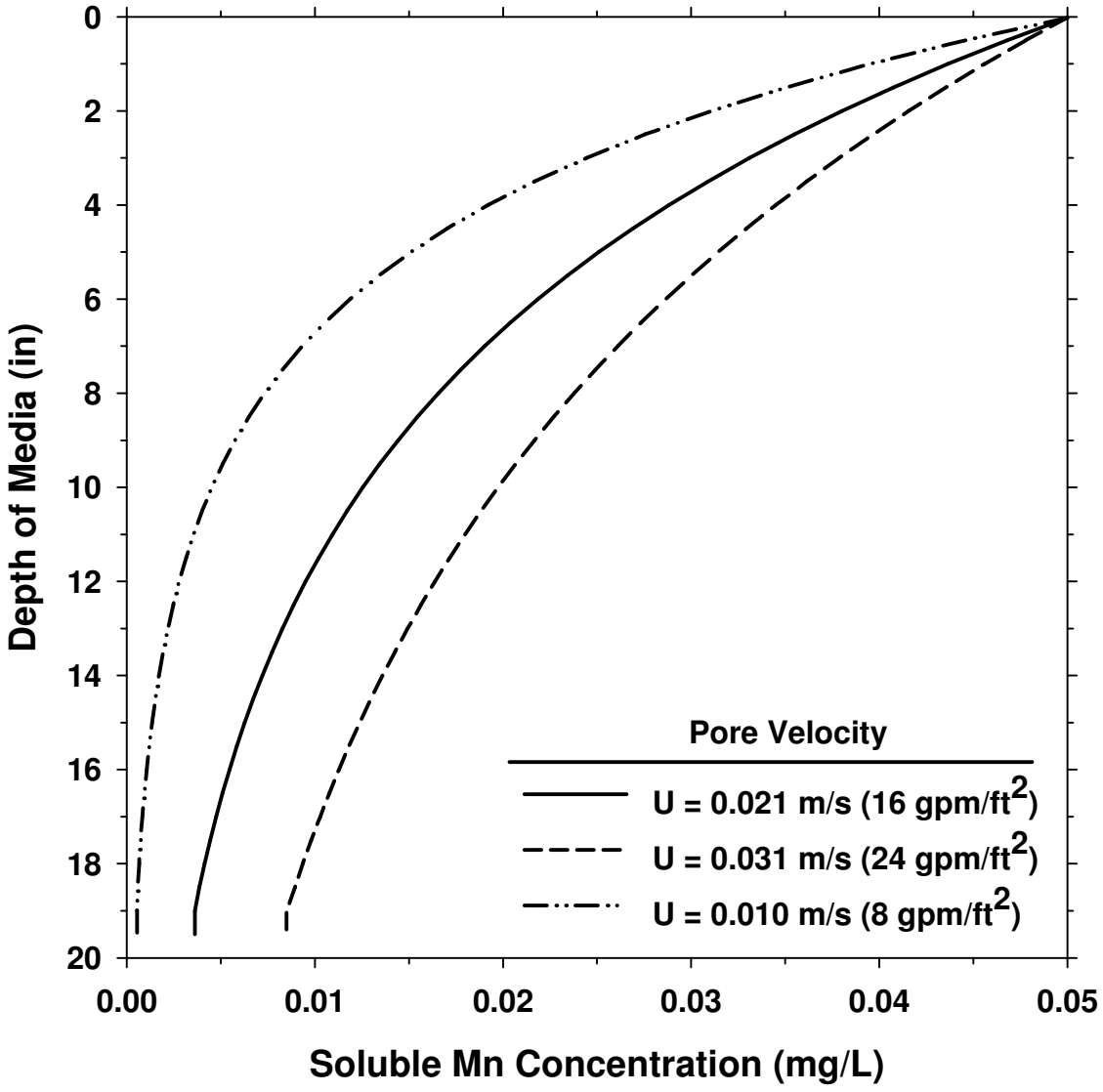

Figure 5.4 Sensitivity analysis: effect of pore velocity on model output

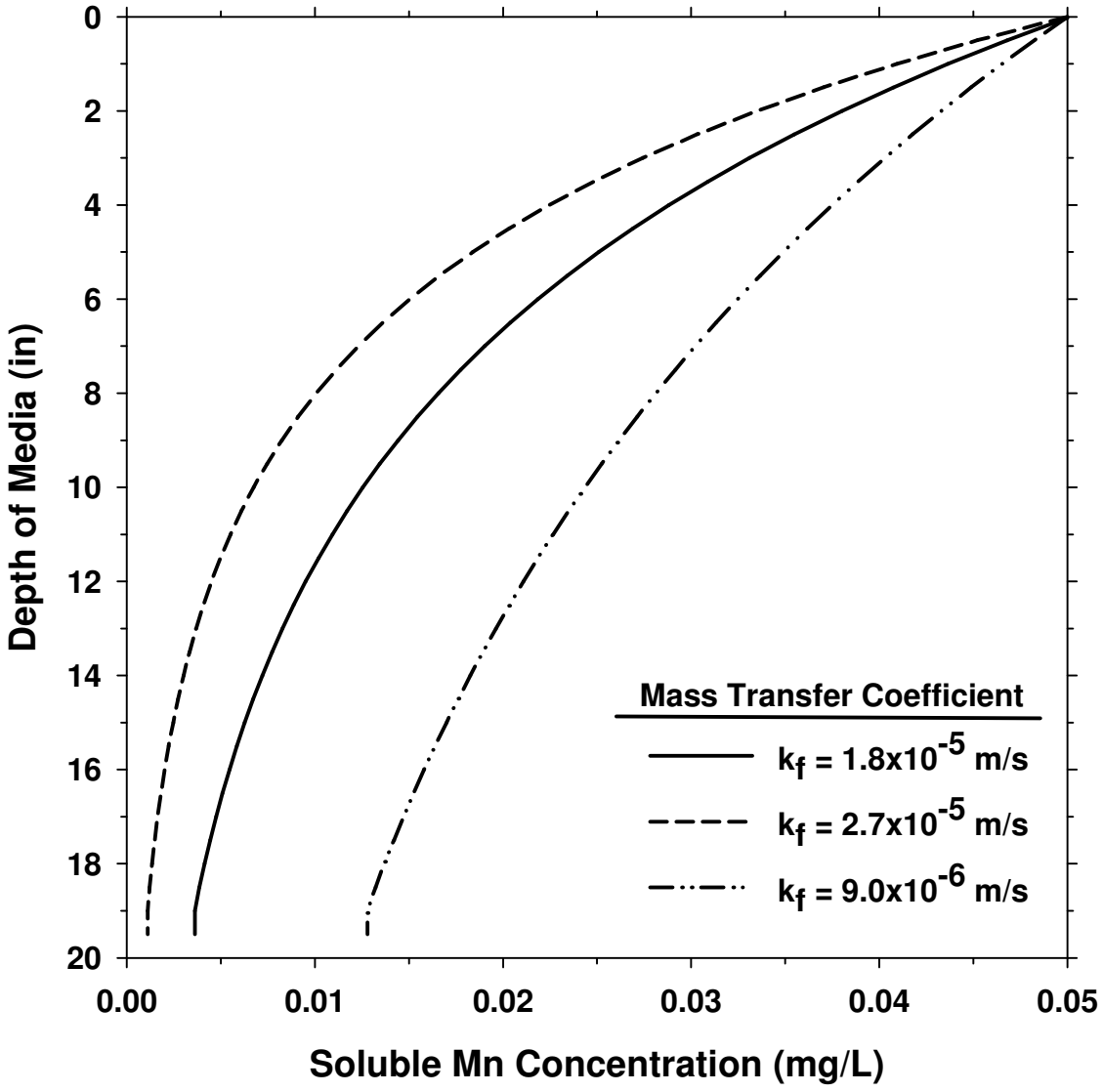

Figure 5.5 Sensitivity analysis: effect of mass transfer coefficient on model output

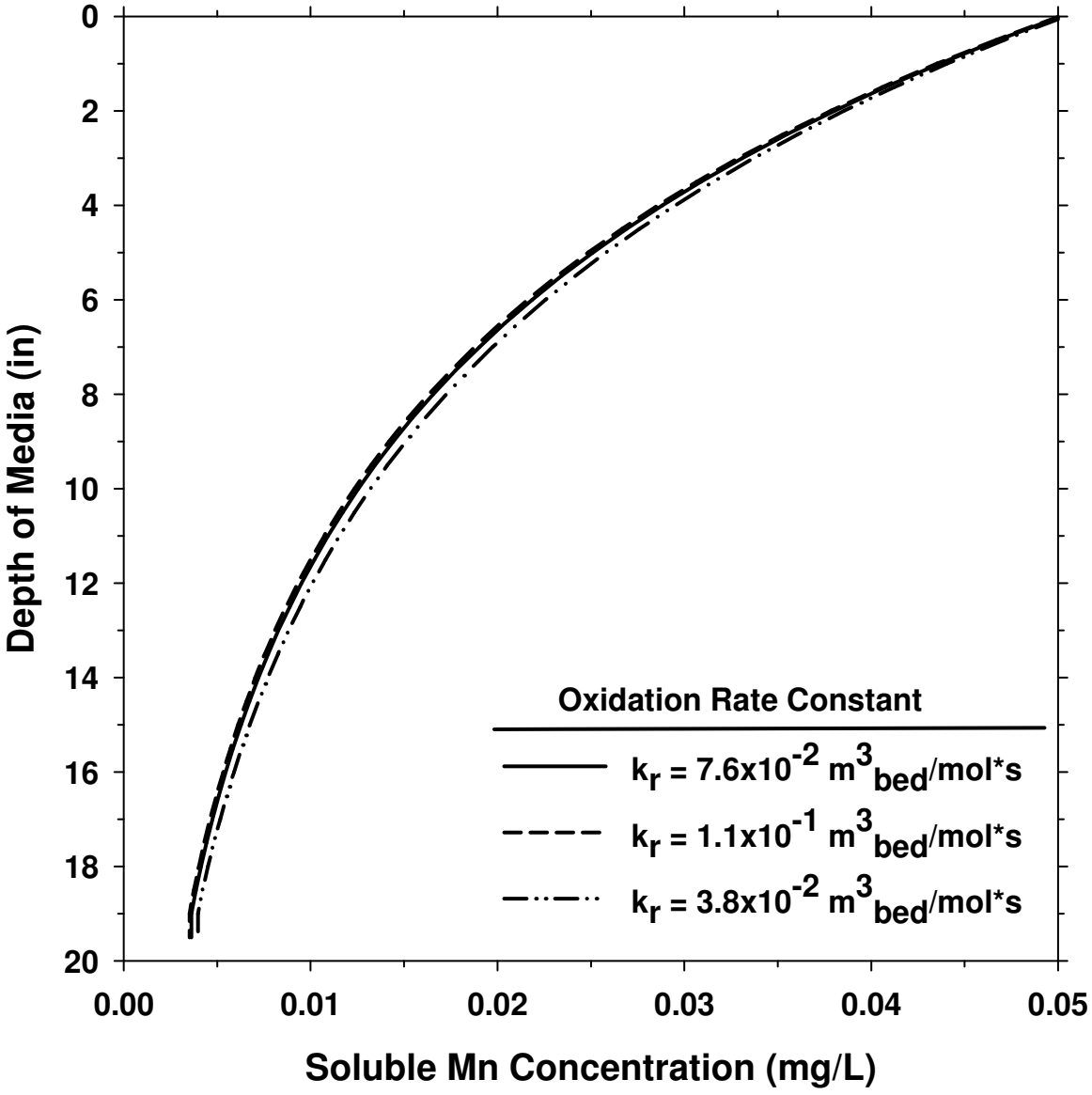

Figure 5.6 Sensitivity analysis: effect of oxidation rate constant on model output

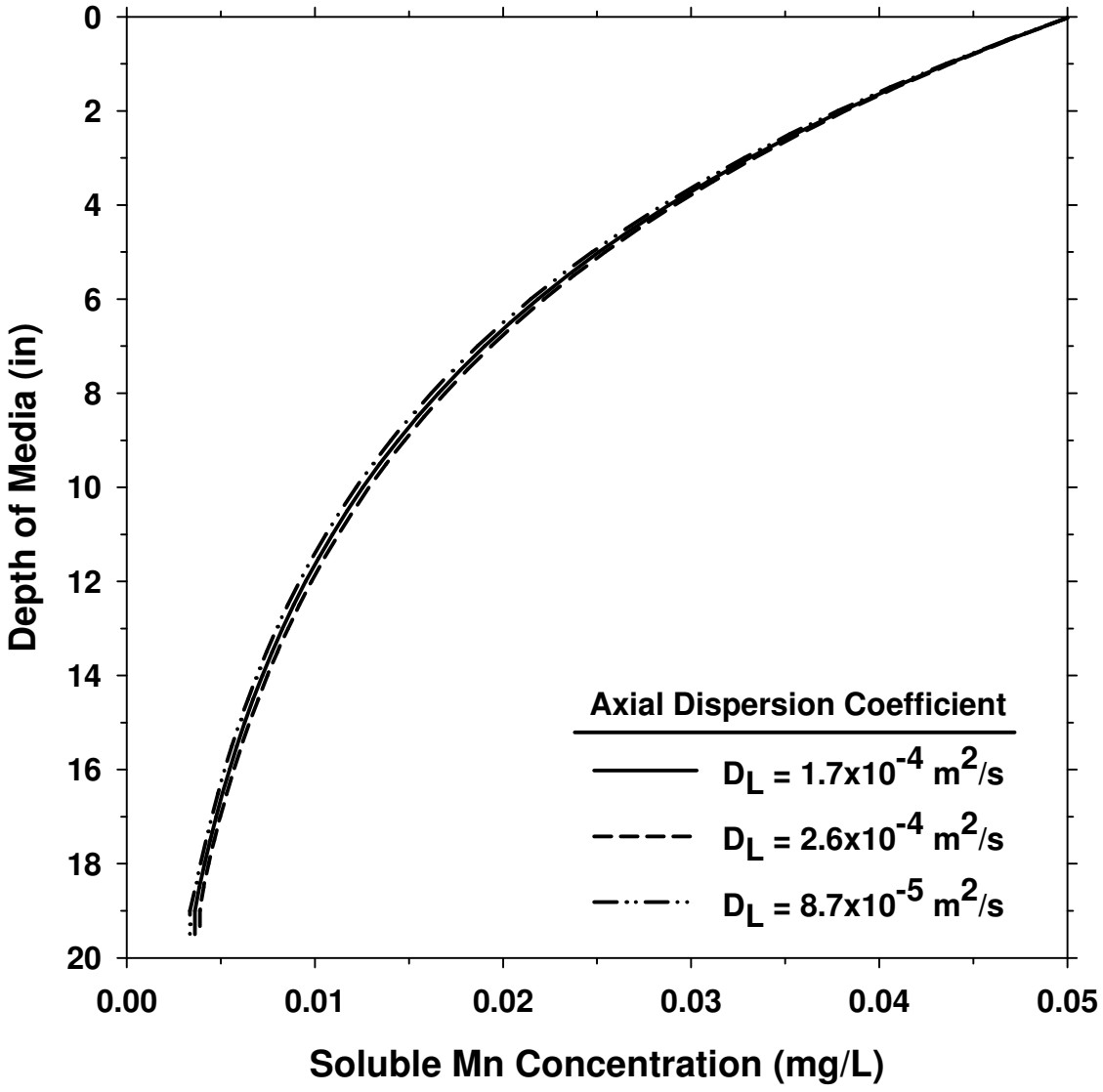

Figure 5.7 Sensitivity analysis: effect of axial dispersion coefficient on model output

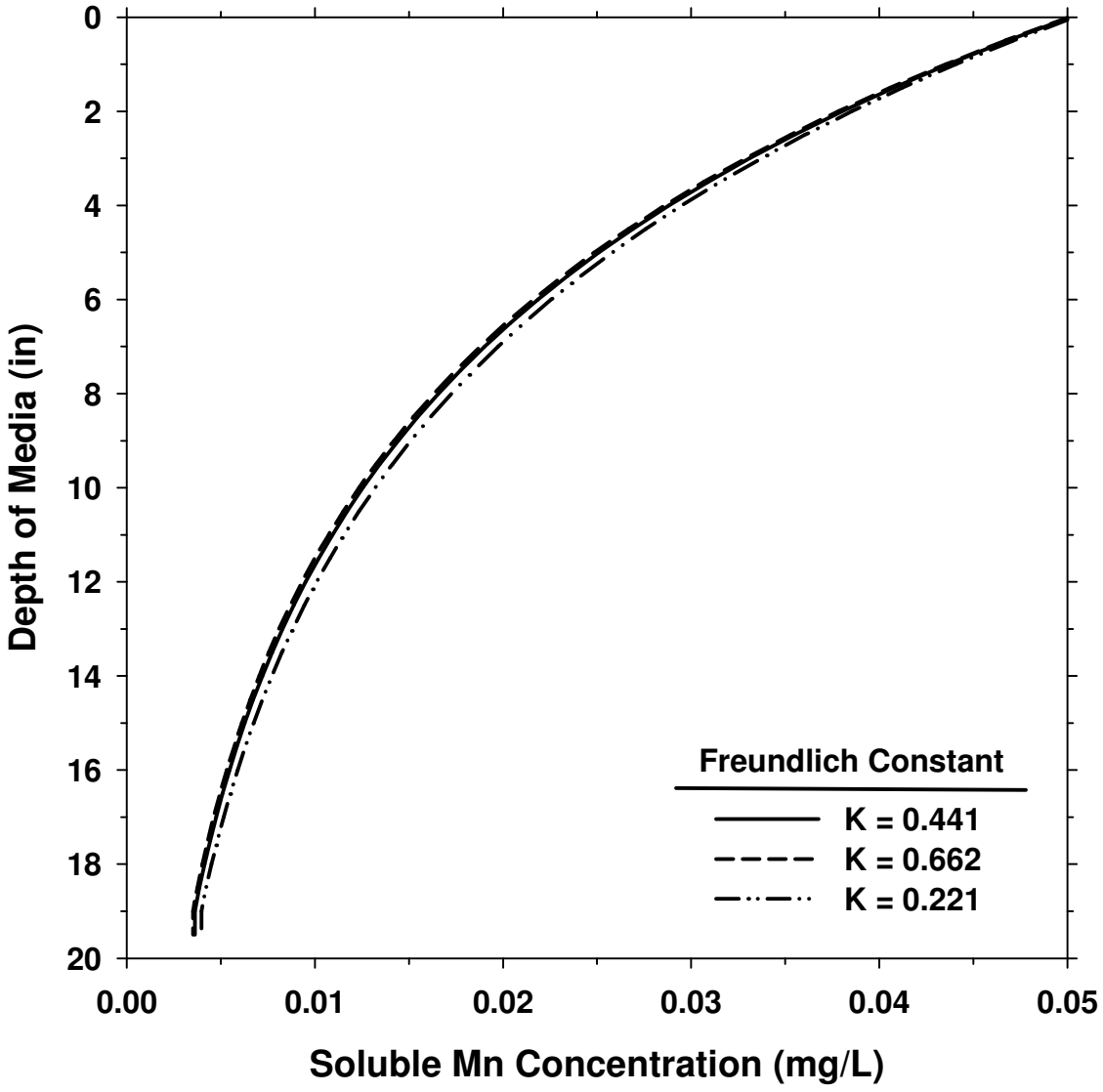

Figure 5.8 Sensitivity analysis: effect of K (Freundlich constant) on model output

CHAPTER 6
DISCUSSION

The purpose of this chapter is to discuss and summarize the results presented in this thesis as well as to relate the findings of this research effort to those published by others in the literature.

Laboratory data from contactor column experiments present the effect of operating parameters on the soluble Mn removal profile across a media bed. Free chlorine concentrations of greater than 1.0 mg/L were required for adequate soluble Mn removal; furthermore, increased concentrations generally improved the soluble Mn removal profile. A slightly alkaline bulk solution pH (7.0-8.0) provided a greater percentage of soluble Mn removal across the contactor depth than a mildly acidic pH (6.3-6.7). Increasing the initial soluble Mn concentration had a slightly positive effect on the soluble Mn removal profile. An increase in HLR did not show a negative effect on the soluble Mn removal profile. The effect of these operating parameters on the soluble Mn removal profile are consistent with earlier research (Morgan and Stumm 1964; Knocke *et al.* 1988; Knocke *et al.* 1990; Knocke *et al.* 1991; Coffey *et al.* 1993).

The process of removing soluble Mn by adsorption and oxidation onto oxide-coated filter media has been proven to be an effective removal technique under previous research conditions of HLR between 2-10 gpm/ft^2 with sand and anthracite filter media. Laboratory data presented in this thesis has also proven that this process is effective under conditions of HLR between 16-24 gpm/ft^2 with large-sized media grains (2.0-6.4 mm diameter).

However, there are differences in the soluble Mn removal performance between the three different media types investigated in this research. Data plotted in Figure 6.1 compare the performance of torpedo sand to pyrolucite at a HLR of 16 gpm/ft^2 and a slightly acidic pH of 6.6. The full depth of torpedo sand media removed approximately 50% of the initial soluble Mn, whereas pyrolucite media removed 50% of the initial soluble Mn concentration in the top three inches of contactor depth. Over the full bed depth, pyrolucite removed 90% of the initial soluble Mn concentration. Data plotted in Figure 6.2 compare the performance of gravel to pyrolucite at a HLR of 20 gpm/ft^2 and a slightly alkaline pH of 7.5-7.6. The results were similar to the data plotted in Figure 6.1, with gravel removing a total of 50% and pyrolucite removing a total of 90% of the initial soluble Mn concentration. When compared at a HLR of 20 gpm/ft^2 and a slightly alkaline pH of 7.5-7.6, data plotted in Figure 6.3 show torpedo sand removing approximately 10% more of the initial soluble Mn concentration than gravel.

Earlier research attributed these differences in soluble Mn removal performance to the amount of extractable oxide-coating present on the media (Coffey *et al.* 1993). However, while pyrolucite media does have a greater amount of extractable MnO_x-coating (11-25 mg/g media) than the gravel (0.2-0.5 mg/g media) or torpedo sand (0.2-0.5 mg/g media), the performance differences could not be correlated with observed differences in extractable Mn-oxide coating. Recent research has shown that the soluble Mn removal performance of oxide-coated media is more directly related to the soluble Mn uptake capacity (Bouchard 2005). As the MnO_x-coating develops on the media grain, previously available sites become inaccessible under the oxide layers (Merkle *et al.* 1997a; Merkle *et al.* 1997b; Bouchard 2005; Goodwill 2006). Therefore, the amount of available adsorption sites on the media surface may in fact control the soluble Mn removal performance of the media.

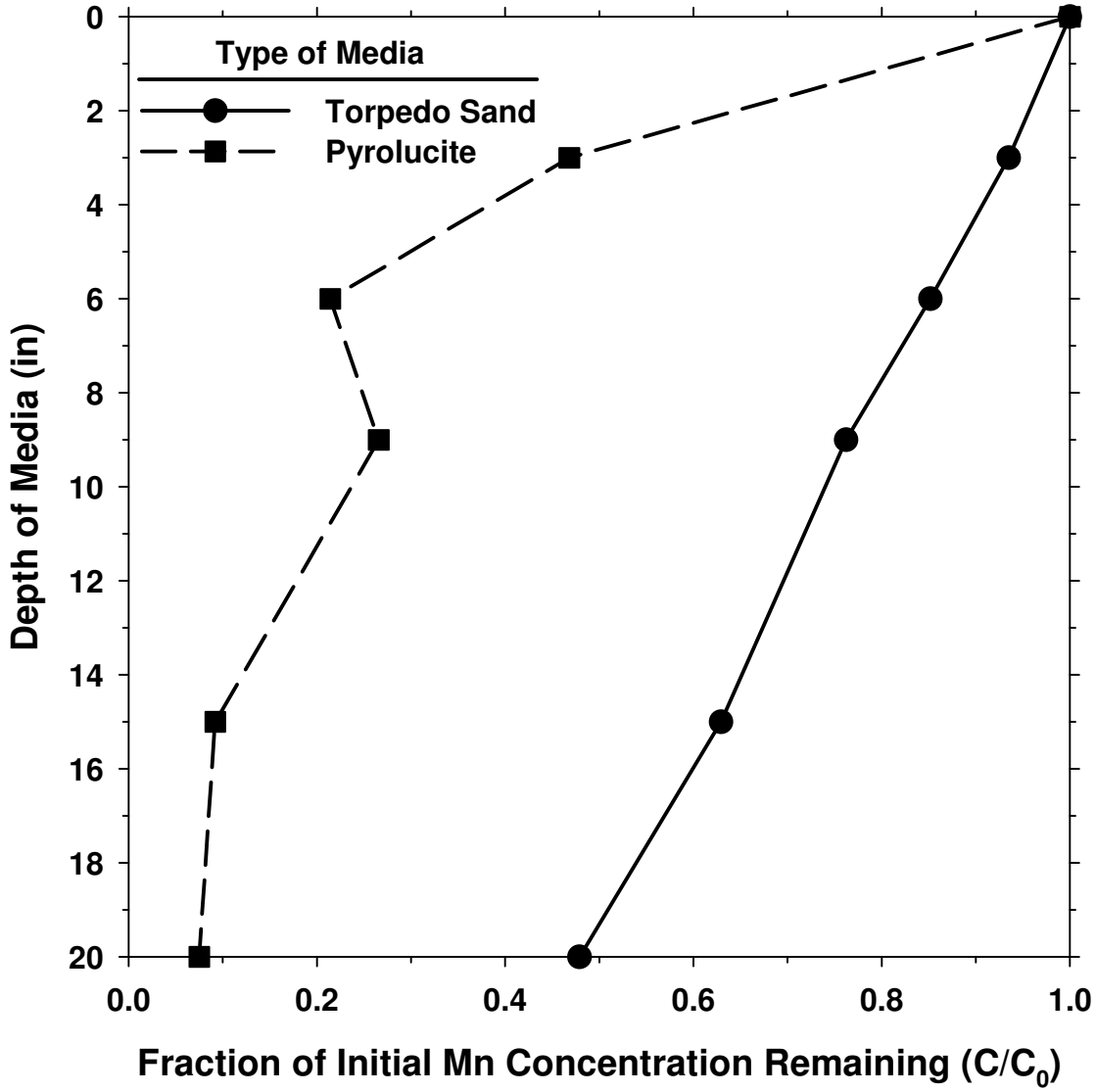

Figure 6.1 Media performance comparison (Influent water: HLR=16 gpm/ft^2, HOCl=1.6-1.7 mg/L, pH=6.6, Mn^{2+}=0.09 mg/L)

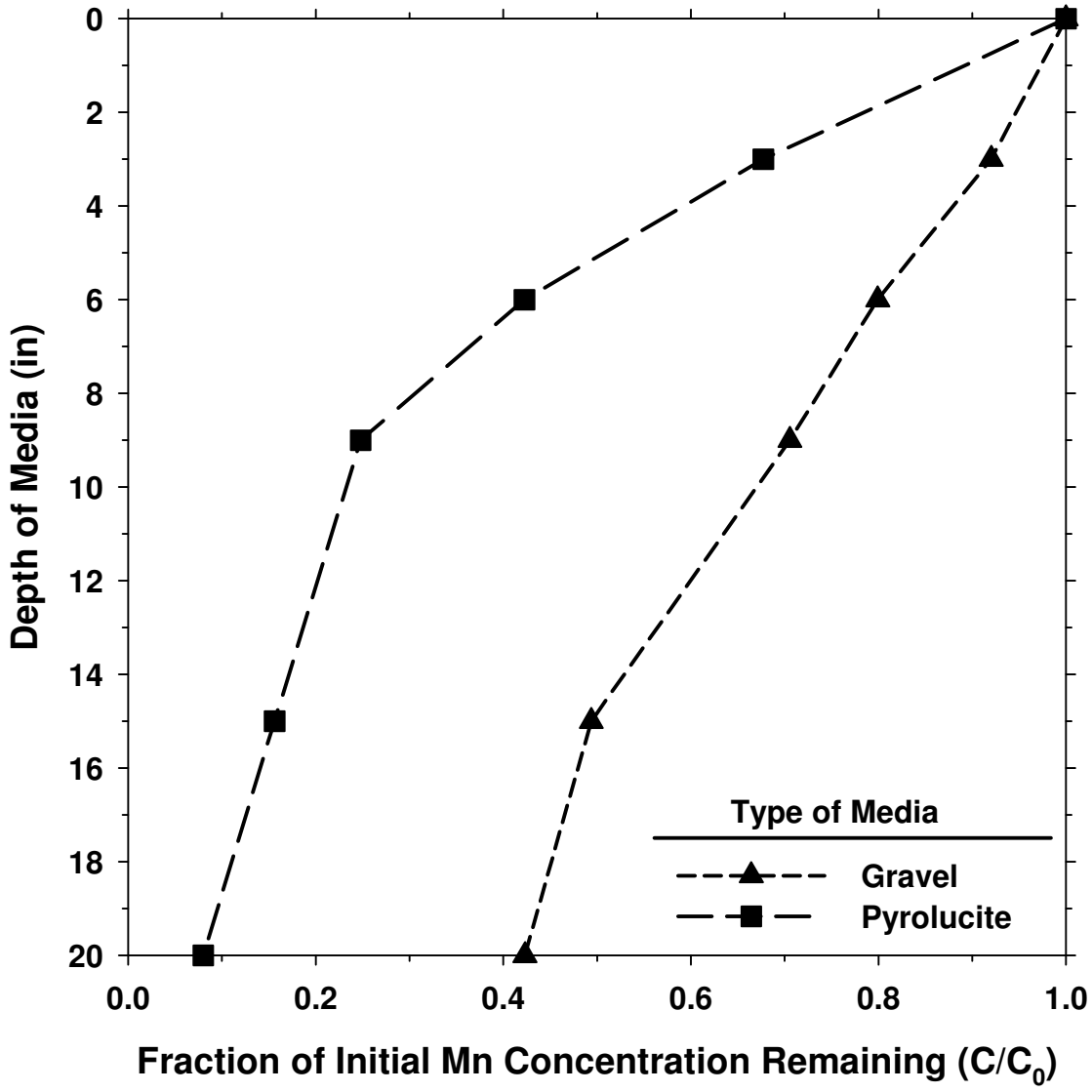

Figure 6.2 Media performance comparison (Influent water: HLR=16 gpm/ft^2, HOCl=1.8-1.9 mg/L, pH=7.5-7.6, Mn^{2+}=0.09-0.10 mg/L)

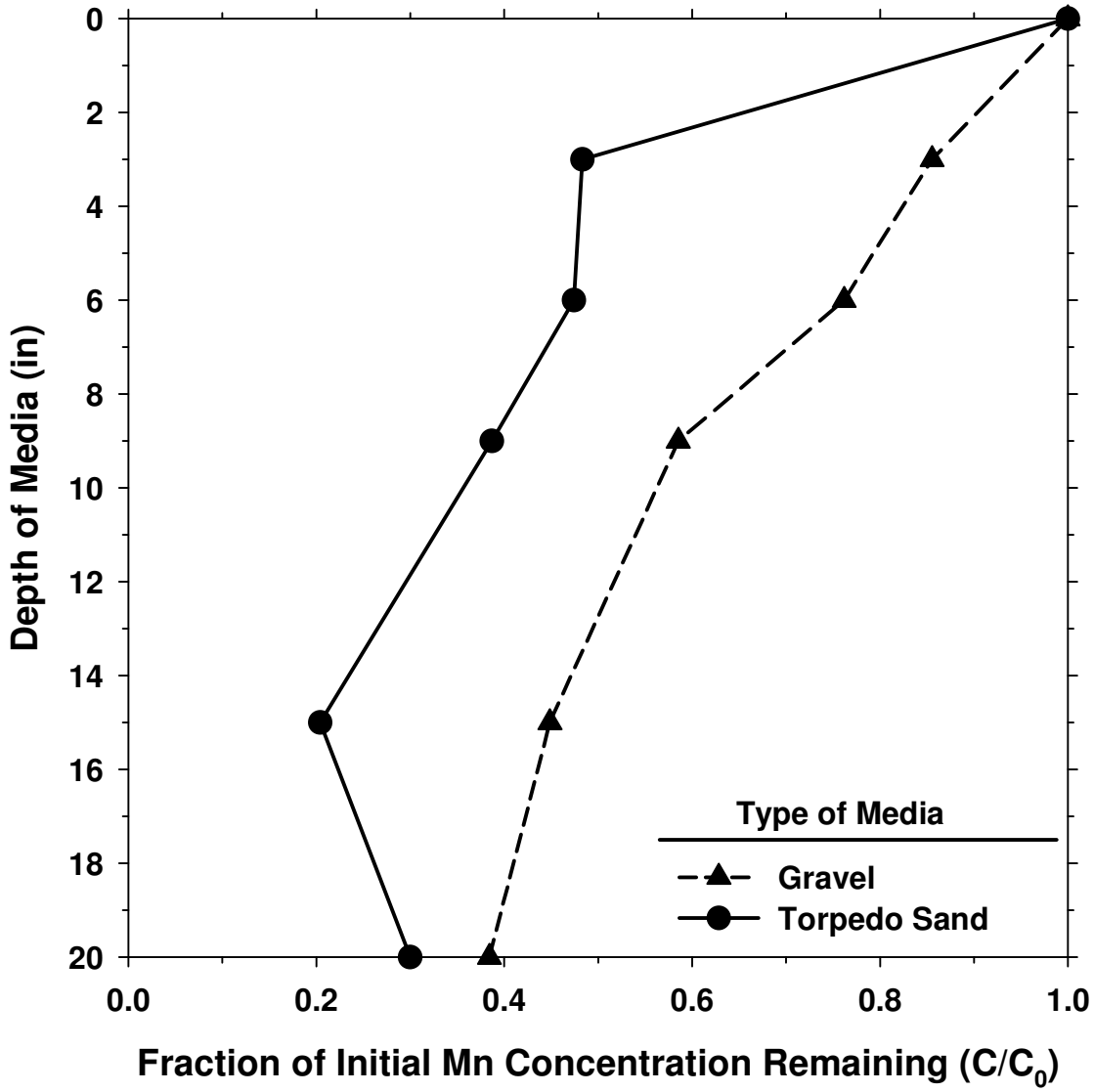

Figure 6.3 Media performance comparison (Influent water: HLR=20 gpm/ft^2, HOCl=1.4-1.5 mg/L, pH=7.5-7.6, Mn^{2+}=0.04-0.05 mg/L)

Data from the soluble Mn uptake capacity experiments shown in Chapter 4 present the different media capacities as a measure of milligrams soluble Mn adsorbed per gram media. This measurement was converted to a measure of milligrams soluble Mn adsorbed per liter of bed volume as shown in Equation 6.1.

$$Capacity_B = Capacity_A * SG * (1- \varepsilon) \quad (6.1)$$

where: SG = Specific gravity
$Capacity_A$ = Soluble Mn uptake capacity (mg Mn/g_{media})
$Capacity_B$ = Soluble Mn uptake capacity (mg Mn/L_{bed})

The soluble Mn uptake capacity measurement was able to be compared across media types in this form. For example, the soluble Mn uptake capacities measured for used media at a bulk solution concentration of 0.03-0.04 mg Mn/L are included in Table 6.1. Pyrolucite uptake capacity is approximately two times the soluble Mn uptake capacity of torpedo sand and three times the soluble Mn uptake capacity of the gravel. Therefore, pyrolucite media is capable of adsorbing three times the mass of soluble Mn per unit bed depth of gravel. Soluble Mn removal profiles presented previously in this report showed soluble Mn concentrations as a function of cumulative media depth. Using the soluble Mn uptake capacity in mg Mn per L bed volume, soluble Mn removal profiles can be presented as soluble Mn concentrations as a function of cumulative soluble Mn uptake capacity. Cumulative soluble Mn uptake capacities were calculated as shown in Equation 6.2.

$$CC = D * 0.1158 \frac{L}{in} * Capacity_B \quad (6.2)$$

where: CC = Cumulative soluble Mn uptake capacity (mg Mn)
D = Cumulative depth of media (in)

Data plotted in Figure 6.4 present the results of pilot-scale experiments conducted at an initial Mn concentration of 0.03-0.04 mg/L. Using the values provided in Table 6.1, soluble Mn concentrations were plotted as a function of cumulative soluble Mn uptake capacity. The appropriate isotherm constants were applied to the calculations as the media was considered to be "used." Pyrolucite media had a large soluble Mn uptake capacity per bed volume. Therefore, the pyrolucite media had a larger overall cumulative soluble Mn uptake capacity which translated to more soluble Mn removal than either gravel or torpedo sand media.

Table 6.1
Soluble Mn uptake capacity in a bulk solution Mn concentration of 0.03-0.04 mg/L

Media	Mn uptake capacity (mg Mn/L media)
Pyrolucite	0.055
Gravel	0.020
Torpedo Sand	0.026

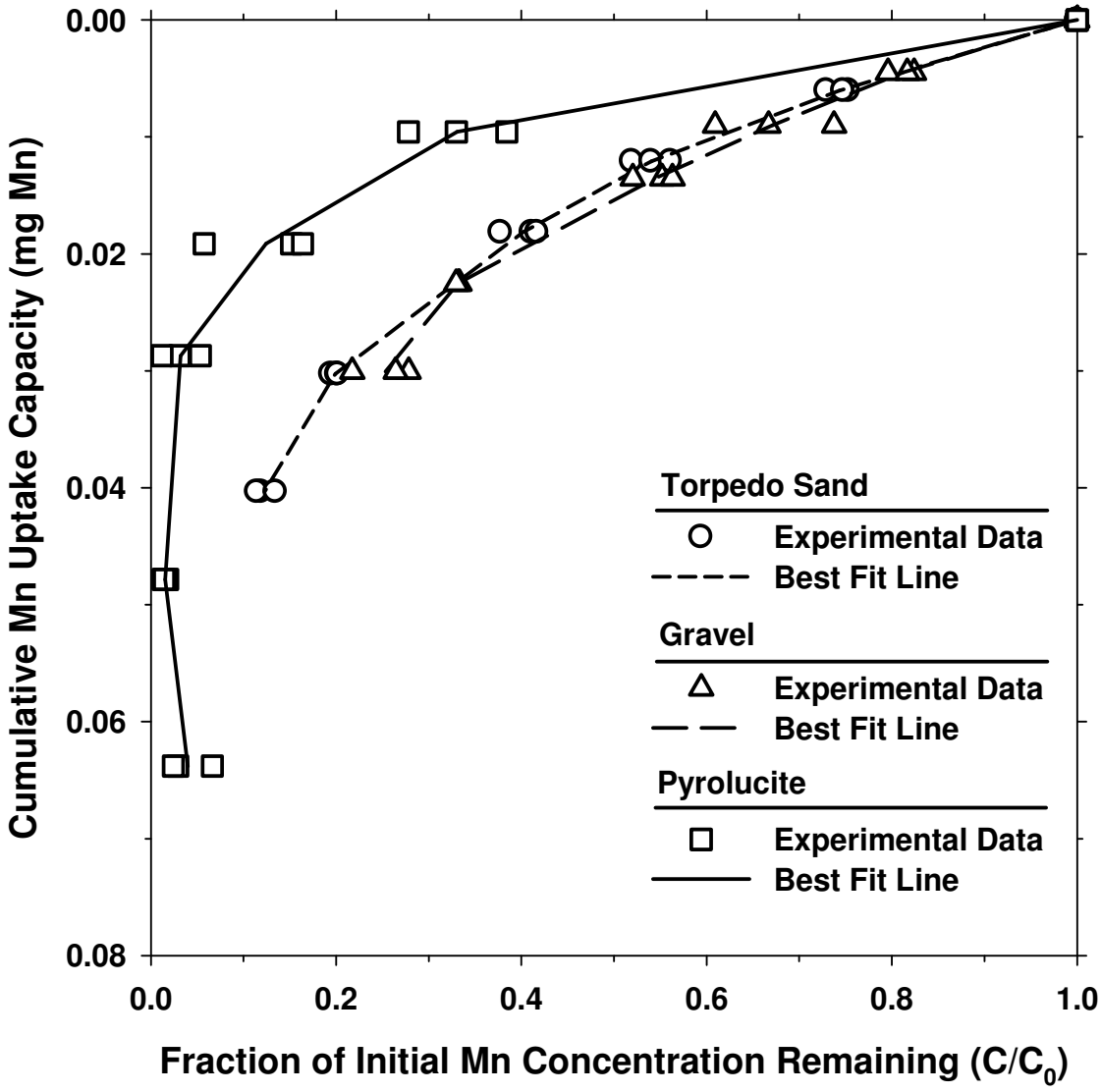

Figure 6.4 Differences in cumulative Mn uptake capacity and Mn removal performance across three used media types (Influent water: HLR=16 gpm/ft^2, HOCl=1.2-2.8 mg/L, pH=7.2, Mn^{2+}=0.03-0.04 mg/L)

Data plotted in Figure 6.2 were plotted again in Figure 6.5 as a function of cumulative soluble Mn uptake capacity. Although, new pyrolucite had three times the soluble Mn uptake capacity of new gravel, data plotted in Figure 6.5 show that the media perform in a similar manner when considering the available cumulative soluble Mn uptake capacity.

The improved soluble Mn removal by pyrolucite was due to increased soluble Mn uptake capacity per bed volume. Data plotted in Figure 6.5 show that the pyrolucite had as much soluble Mn uptake capacity in the top three inches of media bed as the gravel media had in the top nine inches. Researchers have hypothesized that soluble Mn uptake capacity is available on the surface of the media (Bouchard 2005; Goodwill 2006). Therefore, increased pyrolucite soluble Mn uptake capacity could be related to its larger specific surface area.

Soluble Mn uptake capacity was implemented in the model through the use of the Freundlich isotherm. The isotherm constants K and 1/n were determined from the soluble Mn uptake capacity experiments as discussed previously in Chapter 4. Further analysis was conducted to determine the extent to which soluble Mn uptake capacity affected the model prediction for a certain type of media. Using the same parameters provided in Table 5.4 and varying only the Freundlich isotherm constants, data plotted in Figure 6.6 compare model predictions for the same characteristic media with decreased Mn uptake capacity. No significant difference was determined between the Mn removal profiles. This suggested that the pyrolucite media has an increased soluble Mn uptake capacity per bed volume due to the increased surface area per volume.

Therefore, recommendations for media type used in a soluble Mn removal contactor should balance the need for sufficient specific surface area and the ability to apply HLR of $\geq$16gpm/ft^2 with minimal head loss. An increased HLR applied to the media bed would be beneficial to the utility by decreasing the required contactor footprint and incurring capital investment savings. The mass transfer coefficient, k_f, was related to HLR and an increase in HLR should increase this value, as was observed when fitting this parameter to the experimental data. However, a correlation between the increase ratio of both HLR and k_f was not determined. Further research evaluating the correlation between HLR and k_f could be conducted to improve this model prediction capability at HLR of $\geq$16 gpm/ft^2.

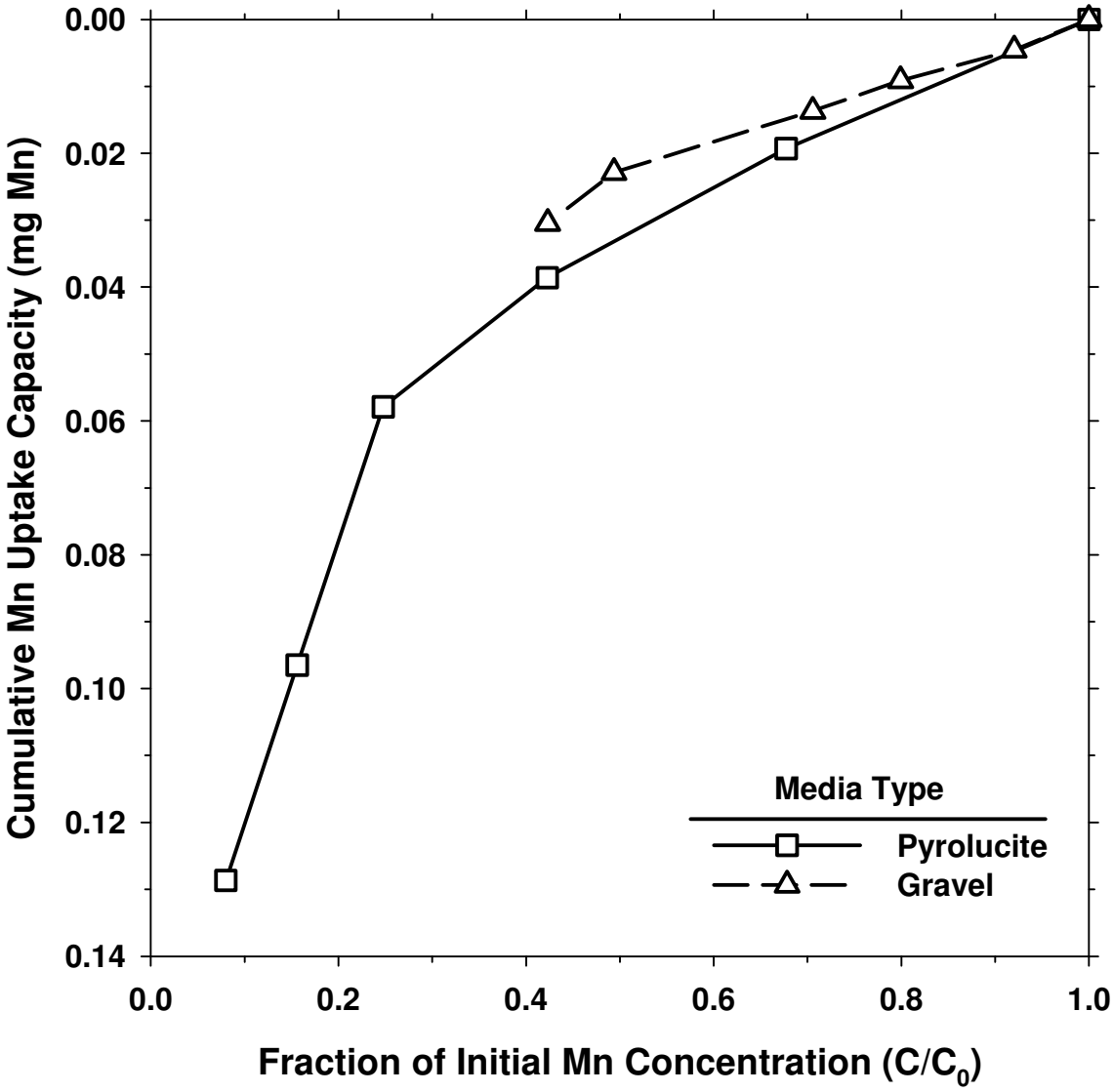

Figure 6.5 Difference in cumulative Mn uptake capacity across two new media types (Influent water: HLR=16 gpm/ft^2, HOCl=1.8-1.9 mg/L, pH=7.5-7.6, Mn^{2+}=0.09-0.10 mg/L)

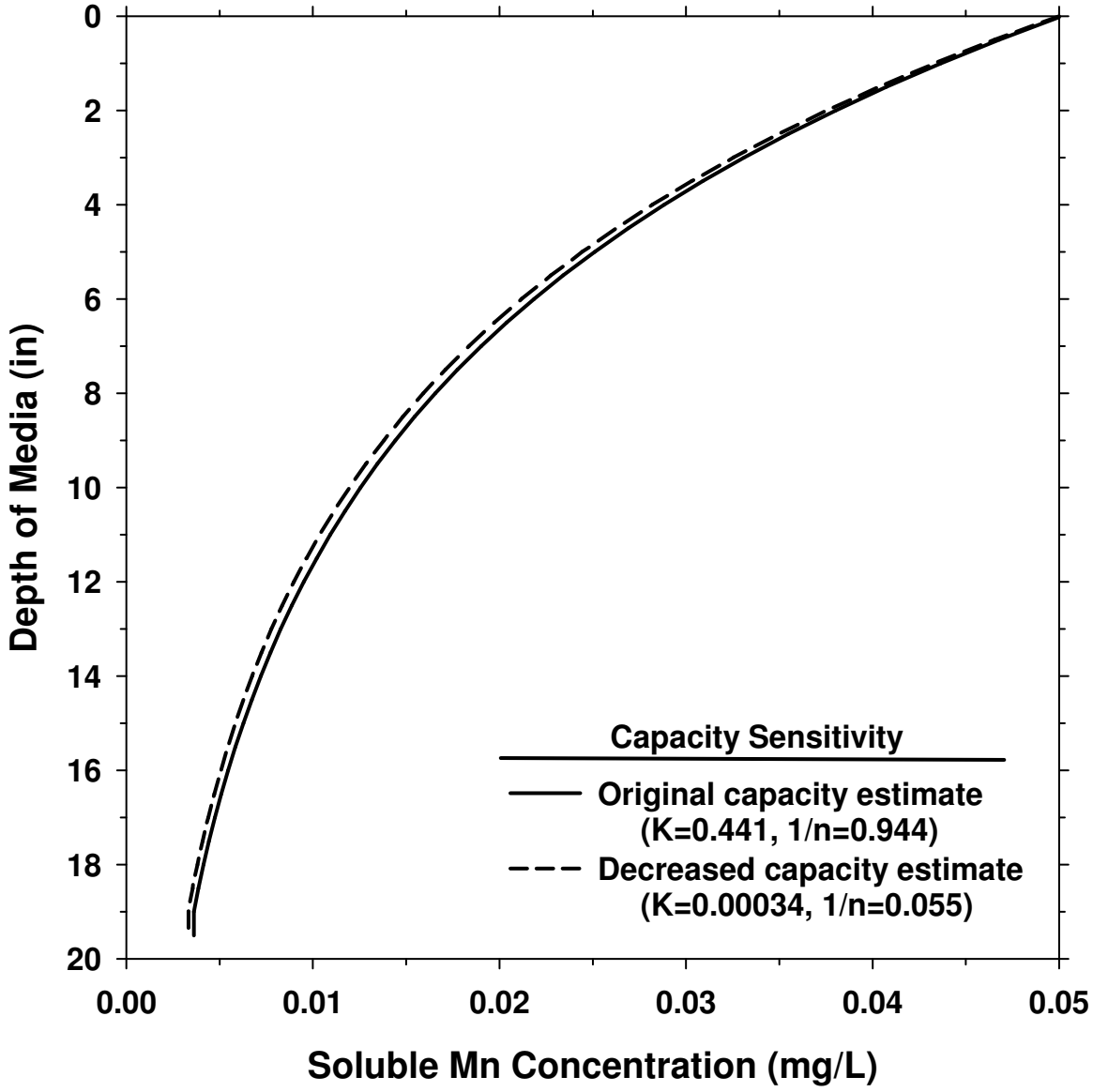

Figure 6.6 Sensitivity of Mn uptake capacity on model prediction for a characteristic media

CHAPTER 7
SUMMARY AND CONCLUSIONS

The objectives of this research involved both experimental data collection and model development and analysis with the overall goal of developing recommendations for implementation of a post-filtration contactor for soluble Mn removal. Laboratory-scale and pilot-scale experiments were conducted to determine the impact of important operational parameters such as initial Mn concentration, free chlorine concentration, hydraulic loading rate and pH on overall Mn removal performance. These parameters were evaluated across three oxide-coated media types: commercially available pyrolucite, MnO_x(s)-coated gravel, and MnO_x(s)-coated torpedo sand. In addition, efforts were undertaken to develop a model based on first principles that could effectively predict contactor performance for soluble Mn removal. Based upon the results obtained in this research effort, the following conclusions were formulated:

CONCLUSIONS

- The process of removing soluble Mn by adsorption and oxidation onto oxide-coated filter media is effective under conditions of HLR = 16-24 gpm/ft^2 with large-sized media grains (2.0-6.4 mm diameter). This validates the use of oxide-coated media under more strenuous conditions than have previously been used in association with traditional filtration applications.

- Four important operation parameters affected the Mn removal profiles across contactor media beds:

    - Free chlorine concentrations of greater than 1.0 mg/L were required for effective soluble Mn removal; furthermore, increased free chlorine concentrations generally improved the soluble Mn removal profile. The presence of free chlorine provides the oxidant required for available sorption site regeneration at the media surface.
    - A slightly alkaline bulk solution pH (7.0-8.0) provided a greater percentage of soluble Mn removal across the contactor depth than a mildly acidic pH (6.3-6.7). Alkaline pH promotes adsorption by increasing the amount of available Mn adsorption sites on the media (Morgan and Stumm 1964).
    - Increasing the initial soluble Mn concentration flow had a slightly positive effect on the soluble Mn removal profile. An increased soluble Mn concentration in solution provides a slightly larger driving force between the bulk solution concentration and concentration at the surface of the media.
    - An increase in HLR did not show a large negative effect on the soluble Mn removal profile. It is important for the successful application of Mn removal via adsorption in a contactor unit that increased HLR does not greatly affect the Mn removal process.

- Overall, pyrolucite media provided the best Mn removal of 80-90% of the initial Mn concentration. Oxide-coated gravel and oxide-coated torpedo sand did provide Mn removal but at a less consistent removal of 50-70% of the initial Mn concentration depending on pH and free chlorine concentration.

- The model developed in this report showed that Mn removal depended on the specific surface area of the contactor media, HLR, and the mass transfer coefficient at the concentrations of Mn expected at a water treatment facility (<0.3 mg/L).

RECOMMENDATIONS

Implementation of an oxide-coated media contactor for soluble Mn removal is recommended for water treatment facilities with certain manganese treatment concerns. These concerns may be related to a removal of the free chlorine residual across the filtration beds which previously had controlled the amount of soluble Mn leaving the facility. The location of the contactor downstream of the filters would ensure that any additional Mn released during the treatment process would be removed as well as provide minimal opportunity for clogging due to solid particles.

Contactor operation is recommended at HLR $\geq$16 gpm/ft^2 with an initial free chlorine concentration of 1.0-2.0 mg/L and a slightly alkaline pH of 7.0-8.0. High values of HLR are recommended to provide capital cost savings due to the decreased contactor footprint required. Facilities with certain disinfection by-product concerns should note that a disinfectant residual is required in the distribution system and free chlorine is often added prior to the clear well after the majority of organics have been removed from the raw water. Placing this free chlorine addition point prior to the proposed soluble Mn removal contactor is recommended for providing continuous regeneration of the oxide-coated media as well as providing the required disinfectant residual. Alkaline pH is recommended for improved Mn removal. Facilities with a slightly acidic pH due to enhanced coagulation practices should consider adjusting the pH of the finished water for corrosion control prior to the Mn removal contactor for improved Mn adsorption performance.

REFERENCES

American Water Works Association (1999). Water Quality and Treatment: A Handbook of Community Water Supplies. New York, McGraw-Hill, Inc.

Bouchard, R. (2005). Evaluation of Manganese Removal at Aquarion Water Company (AWC) Surface Water Treatment Plants. Department of Civil & Environmental Engineering. Amherst, MA, University of Massachusetts. **M.S. in Env. Eng.:** 131.

Burns, F. L. (1998). Case Study: Automatic Reservoir Aeration to Control Manganese in Raw Water Maryborough Town Water Supply Queensland, Australia. *Water Science and Technology,* 37(2):301-308.

Cerrato, J. M., L. P. Reyes, C. N. Alvarado and A. M. Dietrich (2006). Effect of PVC and iron materials in drinking water distribution systems on Mn (II) deposition. *Water Research,* 40(14):2720-2726.

Coffey, B. M., D. L. Gallagher and W. R. Knocke (1993). Modeling Soluble Manganese Removal by Oxide-coated Filter Media. *Journal of Environmental Engineering,* 119(4):679-695.

Elsner, R. and J. Spangler (2005). Neurotoxicity of inhaled manganese: Public health danger in the shower? *Medical Hypotheses,* 65:607–616.

Goodwill, J. E. (2006). Characterization of Metal Oxide Coated Filter Media. Deptment of Civil & Environmental Engineering. Amherst, MA, University of Massachusetts. **M.S. in Env. Eng.:** 115.

Hargette, A. C. and W. R. Knocke (2001). Assessment of Fate of Manganese in Oxide-Coated Filtration Systems. *Journal of Environmental Engineering,* 127(10):1132-1138.

Knocke, W. R., J. R. Hamon and C. P. Thompson (1988). Soluble Manganese Removal on Oxide-Coated Filter Media. *Journal of the American Water Works Association,* 80(12):65-70.

Knocke, W. R., R. C. Hoehn and R. L. Sinsabaugh (1987). Using Alternative Oxidants to Remova Dissolved Manganese from Waters Laden with Organics. *Journal of the American Water Works Association,* 79(3):75-79.

Knocke, W. R., S. Occiano and R. Hungate (1990). Removal of Soluble Manganese from Water by Oxide-Coated Filter Media, AWWA Research Foundation.

Knocke, W. R., S. Occiano and R. Hungate (1991). Removal of Soluble Manganese by Oxide-coated Filter Media: Sorption Rate and Removal Mechanism Issues. *Journal of the American Water Works Association,* 83(8):64-69.

Merkle, P. B., W. R. Knocke and D. L. Gallagher (1997a). Method for Coating Filter Media with Synthetic Manganese Oxide. *Journal of Environmental Engineering,* 123(7):642-649.

Merkle, P. B., W. R. Knocke, D. L. Gallagher and J. C. Little (1997b). Dynamic Model for Soluble Mn2+ Removal by Oxide-Coated Filter Media. *Journal of Environmental Engineering* 123(7):650-658.

Morgan, J. J. and W. Stumm (1964). Colloid-Chemical Properties of Manganese Dioxide. *Journal of Colloid Science,* 19:347-359.

Murdoch, F. and P. G. Smith (1999). Formation of Manganese Micro-Nodules on Water Pipeline Materials. *Water Research,* 33(12):2893-2895.

Rahman, M. A., J. Y. Huang, Y. Iwakami and K. Fujita (2000). Pursuing the effect of aeration, pH increment, and H2O2 coupled with UV irradiation on the removal efficiency of manganese by microfilter membrane. *Water Science and Technology* 41(10-11):25-31.

Reckhow, D. A., W. R. Knocke, M. J. Kearney and C. A. Parks (1991). Oxidation of Iron and Mangnaese by Ozone. *Ozone Science and Engineering,* 13:675-695.

Roberts, P. V., P. Cornel and R. S. Summers (1985). External Mass-Transfer Rate in Fixed-Bed Adsorption. *Journal of Environmental Engineering,* 11(6):891-905.

Rona, P. A. (2003). Resources of the Sea Floor. Science. **299:** 673-674.

Sly, L. I., M. C. Hodgkinson and V. Arunpairojana (1990). Deposition of Manganese in a Drinking Water Distribution System. *Applied and Environmental Microbiology,* 56(3):628-639.

Spangler, J. and R. Elsner (2006). Commentary on possible manganese toxicity from showering: Response to critique. *Medical Hypotheses,* 66:1231–1233.

Suzuki, T., Y. Watanabe, G. Ozawa and S. Ikeda (1998). Removal of soluble organics and manganese by a hybrid MF hollow fiber membrane system. *Desalination,* 117:119-130.

Trace Inorganic Substances Committee (1987). Committee Report: Research Needs for the Treatment of Iron and Manganese. *Journal of the American Water Works Association,* 79(9):119-122.

U.S. Environmental Protection Agency (2003). Contaminant Candidate List Regulatory Determination Support Document for Manganese. Washington, DC 20460, Office of Water (4607M), Standards and Risk Management Division.

Wakao, N. and T. Funazkri (1978). Effect of Fluid Dispersion Coefficients on Particle-to-Fluid Mass Transfer Coefficients in Packed Beds. *Chemical Engineering Science,* 33:1375-1384.

Wong, J. M. (1984). Chlorination-Filtration for Iron and Manganese Removal. *Journal of the American Water Works Association,* 76(1):76-79.

COPYPRIGHT PERMISSIONS

Figure 2.1 – Reprinted from *Journal of Colloid Science,* Volume 19, Morgan J.J. and W. Stumm, Colloid-Chemical Properties of Manganese Dioxide, 347-359, Copyright 1964, with permission from Elsevier.

Figure 2.2 – Reprinted from Knocke, W. R., J. R. Hamon and C. P. Thompson (1988). Soluble Manganese Removal on Oxide-Coated Filter Media. *Journal of the American Water Works Association,* 80(12):65-70., with permission from AWWA.

Figures 2.3, 2.4, & 2.5 – Reprinted from Knocke, W. R., S. Occiano and R. Hungate (1991). Removal of Soluble Manganese by Oxide-coated Filter Media: Sorption Rate and Removal Mechanism Issues. *Journal of the American Water Works Association,* 83(8):64-69., with permission from AWWA.

Figure 2.6 – Reprinted from Bouchard, R. (2005). Evaluation of Manganese Removal at Aquarion Water Company (AWC) Surface Water Treatment Plants. Department of Civil & Environmental Engineering. Amherst, MA, University of Massachusetts. **M.S. in Env. Eng.:** 131., with permission from R. Bouchard.

Figures 2.7 & 2.8 – Reprinted from Hargette, A. C. and W. R. Knocke (2001). Assessment of Fate of Manganese in Oxide-Coated Filtration Systems. *Journal of Environmental Engineering,* 127(10):1132-1138., with permission from ASCE.
This material may be downloaded for personal use only. Any other use requires prior permission of the American Society of Civil Engineers. This material may be found at http://scitation.aip.org/getabs/servlet/GetabsServlet?prog=normal&id=JOEEDU000127000012001132000001&idtype=cvips&gifs=yes.

Figure 2.9 – Reprinted from Merkle, P. B., W. R. Knocke, D. L. Gallagher and J. C. Little (1997b). Dynamic Model for Soluble Mn2+ Removal by Oxide-Coated Filter Media. *Journal of Environmental Engineering* 123(7):650-658., with permission from ASCE.
This material may be downloaded for personal use only. Any other use requires prior permission of the American Society of Civil Engineers. This material may be found at http://scitation.aip.org/getabs/servlet/GetabsServlet?prog=normal&id=JOEEDU000123000007000650000001&idtype=cvips&gifs=yes.

APPENDIX

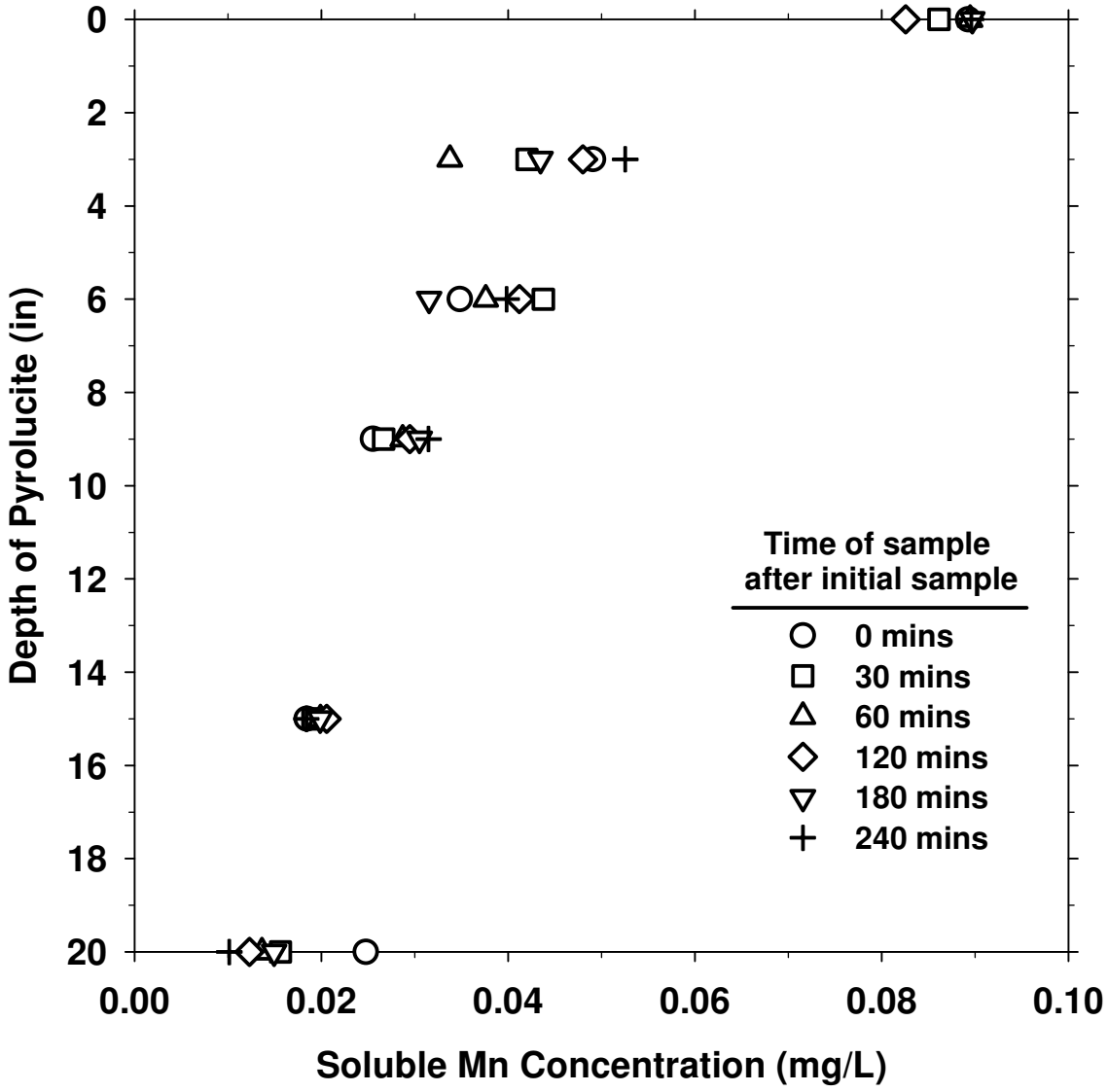

Figure A.1 Soluble Mn removal profiles over depth of pyrolucite as a function of time (Influent water: HLR=20 gpm/ft^2, HOCl=1.2-1.3 mg/L, pH=6.7, Mn^{2+}=0.09 mg/L)

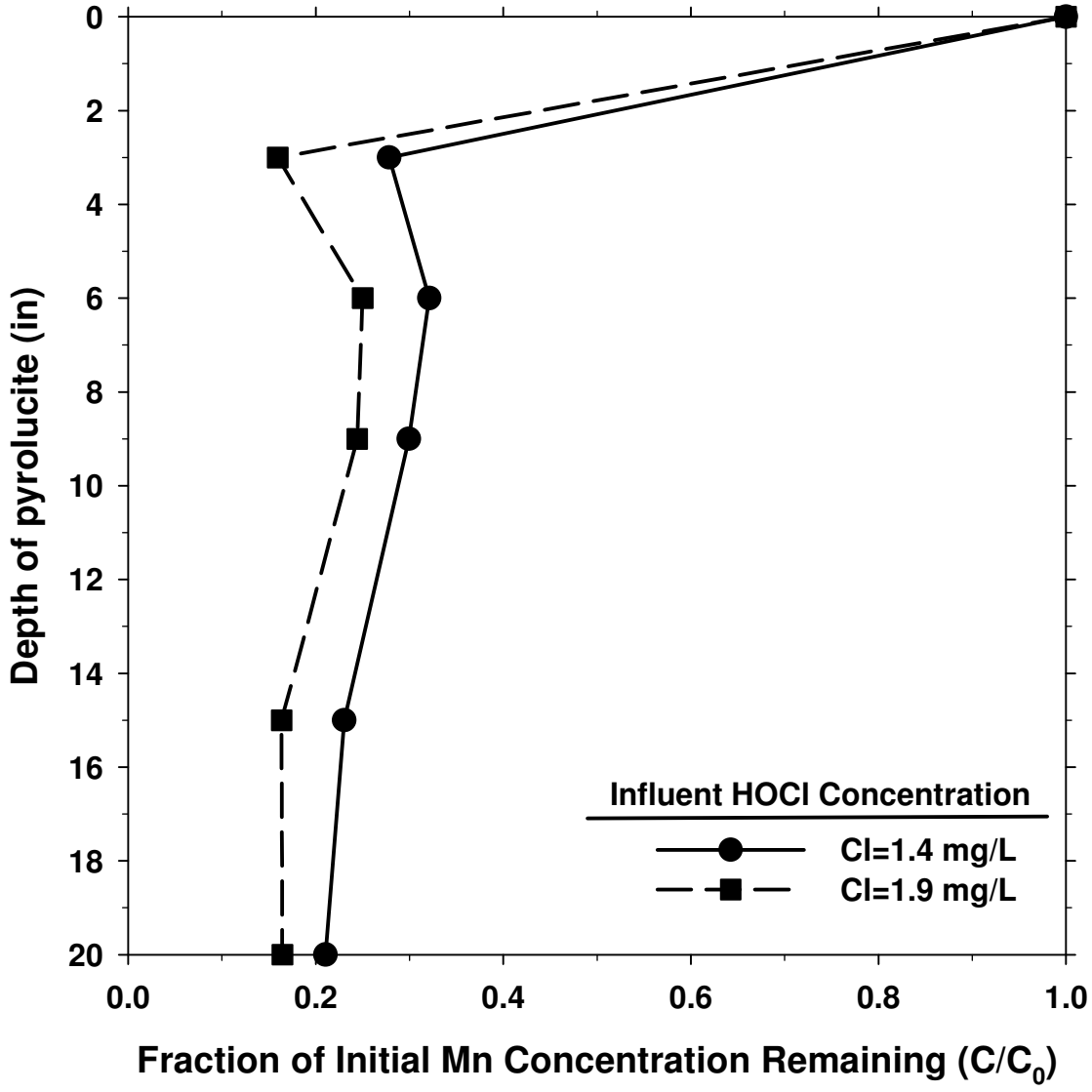

Figure A.2 Effect of free chlorine concentration on soluble Mn removal profile over depth of pyrolucite (Influent water: HLR=20 gpm/ft^2, pH=7.1-7.2, Mn^{2+}=0.05 mg/L)

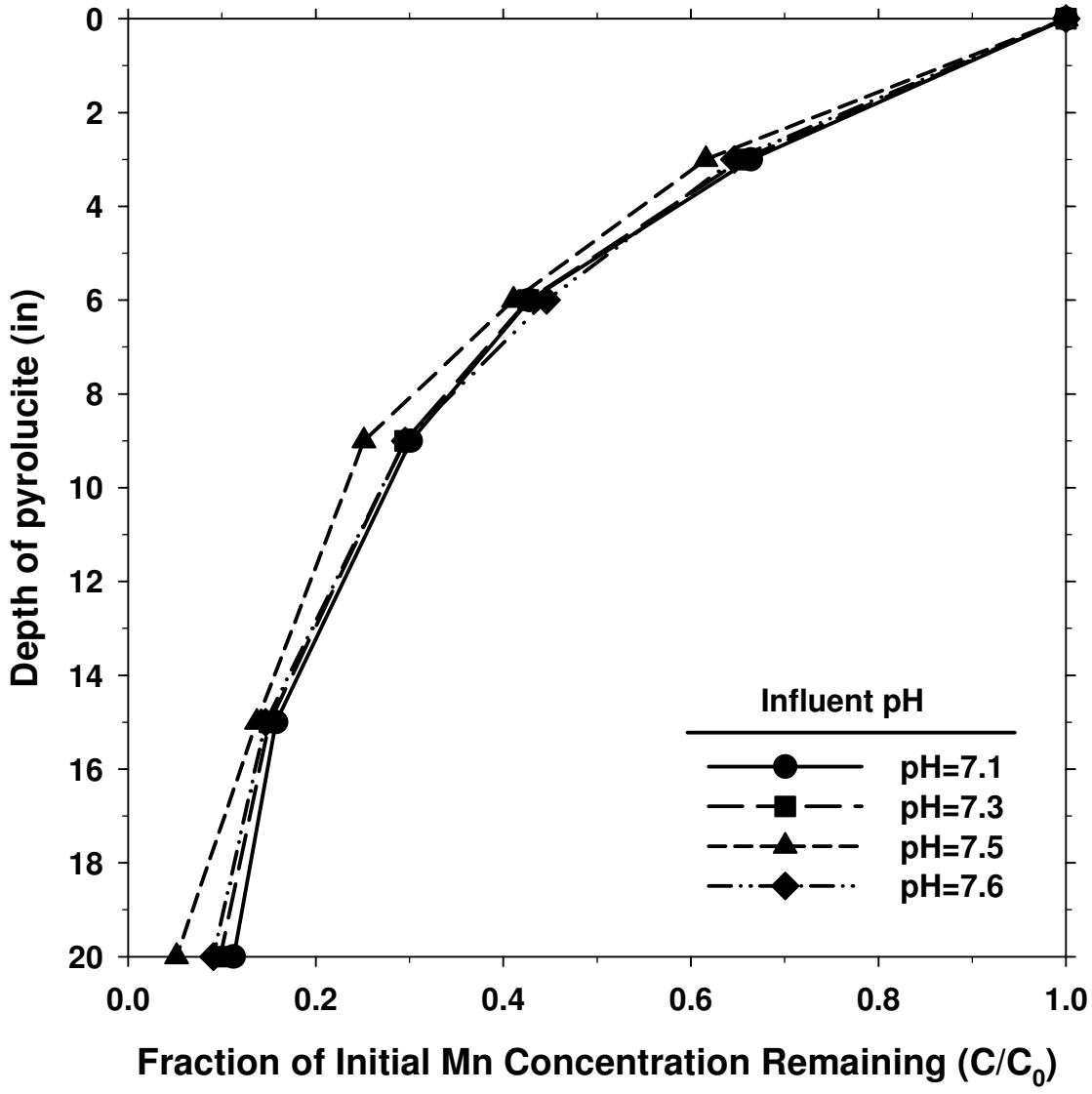

Figure A.3 Effect of pH on soluble Mn removal profile over depth of pyrolucite (Influent water: HLR=16 gpm/ft^2, HOCl=1.9-2.1 mg/L, Mn^{2+}=0.30 mg/L)

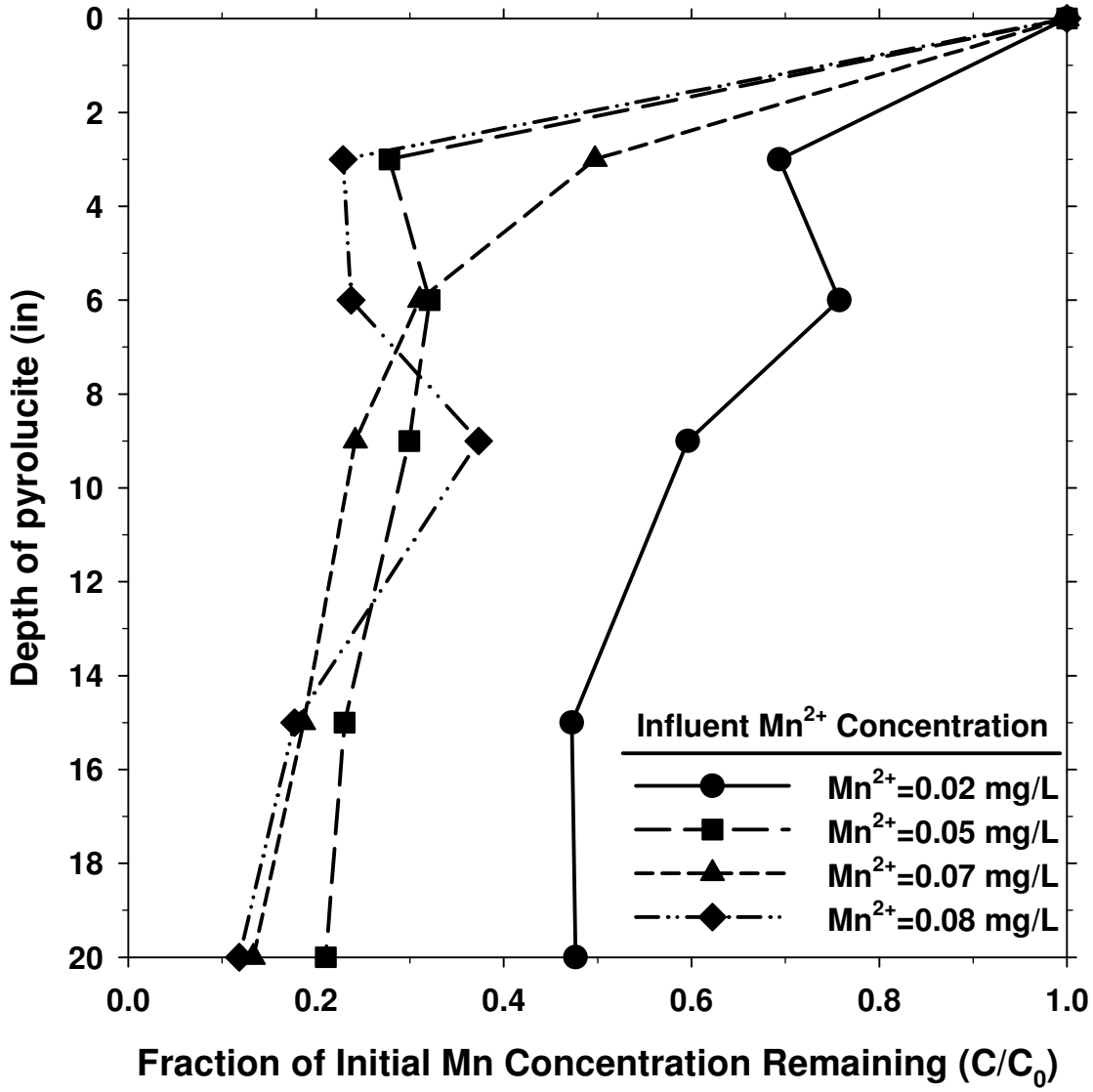

Figure A.4 Effect of influent Mn concentration on soluble Mn^{2+} removal profile over depth of pyrolucite (Influent water: HLR=20 gpm/ft^2, HOCl=1.4-1.6 mg/L, pH=7.1-7.3)

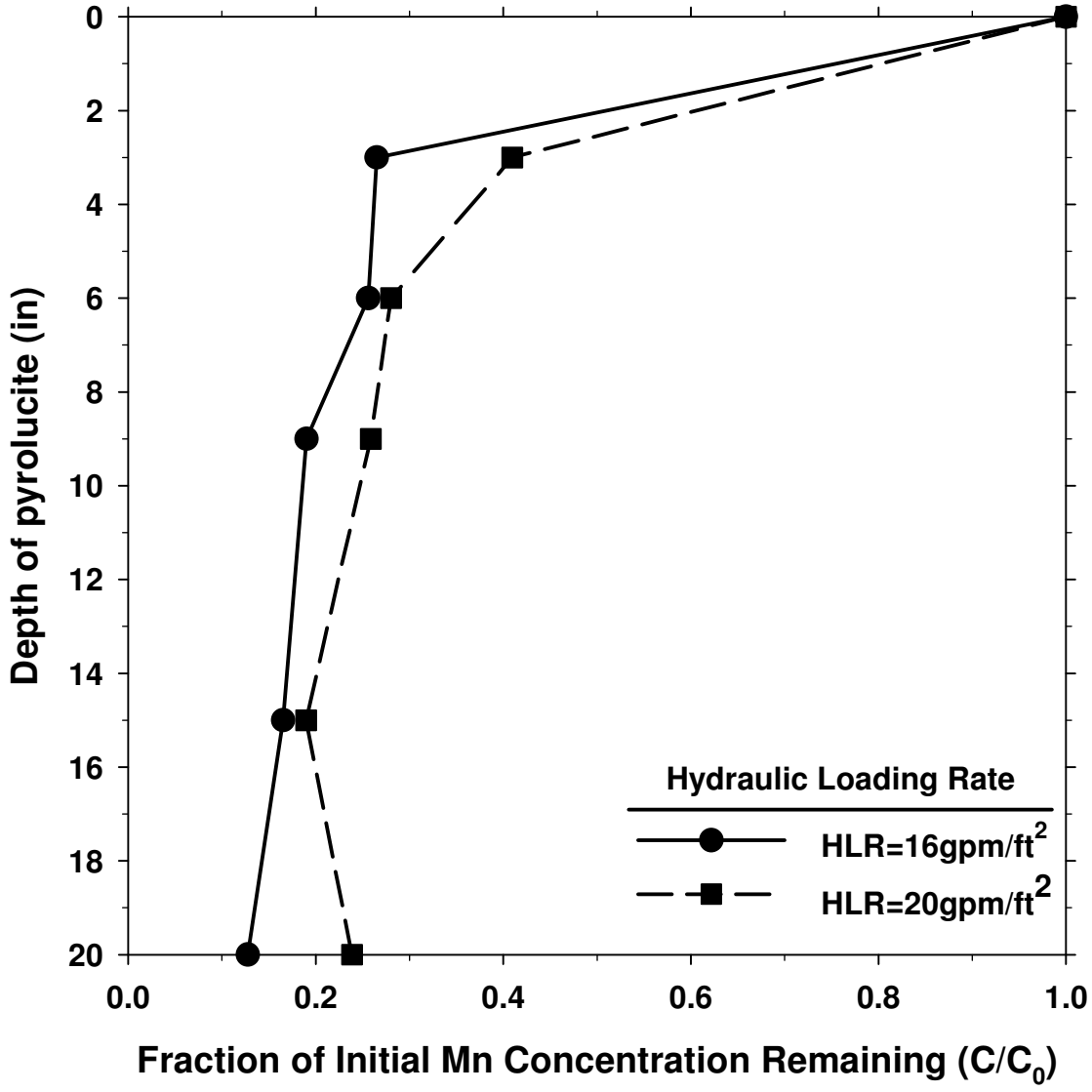

Figure A.5 Effect of HLR on soluble Mn removal profile over depth of pyrolucite (Influent water: HOCl=1.4 mg/L, pH=7.3-7.4, Mn^{2+}=0.06-0.07 mg/L)

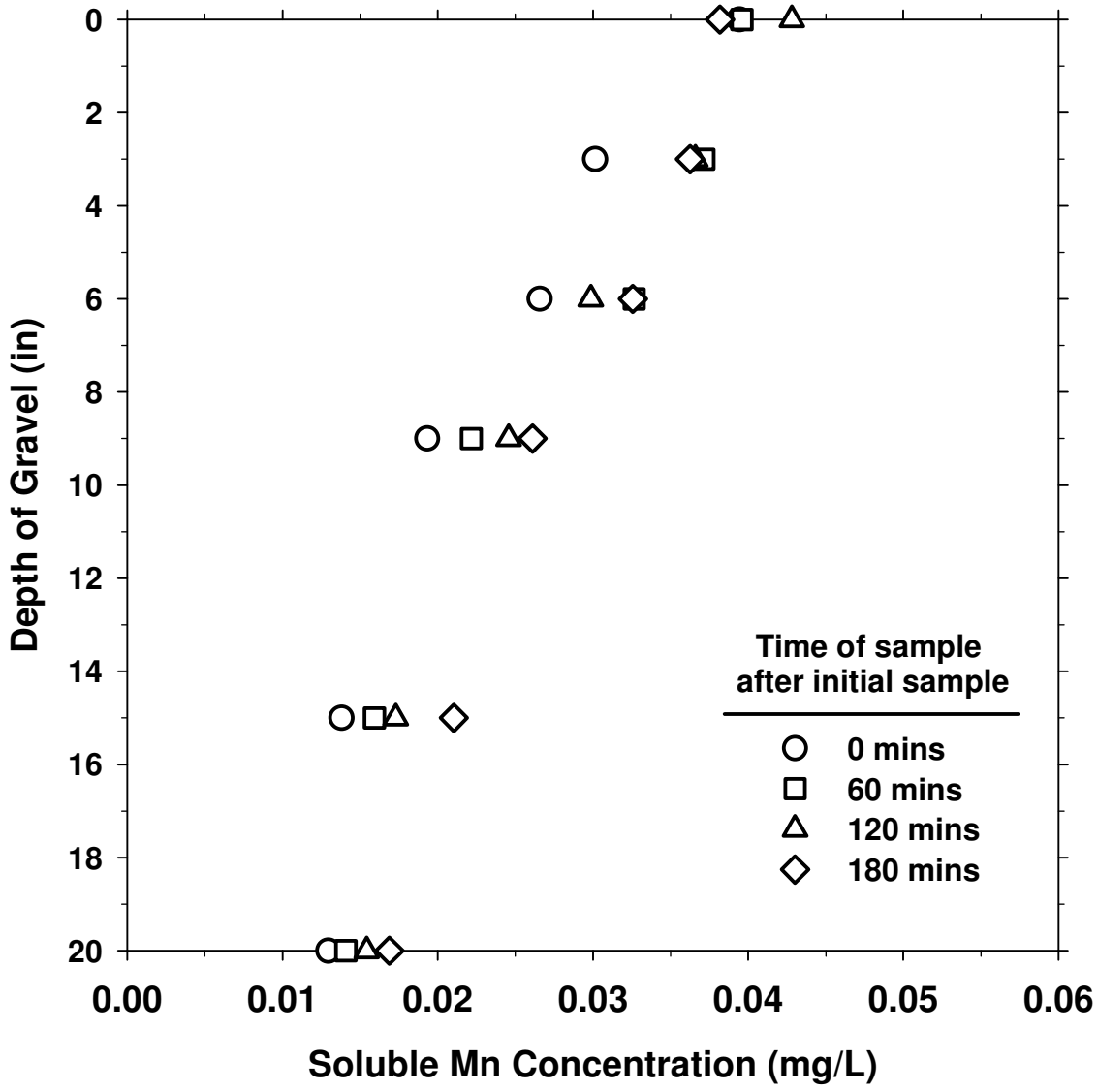

Figure A.6 Soluble Mn removal profiles over depth of gravel as a function of time (Influent water: HLR=20 gpm/ft^2, HOCl=1.4-1.6 mg/L, pH=7.6, Mn^{2+}=0.04 mg/L)

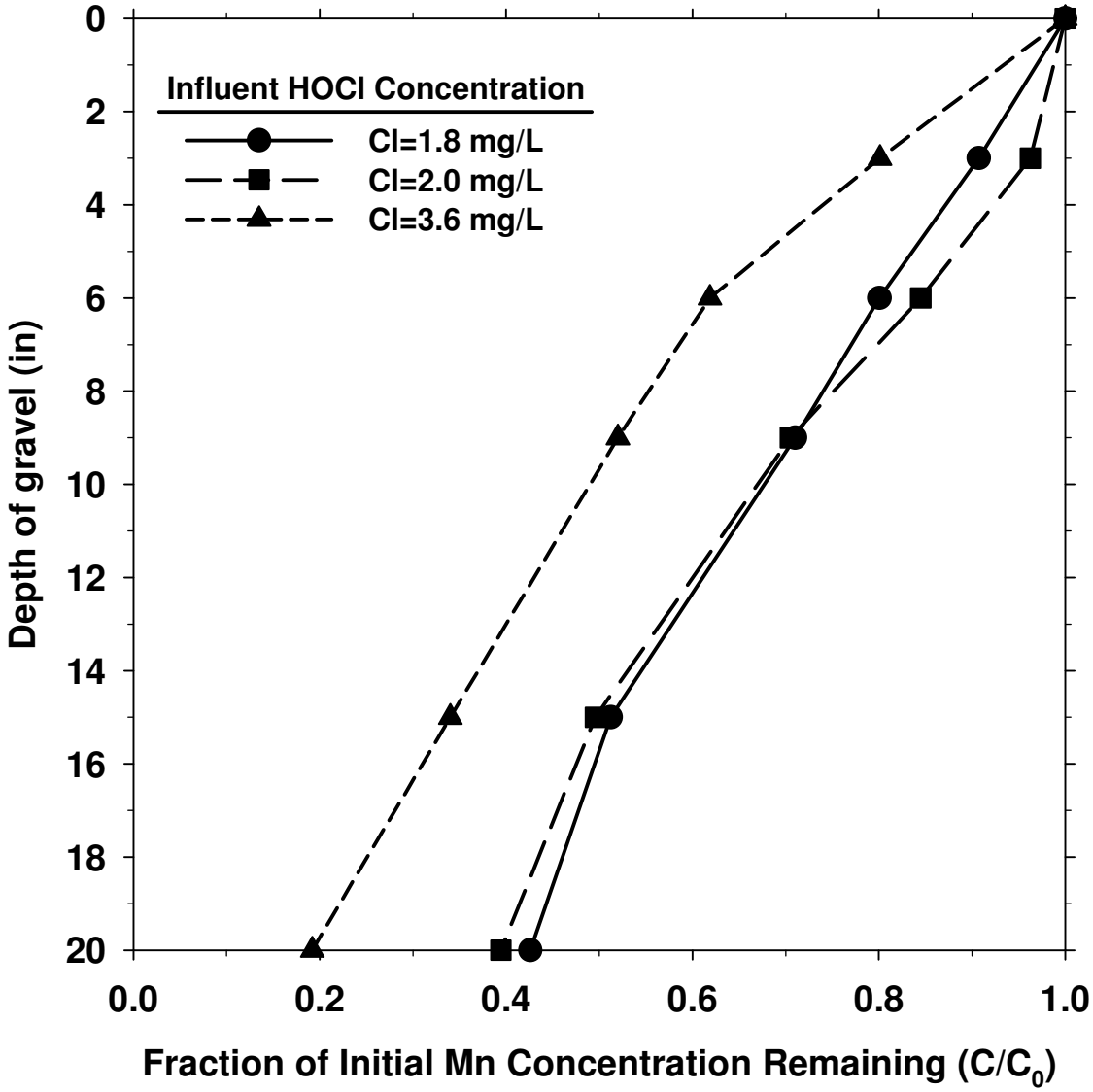

Figure A.7 Effect of free chlorine concentration on soluble Mn removal profile over depth of gravel (Influent water: HLR=16 gpm/ft^2, pH=7.4-7.6, Mn^{2+}=0.09-0.11 mg/L)

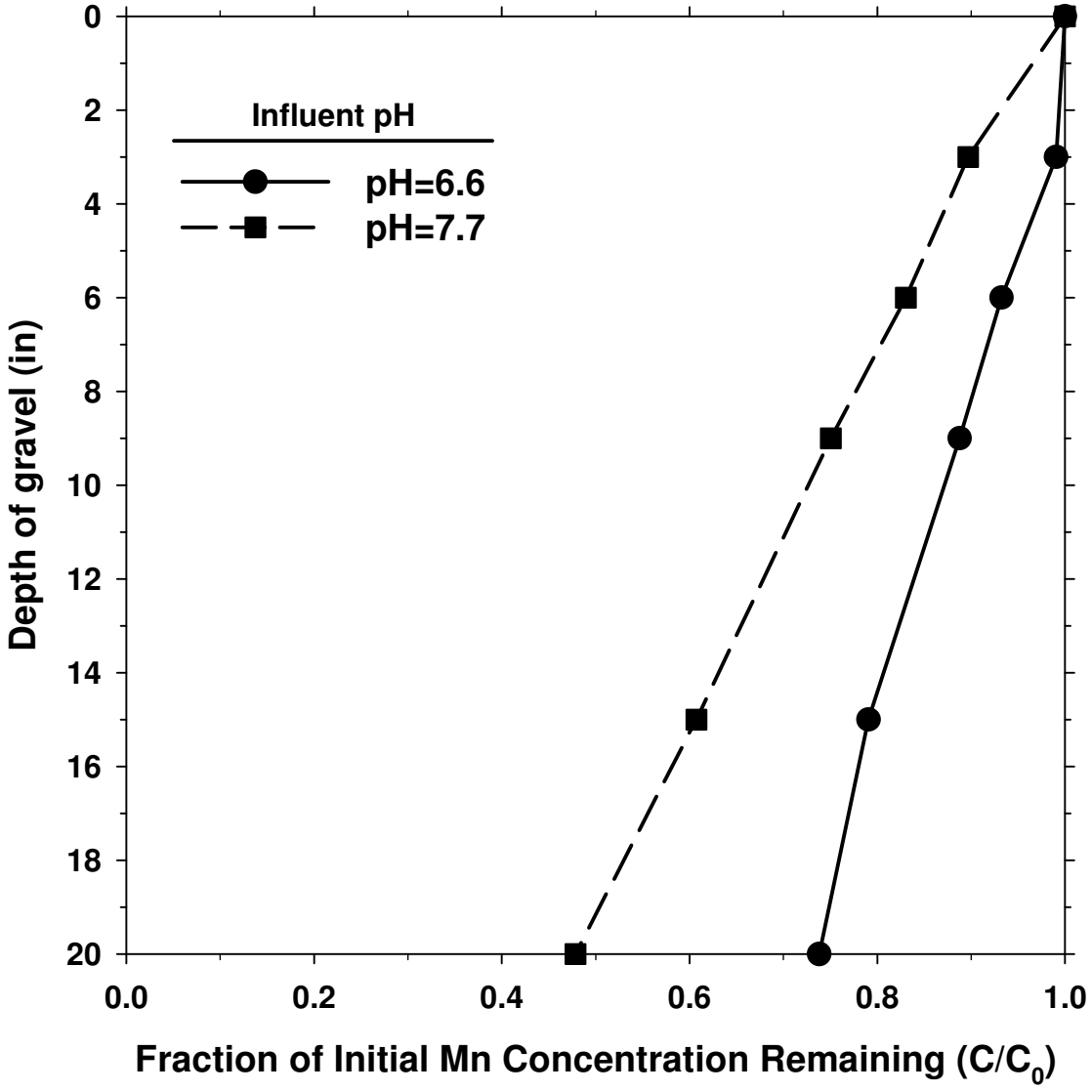

Figure A.8 Effect of pH on soluble Mn removal profile over depth of gravel (Influent water: HLR=16 gpm/ft^2, HOCl=0.8-1.0 mg/L, Mn^{2+}=0.07-0.11 mg/L)

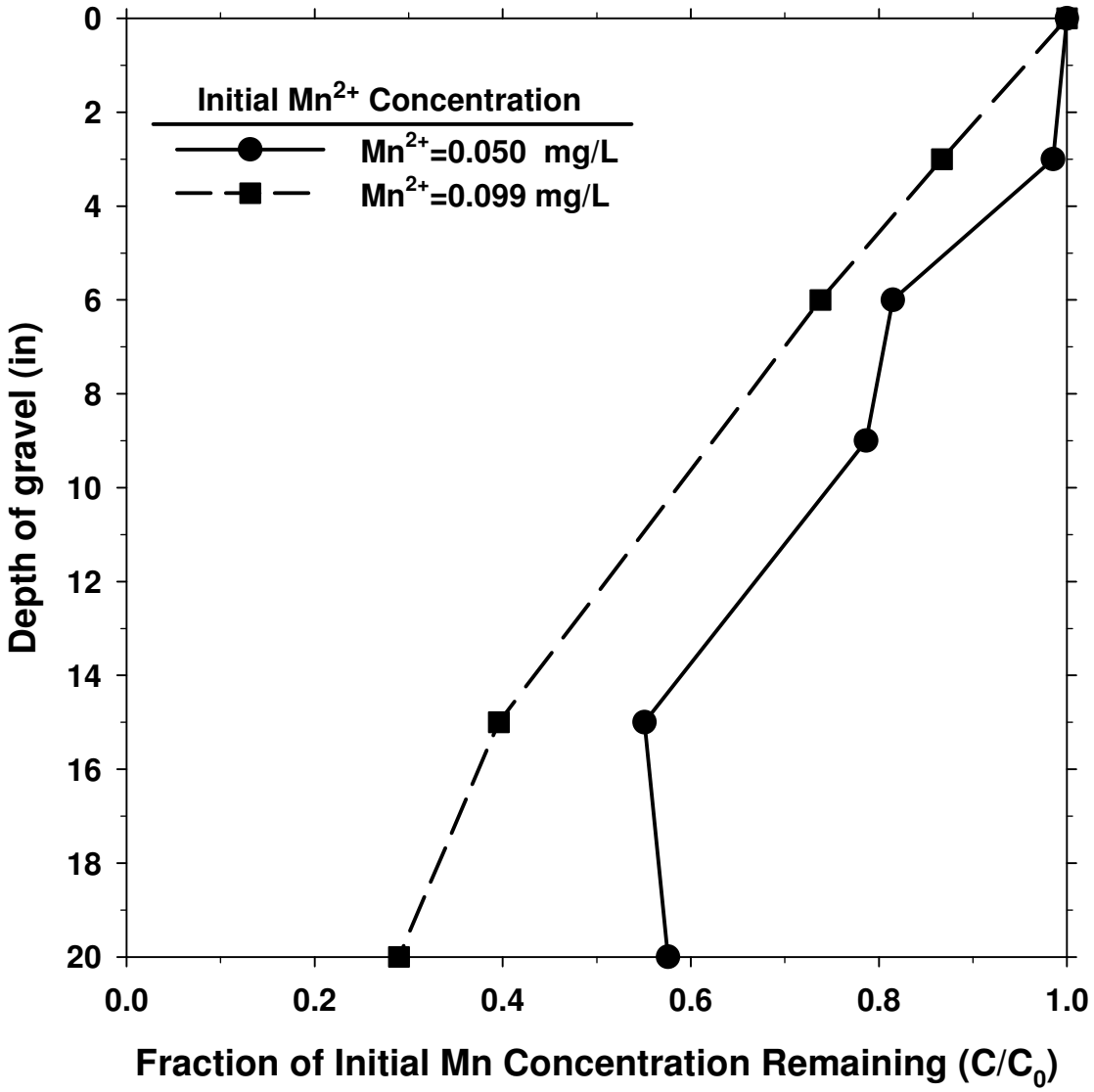

Figure A.9 Effect of influent Mn concentration on soluble Mn removal profile over depth of gravel (Influent water: HLR=16 gpm/ft^2, HOCl=1.2-1.3 mg/L, pH=7.6-7.8)

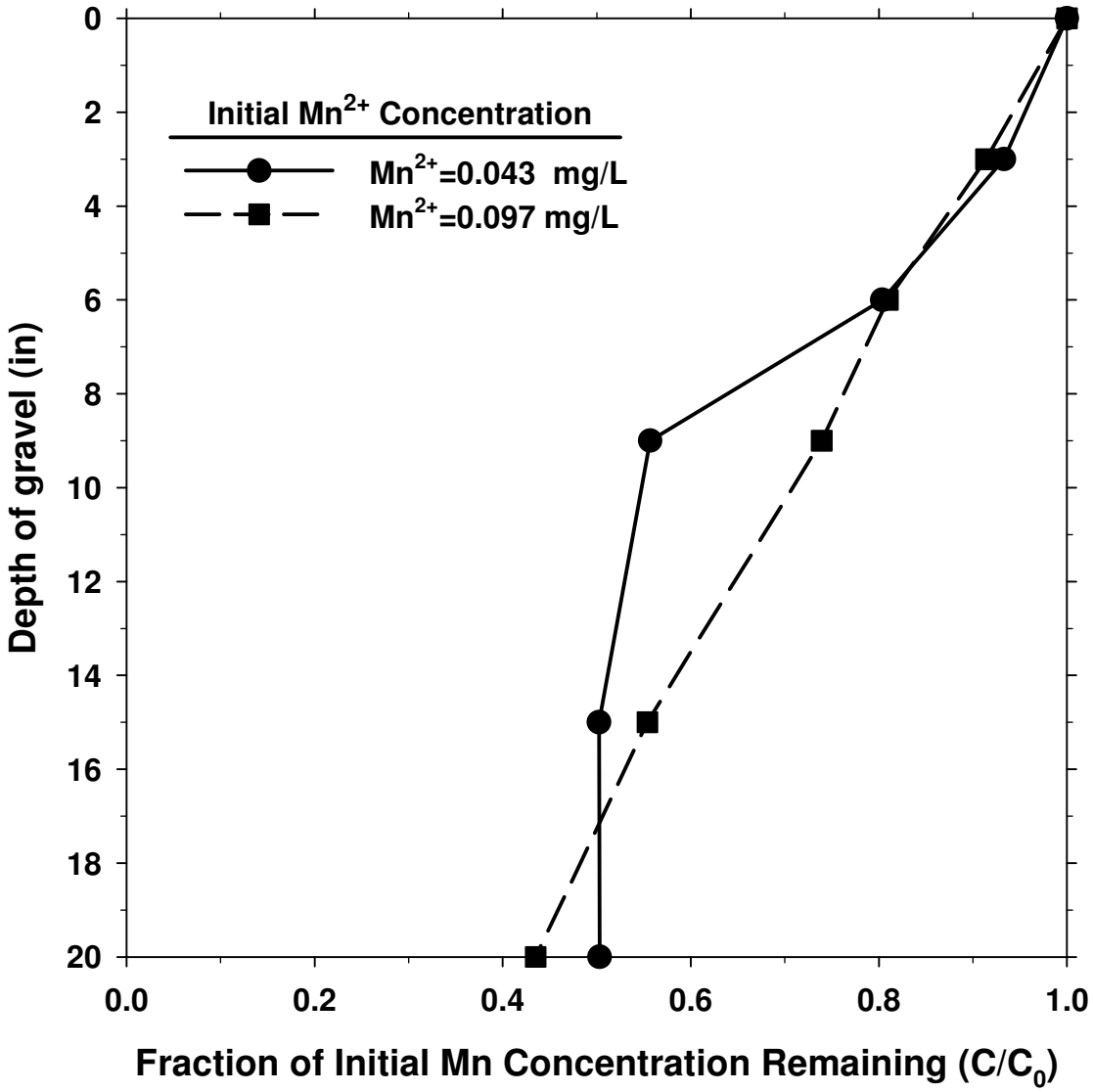

Figure A.10 Effect of influent Mn concentration on soluble Mn removal profile over depth of gravel (Influent water: HLR=20 gpm/ft^2, HOCl=2.0-2.1 mg/L, pH=7.4-7.6)

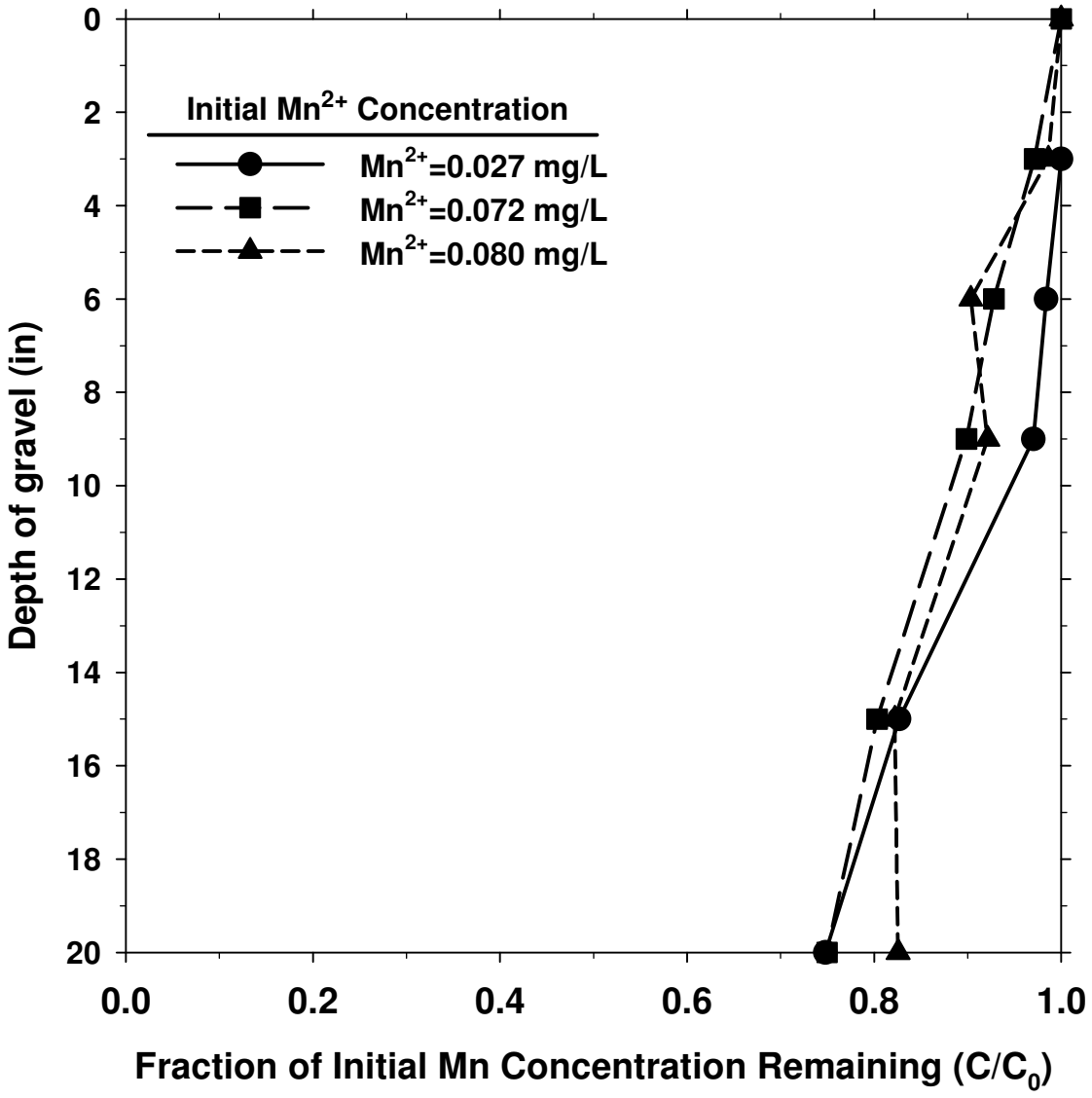

Figure A.11 Effect of influent Mn concentration on soluble Mn removal profile over depth of gravel (Influent water: HLR=16 gpm/ft^2, HOCl=0.7-0.9 mg/L, pH=6.6)

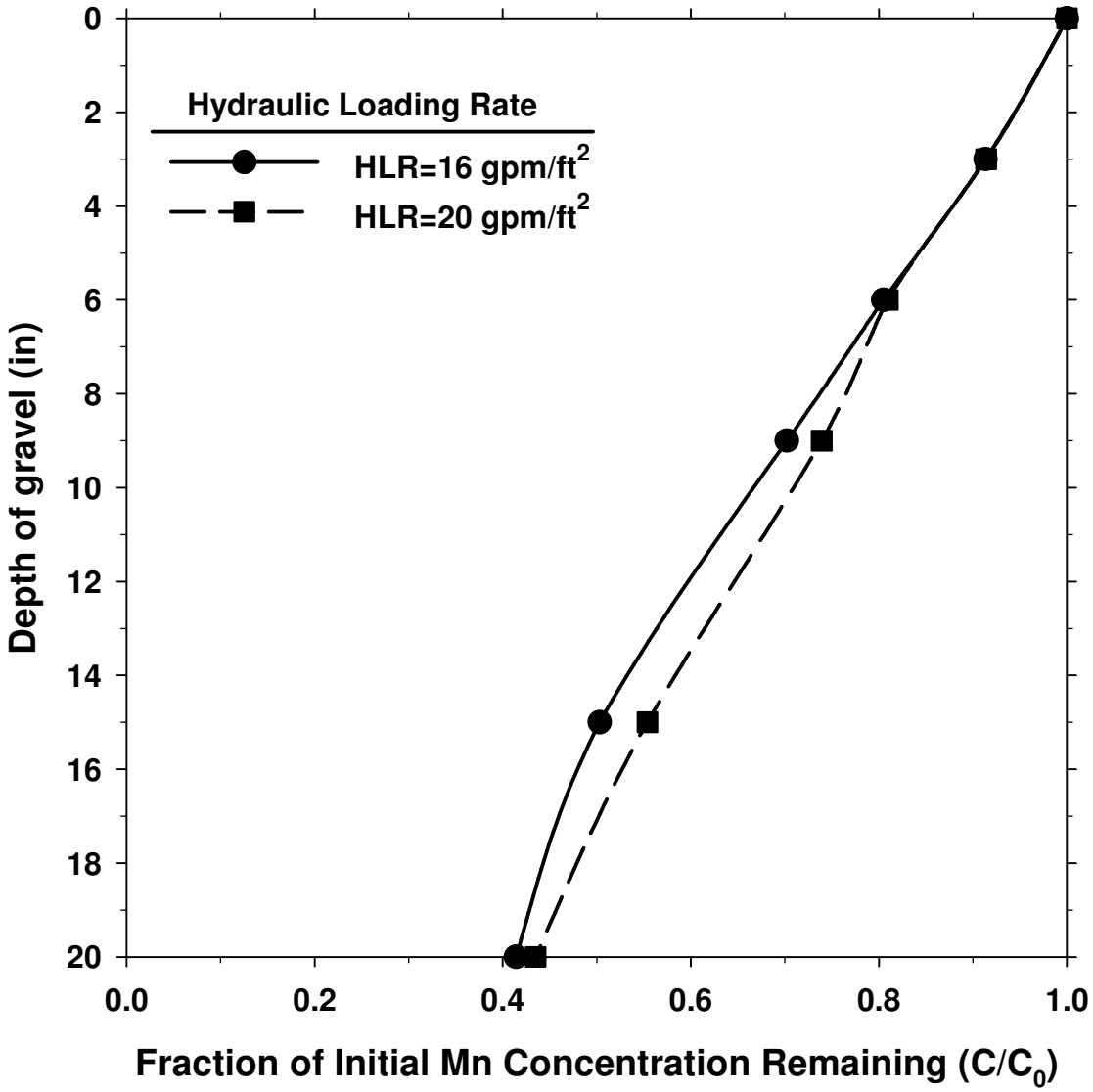

Figure A.12 Effect of HLR on soluble Mn removal profile over depth of gravel (Influent water: HOCl=1.8-2.1 mg/L, pH=7.4-7.6, Mn^{2+}=0.09-0.10 mg/L)

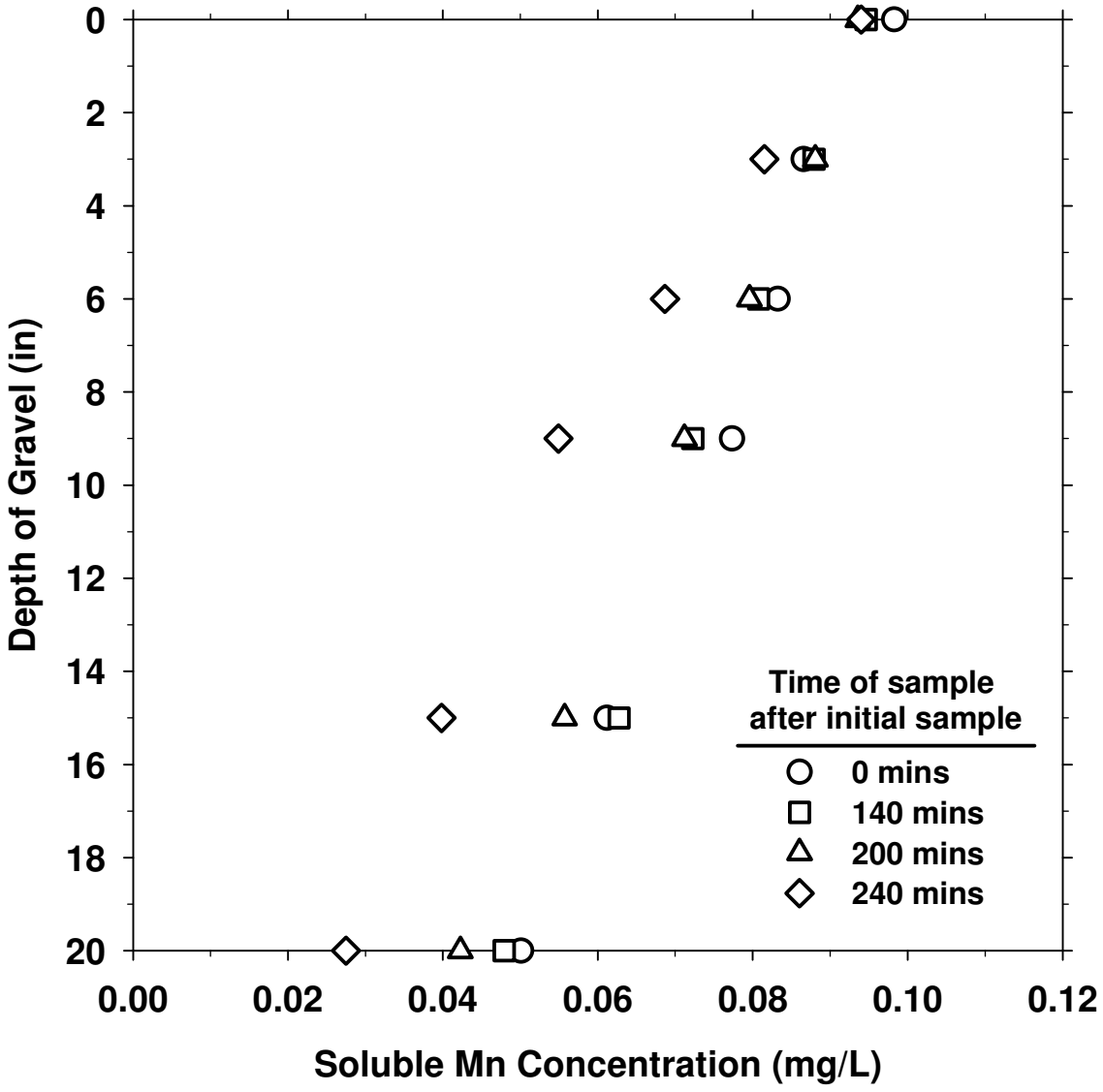

Figure A.13 Soluble Mn removal profiles over depth of torpedo sand as a function of time (Influent water: HLR=16 gpm/ft^2, HOCl=1.5-2.3 mg/L, pH=6.6, Mn^{2+}=0.10 mg/L)

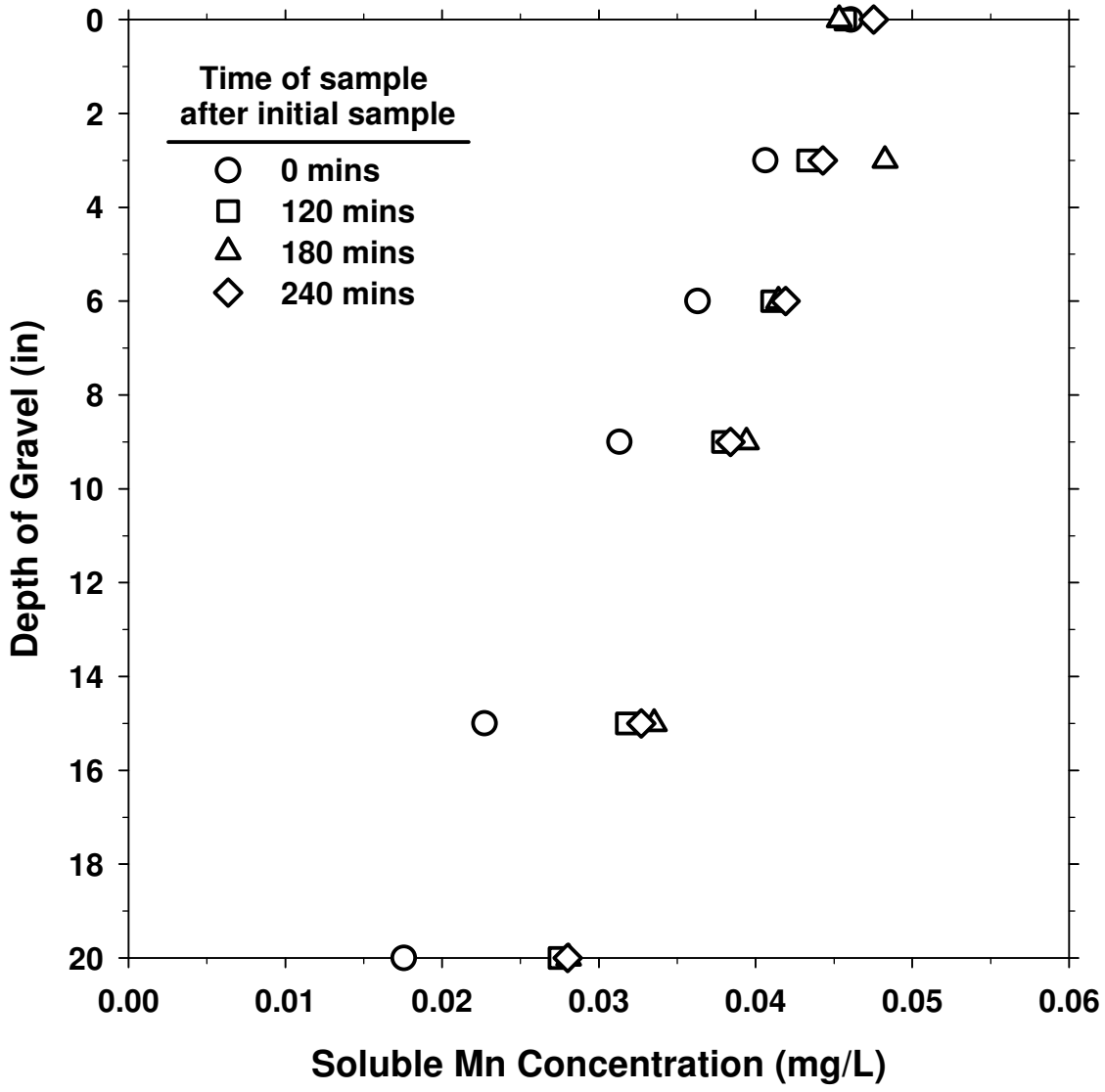

Figure A.14 Soluble Mn removal profiles over depth of torpedo sand as a function of time (Influent water: HLR=20 gpm/ft^2, HOCl=2.0-3.1 mg/L, pH=6.5)

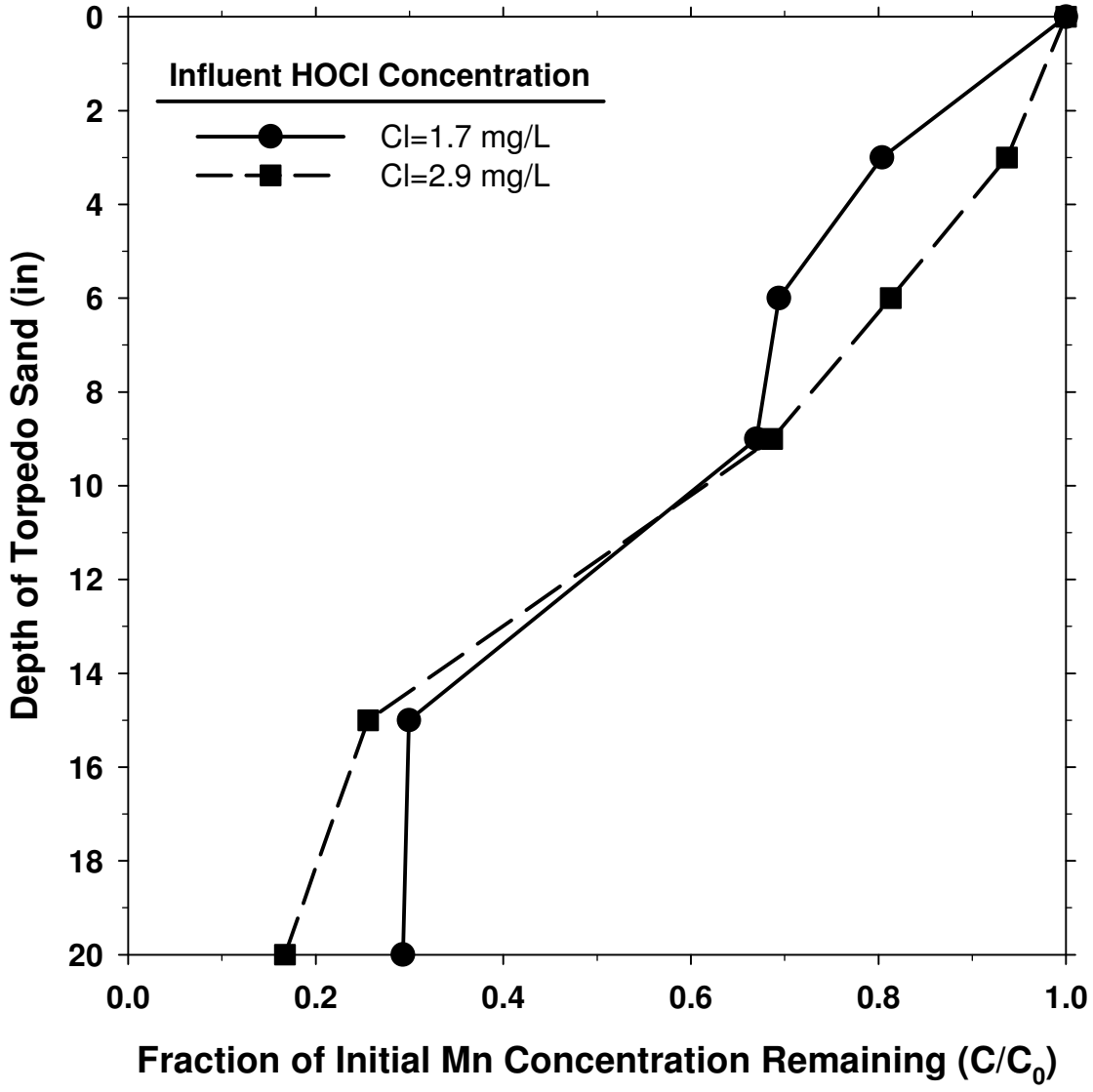

Figure A.15 Effect of free chlorine concentration on soluble Mn removal profile over depth of torpedo sand (Influent water: HLR=20 gpm/ft^2, pH=7.0, Mn^{2+}=0.07-0.08 mg/L)

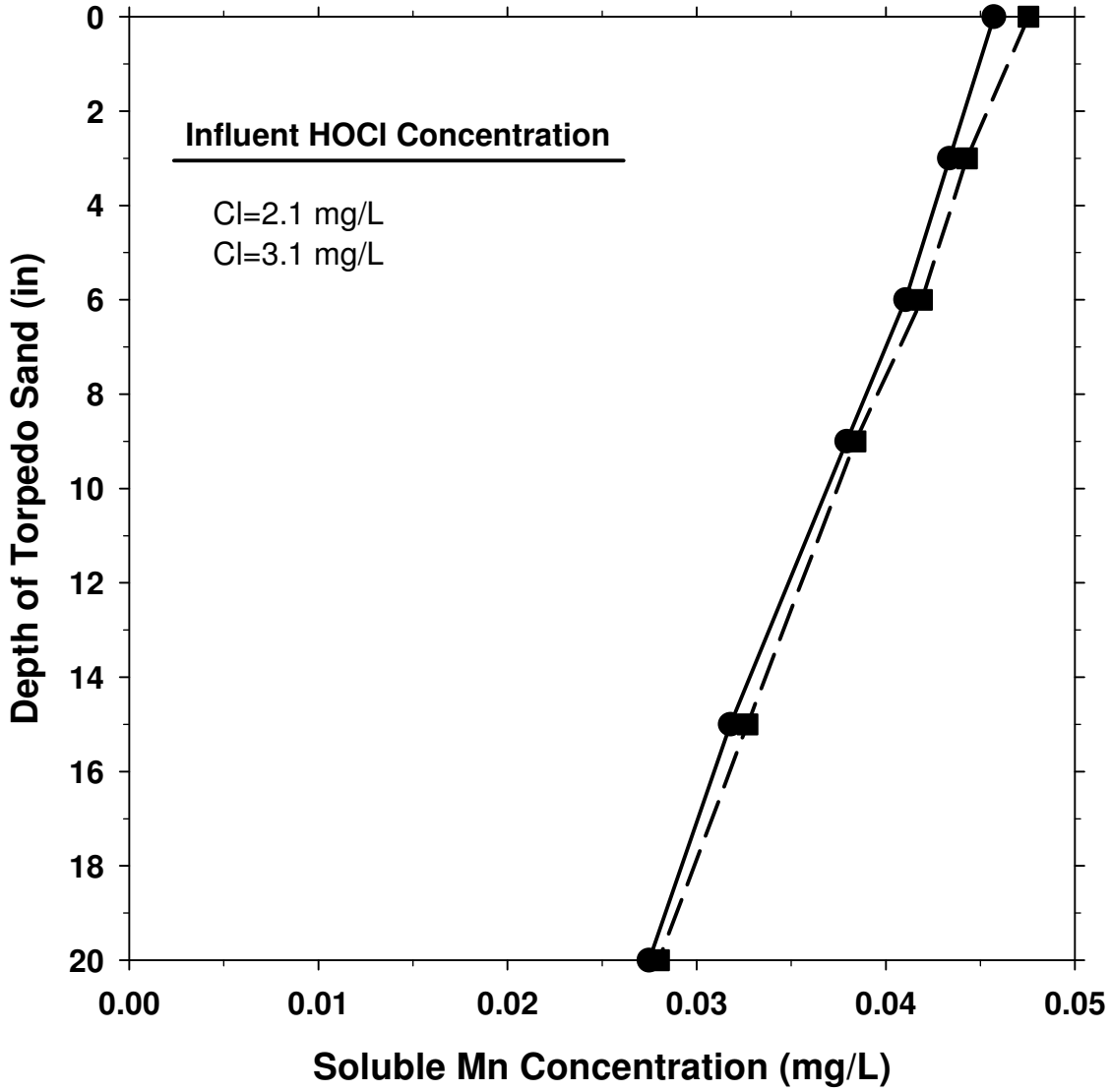

Figure A.16 Effect of free chlorine concentration on soluble Mn removal profile over depth of torpedo sand (Influent water: HLR=20 gpm/ft^2, pH=6.6, Mn^{2+}=0.05 mg/L)

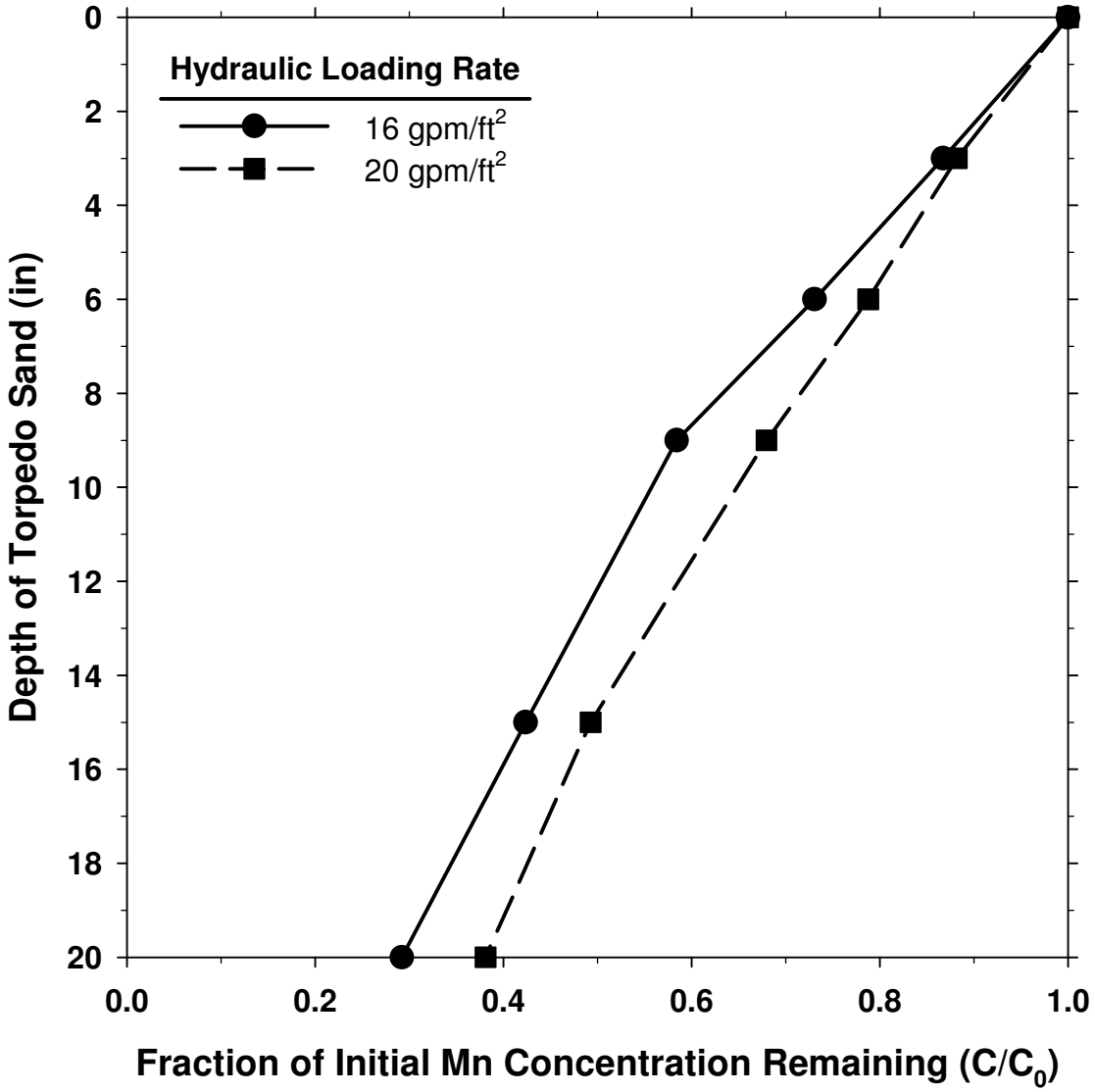

Figure A.17 Effect of HLR on soluble Mn removal profile over depth of torpedo sand (Influent water: HOCl=1.9-2.0 mg/L, pH=6.6, Mn^{2+}=0.05-0.09 mg/L)

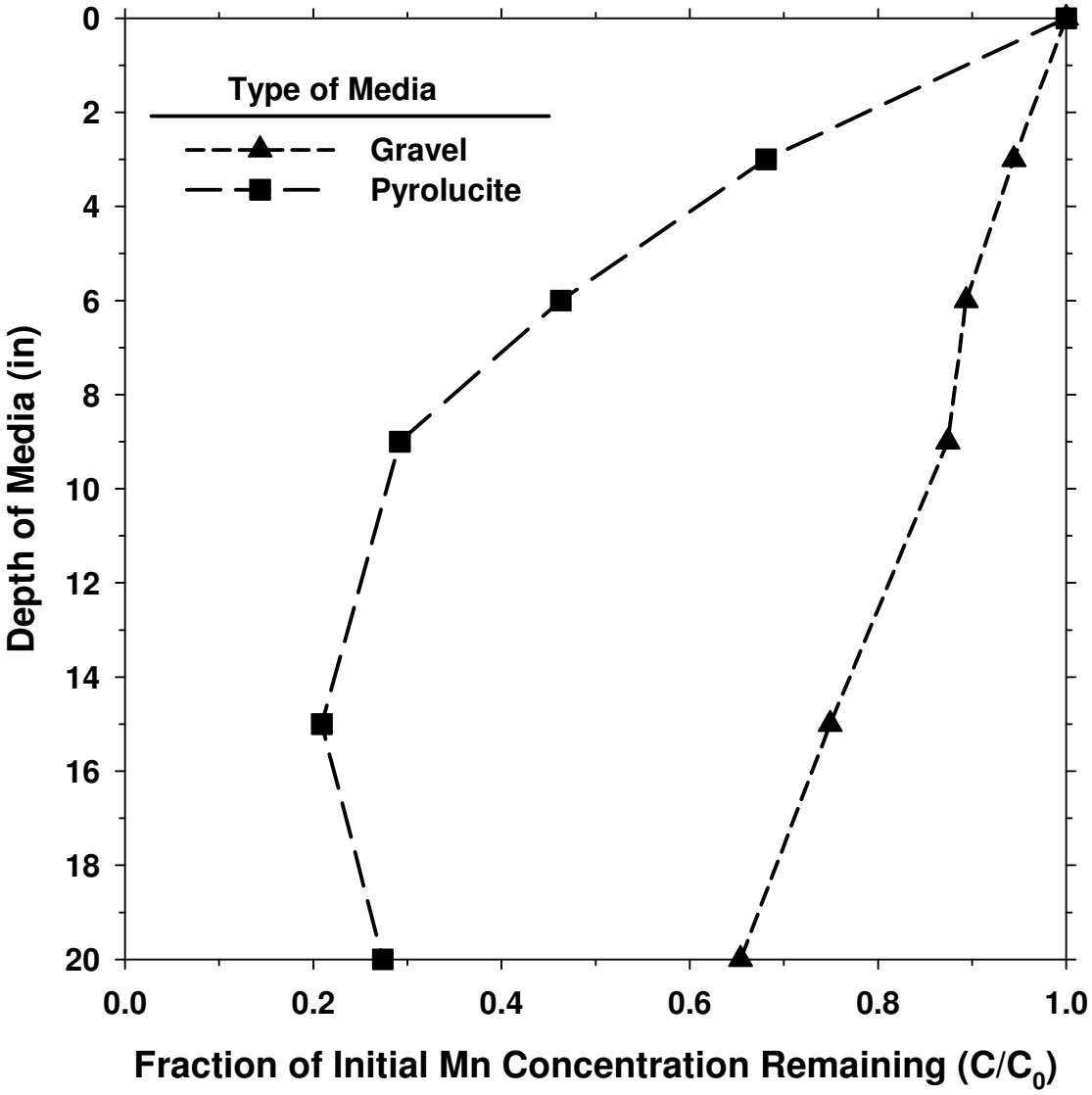

Figure A.18 Media performance comparison (Influent water: HLR=20 gpm/ft^2, HOCl=1.1 mg/L, pH=6.6-6.8, Mn^{2+}=0.07 mg/L)

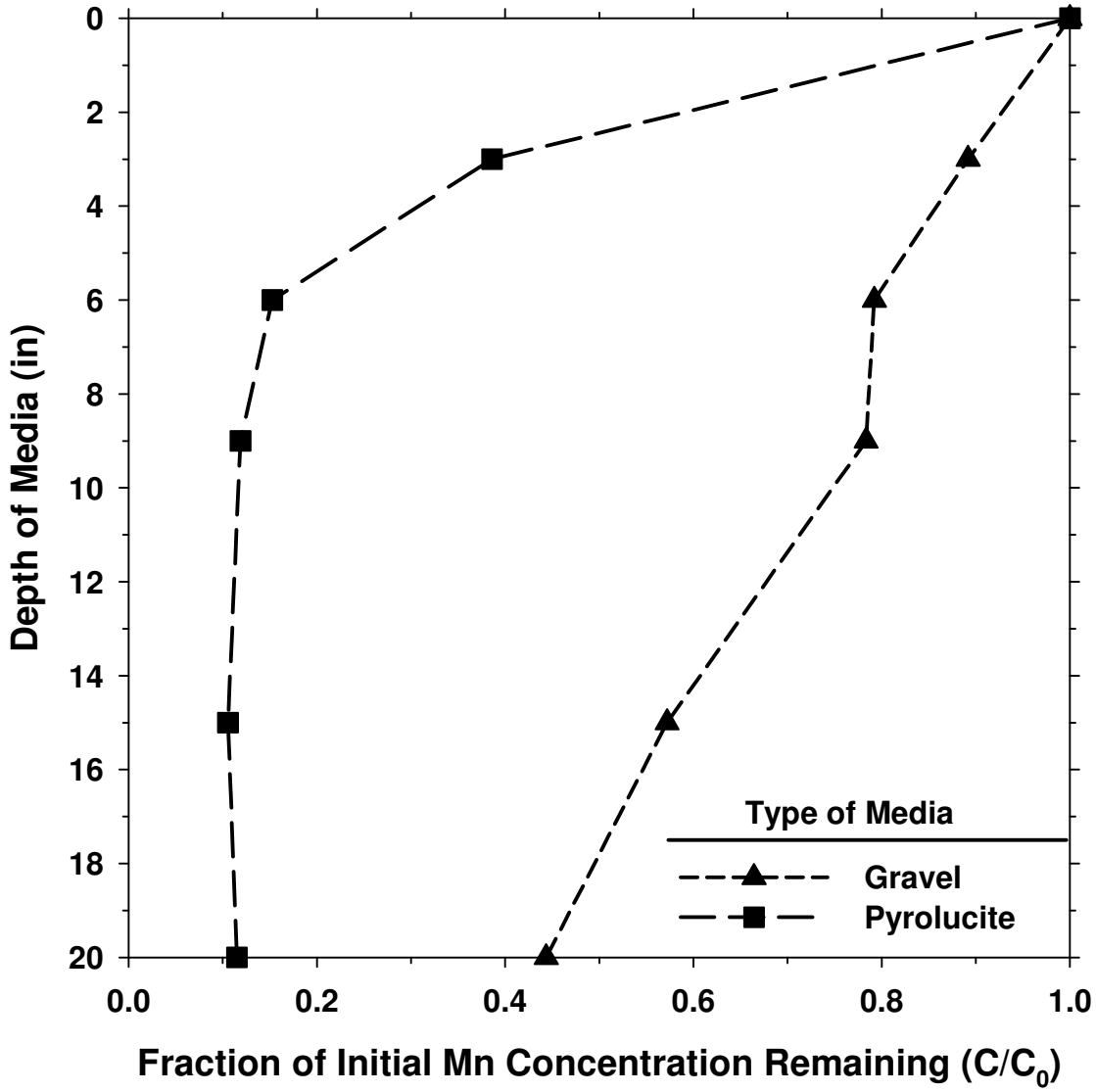

Figure A.19 Media performance comparison (Influent water: HLR=20 gpm/ft^2, HOCl=1.0-1.1 mg/L, pH=7.2-7.4, Mn^{2+}=0.09 mg/L)

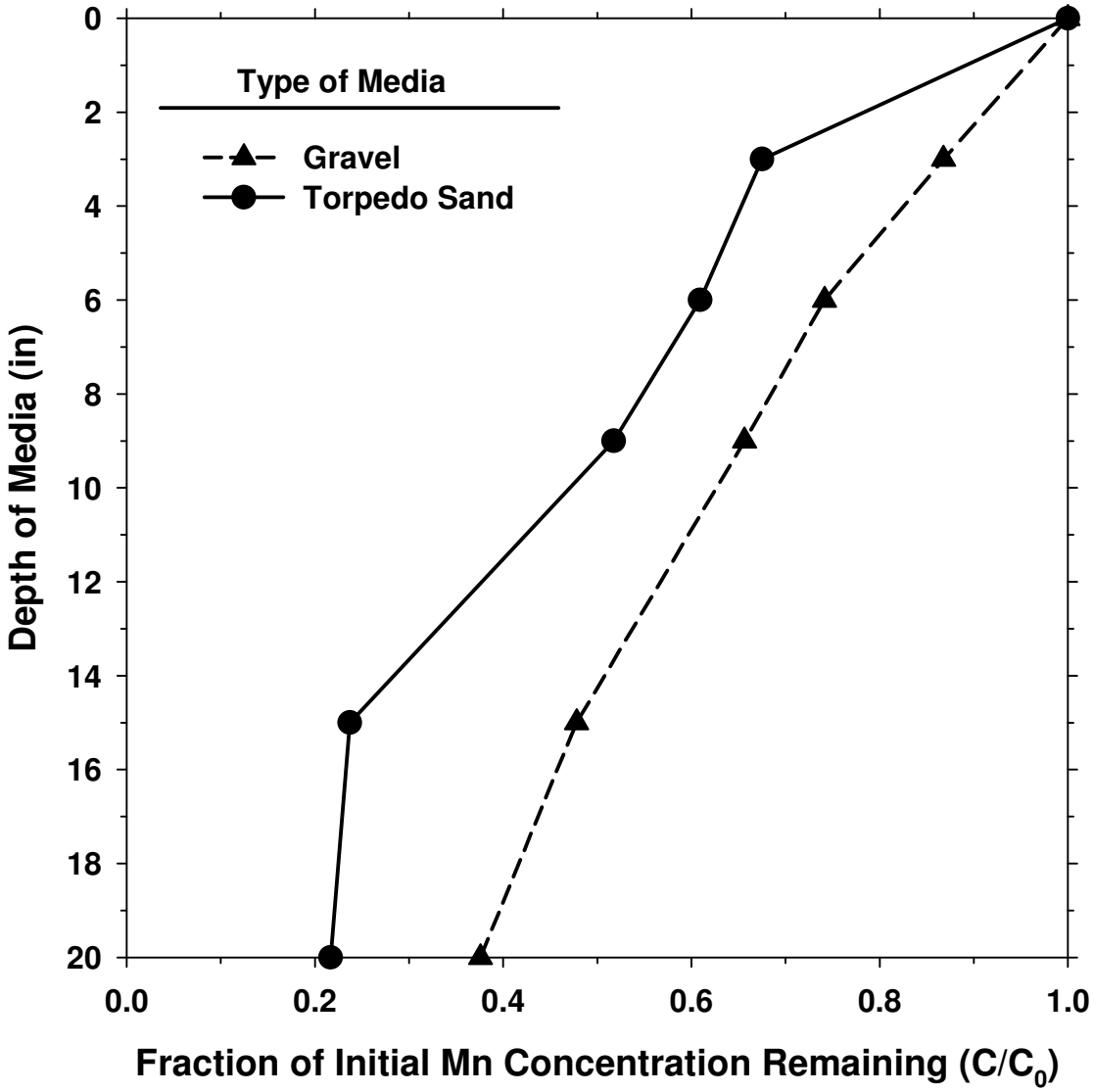

Figure A.20 Media performance comparison (Influent water: HLR=16 gpm/ft^2, HOCl=2.4 mg/L, pH=7.6-7.7, Mn^{2+}=0.08-0.11 mg/L)

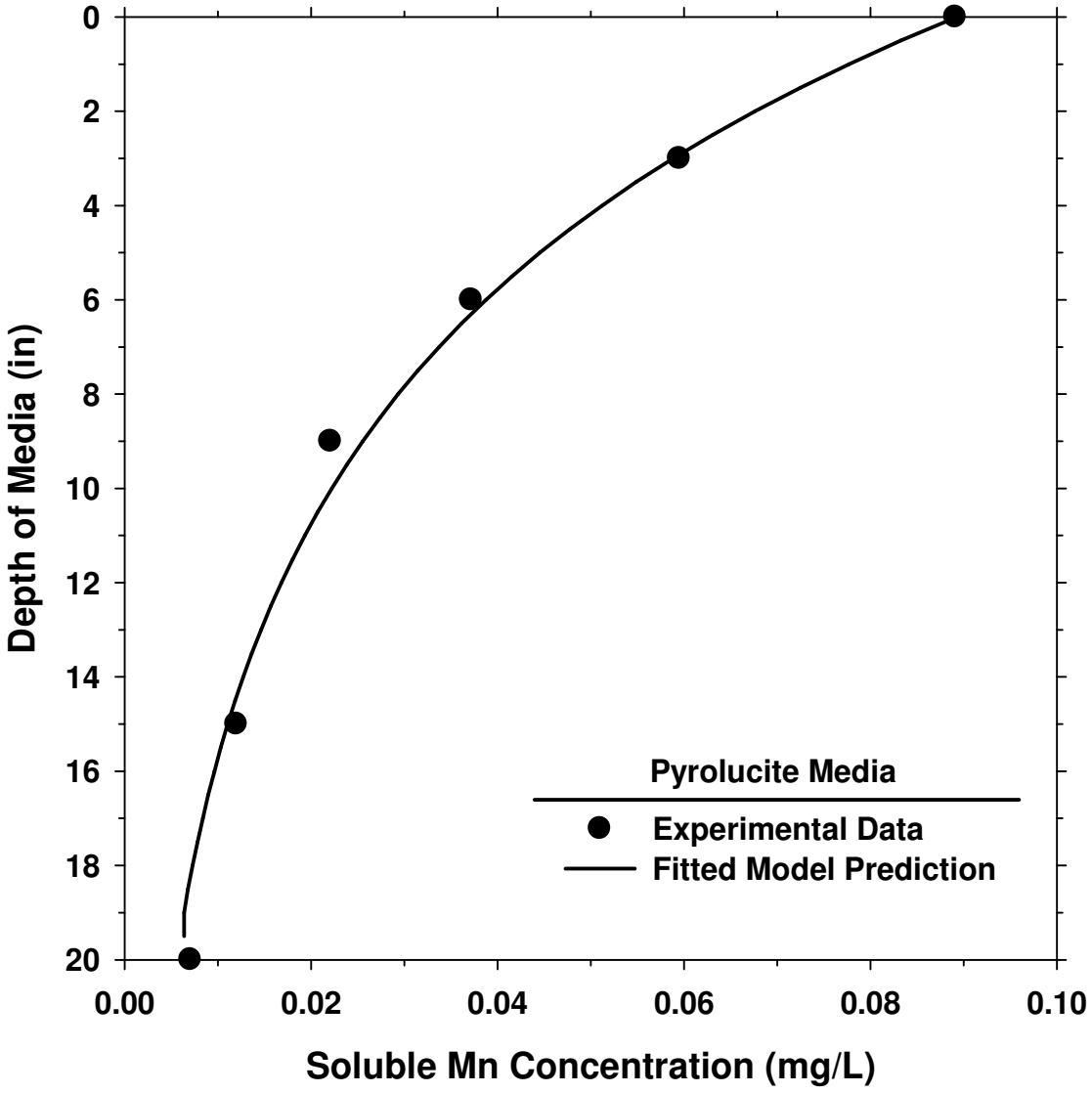

Figure A.21 Model fit to experimental data for pyrolucite media (Influent Water: HLR=16 gpm/ft^2, pH=7.6, HOCl=1.8 mg/L, Mn^{2+}=0.09 mg/L)

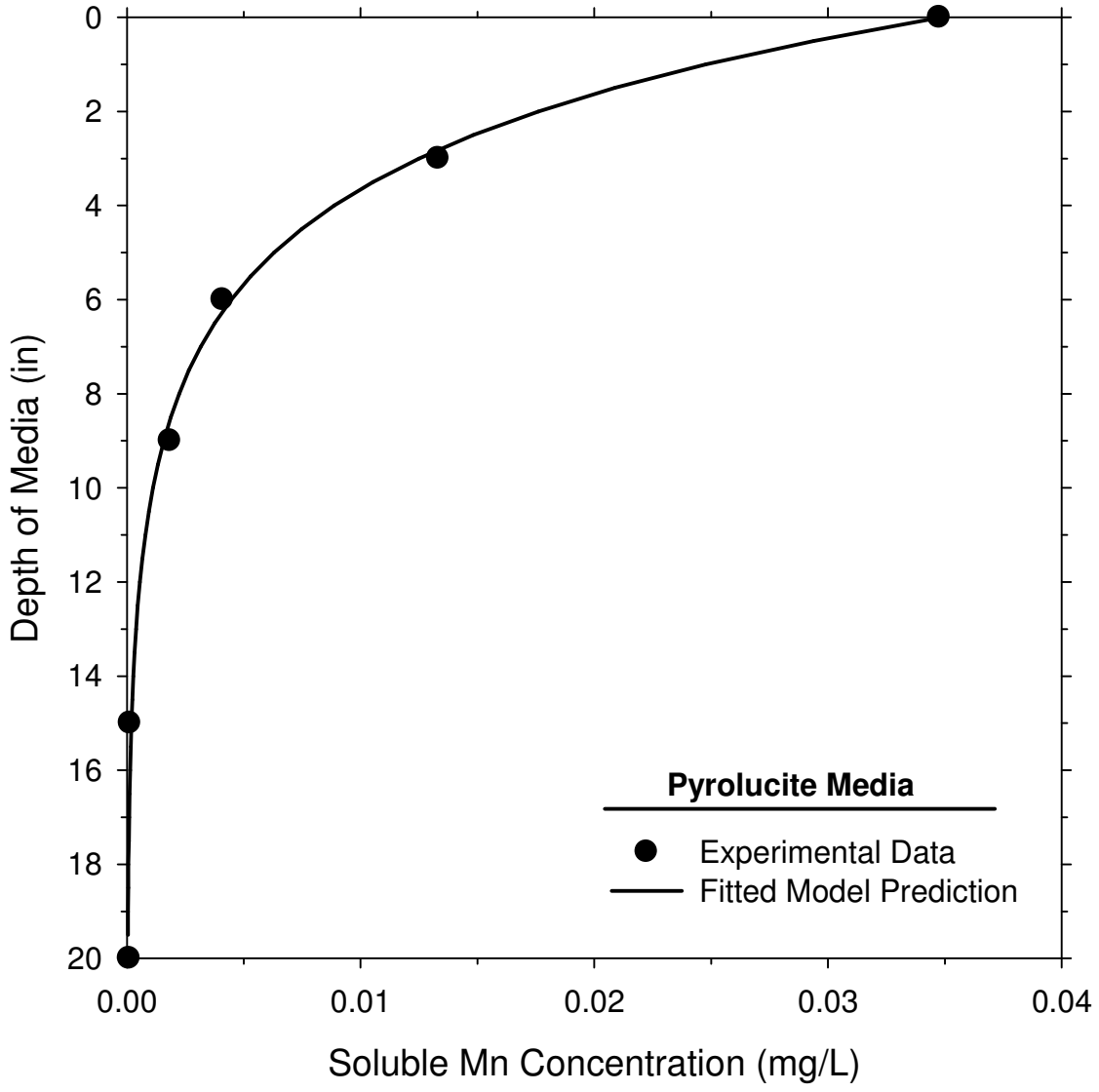

Figure A.22 Model fit to experimental data for gravel media (Influent Water: HLR=16 gpm/ft^2, pH=7.9, HOCl=0.8 mg/L, Mn^{2+}=0.28 mg/L)

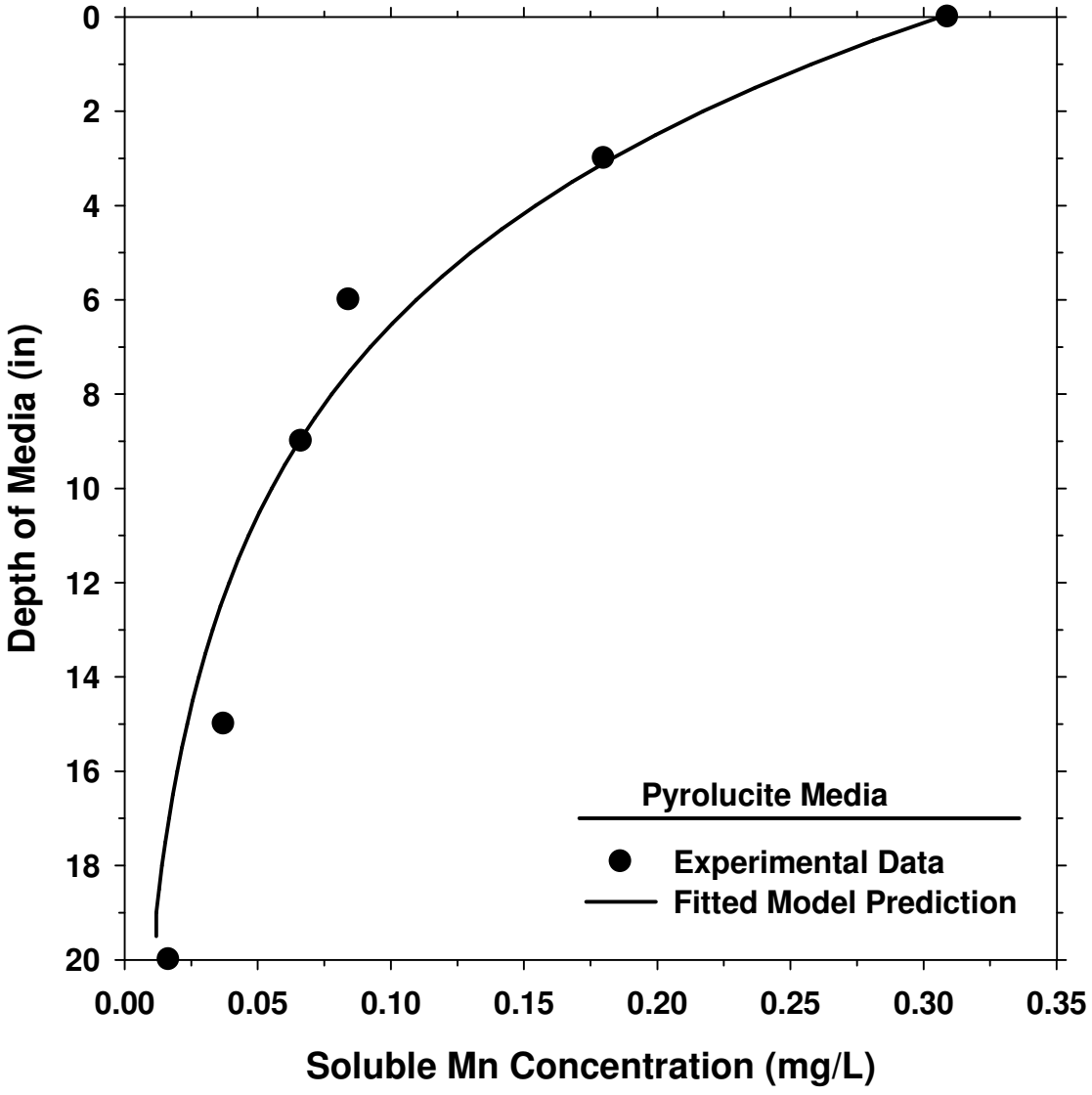

Figure A.23 Model fit to experimental data for pyrolucite media (Influent Water: HLR=16 gpm/ft^2, pH=7.5, HOCl=1.4 mg/L, Mn^{2+}=0.31 mg/L)

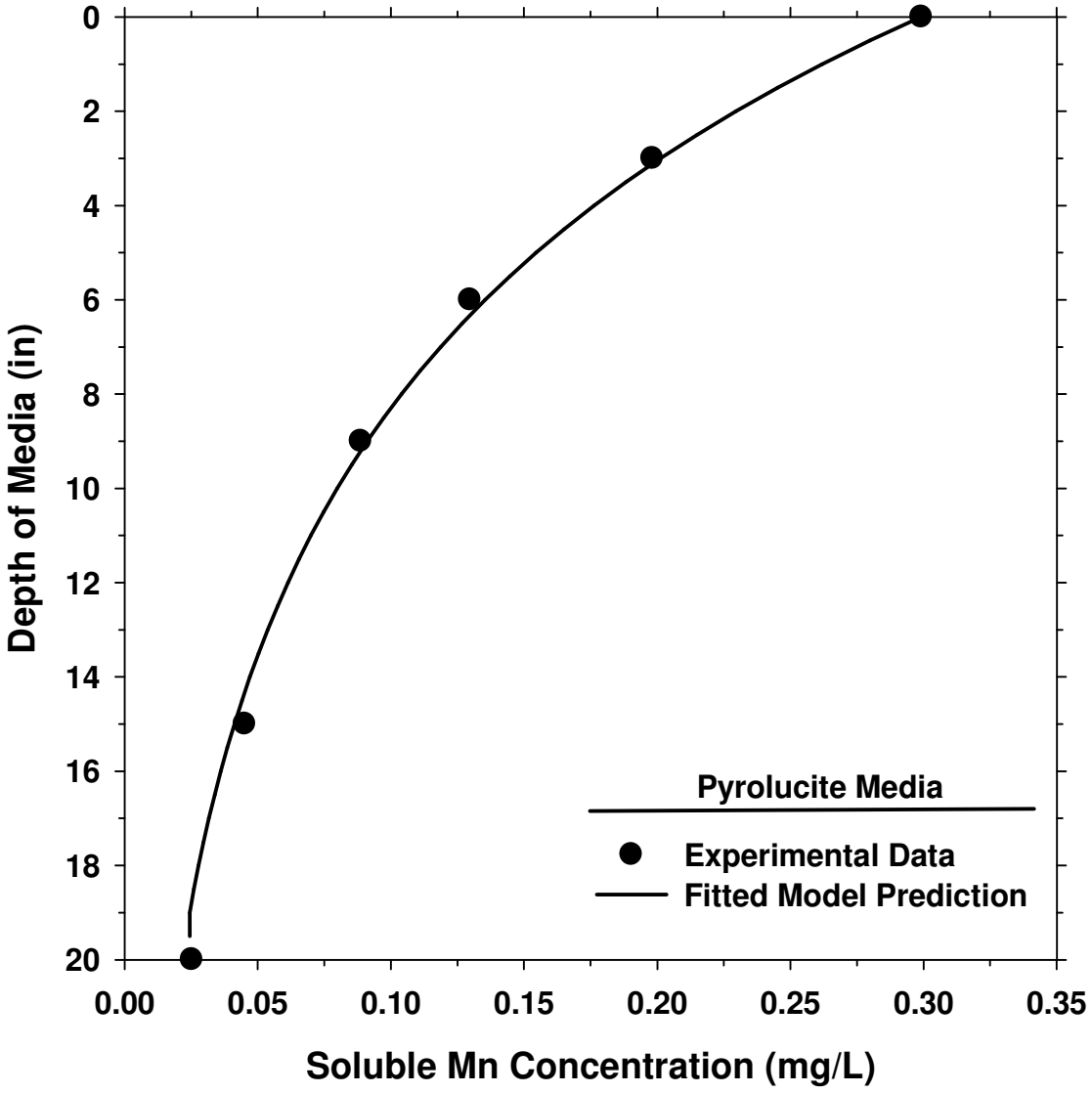

Figure A.24 Model fit to experimental data for pyrolucite media (Influent Water: HLR=16 gpm/ft^2, pH=7.4, HOCl=2.1 mg/L, Mn^{2+}=0.30 mg/L)

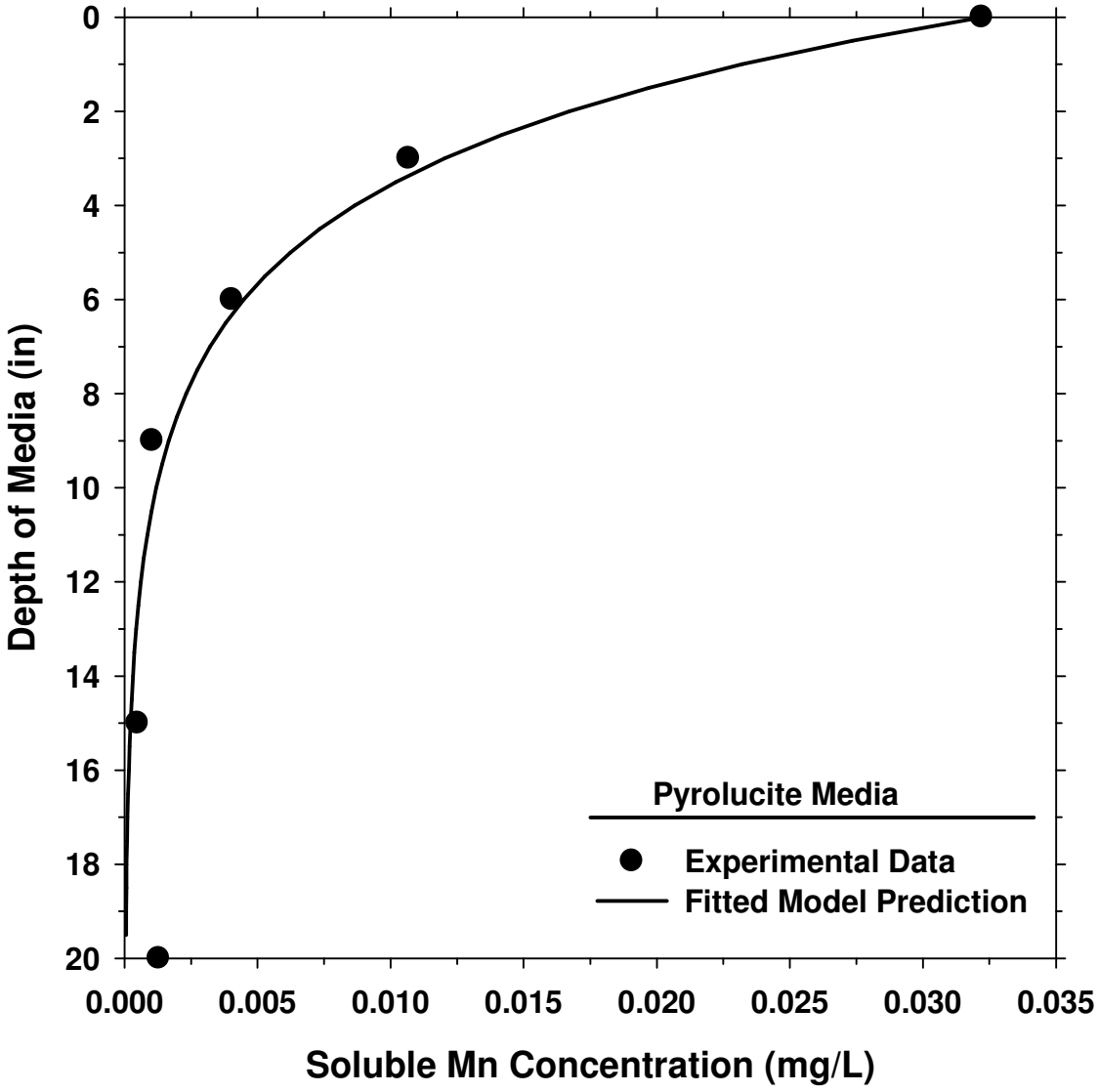

Figure A.25 Model fit to pilot-scale experimental data for pyrolucite media (Influent Water: HLR=16 gpm/ft^2, pH=7.2, HOCl=1.9 mg/L, Mn^{2+}=0.03 mg/L)

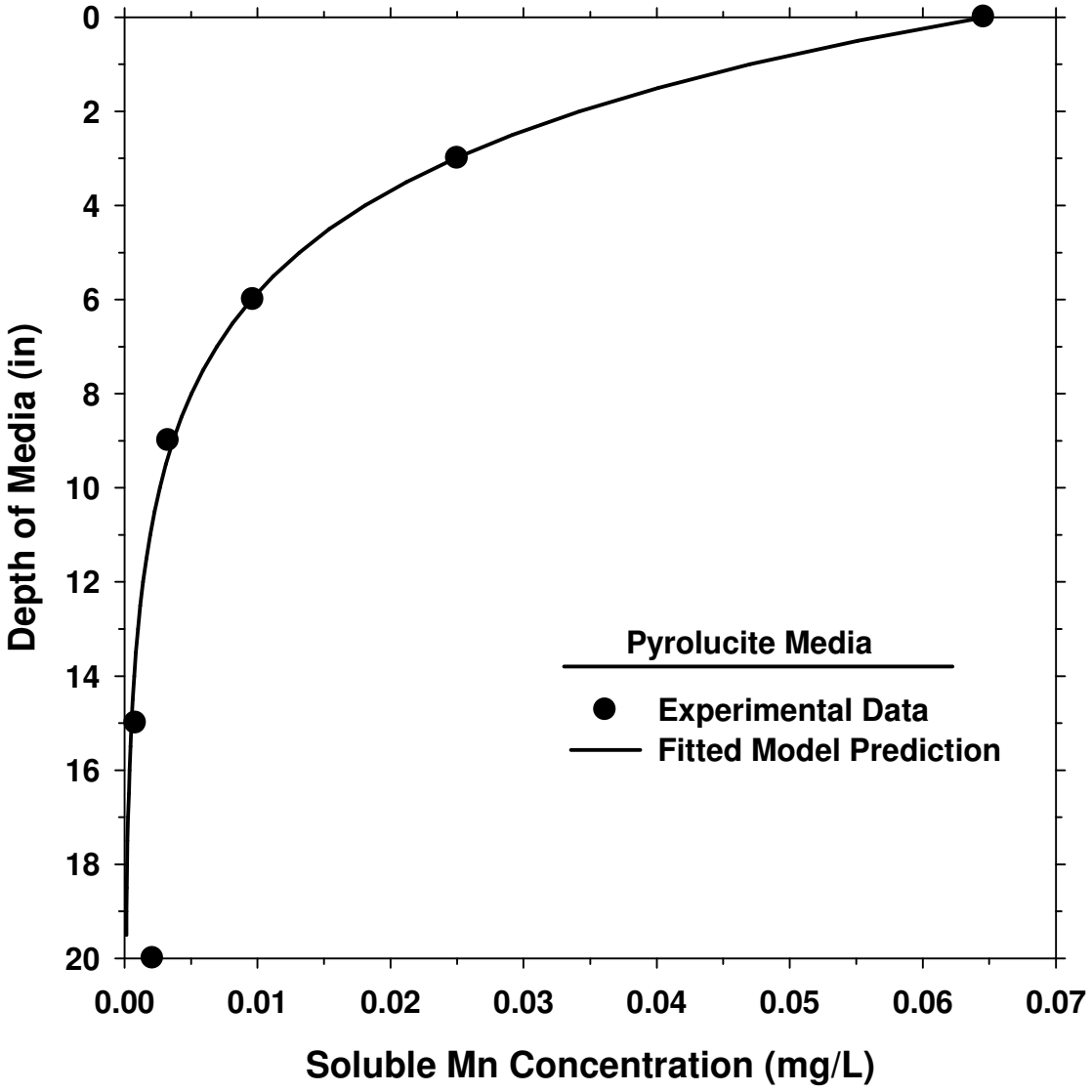

Figure A.26 Model fit to pilot-scale experimental data for pyrolucite media (Influent Water: HLR=16 gpm/ft^2, pH=7.2, HOCl=2.2 mg/L, Mn^{2+}=0.06 mg/L)

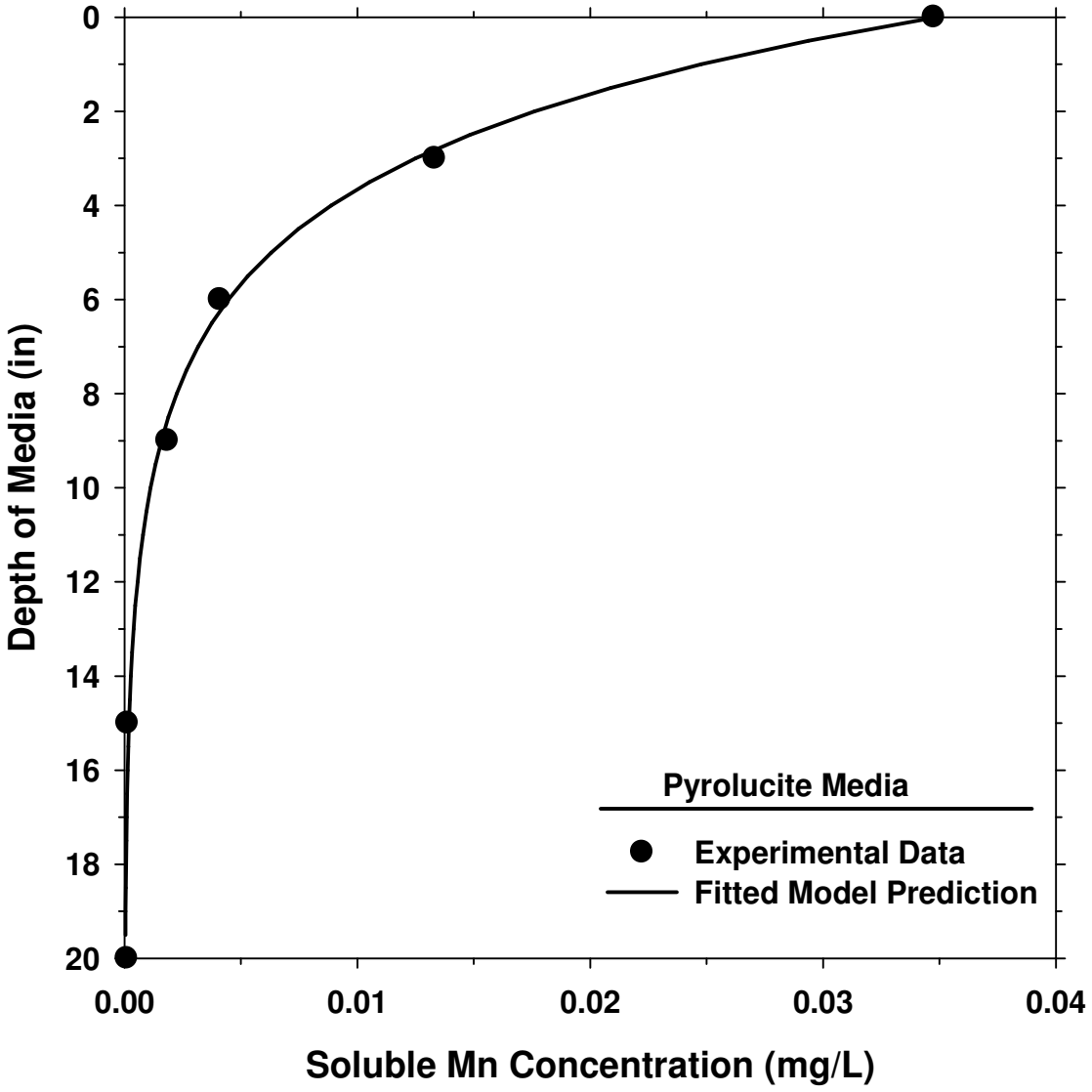

Figure A.27 Model fit to pilot-scale experimental data for pyrolucite media (Influent Water: HLR=22 gpm/ft^2, pH=7.5, HOCl=1.9 mg/L, Mn^{2+}=0.03 mg/L)

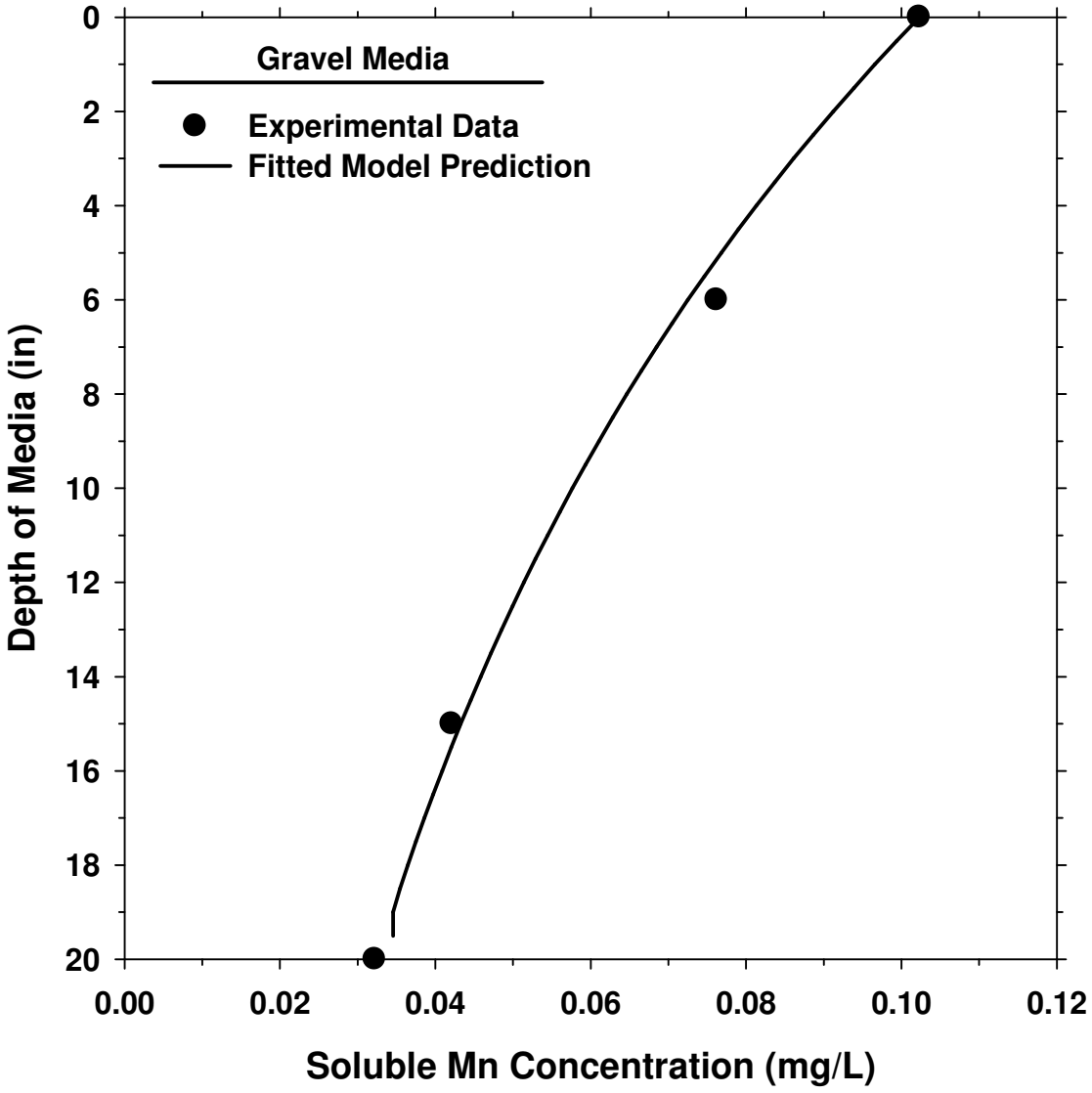

Figure A.28 Model fit to experimental data for gravel media (Influent Water: HLR=16 gpm/ft^2, pH=7.5, HOCl=1.1 mg/L, Mn^{2+}=0.10 mg/L)

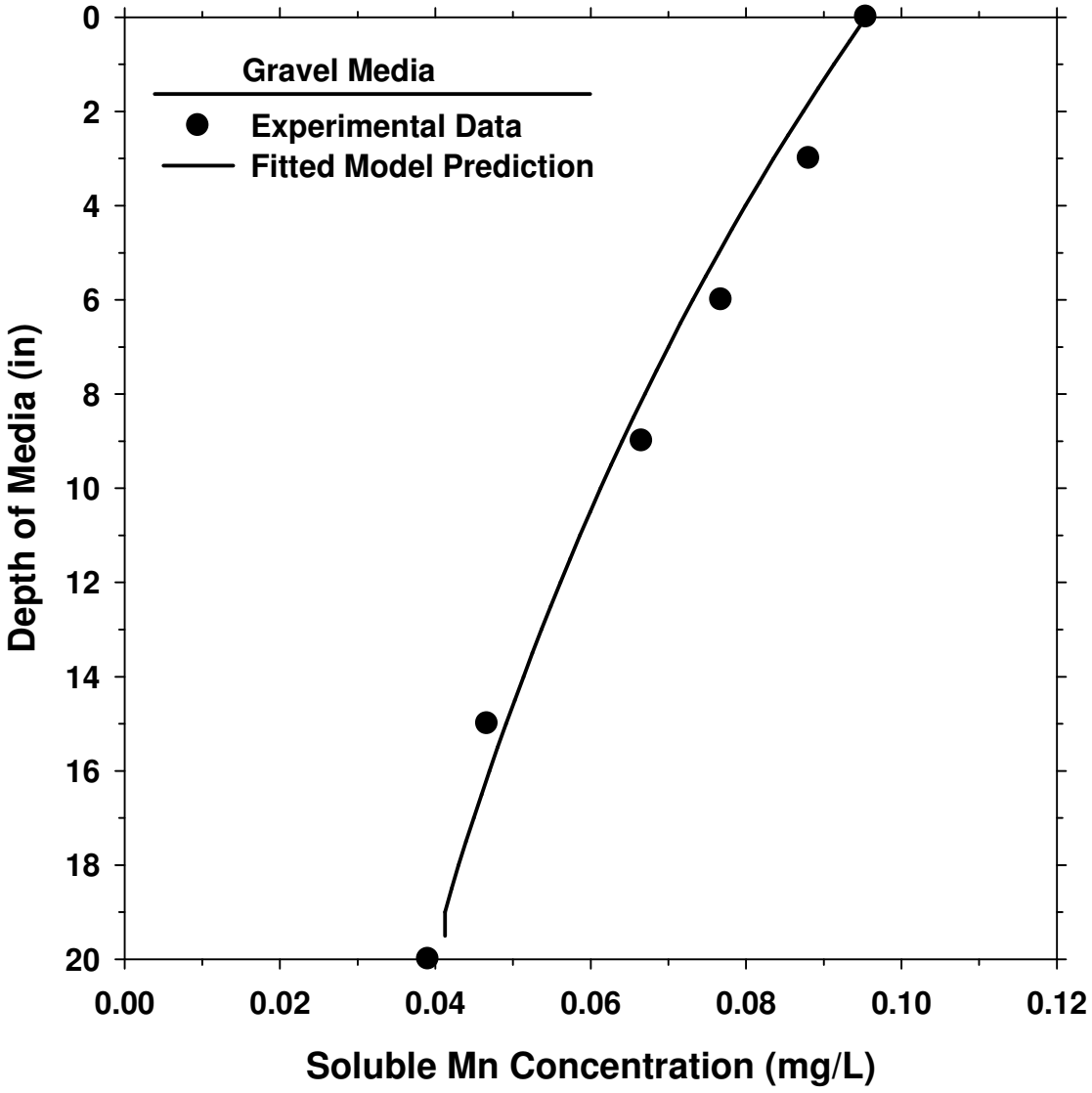

Figure A.29 Model fit to experimental data for gravel media (Influent Water: HLR=16 gpm/ft^2, pH=7.5, HOCl=1.9 mg/L, Mn^{2+}=0.10 mg/L)

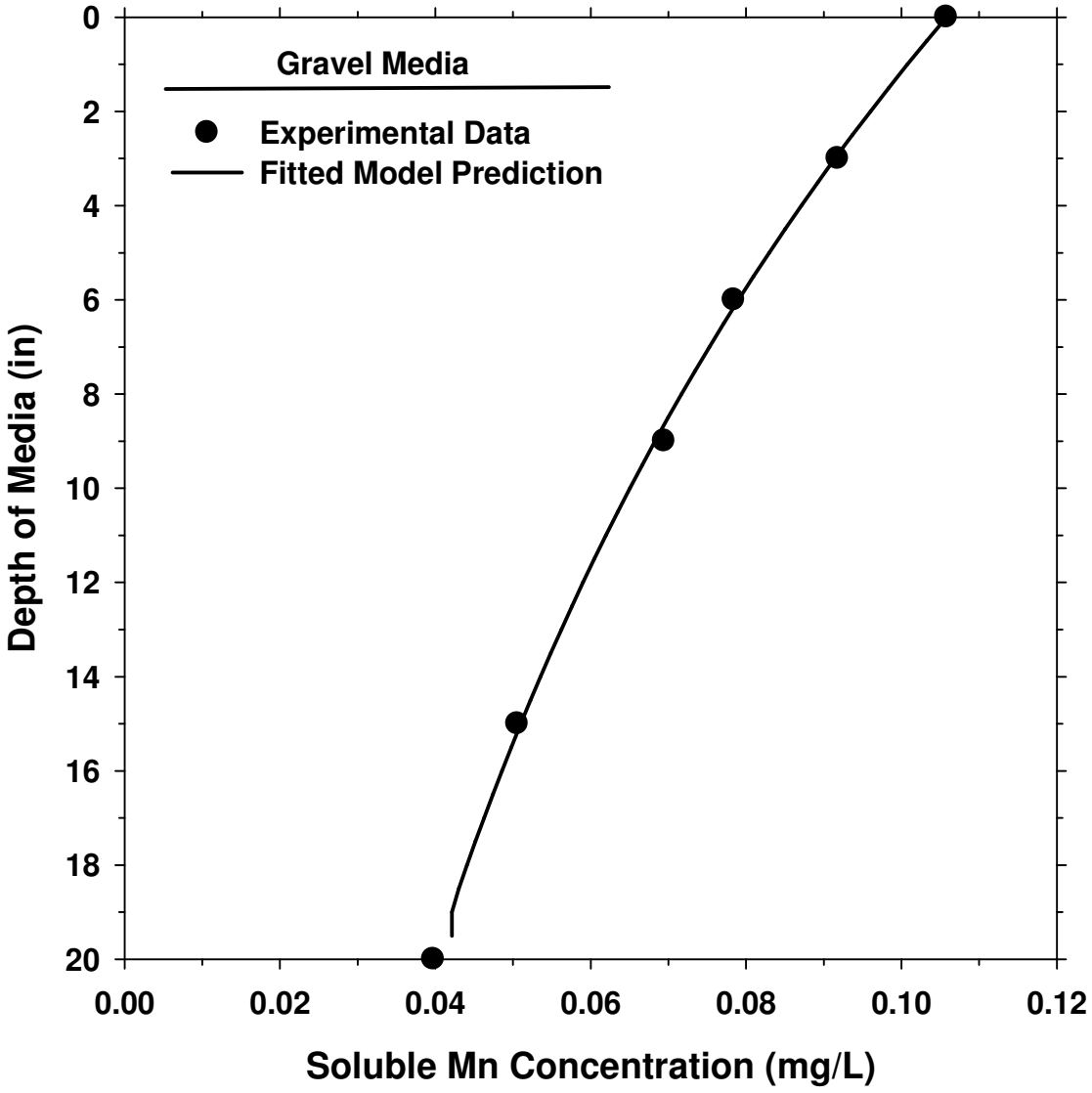

Figure A.30 Model fit to experimental data for gravel media (Influent Water: HLR=16 gpm/ft^2, pH=7.7, HOCl=2.4 mg/L, Mn^{2+}=0.11 mg/L)

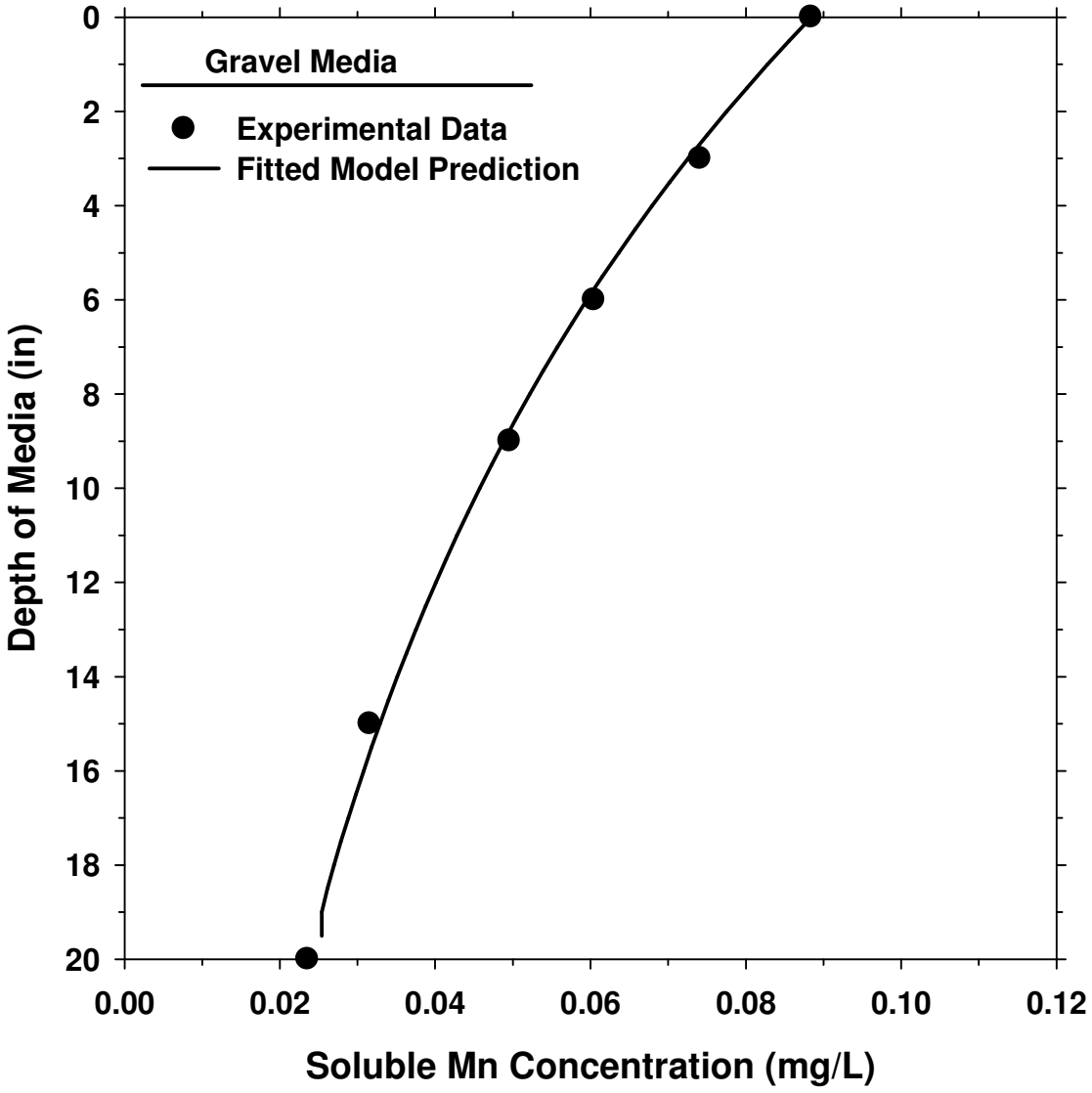

Figure A.31 Model fit to pilot-scale experimental data for gravel media (Influent Water: HLR=16 gpm/ft^2, pH=7.4, HOCl=0.9 mg/L, Mn^{2+}=0.09 mg/L)

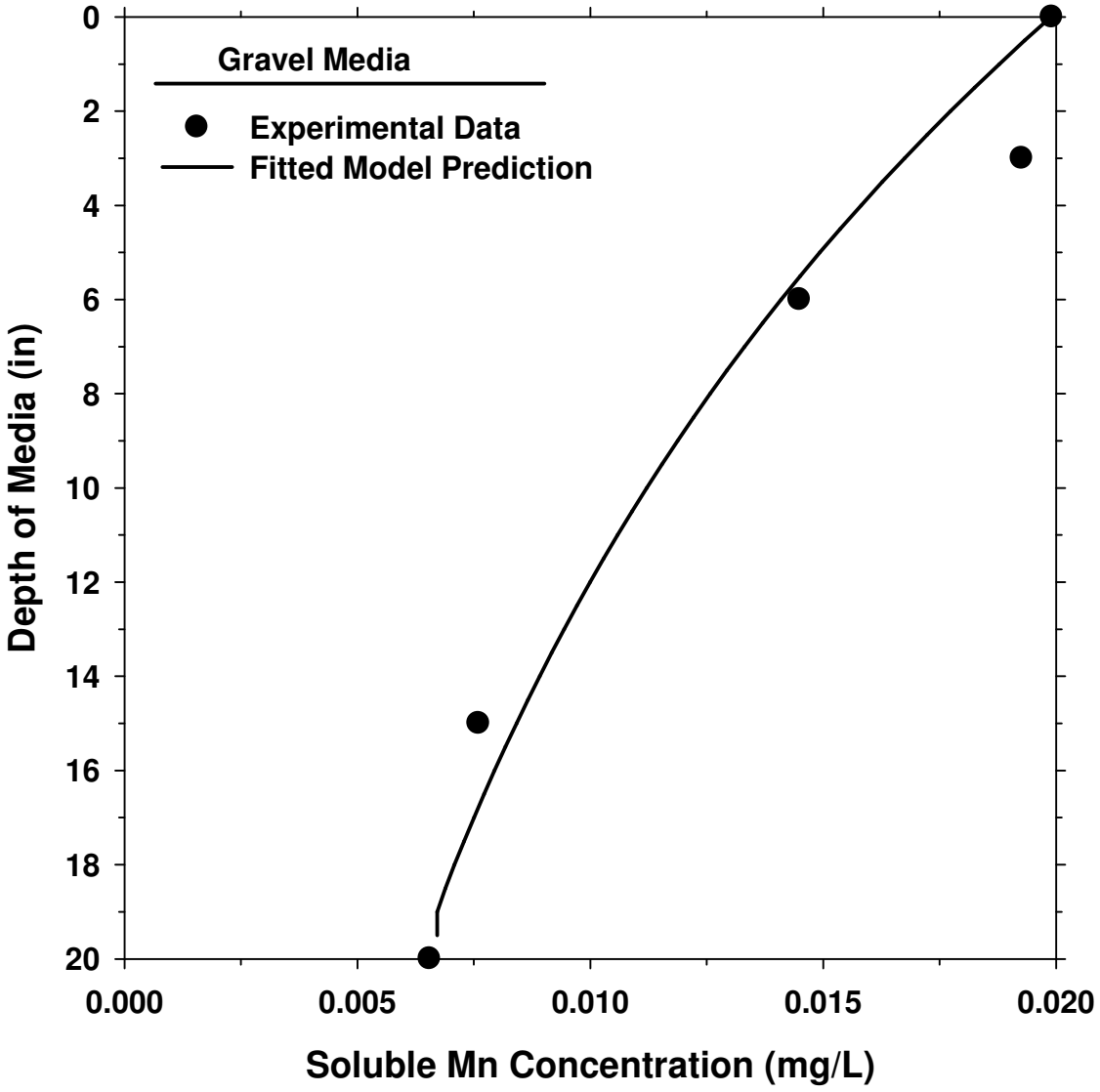

Figure A.32 Model fit to pilot-scale experimental data for gravel media (Influent Water: HLR=16 gpm/ft^2, pH=7.3, HOCl=1.4 mg/L, Mn^{2+}=0.02 mg/L)

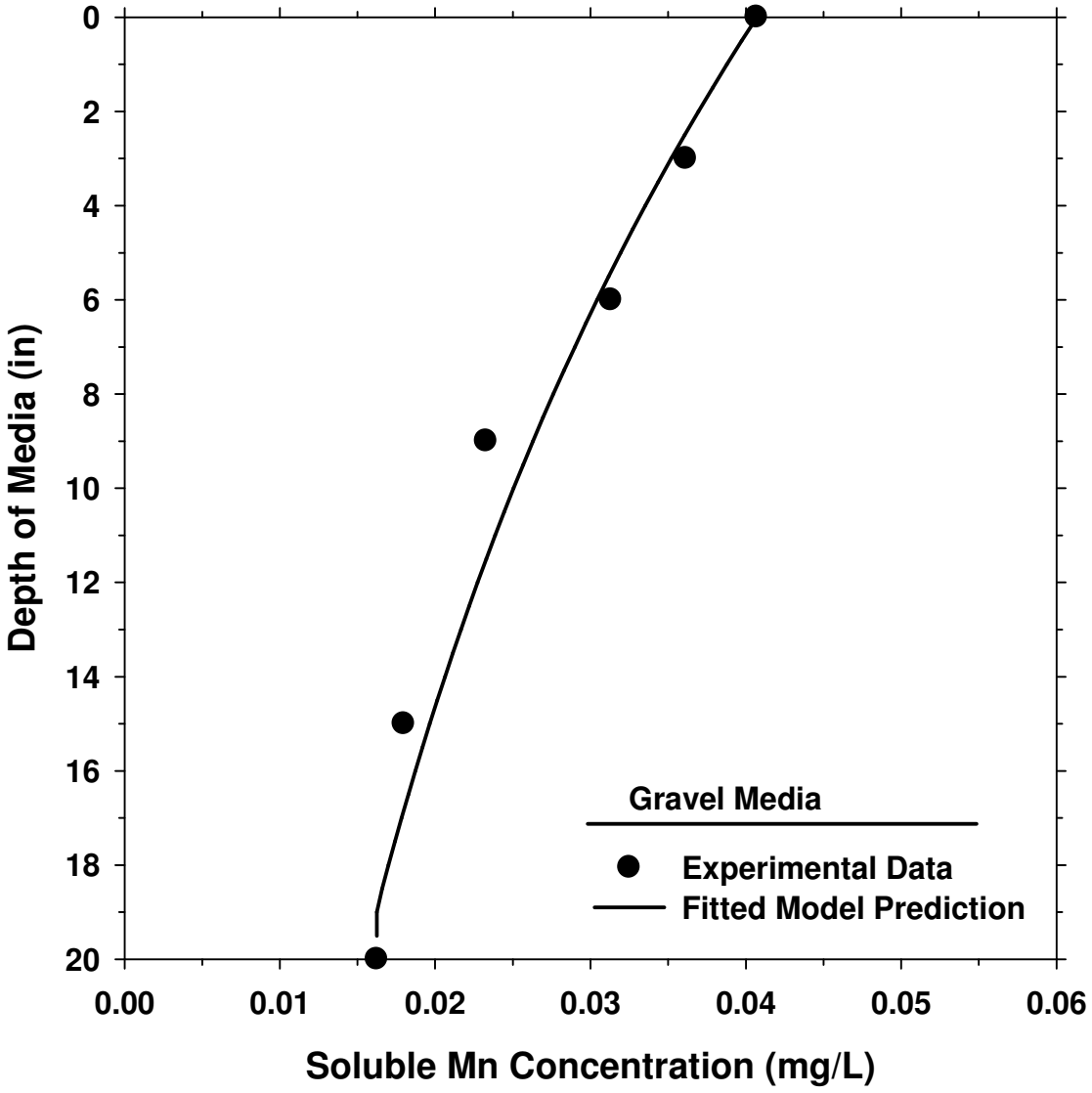

Figure A.33 Model fit to experimental data for gravel media (Influent Water: HLR=20 gpm/ft^2, pH=7.6, HOCl=1.6 mg/L, Mn^{2+}=0.04 mg/L)

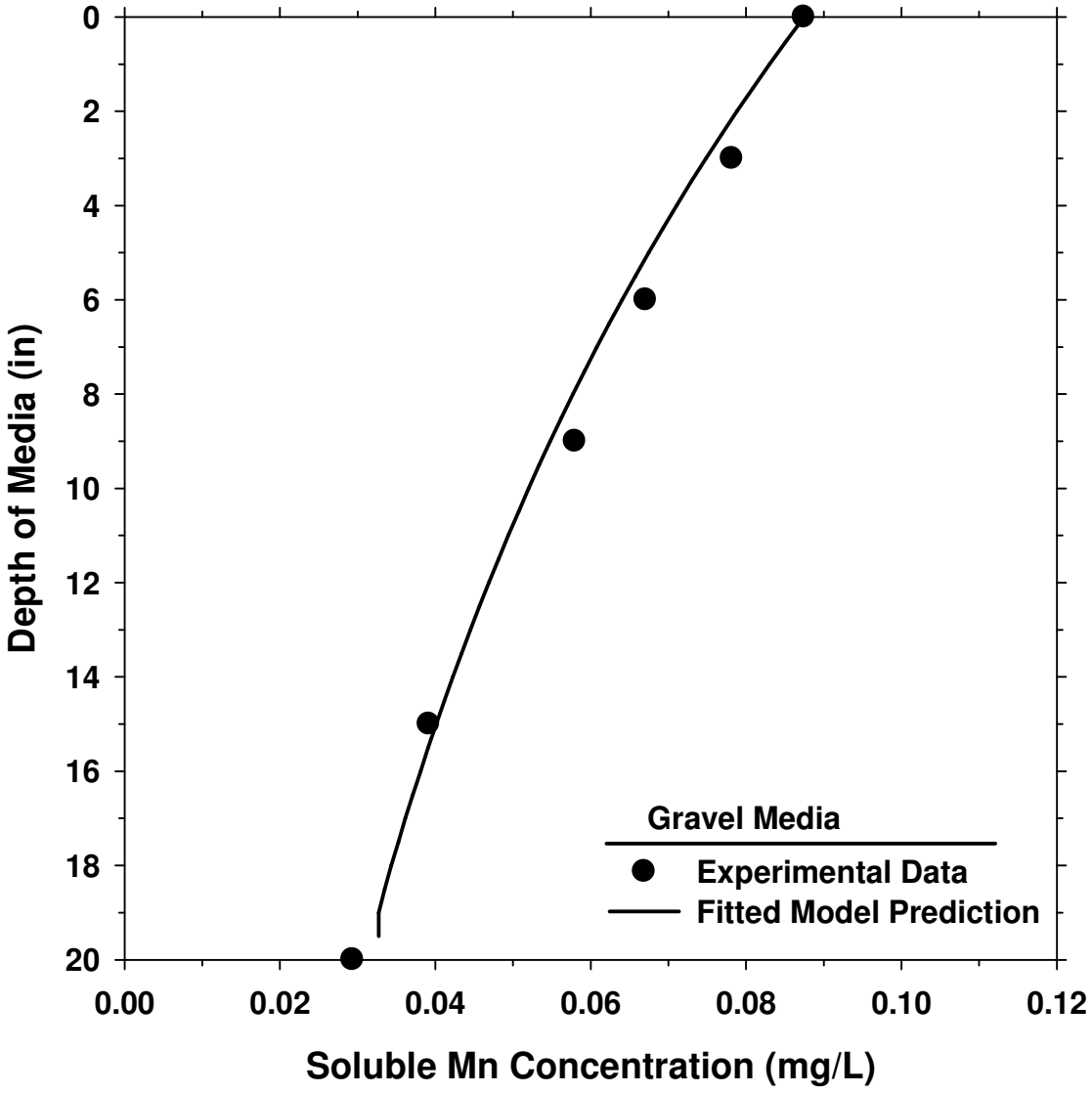

Figure A.34 Model fit to experimental data for gravel media (Influent Water: HLR=20 gpm/ft^2, pH=7.5, HOCl=3.2 mg/L, Mn^{2+}=0.09 mg/L)

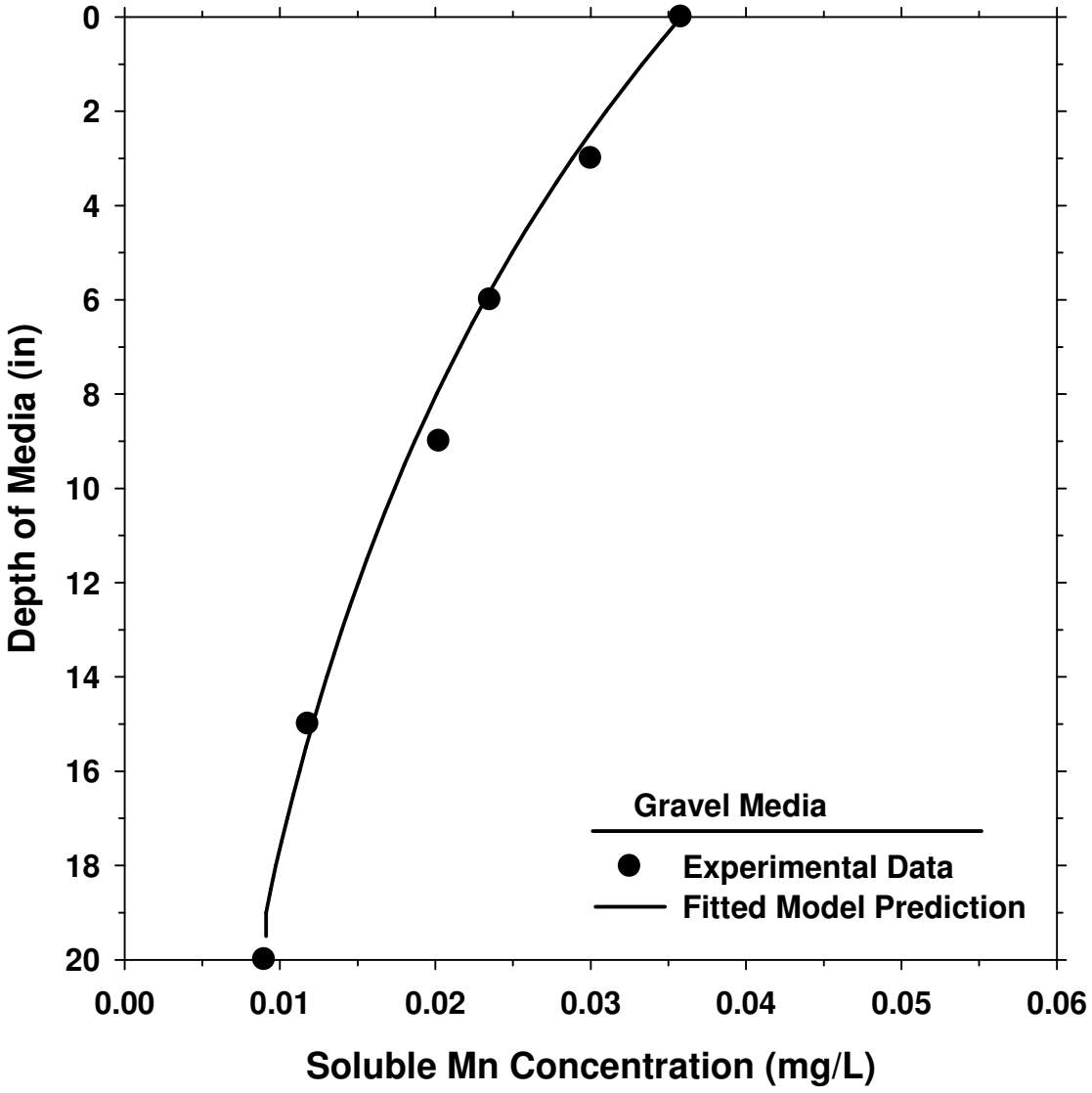

Figure A.35 Model fit to pilot-scale experimental data for gravel media (Influent Water: HLR=24 gpm/ft^2, pH=7.4, HOCl=1.7 mg/L, Mn^{2+}=0.04 mg/L)

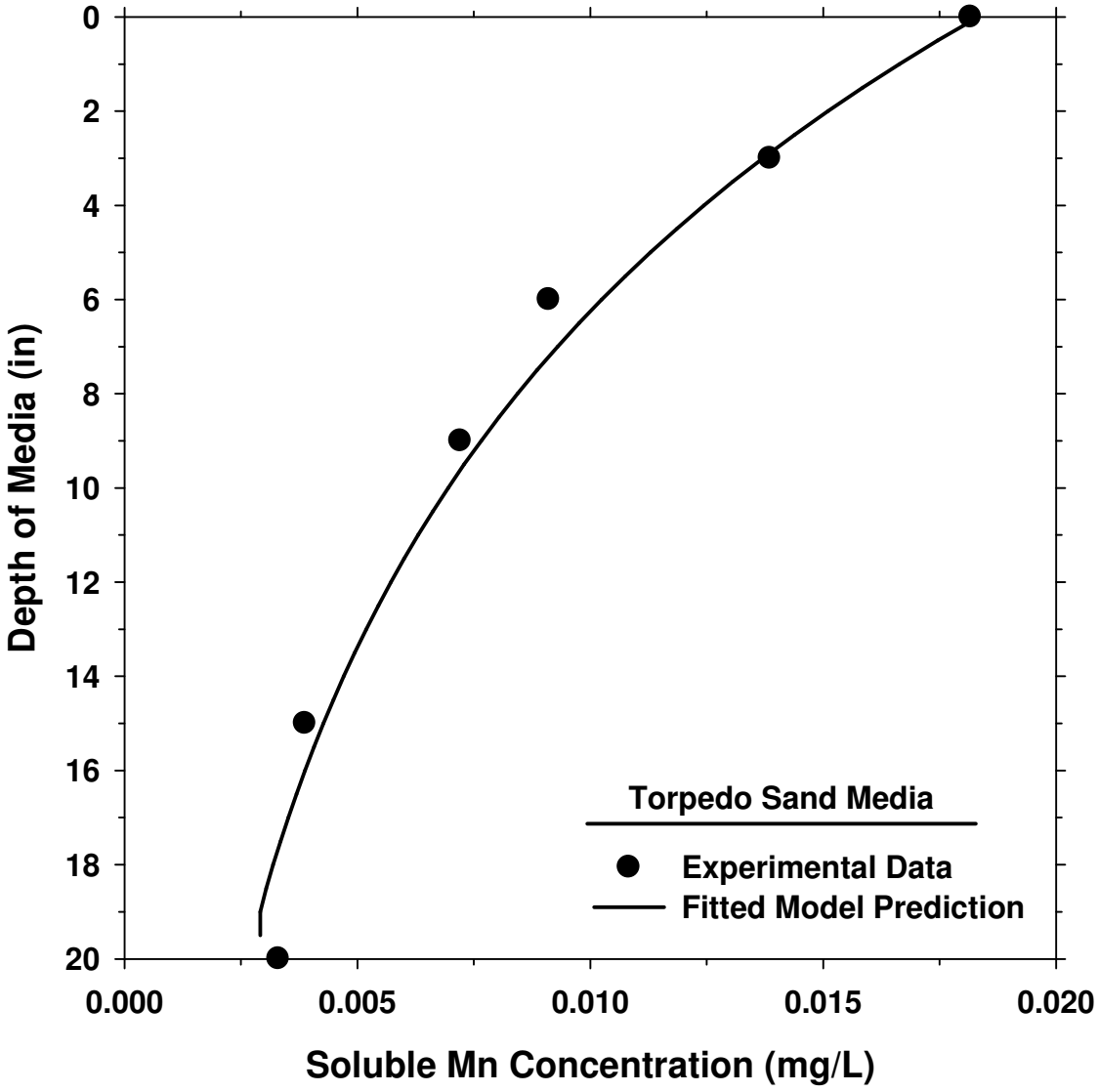

Figure A.36 Model fit to pilot-scale experimental data for torpedo sand media (Influent Water: HLR=16 gpm/ft^2, pH=7.3, HOCl=1.2 mg/L, Mn^{2+}=0.02 mg/L)

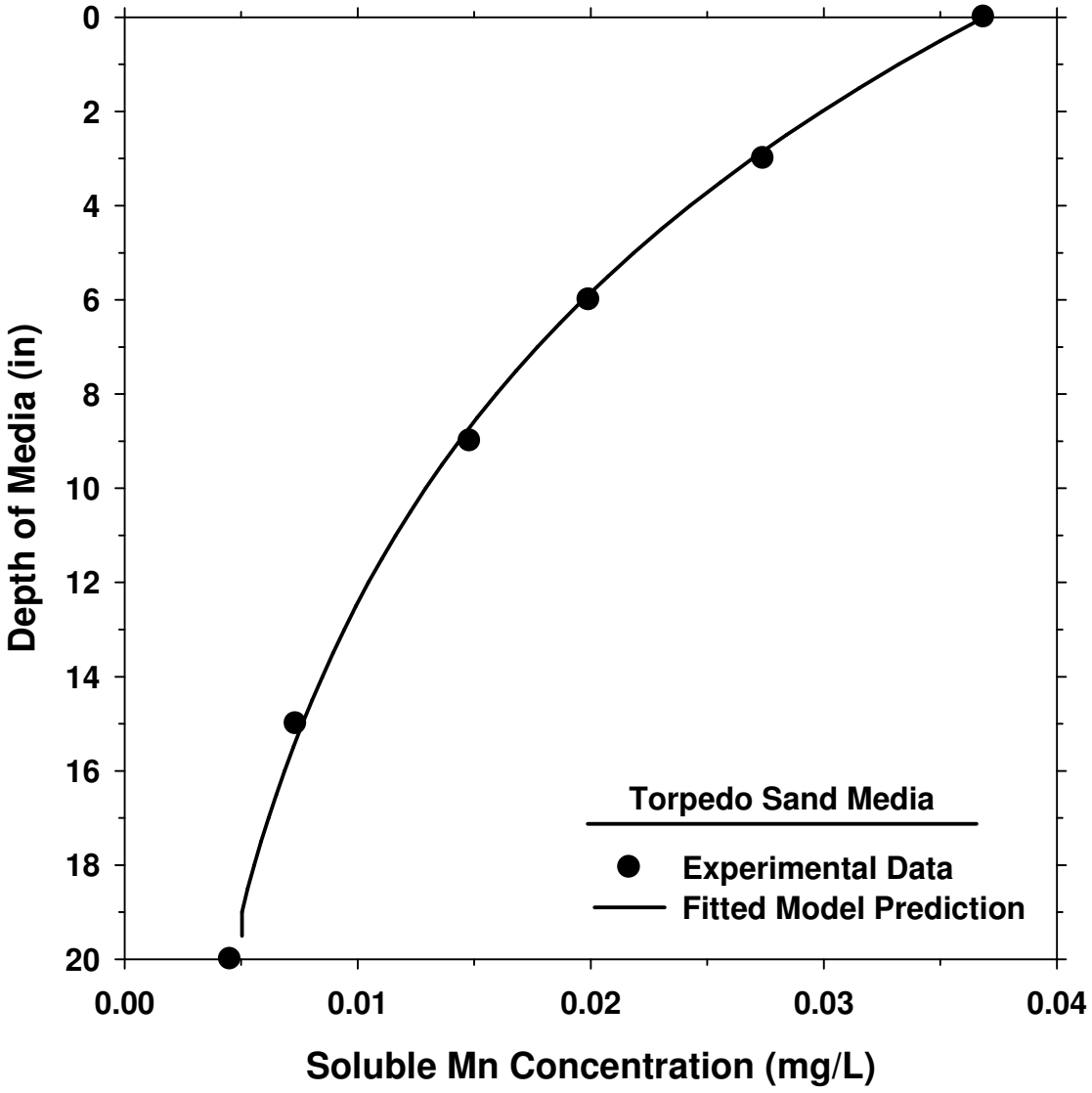

Figure A.37 Model fit to pilot-scale experimental data for torpedo sand media (Influent Water: HLR=16 gpm/ft^2, pH=7.2, HOCl=1.1 mg/L, Mn^{2+}=0.04 mg/L)

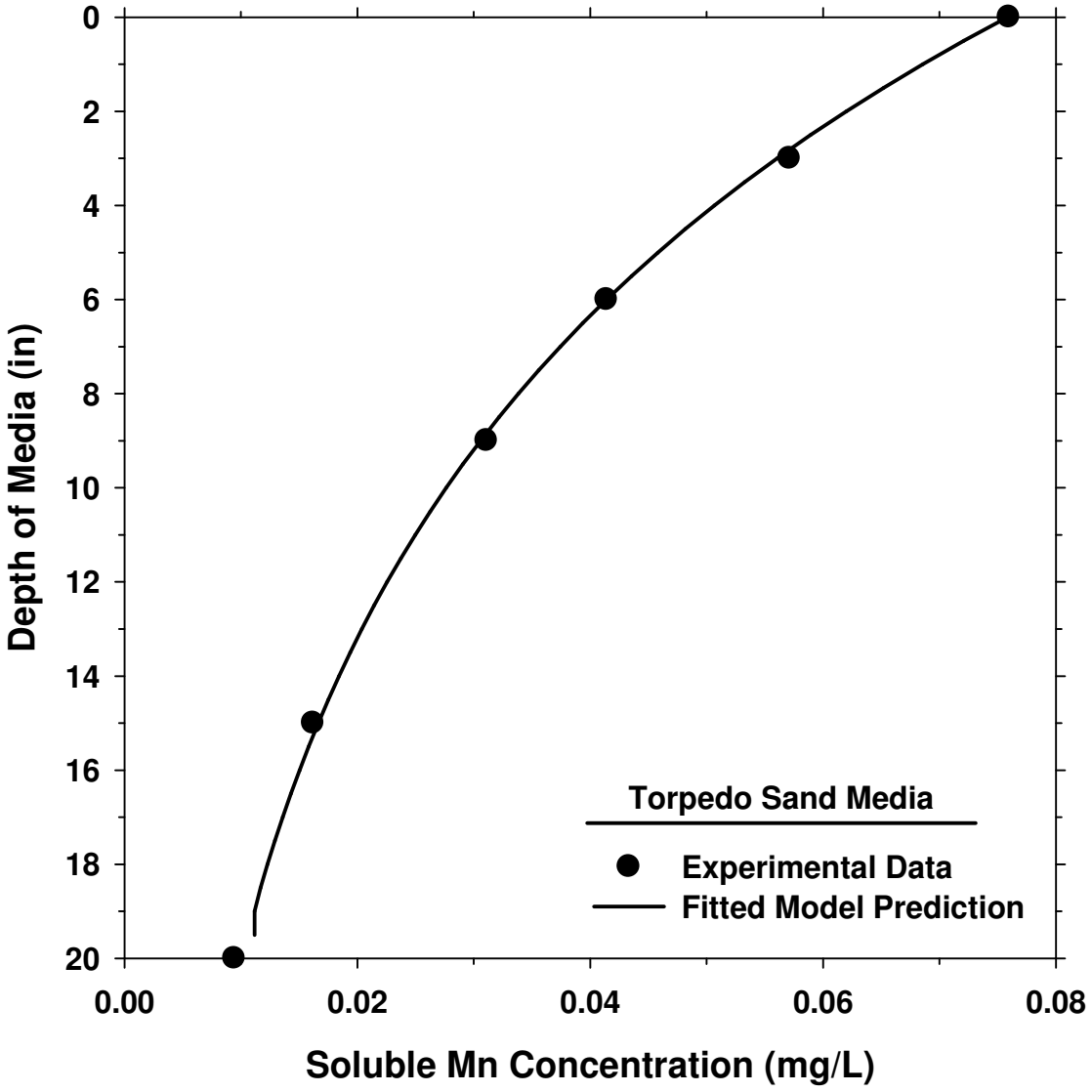

Figure A.38 Model fit to pilot-scale experimental data for torpedo sand media (Influent Water: HLR=16 gpm/ft^2, pH=7.5, HOCl=1.8 mg/L, Mn^{2+}=0.08 mg/L)

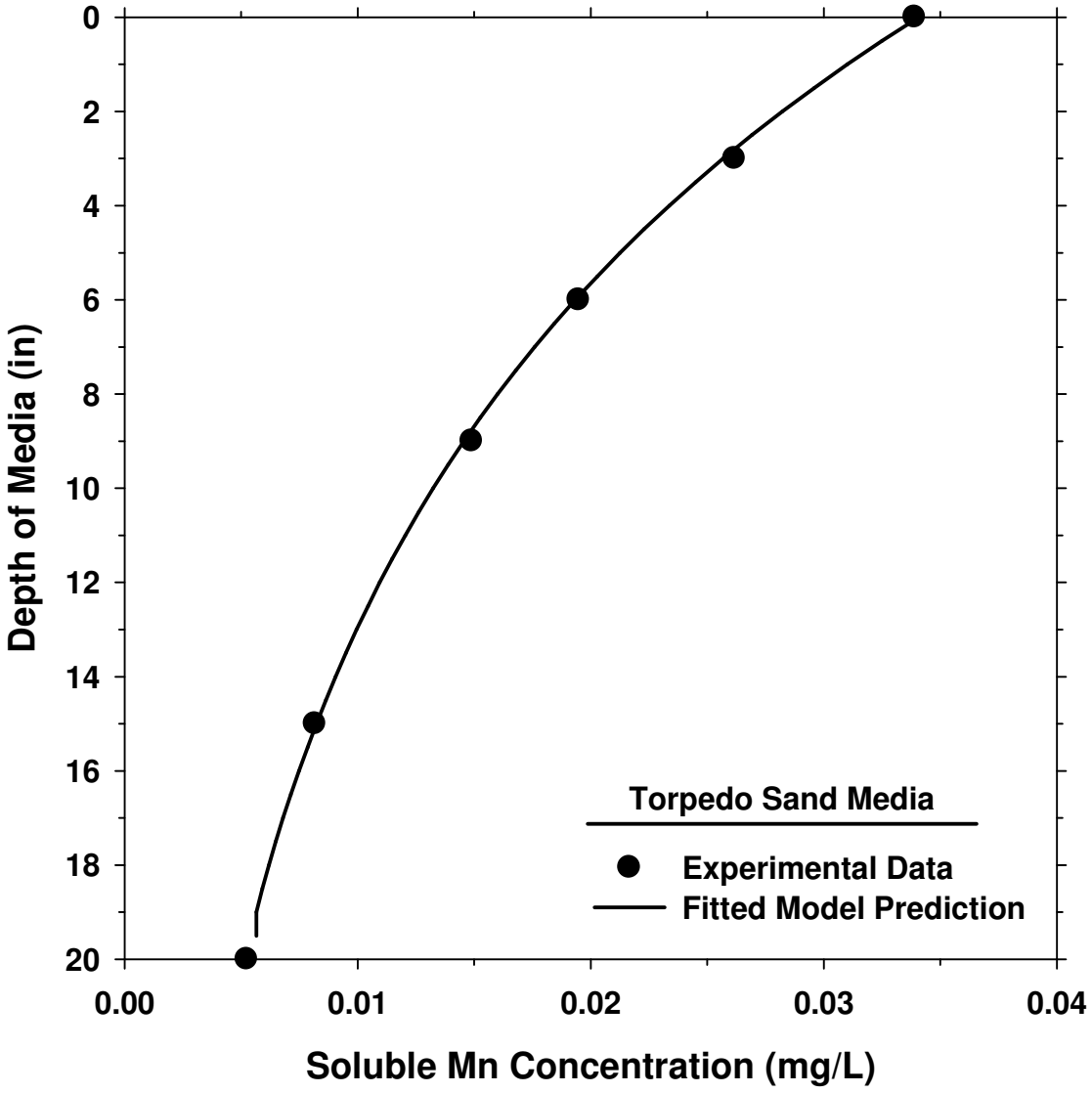

Figure A.39 Model fit to pilot-scale experimental data for torpedo sand media (Influent Water: HLR=24 gpm/ft^2, pH=7.1, HOCl=1.4 mg/L, Mn^{2+}=0.03 mg/L)